

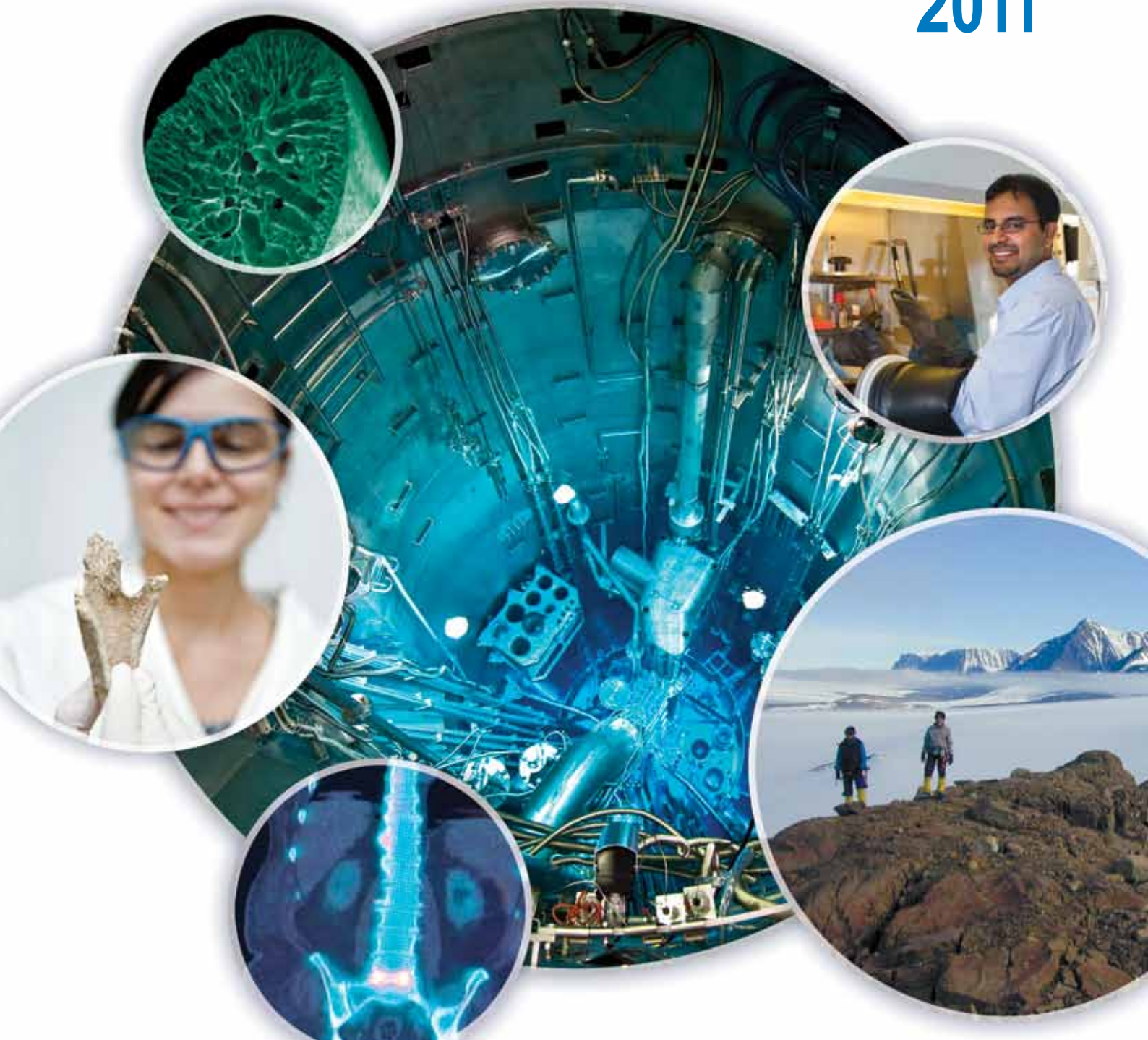


Australian Government

Ansto

Nuclear-based science benefiting all Australians

Research Selections 2011



The Australian Nuclear Science and Technology Organisation (ANSTO) is the home of Australia's nuclear science expertise. This expertise is applied to radiopharmaceutical production and biomedical research, climate change research, water resource management, materials engineering, neutron science and a range of other disciplines.

ANSTO is a Federal Government agency with the mission to apply nuclear science for the benefit of all Australians. It operates Australia's nuclear reactor, OPAL, for research and isotope production. Critical research carried out at ANSTO involves the neutron beam instruments attached to OPAL, run by ANSTO's Bragg Institute, Australia's leading neutron scattering research group.

ANSTO operates particle accelerators to analyse the elemental composition and age of materials. ANSTO has two accelerators, ANTARES and STAR, both of which are used in ion beam analysis and accelerator mass spectrometry. Two new accelerators will be established, putting ANSTO at the forefront of this field worldwide. ANSTO is a founding partner in the national accelerator collaboration – Australian Collaboration for Accelerator Science (ACAS) – aimed at maintaining state-of-the-art facilities and a pool of accelerator experts. ANSTO is also one of the ten foundation investors in the Australian Synchrotron.

As custodian of this world-class infrastructure, ANSTO attracts scientists from around the world to use the facilities. Approximately three hundred scientists use ANSTO's neutron beam instruments each year, enabling productive collaborations, and keeping Australia at the forefront of scientific discovery. ANSTO researchers are engaged in international research through reciprocal arrangements with many organisations. Agreements for collaborations have recently been signed with the French Atomic Energy Commission, the Korean Atomic Energy Research Institute and CERN, home of the Large Hadron Collider in Switzerland.

Table of contents

Foreword	2
Novel materials	5
Visual probes for carbon dioxide and new molecular logic-systems	7
A new way of creating magnetic interfaces in thin films	11
Finding a quantum-forbidden structure	17
Studying interfaces of ionic liquids to improve industrial electrochemical processes	21
Towards a clear understanding of catalytic processes	25
Environment	29
Monitoring evaporation and groundwater inputs to the Darling River during drought	31
Using cosmic rays and radionuclides to measure the contribution of the East Antarctic Ice Sheet to changes in global sea-level	37
Understanding and managing wetland health	45
Unravelling farming and metallurgy in ancient China with nuclear science	49
Plants that can accumulate toxic metals	55
LifeSciences	59
Development of novel imaging radiopharmaceuticals for malignant melanoma	61
Understanding molecular mechanisms to aid in the protection of cell membranes in anhydro- and cryo-biology	67
Identifying optimal conditions for the production of next generation radiopharmaceuticals	71
Materials related to the energy life-cycle	75
Making better Li-ion batteries using neutron diffraction	77
Understanding the kinetic processes of gas-hydrate formation in the marine environment	81
Waste – a resource when using selective separation	87
Developing radiation-tolerant materials	91
Reactor engineering	97
Understanding the vibrational response of thin plates secured using varying strength longitudinal connections	99
Bubbly flow regime and beyond - modelling gas-liquid flow using population balance	103
Facts and figures	106
List of publications	114

Foreword

The world of science, engineering and technology is changing at such a rapid pace, it is crucial that Australia is not left behind.

Many of the most important questions that we face today are within the domain of ANSTO's expertise; whether it is how to create more efficient batteries, better ways to manage scarce water resources, or improved imaging techniques for cancer patients. ANSTO researchers are playing critical roles, providing new solutions for the world we are living in and new insights about what the world will look like in the future. Our researchers and collaborators not only find new solutions, they also provide insights into the past and contribute to the ideas that are so important for informed decision making.

The best science happens at the boundaries of physics; for example, gaining deeper understanding of materials by using neutrons, or new applications for radiopharmaceuticals. With our state-of-the-art research reactor, OPAL, and our accelerators and neutron beam instruments, we are expanding and pushing beyond these boundaries and taking part in vital collaborations with some of the best researchers around the world.

ANSTO has contributed to exciting health research in new imaging techniques for malignant melanoma. This ongoing work provides a solid example of how collaborative research has the potential to bring great benefits to all Australians, and enables tremendous health outcomes globally.

In environmental research, nuclear techniques have been used to gain a baseline understanding of evaporation in the Murray-Darling basin, and how wetlands fluctuate as a result of natural and human-induced changes. Through interpreting historical climate events, this work enables ANSTO and its collaborators to address water resource issues facing the Australian community today and into the future.

ANSTO researchers have also discovered exciting light responsive molecules, with potential applications in detection of toxic levels of carbon dioxide. They are leading the development of functional magnetic interfaces at the atomic level and providing novel insights into the properties of crystals that seem to defy our classical understanding of physics.

Nuclear techniques are also being used to piece together the history of human movements in ancient China, shedding more light about activities on the Silk Road. Other work has uncovered fundamental information about cell membranes; revealed how some plants accumulate toxic metals and provided a better understanding of specific radioactivity. These are all examples of what is being achieved through the combination of great science and strong science platforms.

This tremendous research underpins the immense value of partnerships and collaborations. As a cross section of significant research, this publication demonstrates the ongoing success of our partnerships. Nearly all of these case studies involve collaborations from around the world, and many include experts at Australian universities and other respected Australian science organisations.

To encourage this constant exchange of ideas, ANSTO enters into exciting partnerships with some of the top research organisations around the world, as well as top university researchers around Australia. This trend for collaborative research will continue as the benefits of new partnerships flow through.

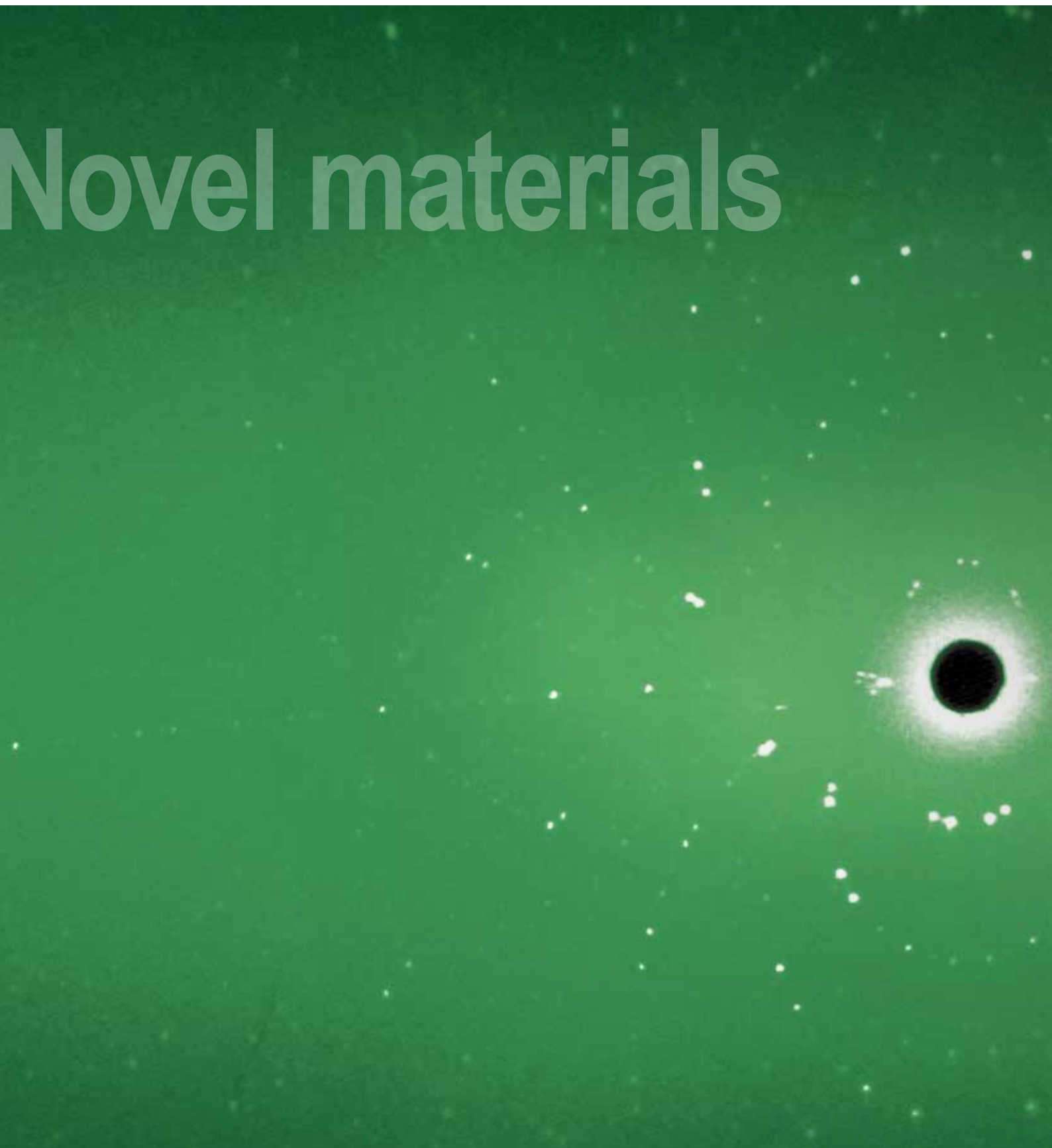
ANSTO takes pride in its mission to use nuclear techniques to benefit all Australians. This publication provides a window into how we use nuclear science and technology to tackle some of the health, environment and industrial challenges of today, to shape our tomorrow.



Dr Adi Paterson
Chief Executive Officer
ANSTO



Novel materials



Novel materials

The research and development of novel materials is essential for the advancement of numerous industries such as health care, electronics and construction industries.

Novel materials are materials such as plastics, metals and ceramics that have been designed in order to exhibit new properties and improve performance.

The research conducted at ANSTO is aimed at developing new materials to tackle industry problems and create innovative new and improved products.



Tamim Darwish pictured is developing chemical sensors that can be used to visually detect toxic levels of CO₂ in the air.

Visual probes for carbon dioxide and new molecular logic-systems

Tamim Darwish¹, Richard Evans², Michael James¹ and Tracey Hanley¹

¹ANSTO, ²CSIRO Materials Science and Engineering

Excessive exposure to high levels of carbon dioxide (CO₂) can endanger human health and even be fatal. As CO₂ is invisible to the naked eye it can only be monitored using electronic equipment. Therefore we are developing chemical sensors for CO₂ based on a spirocyan molecule with an amidine moiety conjugated to its backbone, that have generated a single molecule that is highly sensitive to the presence of CO₂ and more importantly can be used to visually detect toxic levels of CO₂ in the air.

A spectrum of colours, from purple to yellow, can be obtained depending on the concentration of CO₂ being introduced. Just like photochromic (light-responsive) molecules darken UV sensitive sunglasses when exposed to the sun, this research has the potential to develop products that will change colour when exposed to high levels of CO₂.

Photochromic molecules

Photochromic dyes (e.g. spirocyan – Fig. 1) are light-responsive molecules. They reversibly transform between two forms which have exactly the same atoms but different structures, also called photo-isomerisation. The light effect results in clear and coloured states, where molecular structure and polarity are dramatically different. When irradiated by UV light, spirocyan molecules adopt an ionic, planar merocyanine (MC) form and a deep purple colour; while under heat or visible light they revert to the neutral, orthogonal spiro (SP) form and are colourless.

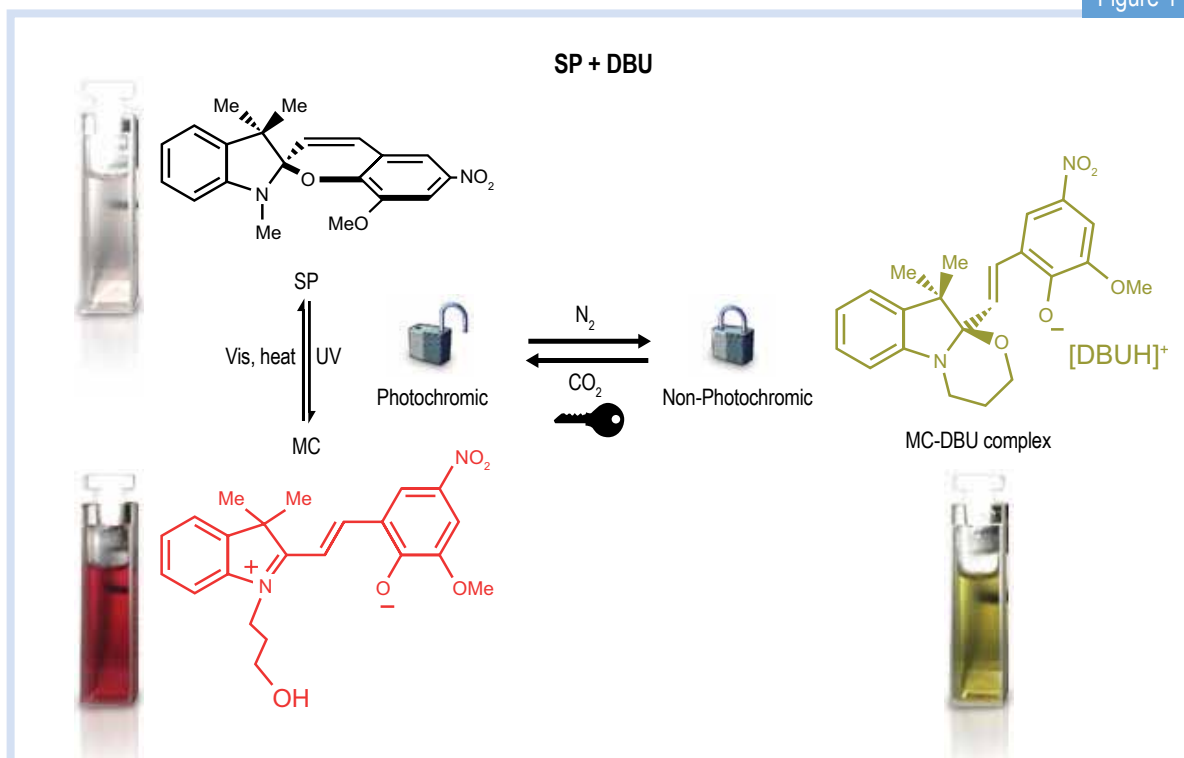
Commercially, photochromic compounds have been applied in ophthalmic lenses and consequently, substantial research has concentrated in this domain [1]. More recently, the remote triggering and reversible behaviour of these compounds has led to their evaluation in numerous applications such as the modulation of stem-cell attachment and self assembly among other biological and chemical processes.

Carbon-dioxide and nitrogen gases as new triggers for spirocyan systems

Carbon dioxide (CO₂) has excellent potential to act as a new mild stimulus that can be easily added and removed from solutions of photochromic molecules. We have found that the photochromic effect of spirocyan molecules can be reversibly activated/deactivated by the addition and removal of CO₂ from solutions of spirocyan containing an amidine species (e.g. DBU) [2].

The spirocyan/amidine complexes are yellow in solution and non-photochromic, but become photochromic again when CO₂ is subsequently added to the solution (Fig. 1). The CO₂ is readily removed by inert gas sparging which leads to the deactivation of photochromism and the reappearance of the yellow colour. Our work suggests a number of applications in developing bio-responsive materials based on CO₂ gradients found in industry and nature.

Figure 1



Different forms of spiropyran (SP, MC and MC-DBU) and the reversibility of their associated reactions with different stimuli.

Photochromics and molecular logics

Other photochromic dye classes such as spirooxazines and chromenes are not affected by the CO₂/amidine stimulus. As a result, we have developed a system of molecular switches based on mixtures of spirooxazine, chromene and spiropyran that respond differently to UV and visible light as well as CO₂ (Fig. 2). This allows the photochromism of some molecules to be selectively preserved while reversibly deactivating the photochromism of others.

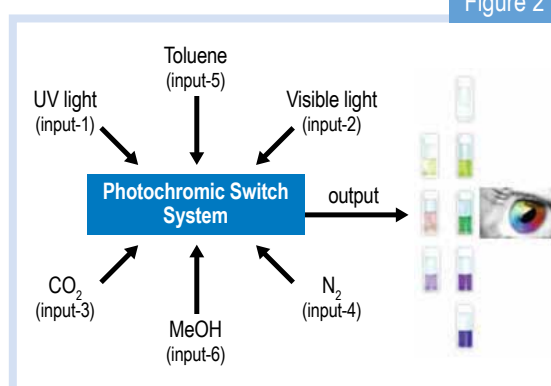
We have investigated the potential of our new solution systems for the application in molecular logics. Essentially, the ON or OFF states of solution photochromism represent “1” or “0” of a digital binary code. Different combinations of stimuli (inputs) give unique visual response (output), which is a blend of different individual colours (Table 1).

Traditionally, molecular logics suffer from dilution and fatigue effects which make the systems non-reversible. In our system, the use of benign triggers such as visible light, UV, CO₂ and N₂ gives us a more robust logic system that does not suffer dilution effects, and hence becomes truly reversible [3].

A new carbon dioxide sensor

CO₂ is an environmental hazard in many areas and a simple visual method of detection remains elusive. Monitoring the air quality continuously, where the output

Figure 2



Multiple inputs for the same solution that can display eight different output colours, all of the changes are fully reversible allowing a more robust molecular logic-system [3].

is monitored by the naked eye and no assay kit or instruments are required would be very beneficial in remote and confined places. We have developed a new visual probe for CO₂ based on a spiropyran molecule with an amidine moiety conjugated to its backbone (SP-Am).

This has generated a single molecule that is highly sensitive to the presence of CO₂ and more importantly can be used to visually detect toxic levels of CO₂ in air; essentially acting as a modern-day molecular canary [4]. A spectrum of colours, from purple to yellow, can be obtained depending on the concentration of CO₂ being introduced (Fig. 3). Also the solution is sufficiently sensitive for which colour changes are observed simply by having the CO₂ in the air above the solutions.

Table 1

Input Data						Output Data							
in ₁	in ₂	in ₃	in ₄	in ₅	in ₆								
UV	Vis	CO ₂	N ₂	Toluene	MeOH								
0	1	0	1	1	0	1	0	0	0	0	0	0	0
0	0	1	0	1	0	0	0	0	1	0	0	0	0
0	1	1	0	1	0	0	0	1	0	0	0	0	0
1	0	0	1	1	0	0	0	0	1	0	0	0	0
1	0	1	0	1	0	0	0	0	0	0	0	0	1
0	1	0	1	0	1	0	0	0	0	0	1	0	0
0	0	1	0	0	1	0	1	0	0	0	0	0	0
0	1	1	0	0	1	0	0	1	0	0	0	0	0
1	0	0	1	0	1	0	0	0	0	0	0	1	0
1	0	1	0	0	1	0	0	0	0	1	0	0	0

Truth Table for a mixture of chromene, spirooxazine and spiropyran with amidine, where a 0 indicates that the corresponding signal is Off and a 1 that is On [3].

Future work

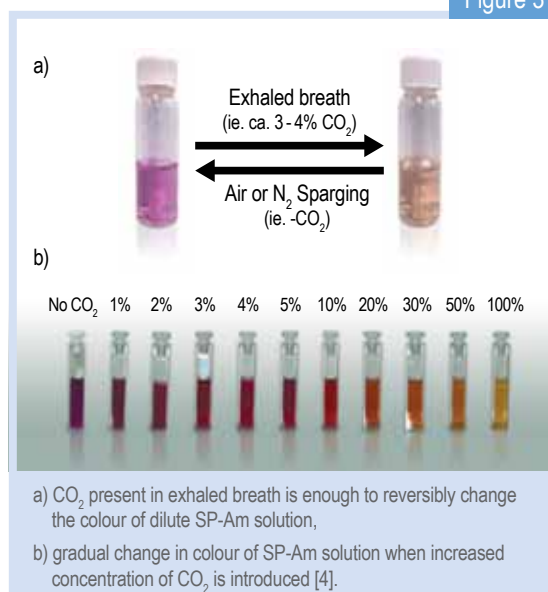
Development of new applications based on these photochromic switches is expected to be widespread. This is in addition to finding roles in fundamental scientific studies. We have opened the door to a new method of triggering response of photochromic spiropyrans, as well as, providing a direct visual method for the detection of hazardous levels of CO₂. The path of absorption of the CO₂ in solution for example can be visually monitored as it diffuses down an unstirred column of Sp-Am in solution. Such a system acts as a CO₂ clock where the length of the yellow coloration provides an indication of time since CO₂ became present above the solution.

Example of future work in this area would be focussed on fundamental studies of CO₂ diffusion in liquids; as well as applications of these dyes in a solid matrix form.

References

- [1] Evans, R. A., Hanley, T. L., Skidmore, M. A., Davis, T. P., Such, G. K., Yee, L. H., et al. (2005). The generic enhancement of photochromic dye switching speeds in a rigid polymer matrix. *Nature Materials*, 4(3), 249-253.
- [2] Darwish, T. A., Evans, R. A., James, M., Malic, N., Triani, G., & Hanley, T. L. (2010). CO₂ Triggering and Controlling Orthogonally Multiresponsive Photochromic Systems. *Journal of the American Chemical Society*, 132(31), 10748–10755.
- [3] Darwish, T. A., Evans, R. A., & Hanley, T. L., Spiropyran, chromene and spirooxazine, mélange à trois: Molecular logic systems through selective and reversible deactivation of photochromism mediated by CO₂ gas. *Dyes and Pigments* (2011), Article in Press doi: 10.1016/j.dyepig.2011.03.021.
- [4] Darwish, T. A., Evans, R. A., James, M., & Hanley, T. L. (2011). Spiropyran-Amidine: A Molecular Canary for Visual Detection of Carbon Dioxide Gas. *Chemistry-A European Journal*, Article in press doi: 10.1002/chem.201101723. (Published online 29 Aug 2011)

Figure 3





Taipan, a neutron three-axis spectrometer, was used for obtaining the results in this article.

A new way of creating magnetic interfaces in thin films

Thomas Saerbeck¹, Frank Klose², Anton Stampff², Sergey Danilkin², Mohana Yethiraj³, Dieter Lott⁴, Andreas Schreyer⁴, Gary Mankey⁵, Zhihong Lu⁵, Patrick LeClair⁵ and Wolfgang Schmidt⁶

¹University of Western Australia and ANSTO, ²ANSTO, ³Alta, Utah, USA, ⁴GKSS, Geesthacht, Germany, ⁵University of Alabama, USA, ⁶Forschungszentrum Jülich, Germany

Since their discovery last century, neutrons have been established as an excellent tool for use in magnetism research, which has a wide range of technological applications such as increasing the storage capacity of computer hard drives. The neutron's high magnetic moment and its large penetration depth enables scientists to perform magnetometry at atomic to mesoscopic length-scales in bulk and thin-film materials.

This study focused on the chemical order in a thin film of FePt₃, which features a completely new way of creating functional magnetic interfaces. Using neutron reflectometry and neutron diffraction, we can elucidate important physics of the magnetic interactions in our system. This could potentially have technological applications for the information and communication technology industry.

Thin film and multilayer magnetism

The area of thin magnetic films and multilayers offers a wide range of technological applications. A prime example is the discovery of the giant magnetoresistance (GMR) effect in layered magnetic systems for which P. Gruenberg and A. Fert were awarded the Nobel Prize in 2007. Only discovered in 1986, GMR-based devices are already implemented as read heads in most hard-disc drives of computers. This has resulted in increased data-storage density in these devices.

The magnetic exchange-bias phenomenon is another extremely useful tool in magnetic recording which is being implemented in modern hard-disc drives. Temperature dependent exchange-bias results from pinning a ferromagnetic magnetisation in one layer by direct contact with a second, antiferromagnetic layer [1].

In detail, if we cool a ferromagnetic/antiferromagnetic layered system in a magnetic field, the ferromagnetic orientation will be "glued" to the magnetic-field

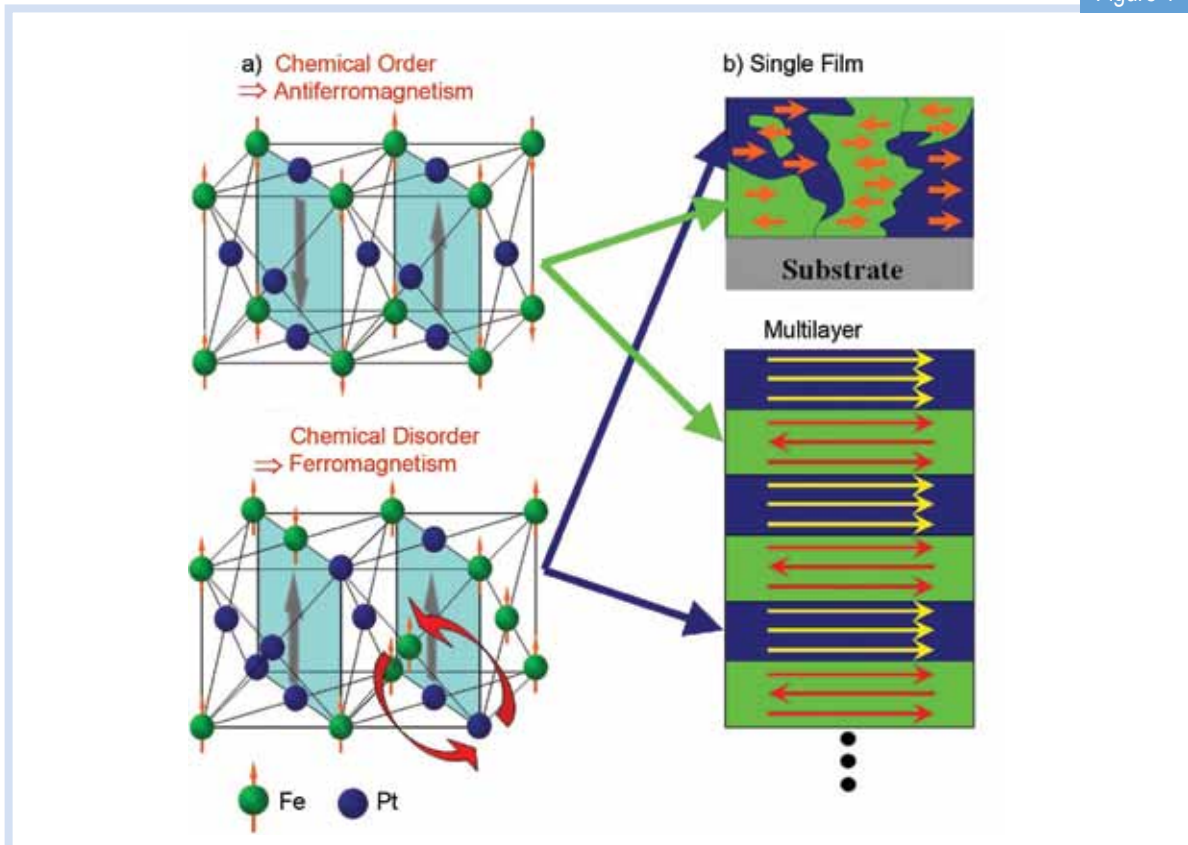
orientation and it will be harder to reverse.

Although this has been known for over 50 years and heavily used in many technological applications, there is still no complete understanding of the effect and therefore preparing and producing exchange-bias devices can have diverse results.

The strength of the effect is directly related to the quality of the contact between the ferromagnet and antiferromagnet. In thin layered films, this contact quality can be described in terms of compatibility of the two materials and quality of the contact area, or "the right glue for the right surface".

Neutrons play an essential role in the search for the "right glue", as they provide information on magnetic structures with high accuracy. The ability to perform direction resolved depth dependent investigations as a function of temperature is unmatched by any complementary magnetometry technique.

Figure 1



Schematic view of chemical order and magnetism in FePt₃.

a) Depending on the growth temperature, either antiferromagnetic or ferromagnetic phases evolve in the system.

b) Top: Intermediate growth temperatures lead to a separation in ferromagnetic and antiferromagnetic domains.

Bottom: The two magnetic phases can be combined in a multilayer, in which each interface between ferromagnetic and antiferromagnetic regions forms an exchange-bias subsystem.

FePt₃: Order makes the difference

We have adopted a new approach to create a magnetically modulated exchange-bias system with perfect structural interfaces in mono-material FePt₃ thin films [2]. The material FePt₃ can exhibit both ferromagnetic and antiferromagnetic properties, only depending on the chemical ordering, i.e. the regular arrangement of the Fe and Pt atoms in the lattice [3].

In perfect order, with Fe only occupying corners of a face-centred cubic lattice (Fig. 1a.), the system develops antiferromagnetism below a temperature called the Néel temperature. If a random distribution of Fe and Pt is present, the system shows ferromagnetic properties (Fig. 1a).

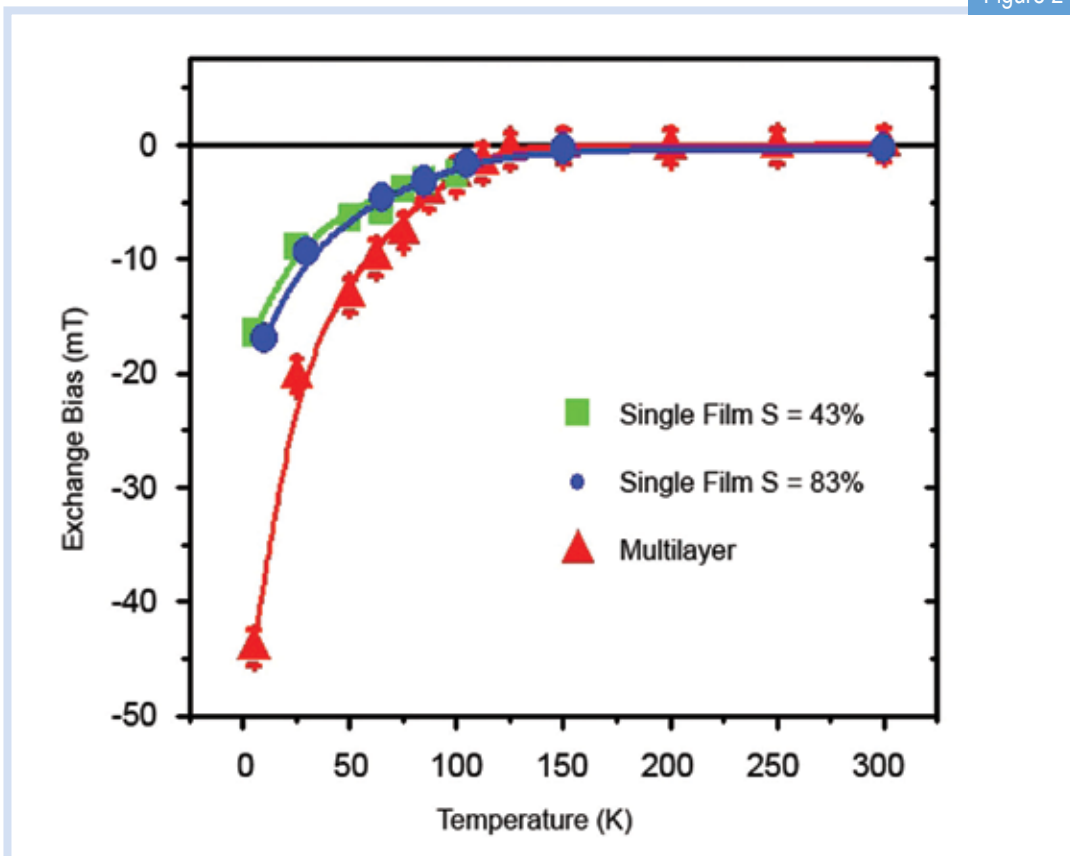
It turned out that this chemical ordering can easily be controlled by the temperature under which the thin film

is grown, below 900 K for disordered FePt₃ and above 900 K for high degrees of order. Therefore we can choose whichever property, ferromagnetic or antiferromagnetic, is preferred and as such we can grow a system representing one material with two different magnetic phases, determined by the degree of ordering.

By modulating the growth temperature successive layers of ordered and disordered FePt₃ in an alternating fashion can be grown with each interface composed of ferromagnetic/antiferromagnetic transition (see Fig. 1b).

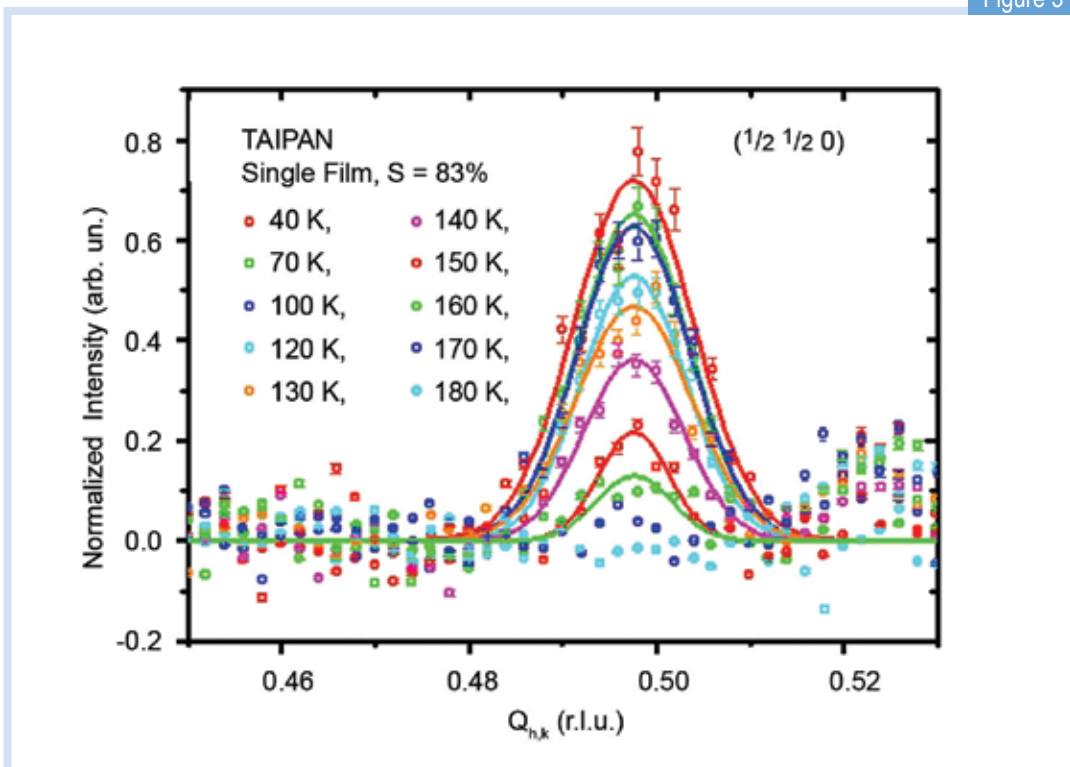
Standard magnetometry experiments prove that our created materials indeed show the desired exchange-bias effect, identifiable by a temperature-dependent horizontal shift of the magnetic hysteresis loop by an amount called the exchange-bias field (Fig. 2).

Figure 2



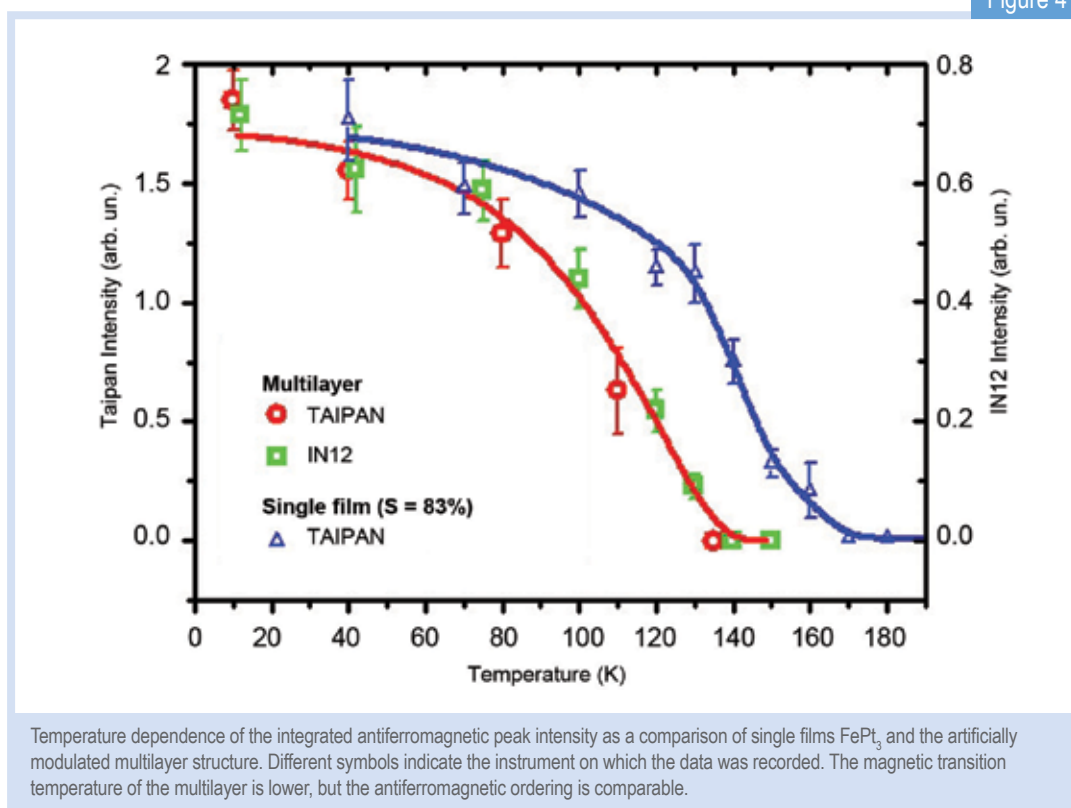
Exchange bias measured as a function of temperature for the thin film and multilayer samples.

Figure 3



High-angle neutron diffraction along the $(\frac{1}{2} \frac{1}{2} 0)$ direction as a function of temperature. The half-order peak is a direct indication of the antiferromagnetism along this direction.

Figure 4



Magnetism and neutron diffraction

In order to distinguish the two magnetic phases and gain insight into the characteristics of our artificial mono-material magnetic multilayer, a combination of neutron techniques is used. No other probe is sensitive to structural and magnetic compositions even far below the surface without damaging the sample.

High-angle neutron diffraction resolves atomic positions and atomic magnetic moments and their respective orientations. Similar to atomic structures in a confined lattice, magnetic moments and their periodicities give rise to observable Bragg diffraction peaks. Antiferromagnetic peaks can easily be identified, as they show a periodicity of twice the structural lattice, which gives rise to a 'half-order' peak.

The crystallographic direction under which this half-order peak occurs represents the ordering direction of the magnetic moments, which can successively

be traced in temperature until close to the magnetic ordering temperature (Fig. 3 and 4). In the case of our artificial FePt₃ magnetic multilayer, we observe a strong, temperature-dependent half-order diffraction peak (see Fig. 3), which identifies the same antiferromagnetic order as drawn schematically in Fig. 1a. The temperature, below which the peak is observed, is characteristic for the antiferromagnetic transition, which in turn defines the temperature of the exchange-bias onset.

In general, the same principle applies for ferromagnetic orientations. However, due to the superposition with intensities from structural diffraction peaks, these can be harder to separate.

Magnetism and neutron reflectometry

The depth-dependent multilayered structure of the samples has been investigated using the polarised neutron reflectometry technique. Neutrons of preferential spin polarisation (“spin up” and “spin down”) are illuminated onto the sample under shallow incident angles and reflected from the surface. After the reflection process, the neutron carries important information of the materials composition, structure and magnetisation. The technique is especially sensitive to interfaces and structures on a nanometre length-scale.

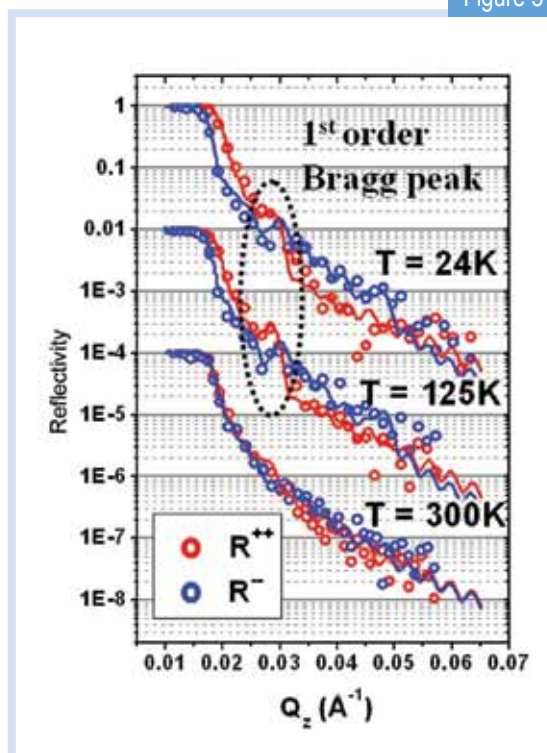
Due to the mono-compositional property of the film, we only expect a contrast from layers of different magnetisations. The difference between two-spin polarisations is directly related to the average magnetic moment, while the first-order Bragg peak indicates the thickness of the ferromagnetic/antiferromagnetic layers and their individual magnetisation (Fig. 5).

By fitting the reflectometry data, a detailed depth-resolved model of the ferromagnetic regions can be obtained. The temperature evolution of this model provides essential information for the interpretation of the observed exchange-bias signal.

In summary, the combination of polarised neutron reflectometry and neutron diffraction allows us to elucidate the important physics of the magnetic interactions in our exchange-bias systems. We succeeded in creating an artificial magnetic modulation without changing material constituents and exchange bias was observed for single and multilayered films.

Furthermore, this example highlights the unique possibility of studying exchange-bias phenomena in systems without structural roughness or incommensurate material. A detailed study of the observed exchange-bias effect in view of existing theories will bring new insights into the physics of exchange bias to extend existing models.

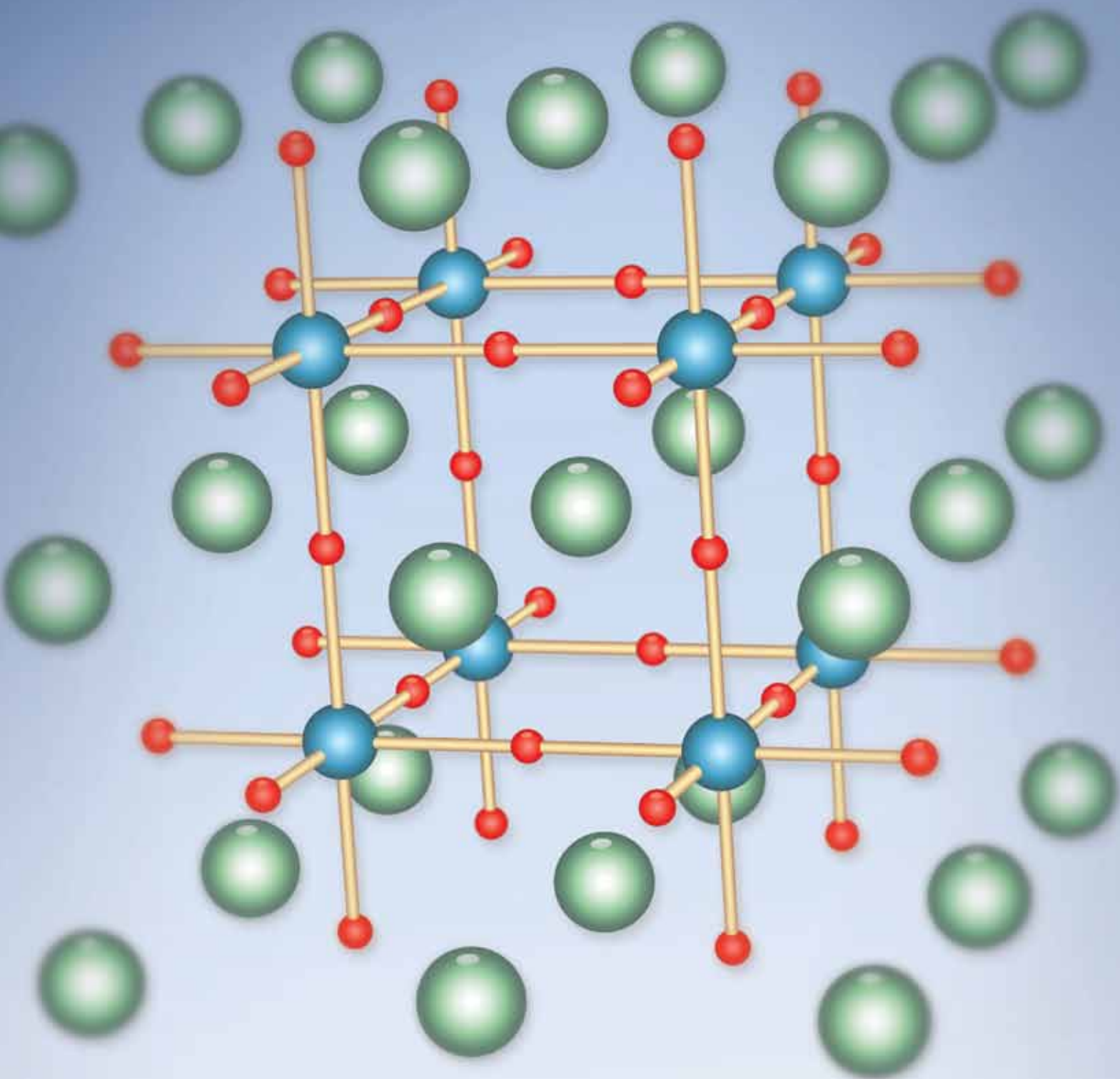
Figure 5



Polarised neutron reflectometry (symbols) and fits (lines) of the FePt₄ multilayer. The splitting between the two channels is proportional to the magnetisation and the first-order Bragg peak indicates the ferromagnetic/antiferromagnetic modulation periodicity.

References

- [1] Stamps, R. L. (2000). Mechanisms for exchange bias. *Journal of Physics D: Applied Physics*, 33(23), R247.
- [2] Saerbeck, T., Klose, F., Lott, D., Mankey, G. J., Lu, Z., LeClair, P. R., et al. (2010). Artificially modulated chemical order in thin films: A different approach to create ferro/antiferromagnetic interfaces. *Physical Review B*, 82(13), 134409.
- [3] Bacon, G. E., & Crangle, J. (1963). Chemical and magnetic order in platinum-rich Pt+Fe alloys. *Proceedings of the Royal Society of London A: Mathematical, Physical & Engineering Sciences*, 272(1350), 272-387.



Structure of strontium titanate.
Oxygen is red, titanium is blue and
strontium is green.

Finding a quantum-forbidden structure

M. Bartkowiak^{1,2}, G. J. Kearley¹, M. Yethiraj¹, and A. M. Mulders²

¹ANSTO, ²School of Physical, Environmental and Mathematical Sciences, UNSW@ADFA

Strontium titanate (SrTiO_3) had been analysed so thoroughly that it appeared it could hold no further secrets. But in 1999, a surprising discovery showed that electric properties of the crystal could be changed simply by increasing the mass of oxygen atoms.

As is usually the case with unexpected phenomena, the explanation lies outside of classical physics and has to be found in the domain of elusive quantum-mechanical effects.

The phenomenon is as puzzling as it is useful: changing the mass of oxygen atoms in the system gives strontium titanate an electronic polarisation and therefore the ability to 'remember' its electrical state, yet all we have changed is the nucleus - nothing to do with the electrons.

Understanding the origins of the process could let us modify compounds used in computing and create new options for information storage.

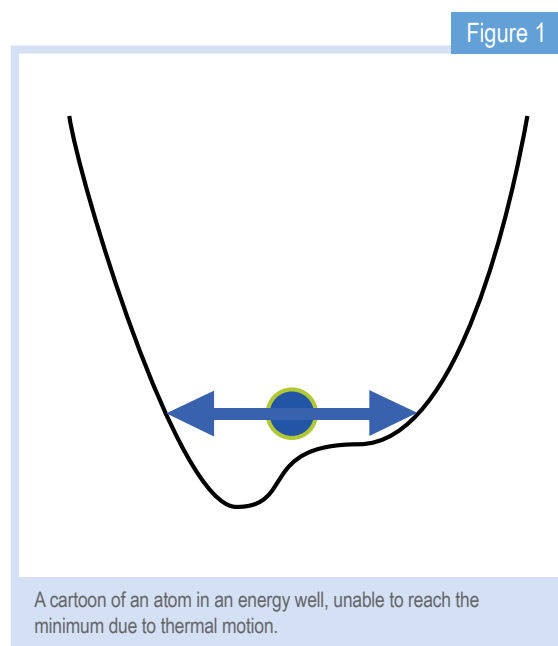
Experiments immediately followed the discovery of electrically polarised strontium titanate and its properties were determined, but produced ambiguous answers to the question of the system's structure.

It appeared that the static structure of the lattice resulted from the dynamic behaviour of the atoms, and more precisely from the quantum motion that is required by the uncertainty principle. Inelastic neutron scattering is the best tool for studying the dynamic behaviour of atoms in a crystal, but only by applying computational techniques together with experimental methods can the crucial link between the static and dynamic properties of the crystalline lattice be unravelled.

By using a heavy isotope of oxygen, the crystal can be tricked into the structure that is quantum-forbidden for the ^{16}O crystal. We elucidate [1] the arrangement of atoms in the quantum-forbidden structure and show that its properties are the same as those observed experimentally in the isotopically tricked crystal.

The root of the problem

The way in which atoms arrange themselves in a crystal depends on the amount of thermal energy. At high temperature the atoms overcome the forces and interactions that distort the internal structure of the crystal at low temperature. At very low temperatures it is the weakest interaction that finally pulls the atoms into their lowest-energy arrangement.



The structural changes that occur as atoms occupy lower energy positions with decreasing temperature are known as phase transitions. Quantum theory tells us that we cannot know both the energy and the position of particles with perfect accuracy; so what happens if there is a lower-energy arrangement of the atoms that cannot be reached due to this enforced uncertainty?

Fig. 1 is a schematic illustration of this situation where the uncertainty of position (effectively a quantum motion) keeps the atom at an average position that is different from the lowest-energy position.

Careful analysis of the low-temperature properties of strontium titanate, SrTiO_3 (STO), implies that this crystal is indeed such a case. This can be visualised as the atoms vibrating with an uncertainty-amplitude that is too big to fit into the energy minimum (similar to the ball in Fig. 1). Some years ago an interesting experimental trick was found [2] to force STO into this lowest-energy structure.

A regular oxygen nucleus contains 16 nucleons (8 protons and 8 neutrons), but isotopes containing 1 or 2 additional neutrons are also stable and exist in nature, although in much lower concentrations. ^{17}O is well known for its magnetic properties that make it useful in magnetic resonance imaging, and ^{18}O is virtually identical to the regular ^{16}O apart from being heavier by the mass of two neutrons.

By substituting this heavier isotope to get $\text{SrTi}^{18}\text{O}_3$ (labelled STO18), the quantum uncertainty in atomic position diminishes slightly and a new low-symmetry phase appears below 23 K. The clearest signature of this new phase is the electric field in the crystal even when there is no external electric field applied to it, this being known as a ferroelectric.

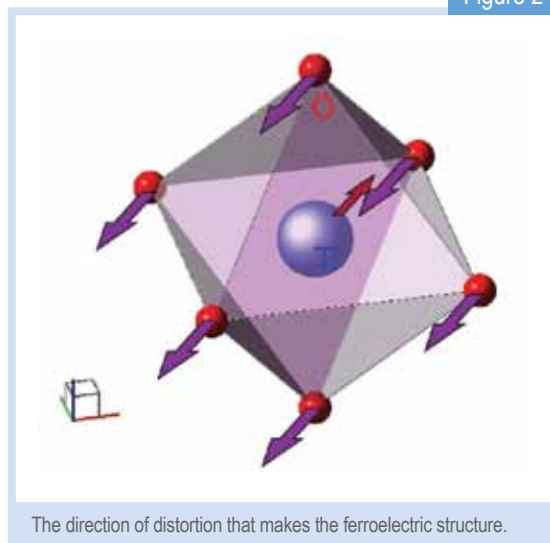
The change in symmetry causes the electrons to interact differently with atomic motion which causes new spectra to be seen that also characterise the phase change. Not surprisingly, the change in positions of the atoms at the phase transition is very slight, and so far it has not been possible to determine these new positions experimentally.

The route to a solution

This is where computers can really help because they can simulate crystals that reach totally artificial situations - such as the absence of quantum uncertainty. For this we need to know how the energy of the crystal changes when we move the atoms around inside it. We used density functional theory (DFT) calculations implemented by Vienna Ab-initio Software Package (VASP [3]).

DFT simulates the state of electrons at absolute zero temperature and can determine ion charges, forces

Figure 2



The direction of distortion that makes the ferroelectric structure.

acting on atoms and the total energy of the system. It can also displace atoms into more favourable positions within a small area around the starting point. Our calculations started from a tetragonal structure of STO observed in a STO16 sample at 1.5 K temperature, later referred to as Structure 1.

Perhaps surprisingly, when we took all of the thermal energy out of the crystal the atoms did not move to new positions, that is, there was no phase transition.

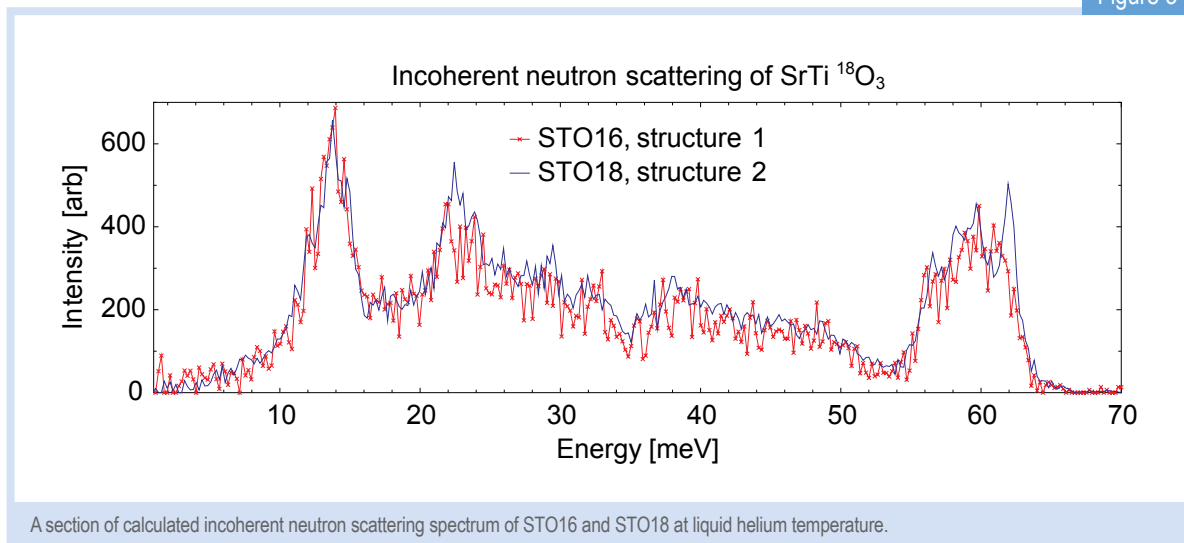
However by calculating the dynamical properties of the atoms within the lattice (PHONON [4]) using force constants (like the ones that describe springs) calculated by DFT we found collective motions of the atoms that led to an even lower-energy arrangement of the atoms, that is a phase transition. The atomic motions we found are illustrated schematically in Fig. 2.

The route to comprehension

We have to analyse the result of the calculations in the context of experimental data. These are only available for the ^{18}O substituted crystal and are limited due to the high cost of this substitution, the low temperatures required and the subtlety of the changes.

However, having obtained a computer-generated crystal structure we can easily computer-generate its properties and compare them with those measured experimentally. If they are the same then it is safe to assume that we have found the quantum-forbidden

Figure 3



structure of the isotopically normal STO which can be used to make other predictions about the properties of the new phase.

Most important: the new structure is orthorhombic and has no centre of symmetry, therefore satisfying the necessary condition for electric polarisation to be present in the system. Calculated lattice vibrations of the new structure show that there is no lower-energy arrangement possible, and the vibrational frequencies of the atoms are in good agreement with the ones observed experimentally for STO18 by other groups [5] via Raman spectroscopy.

Finally, although crystallography could not solve the structure of the new phase, it could propose most likely candidates [6] based on diffraction patterns. Our calculated structure corresponds to one of the most likely candidates.

We have confirmed that the atom positions we determined are valid, but now it is time to see if we are right about atom motion. Analysing the lattice vibrations let us predict the result of incoherent neutron-scattering experiments on STO16 and STO18 and we see that the differences in atom vibrations spectra (shown in Fig. 3) of Structures 1 and 2 should be visible in the experiment results.

In future studies we will use Taipan, ANSTO's triple-axis spectrometer, to measure the incoherent neutron scattering of STO16 and STO18 samples and verify our prediction.

References:

- [1] Bartkowiak, M., Kearley, G. J., Yethiraj, M., & Mulders, A. M. (2011). Symmetry of ferroelectric phase of SrTi18O3 determined by ab initio calculations. *Physical Review B*, 83(6), 064102.
- [2] Itoh, M., Wang, R., Inaguma, Y., Yamaguchi, T., Shan, Y. -J., & Nakamura, T. (1999). Ferroelectricity induced by oxygen isotope exchange in strontium titanate perovskite. *Physical Review Letters*, 82(17), 3540–3543.
- [3] Kresse, G., & Furthmüller, J. (1996). Efficient iterative schemes for ab initio total-energy calculations using a plane-wave basis set. *Physical Review B*, 54(16), 11169–11186.
- [4] Parlinski, K. (2003). PHONON software. Retrieved 4 April 2011, from www.computingformaterials.com/index.html
- [5] Shigenari, T., Abe, K., Takemoto, T., Sanaka, O., Akaike, T., Sakai, Y., et al. (2006). Raman spectra of the ferroelectric phase of SrTi18O3: Symmetry and domains below Tc and the origin of the phase transition. *Physical Review B*, 74(17), 174121.
- [6] Noda, Y., Mochizuki, Y., Kimura, H., Itoh, M., Kyomen, T., & Wang, R. (2005). Possibility of Slater-mode condensation in ferroelectric SrTi18O3. *Journal of the Korean Physical Society*, 46(1), 69-72.



Andrew Nelson pictured with ANSTO's neutron reflectometer, Platypus. Platypus is enabling Andrew and the research team to study ionic liquids at the electrode-liquid interface.

Studying interfaces of ionic liquids to improve industrial electrochemical processes

Andrew Nelson¹, Yansen Lauw^{1,2}, Mike Horne², Theo Rodopoulos²

¹ANSTO, ²CSIRO Process Science and Engineering, Clayton South, Australia

Ionic liquids are simply salts with a melting point below 100°C. Many melt below room temperature, hence their name. Their rather varied physical and chemical properties are interesting because they can be employed in improving various chemical processes, such as the electrodeposition of metals.

Ionic liquids have attracted particular interest because they allow aluminium to be electrodeposited at room temperature. We have used modelling combined with neutron and X-ray reflectometry to examine the structure of ionic liquids at the air-liquid and electrode-liquid interfaces to understand the electrochemical processes.

Ionic liquids

Most ionic salts have very high melting points as a consequence of strong ionic bonding between the small cation and anion (for example NaCl has a melting point of 801°C). However, if the ionic bonds are weaker it is possible for the ionic salt to be molten at much lower temperatures (<100° Celsius), such salts are referred to as ionic liquids. They are typically composed of a large asymmetric organic cation and a smaller organic or inorganic anion.

Ionic liquids have many important physical and chemical properties that are extremely attractive to industries. These properties include low vapour pressure, high viscosity, high temperature and electrochemical stability and a wide electrochemical window. It is this last property that has spurred a collaborative research project between ANSTO and CSIRO Minerals over the past four years.

The reason is that current production of aluminium requires a huge amount of energy because alumina has to be dissolved in molten cryolite at ~960° Celsius before electrodeposition can occur.

This expensive process is required because aluminium cannot be electrodeposited from water because its reduction potential is outside the electrochemical window of water.

However, electrodeposition should be possible from some ionic liquids as their electrochemical windows encompass the reduction potential of aluminium, giving the tantalizing vision of large scale aluminium production at room temperature (no massive heating bills).

One candidate for this process is 1-butyl-1-methylpyrrolidinium bis(trifluoromethylsulfonyl)imide (P14Tf2N). In our project, we performed a fundamental examination of the interfacial structure of this liquid at the air-liquid and electrode-liquid surfaces.

Indeed, the behaviour of ions at charged interfaces is already well known for aqueous electrolytes, with theory from Helmholtz and Gouy and Chapman (in the early 20th century), but much less so for ionic liquids. The behaviour of this structure plays an essential role in all interfacial electrochemical processes.

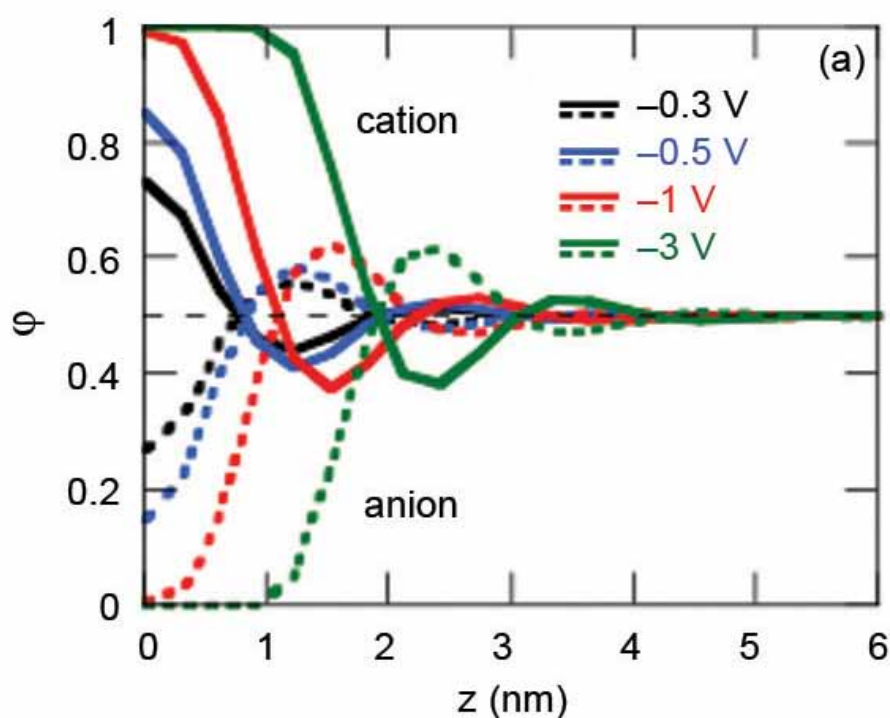


Figure 1

Profile of the volume fraction of cation and anion at the interface with different surface potential values. Taken from [1].

Modelling approaches

The first approach used theoretical modelling techniques to predict the equilibrium structure of ionic liquids at a charged electrode surface (also termed the electrical double-layer) and the correlation between the electrical double-layer and its electrochemical capacitance [1].

The capacitance of the electrical double-layer is an indication of how the electrostatic potential of the electrode surface is screened by the ions that accumulate there. The modelling was able to predict the volume fraction profiles of the cation and anion, revealing an oscillatory nature that depends on the surface potential of the electrode surface, Fig. 1.

Quite simply, as electrode potential increases there is a greater excess of counter ion in the layer adjacent to the electrode and the ordering increases.

Subsequent modelling investigated the effect of size asymmetry on the electrical double-layer structure, revealing that the ordering becomes damped when size asymmetry between the cations and anions is larger [2].

Experimental Approaches

To complement the information obtained from the theoretical approaches we used neutron and X-ray reflectometry at ANSTO.

These techniques are ideal for studying chemical composition gradients across interfaces, especially when the interface of interest is buried – such as the electrode-ionic liquid interface. The initial X-ray reflectometry work found [3] that cations preferentially adsorb at the air-liquid boundary.

When water impurities were doped into the ionic liquid they also (ionic liquids are very hygroscopic) adsorbed at the air-liquid boundary, but had a non-monotonic effect on the overall thickness of the surface layer.

The trend in surface thickness was able to explain the trend in surface tension of ionic liquid-water mixtures reported in the literature. Understanding where water impurities concentrate is important as they greatly affect the electrochemical behaviour of ionic liquids at solid electrodes.

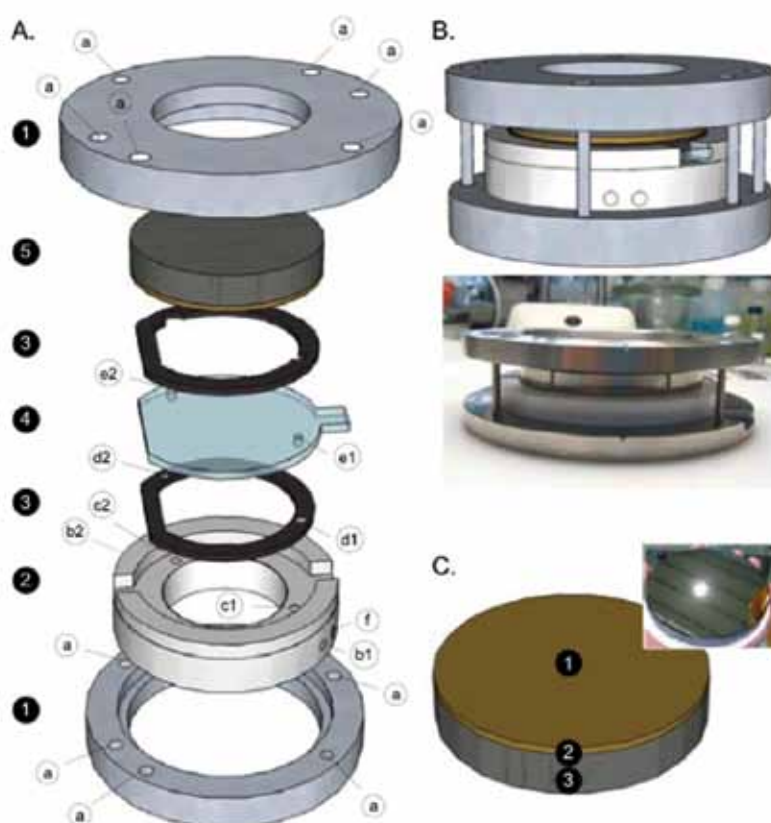


Figure 2

The *in situ* electrochemical cell used for the investigation of the electrical double-layer structure at different electrode potentials. The silicon wafer is 100 mm in diameter.

In order to study the ionic liquids at the electrode-liquid interface we performed several neutron reflectometry experiments on Platypus, ANSTO's neutron reflectometer. By constructing a unique electrochemical cell [4], Fig. 2, we were able to characterise the electrical double-layer at different surface potentials.

This data is still in the process of being analysed, but early results give the unusual conclusion that cations preferentially adsorb even at positive surface potentials.

References:

- [1] Lauw, Y., Horne, M. D., Rodopoulos, T., & Leermakers, F. A. M. (2009). Room-temperature ionic liquids: excluded volume and ion polarizability effects in the electrical double-layer structure and capacitance. *Physical Review Letters*, 103(11), 117801-117804.
- [2] Lauw, Y., Horne, M. D., Rodopoulos, T., Nelson, A., & Leermakers, F. A. M. (2010). Electrical double-layer capacitance in room temperature ionic liquids: ion-size and specific adsorption effects. *Journal of Physical Chemistry B*, 114(34), 11149-11154).
- [3] Lauw, Y., Horne, M. D., Rodopoulos, T., Webster, N. A. S., Minofar, B., & Nelson, A. (2009). X-Ray reflectometry studies on the effect of water on the surface structure of [C4mpyr][NTf2] ionic liquid. *Physical Chemistry Chemical Physics*, 11(48), 11507-11514.
- [4] Lauw, Y., Rodopoulos, T., Gross, M., Nelson, A., Gardner, R., & Horne, M. D. (2010). Electrochemical cell for neutron reflectometry studies of the structure of ionic liquids at electrified interface. *Review of Scientific Instruments*, 81(7), 074101.



Alison Edwards with Koala, a Laue diffractometer, in ANSTO's Neutron Beam Guide Hall.

Towards a clear understanding of catalytic processes

Alison J. Edwards¹, Michael G. Gardiner²

¹ANSTO, ²School of Chemistry, University of Tasmania

Materials which are required to allow a chemical reaction to proceed at a useful rate, but are left unchanged by the overall chemical reaction, are called catalysts. The use of catalysts to facilitate the reactivity of processes which are otherwise energetically unfavourable is a major area of chemistry research.

Catalysis finds applications in both the industrial setting, and in widely distributed consumer devices. For example, considerable effort is directed at finding a catalyst which would facilitate the oxidation of highly abundant gaseous methane into the more easily handled and transported liquid methanol. Catalytic converters which facilitate pollutant reduction are now present in most cars, and the search for a catalyst that can safely be used to generate hydrogen and oxygen from water for combustion in consumer fuel cell devices is the current holy grail of chemical catalysis.

Catalysis

The systematic pursuit of chemical compounds that can facilitate the lowering of the energetic pathway of particular chemical reactions relies on an ability to fully characterise the compounds targeted either as potential catalysts or as suitable model systems from which the operation of catalytic systems may be better understood.

In this regard it is imperative that the structure of the compounds be fully understood in terms of their atomic composition, connectivity and bonding.

Why use neutrons for finding hydrogen?

Since the work of Bragg gave rise to the means for determining the structure of complex crystalline materials at the atomic level, the application of crystallographic methods to characterise potential catalysts has become an integral part of catalysis studies.

X-ray diffraction studies find large-scale application to this problem, but are inherently less sensitive to the positions of hydrogen atoms than the heavier elements. This is due to the physical process in which the X-rays are scattered by the electrons of the crystal.

Hydrogen atoms present in a compound may have no electrons at all, when in the formal +1

oxidation state. Electrons which are formally considered to “belong” to the hydrogen – one if neutral and two if carrying a negative charge – although present near the atomic nucleus, will typically be distorted away from the hydrogen atom's nuclear position by chemical bond formation leading to a comparable distortion of any model built from X-ray diffraction data.

Neutron diffraction, by contrast, is effected by the interaction of the neutron beam with the nuclear density of a crystal (not the electron density). The interaction of neutrons with the H nucleus is especially strong, and the position of hydrogen nuclei is thereby well determined.

Structure of the catalyst under investigation

Materials of potential catalytic relevance are the subject of ongoing investigations by Michael Gardiner at the University of Tasmania. His work aims to improve the fundamental understanding of the way catalysts work especially at the level of how the electrons are distributed about the true atomic positions, how they form bonds to reactant molecules in the catalytic process and how this can give a catalytic effect.

Whilst the presence of an hydridic (H^-) hydrogen was suspected in the novel binuclear palladium molecular cation shown in Fig. 1 [1], neither the

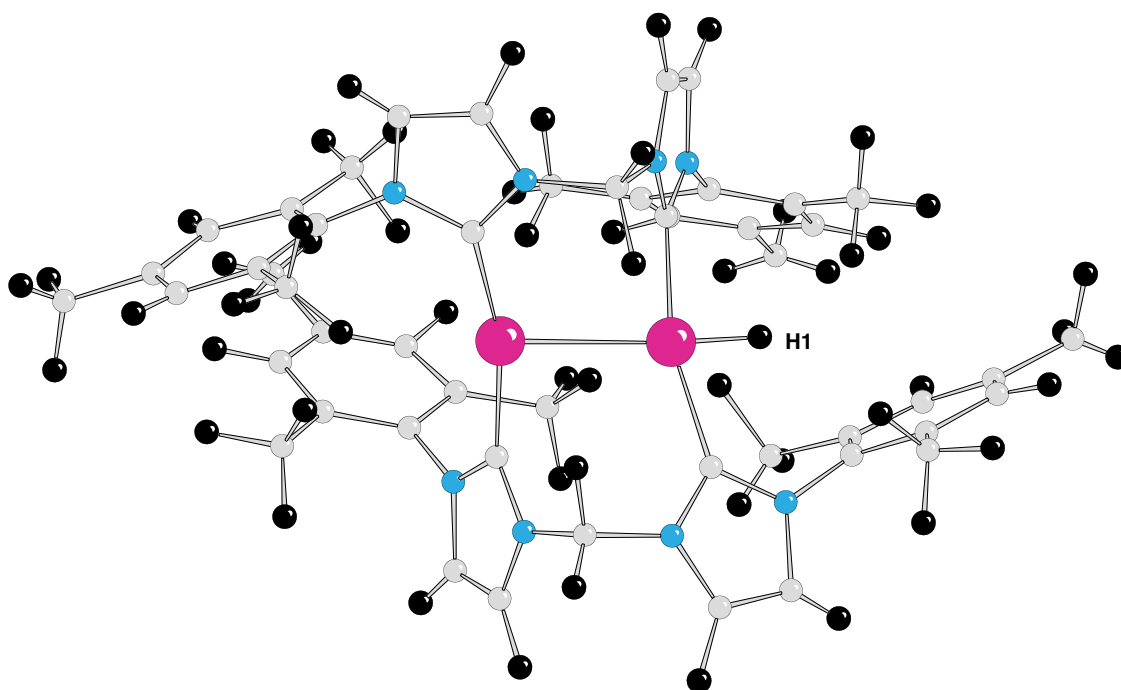


Figure 1

A novel dipalladium molecular cation of potential catalytic relevance [Formula: $C_{50}H_{57}N_8Pd_2PF_6 \cdot 4(C_4H_8O)$ (Cation : Anion : Solvent = 1 : 1 : 4)]. All hydrogen atoms (black) are observed. The hydridic hydrogen H1 is bonded to one of the two palladium atoms (pink); carbon atoms are shown in grey and nitrogen in blue. The molecule as depicted is monocationic - i.e. carries a charge of +1 and crystallises with a PF_6^- anion as a tetrahydrofuran solvate.

spectroscopic observations nor the theoretical modelling provided sufficient evidence for the development of a complete and accurate structural model of the material incorporating this species.

Neutron-diffraction studies using ANSTO's Laue Diffractometer, Koala have proved that a hydride (H1) is indeed present in crystals of the material and further, that it is located in a terminal position at one end of a palladium-palladium bond (see Fig. 1) rather than in a bridging configuration as suggested by an earlier computer modelling study.

This means that in the crystal the two ends of the molecule are clearly different from each other and have two different metal atom sites with which reactants could interact, rather than having a pair of chemically equivalent metal atoms.

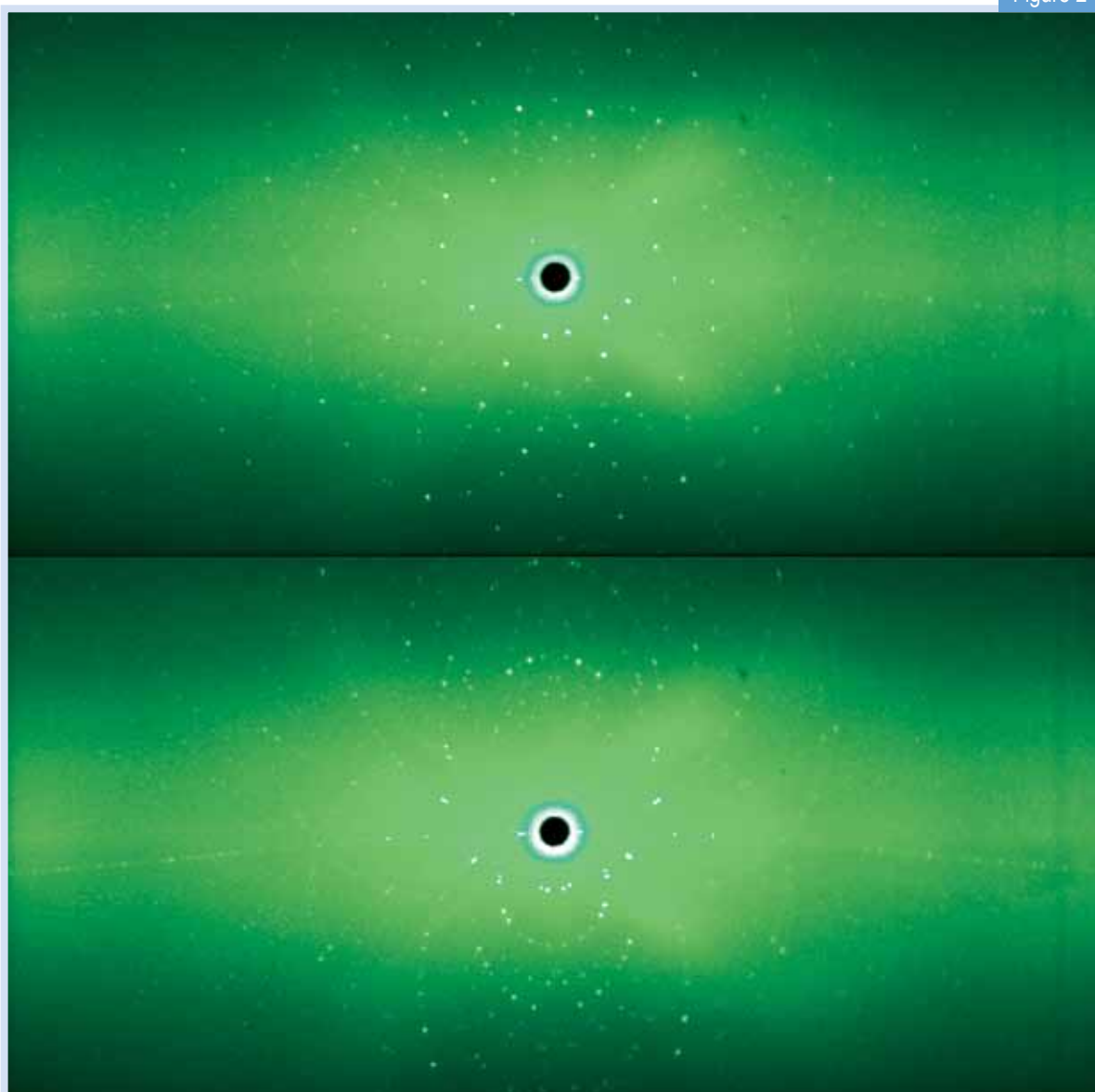
The diffraction patterns we obtain from our single-crystal neutron-diffraction experiments on Koala are shown in Fig. 2: at 150 K (at top) from which this structure has been determined and at bottom,

the analogous experiment at 100 K yields a clearly related pattern in which most of the spots on the upper image are split into two nearly equal components. Cycling between the two temperatures switches reversibly between the two distinct patterns. The characterisation of this fully reversible phase change demonstrated in Fig. 2 for this material will be the subject of further neutron-diffraction studies and neutron spectroscopy.

References

- [1] Boyd, P. D. W., Edwards, A. J., Gardiner, M. G., Ho, C. C., Lemée-Cailleau, M-H., McGuinness, D. S., et al. (2010). Reduction of a chelating bis(NHC) palladium(II) complex to $[\mu\text{-bis(NHC)}_2\text{Pd}_2\text{H}]^+$: a terminal hydride in a binuclear palladium(I) species formed under catalytically relevant conditions. *Angewandte Chemie International Edition*, 49(36), 6315-6318).

Figure 2



Neutron diffraction patterns for a crystal of the dipalladium cation as a PF_6 salt at 150 K (top) and 100 K (bottom). The crystal orientation is unchanged and a phase change, which may shed further light on potential catalytic behaviour, is evident by the change of the diffraction pattern.



Environment

Environment

Understanding and improving the health of our planet's fragile environment is one of the most important research areas of our time.

ANSTO's studies look at many aspects of our environmental systems, from the impact of drought and human activities on the health of our wetlands and river systems to the potential of certain plants to extract metal from contaminated soils and to the impact the East Antarctic Ice Sheet has and will continue to have on global sea-levels.

ANSTO scientists are collaborating with top researchers in this field from across the globe to help understand and provide solutions to these and many other of the environmental problems we face.



ANSTO's isotopic tracers are being used to establish baseline signatures of Australian river systems.

Monitoring evaporation and groundwater inputs to the Darling River during drought

Cath Hughes¹, Karina Meredith¹, Dioni Cendón¹, Suzanne Hollins¹, Tim Morrison²

¹ANSTO, ²University of Technology, Sydney

The Darling River faces environmental pressures from both direct human influence and also climate change. Irrigation demands have dramatically altered the riverine ecosystem over the last century, but during drought it is evaporation and saline groundwater input that impacts the water quality of the river through the formation of algal blooms, salinisation and acidification.

Dryland rivers are particularly challenging to monitor because they experience variable rainfall, low flow and evaporation. This is why more sophisticated tools such as isotopic tracers are being used to establish baseline signatures of these river systems.

Since mid-2002 we have monitored the changes along the Darling River using stable isotopes and subsequently have modelled evaporative losses and saline groundwater input to the river during the long drought of the last decade. Research such as this is being used to help inform decision makers in charge of managing the river system.

Why do we study the Darling River?

The Darling River is Australia's longest river (Fig. 1), draining over 8% of the Australian continent, but finally discharging less than 1% of the precipitation that falls in its catchment, into the receiving waters of the Murray River.

This river forms one of the only freshwater supplies in western New South Wales and suffers environmental pressures from over-abstraction, unpredictable flow regimes, evaporative losses, drought and saline groundwater exchange. The highly regulated nature of this system means that dams divert the vast majority of potential inflows to irrigation, preventing them from flowing into the Murray River.

During drought the main channel of the Darling River often dries up between Bourke and Menindee (Fig. 1), resulting in water quality decline and ecological damage. In this dryland system, evaporative losses and groundwater inputs are very important but difficult to quantify.

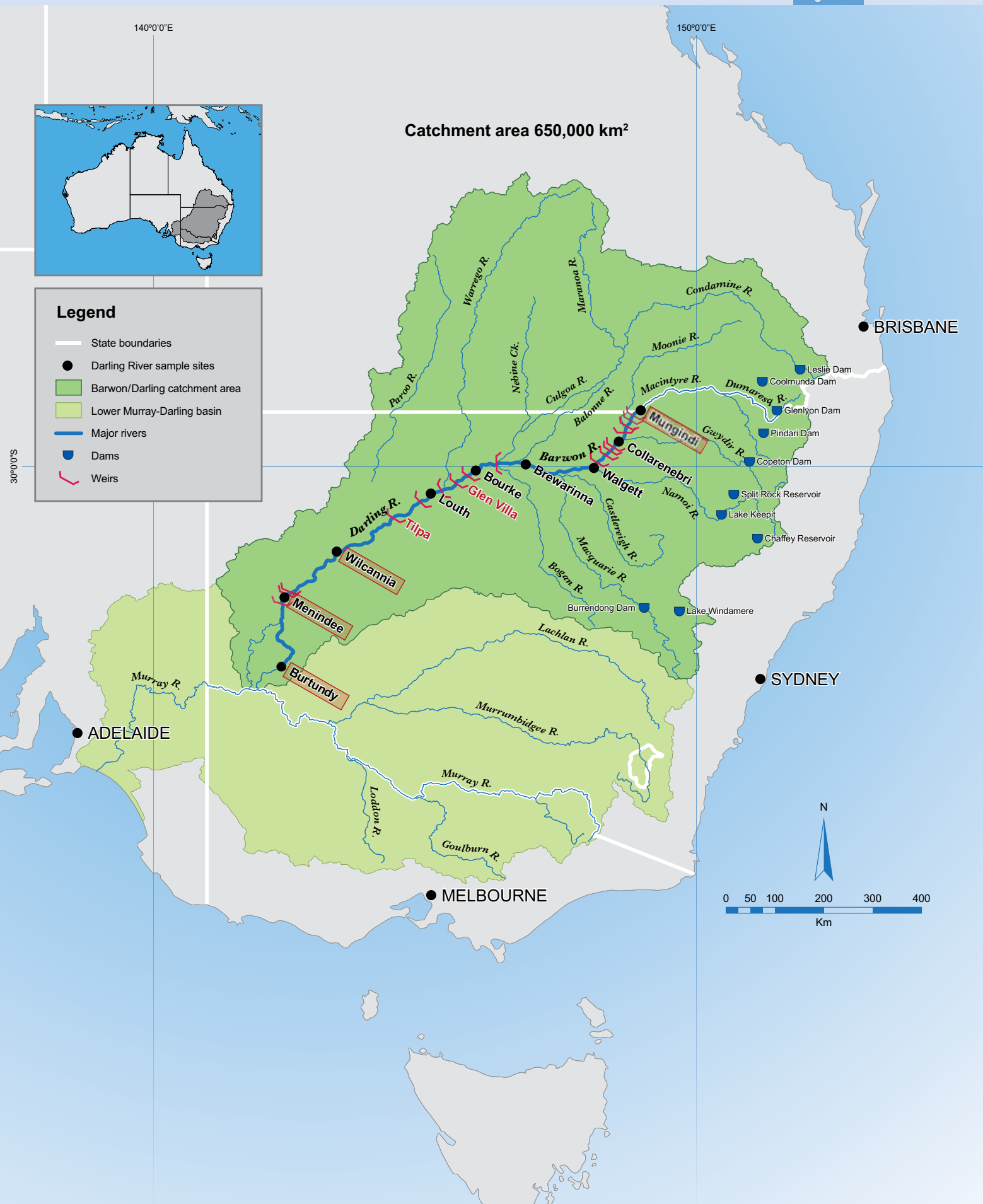
How stable isotopes trace water

The stable isotopes of water are very useful tracers to help understand the processes in this catchment. Variations in the number of neutrons in both the H and O atoms in water mean that some water molecules (e.g. $^2\text{H}_2^{16}\text{O}$) are heavier than others (e.g. $^1\text{H}_2^{16}\text{O}$).

Consequently, the mass imbalance between these water molecules means they behave differently during phase changes in the water cycle, i.e. there is isotopic fractionation. In different parts of the water cycle, water thus becomes naturally tagged with isotopic "signatures", which vary according to the history of a particular body of water and its pathway through the water cycle.

The stable isotope concentrations are measured as the difference between the ratio of the heavier to lighter isotopes (i.e. $\text{H}^2:\text{H}^1$ and $\text{O}^{18}:\text{O}^{16}$) in a water sample and an international reference water, known as δ notation [1]. As changes in the isotope concentrations are very small, for convenience the δ -values ($\delta^2\text{H}$ and $\delta^{18}\text{O}$) are expressed in parts per thousand (‰).

Figure 1



In general, isotopic fractionation during precipitation results in a linear relationship between hydrogen and oxygen isotope concentrations in natural waters, also known as a meteoric water line [1].

Variability in precipitation isotope composition is related mainly to the sources of water vapour and evolution of air masses that lead to rainfall as well as temperature and elevation.

Studying evaporation from the Darling River using $\delta^2\text{H}$ and $\delta^{18}\text{O}$

Isotopic fractionation during evaporation increases the proportion of heavy isotope species in surface waters producing enrichment along so-called “evaporation lines” of slopes less than the meteoric water line.

The measured stable isotope composition of river water samples reflects the average of the rainfall events that resulted in the flow. This composition is then modified by the enrichment of heavy isotopes ($\delta^2\text{H}$ and $\delta^{18}\text{O}$) during evaporation and the inflow of groundwater with a more depleted signature.

This evaporative enrichment is clearly seen along the Darling River (Fig. 2) during the drought from 2002-2005 with river waters only intersecting the Global Meteoric Water Line briefly following a new inflow (Fig. 2B and C), then enriching rapidly along an evaporation line.

The isotopic enrichment can be modelled using local climate data [3] to determine the proportion of water remaining as indicated in Fig. 2A, which shows the most evaporated waters represent only 20% of their original volume.

Isotopic modelling of the river from June 2002 to December 2003 [2] found that only 0.1 to 1% of precipitation in the catchment reached the river. Evaporative losses exceeded inflow in many reaches prior to a flow event in March 2003.

During these low flow periods the Darling River is particularly susceptible to contamination from agricultural and urban inputs and increasing salinity from groundwater exchange. Algal blooms and high salinity levels can result in large numbers of fish dying and prevent human and stock use of the precious remaining water.

Identifying saline groundwater input to the Darling River

Stable isotopes and chloride (salt) or electrical conductivity (EC) data can also be used to determine the input of saline groundwater into the river. In order to find zones of groundwater inflow to the river, higher density sampling was undertaken in May 2007 along the Bourke to Louth reach of the Darling River (Fig. 3).

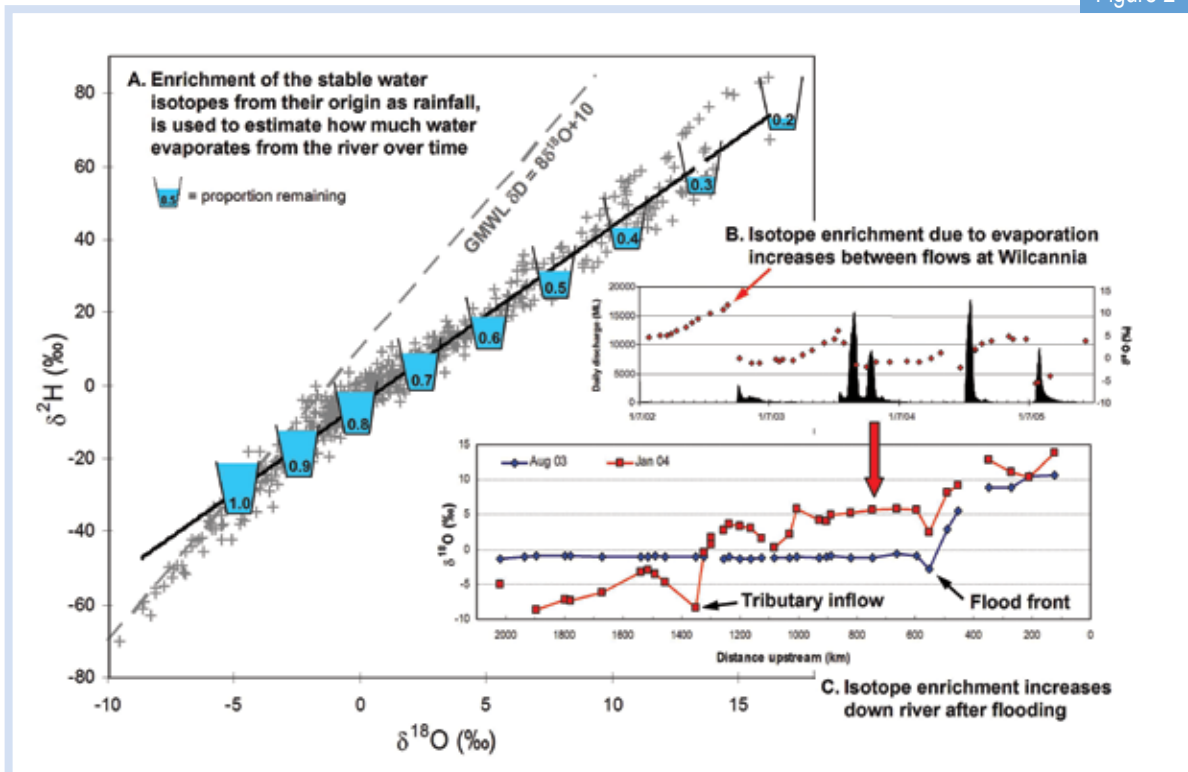
During this period $\sim 2400 \text{ m}^3 \text{ day}^{-1}$ flowed past Bourke, but zero flow arrived at Louth. Results showed that chloride and stable isotope concentrations varied significantly over relatively short distances.

At location DR07 (above Glen Villa Weir 19A), the chloride concentration was very low, while $\delta^{18}\text{O}$ values were enriched relative to other river samples indicating evaporative losses but little groundwater input. River waters approximately 100 m downstream of the weir at DR08 contained elevated chloride concentrations and $\delta^{18}\text{O}$ values were depleted.



(Left, p. 32) The Darling River catchment showing the major stable isotope sampling sites. The photos above from left to right show the Darling River in the late 19th century, Weir 19A at Glen Villa and the dry river bed at Tilpa in May 2007.

Figure 2



A. Stable isotope data for the Barwon-Darling River system showing evaporative enrichment relative to the Global Meteoric Water Line (GMWL, [1]). The proportion of water remaining is shown with the most enriched or evaporated waters found in the Menindee Lakes system.

B. Time series showing evaporative enrichment or increase in the $\delta^{18}\text{O}$ (red dots) between small flow events (black peaks) during a drought period at Wilcannia.

C. Two snapshots of the stable-isotope composition of the river from Mungindi on the Queensland border to Burtundy upstream of the Murray R. These show the effect of a flow or flood on resetting the isotope values (Aug '03), then the gradual increase in enrichment as the water moves downstream in Jan '04 (left to right). The red arrow indicates the position of Wilcannia.

The combination of the salt and isotope tracers allows us to prove that groundwater inflow rather than evaporation of stagnant water has caused the saline spike in the river. A mixing model of surface and groundwaters [4] estimated that between 60 and 99 percent of water in the river at Glen Villa came from groundwater during this period.

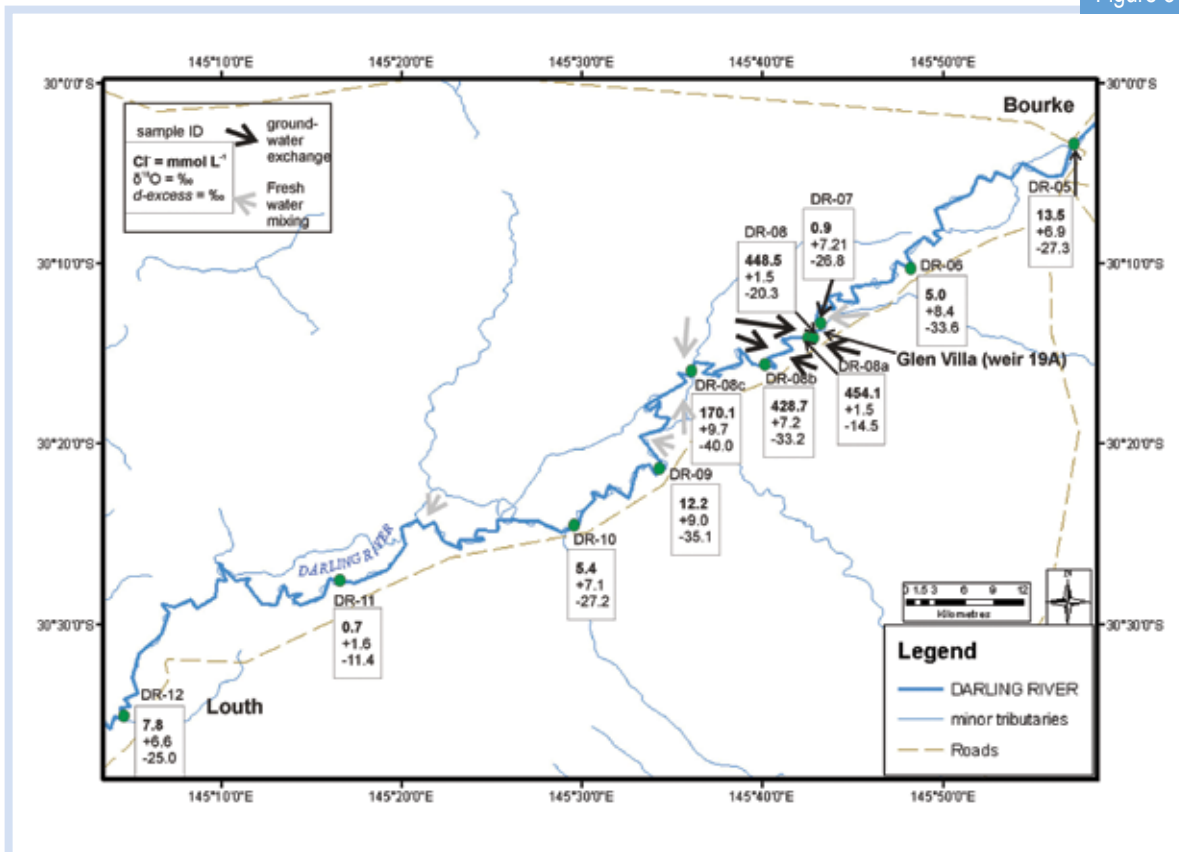
This analysis repeated along the river enables us to detect both saline and freshwater inflows to the river (Fig. 3). The flux of saline groundwaters into the river during zero or low-flow periods, such as occurred in mid-2002 to mid-2003 and 2006 to 2007 create ideal environmental conditions for cyanobacteria blooms to develop and cause fish kills, as seen in May 2007.

To look at the impact of this groundwater input over a larger scale for a longer period of less-extreme drought, a model of river flow (MIKE-11) was combined with an

EC mixing model and run from May 2003 to Sept. 2005. This model found that the saline groundwater input represented less than 0.01% of the total flow volume and provided only 12% of the total salt load during that period. So whilst the saline groundwater discharge has an extreme localised impact when the river flow is zero, it is a less significant source of salinity downstream when the river is flowing.

A combined hydrodynamic and mixing model (R-WSIBal) which incorporates both stable water isotopes and EC is under development with promising initial results. Recent flooding along the Darling River now gives us the opportunity to study the system under a different hydrological regime.

Figure 3



Location of the surface water sample points with Cl⁻ (mmol L⁻¹), δ¹⁸O (‰) and the deuterium excess (d) values for May 2007 from Bourke to Louth. Arrows indicate possible water influx locations along the reach.

Acknowledgements

We would like to acknowledge the support of the New South Wales Office of Water for ongoing access to samples and data. We also thank Tony Barr and Jeff Turner from CSIRO and John Gibson from the University of Victoria in Canada and many ANSTO colleagues for their collaboration.

References

- [1] Craig, H. (1961). Isotopic variations in meteoric waters. *Science*, 133(3465), 1702-1703.
- [2] Gibson, J. J., Sadek, M. A., Stone, D. J. M., Hughes, C. E., Hankin, S., Cendón, D. I., et al. (2008). Evaporative isotope enrichment as a constraint on reach water balance along a dryland river. *Isotopes in Environmental and Health Studies*, 44(1), 83-98.
- [3] Gonfiantini, R. (1986). Environmental isotopes in lake studies. In P. Fritz & J. Ch. Fontes (Eds.), *Handbook of Environmental Isotope Geochemistry* (volume 3, pp. 113-168). New York, United States of America: Elsevier.
- [4] Meredith, K. T., Hollins, S. E., Hughes, C. E., Cendón, D. I., Hankin, S., & Stone, D. J. M. (2009). Temporal variation in stable isotopes (¹⁸O and ²H) and major ion concentrations within the Darling River between Bourke and Wilcannia due to variable flows, saline groundwater influx and evaporation. *Journal of Hydrology*, 378(3-4), 313-324.



View of the Prince Charles Mountain flanking the Lambert Glacier near Loewe Massif.

Using cosmic rays and radionuclides to measure the contribution of the East Antarctic Ice Sheet to changes in global sea-level

David Fink¹, Charles Mifsud¹, Duanne White², Kat Lilly³, Andrew Makintosh⁴, Derek Fabel⁵

¹ANSTO, ²Macquarie University, ³University of Otago (NZ), ⁴Victoria University (NZ),

⁵University of Glasgow (UK)

Current global climate models do not fully incorporate the contribution of Antarctic Ice Sheets to changes in sea level despite dramatic changes in the past. Projected sea-level rise by the end of the 21st century ranges from 20 to 60 centimetres, mainly attributed to the Antarctic Peninsula, Greenland and ocean thermal expansion.

However during the last ice age, about 20,000-25,000 years ago, the sea-level was 120 metres lower and Antarctic ice volume three times larger than today. Hence, documenting the size and retreat rate of the East Antarctic Ice Sheet since the last ice age (called the Last Glacial Maximum) will allow a better understanding of ice-sheet dynamics, improve sensitivity to increasing warming and validate predictions of future sea-level change.

Using the new innovative technique of *in situ* cosmogenic radionuclide surface exposure dating, we can for the first time provide quantitative geochronological constraints on the variability and sensitivity of East Antarctic ice volume, suggesting that parts of the Ice Sheet respond more rapidly to global climate change than previously assumed, and that East Antarctica was not responsible for a controversial dramatic pulse in sea-level rise of 20 metres 14,500 years ago.

Tackling ice-volume changes of the East Antarctic Ice Sheet

The East Antarctic Ice Sheet (EAIS) holds enough ice to raise global sea level by ~60 metres, but because surface temperatures are well below freezing point, this ice is relatively stable, and thus unlikely to contribute significantly to sea level rise during the next few centuries.

Most of the contribution to sea level from melted ice occurs along the coastal perimeter of East Antarctica where the slow moving ice-sheet calves directly into the ocean and via large outlet glaciers which stream through deep and extensive basins that act like drainage channels. Little is known on the magnitude and rates of change of these two mechanisms.

As glaciers advance down a valley scouring and cutting bedrock they accumulate and transport debris, ranging in size from small cobbles to large boulders. Moraines are piles of accumulated boulders which

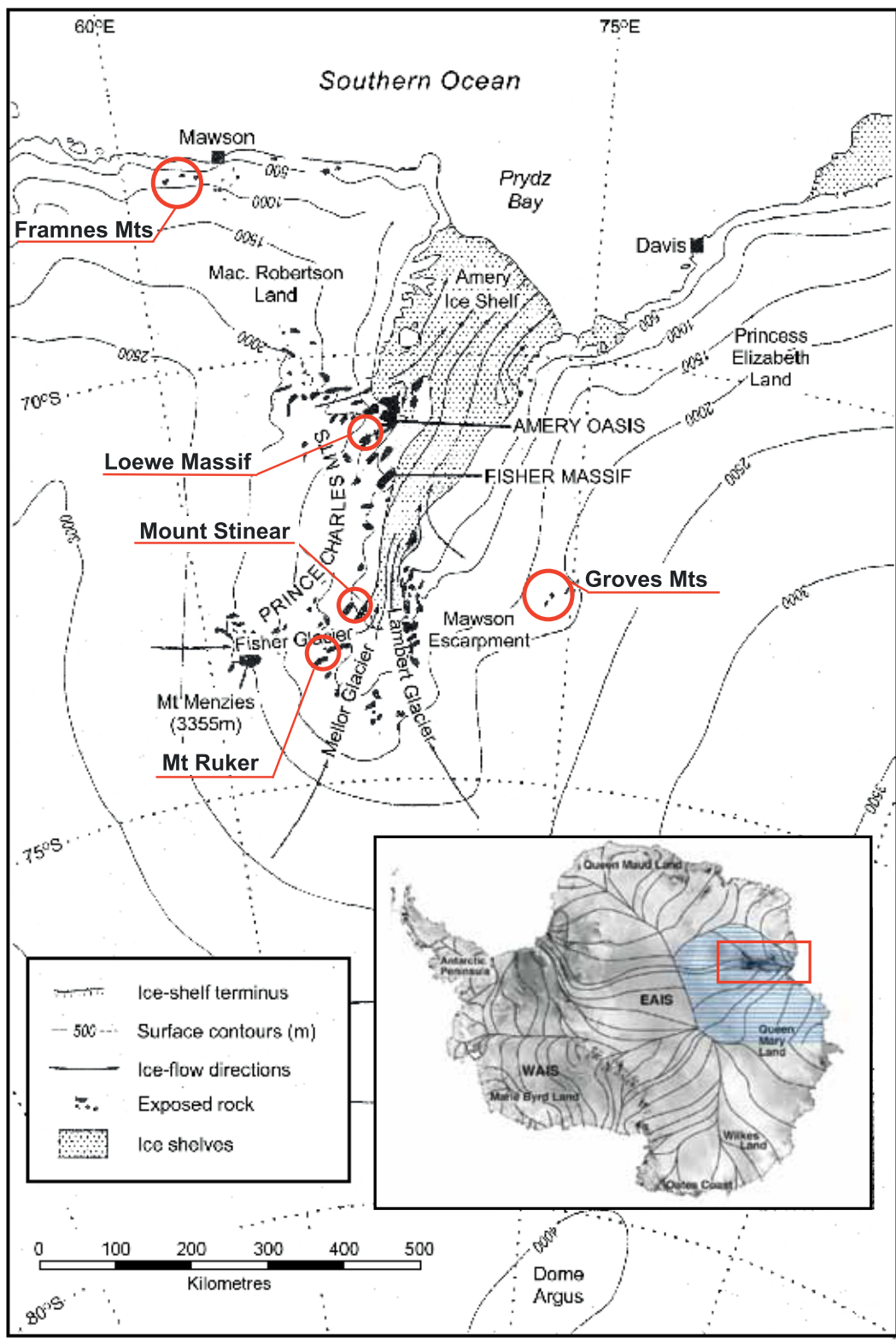
are deposited at the perimeter of a glacier when the advance ceases and it begins to retreat up a valley.

Hence, moraines represent past ice limits and changes in climatic conditions. The boulders of such moraines deposited over the flanks of mountain ranges, which constrain the passage of outlet glaciers of the Antarctica ice sheet, form the basis of our study.

We used the mountain ranges that protrude above the ice sheet as 'dipsticks' to measure past ice-sheet elevation. By correlating exposure ages (i.e. boulder deposition age) of glacially transported boulders on a moraine with altitude, we can map the evolution of the ice sheet and quantify ice-volume changes as a function of time.

New cosmogenic exposure ages and field-based studies indicate that since the Last Glacial Maximum, increased atmospheric temperatures and coastal instability due to sea level increase causes ice-streaming sections of the EAIS to respond more rapidly to global climate change than previously assumed.

Figure 1



Map of the 5 locations (red underline) in the Prince Charles-Lambert-Amery region where transported boulders and exposed bedrock were sampled for radionuclide analyses at the ANTARES AMS facility at ANSTO. The stippled area is floating Amery Ice Shelf; continuous numbered lines represent contours of altitude above sea level of today's ice sheet surface. Inset shows full Antarctic continent with darker blue shaded region indicating the area of the ice sheet which drains through the Prince Charles-Lambert basin shown within the red rectangle.

Figure 2



How do we measure cosmogenic exposure ages?

The radionuclides ^{10}Be ($T_{1/2}=1.38$ million years) and ^{26}Al (0.70 million years) are produced in exposed surface rocks and within a metre or so of the Earth's crust by the secondary cosmic ray flux (fast neutrons) which penetrate Earth's atmosphere. Despite ultra-low *in situ* production rates only five atoms of ^{10}Be are produced each year per gram of rock.

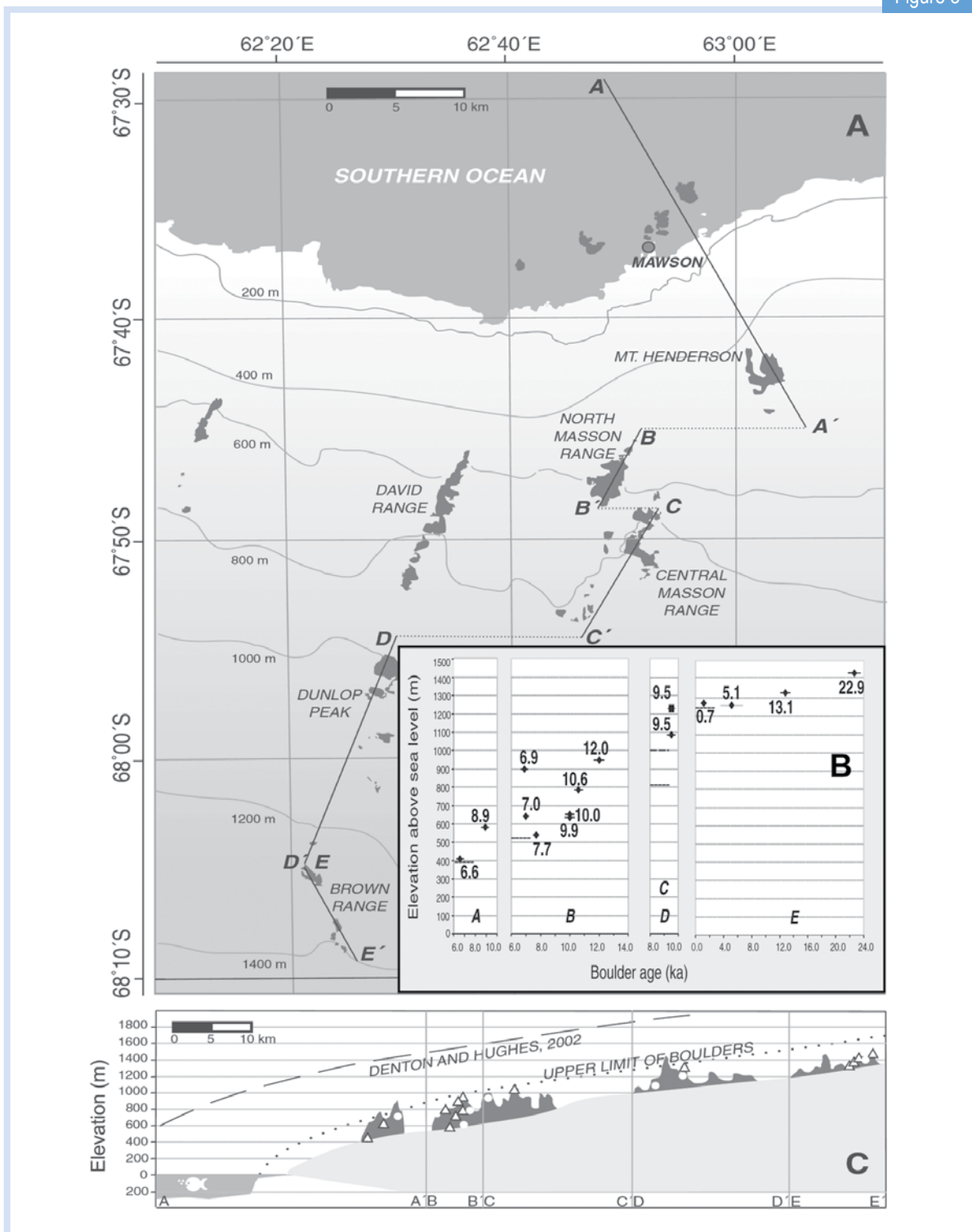
The technique of Accelerator Mass Spectrometry (AMS) [1] using ANSTO's ANTARES Facility can measure this tell-tale signal. As the concentration builds up over time with continued exposure to cosmic rays, *in situ* cosmogenic radionuclides act as nuclear clocks which measure an 'exposure age'.

This technique has revolutionised our understating of changing landscapes and of continental glacial chronologies.

Various photographs of sampling sites:

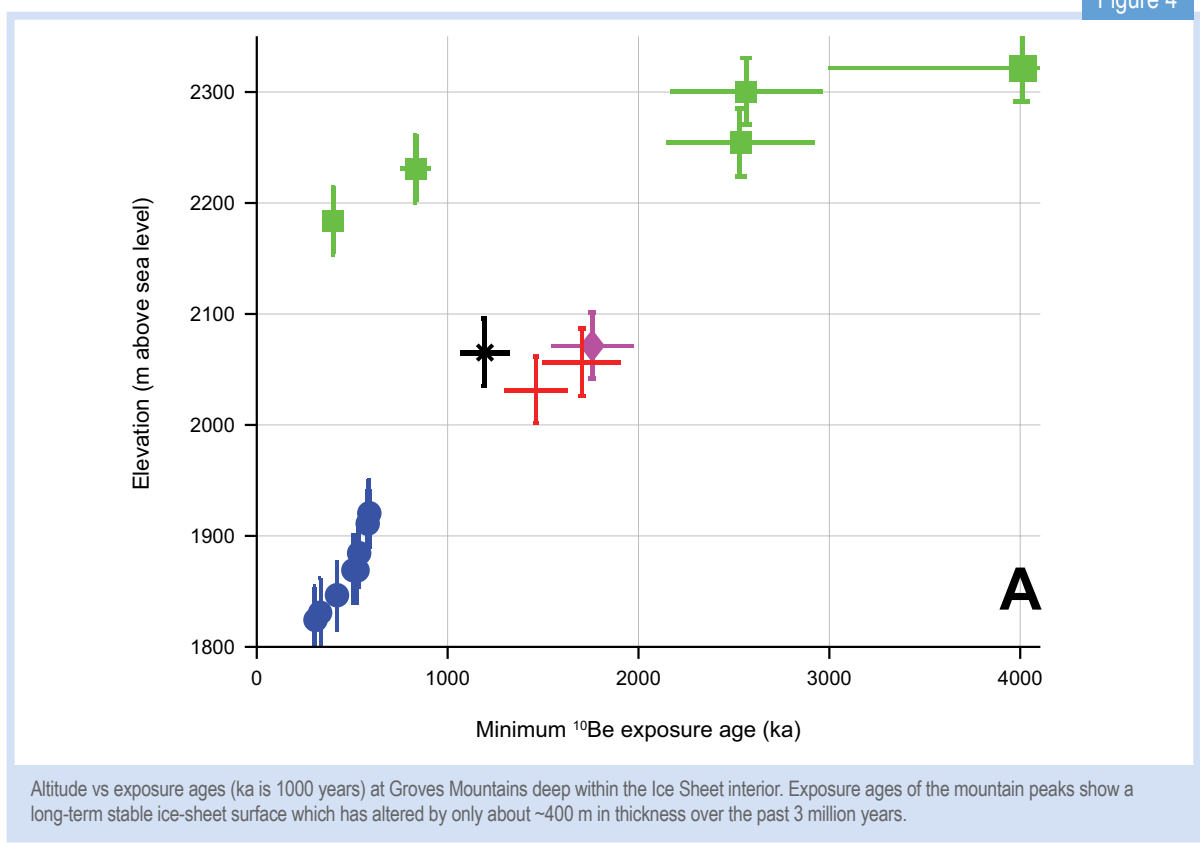
- (A) View of the Prince Charles Mountain flanking the Lambert Glacier near Loewe Massif. Light coloured rocks or cobbles contrast with the darker local bedrock lithology. Two samples gave exposure ages of 18,500 and 17,400 years suggesting that at that time the surface of the Lambert glacier was about 300 metres higher than today.
- (B) Small cobble on the peak of Central Mason Range (1035 m above sea level and 330 metres above today's ice surface) in Framnes Mountains, which gave an exposure age of 9500 years. Note the ocean coastline in background.
- (C) View of Groves Mountains looking south towards the centre of the East Antarctic Ice Sheet. These mountains protruding only 100-150 metres above the Ice Sheet are the most southern of any in the region. The red dot indicates one of the bedrock sample sites which gave an exposure age of about 2.5 million years indicating relatively little change of ice volume and hence a static ice-sheet surface.
- (D) An example of a very large boulder transported and deposited by the Lambert glacier. Samples for exposure dating are taken from the very uppermost flat surface of the boulder usually a few centimetres in thickness, by chisel and hammer.

Figure 3



- (A) Map of Framnes Mountains, Mac.Robertson Land, near Mawson Station. Transect A-E traces the chain of mountains which act as elevation 'dipsticks' allowing past changes in ice sheet volume to be constrained.
- (B) Inset shows elevation against exposure age (in thousand years) for each mountain range labeled A to E in the transect. Dashed lines denote present day local ice sheet elevation at individual sections. For example, panel A (Mt. Henderson) shows ~200 m of ice sheet lowering occurred between ~8900 and 6600 years; panel B (North Masson Range) provides evidence for 350 m of ice sheet lowering between 12,000 and 7000 years.
- (C) Modelled ice sheet surface during the last ice age—compared to measured surface based on exposure age dating (dotted line represents upper limit of boulders with exposure ages). The measured profile suggests a much smaller ice sheet in the past (500-1000 metres thinner and ~10 km less in extension over the continental shelf). Also coastal ice sheet deglaciation commences at 13,000 years - about 1000-2000 years before Meltwater pulse-1a which has previously been attributed to Antarctic ice melt.

Figure 4



Study region - Lambert Glacier and Prince Charles Mountains

We measured exposure ages of glacial boulders from three distinct regions of the EAIS that are characterised by vastly different modes of dynamical ice behaviour (see Fig. 1).

1. The Southern and Northern Prince Charles Mountains border the Lambert Glacier-Amery Ice Shelf region (Fig. 2A), which acts as an extensive ice-stream drainage basin extending ~800 km inland funnelling an estimated ~15% of East Antarctica's ice onto the Amery Shelf. As an outlet glacier system rapidly conveying ice from the deep interior to the coast, it effectively propagates large ocean-atmospheric variability to regions of static ice-sheet frozen to its bed which otherwise would be decoupled from external forcing.
2. The Framnes Mountains (Fig. 2B) near Mawson station are a string of localised coastal mountain peaks previously overridden by the EAIS, which today act as obstructive dipsticks protruding through the ice surface. At Framnes, the EAIS is slow and calves directly into the ocean; hence rising sea-level can unhinge basal ice-flow and change the rate of ice-sheet loss.
3. The Groves Mountains (Fig. 2C), smaller in area and only 200 m above the present ice surface, is fully encircled by the EAIS to the south-east beyond the drainage contours of the Lambert Glacier. The Groves Mountains are considered to be the most isolated land-mass within the deep interior of the EAIS.



Exposure ages document ice-sheet volume changes

Our results indicate that after the last ice age, ice thickness in the Lambert Glacier ice-streaming region began to decrease 18,000 to 14,000 years ago [2,3].

At the adjacent regions of the Framnes Mountains, where the EAIS reaches the coastline, our exposure ages [4] indicate that the ice-sheet retreat commenced only at 13,000 years and continued to 6000-7000 years at which time the ice sheet stabilises [4] (Fig. 3B).

This phase of ice-volume reduction at Framnes occurred about 4000 - 6000 years later than registered by the Lambert Glacier. Earlier onset of deglaciation of drainage basins suggests a heightened sensitivity of the EAIS to climate change.

Such effects are not included in any climate models. In contrast to these short-term ice-volume changes, our exposure ages at Groves Mountains tells a far different story, varying in thickness by ~100 metres at each mountain 'dipstick' with a total ice-thickness reduction of ~300 metres compared to today's ice surface in the past three million years – effectively a passive ice surface with little overall change during this time (Fig. 4).

Our exposure ages do not only provide dates, but also information on the spatial distribution of ice volume. By combining all ice limits traced out by the dated moraines across the Framnes region, we can reconstruct a picture of the dimensions of the coastal ice-sheet surface at the Last Glacial Maximum and thus predict how far it extended over the surrounding Southern Ocean (Fig. 3C).

Our surface reconstruction indicates an ice-sheet thickness only a few hundred metres thick and a few kilometres out to sea rather than predicted by some contemporary ice-sheet models which show ice 1000 metres thicker and tens of kilometres larger over the ocean.

Hence, we argue that there were only minor reductions in East Antarctic Ice Sheet thickness from 13,000 - 6000 years, a period during which northern hemisphere ice-sheets all but disappeared and sea levels rose by about 100 metres.

This discovery leads onto a second very exciting conclusion. Past sea-level records across global oceans



An iceberg off the coast of Antarctica.

document a continuous increasing sea-level totalling 120 metres from 20,000 years to about 6000 years ago. This trend is punctuated by a dramatic short pulse of a 20 metre rise about 14,500 years ago called Meltwater Pulse-1a. Most scientists point at Antarctica as the only source of such a large volume of water. Our results indicate that ice-streaming melt occurred well before this pulse, and coastal ice-sheet melt initiated about 1000 to 2000 years after it. Hence, we present a controversial conclusion that coastal EAIS retreat is not a contributor to Meltwater Pulse-1a because of a far smaller available ice volume and because coastal deglaciation postdates the pulse by 1000 - 2000 years.

We have shown that the EAIS does not respond uniformly both in space and time across all sectors to global climate change. Our improved documentation of size and thickness of the EAIS at the Last Glacial Maximum, as well as comparison of retreat rates between coastal margins and drainage basins are essential input to improving ice-sheet modelling and predicting future sea-level rise.

References

- [1] Tuniz, C., Bird, R., Fink, D., & Herzog, G. (1998). *Accelerator Mass Spectrometry: Ultrasensitive Analysis for Global Science*. Boca Raton, Florida, United States of America: CRC Press. 371p.
- [2] White, D., Fink, D., & Gore, D., Cosmogenic nuclide evidence for enhanced sensitivity of an East Antarctic ice stream to change during the last deglaciation. *Geology*, 39(1), 23-26.
- [3] Fink, D., McKelvey, B., Hambrey, M. J., Fabel, D., & Brown, R. (2006). Pleistocene deglaciation chronology of the Amery Oasis and Radok Lake, northern Prince Charles Mountains, Antarctica. *Earth and Planetary Science Letters*, 243(1-2), 229-243.
- [4] Mackintosh, A., White, D., Fink, D., Gore, D. B., Pickard, J., & Fanning, P. C. (2007). Exposure ages from mountain dipsticks in Mac. Robertson Land, East Antarctica, indicate little change in ice-sheet thickness since the Last Glacial Maximum. *Geology*, 35(6), 551-554.
- [5] Lilly, K., Fink, D., Fabel, D., & Lambeck, K. (2010). Pleistocene dynamics of the interior East Antarctic ice sheet. *Geology*, 38(8), 703-706.



Debashish Mazumder (right) and Jordan Iles taking samples from Australian wetlands.

Understanding and managing wetland health

Debashish Mazumder¹, Mathew Johansen¹, Suzanne Hollins¹, Yoshi Kobayashi², Jordan Iles², and Neil Saintilan²

¹ANSTO and ²Office of Environment and Heritage, Department of Premier and Cabinet, NSW

Australia's wetlands undergo frequent stresses from droughts and floods that impact life-sustaining wetland functions for a diverse range of aquatic, avian, and terrestrial biota. During these periods of changes in water levels, the food webs of the wetland shift, increasing the competition between native and introduced species.

The impacts that occur can be measured using the isotopes of carbon and nitrogen - the fundamental building blocks of wetland animals and plants. Our study adds to the understanding of how wetland health fluctuates as a result of natural and human-caused changes, and aids in knowing what actions are needed to sustain functioning wetlands.

Wetland ecology

Wetlands in the Murray-Darling basin are internationally recognised for their unique qualities in providing breeding and nursery grounds for numerous species, and providing food and water for aquatic, avian, and terrestrial biota as well as supporting human activities that depend on healthy functioning river-systems.

However, over the past decade these wetlands became increasingly isolated, diminished in area, and subject to dry periods due to land-use practices, water diversion, drought and climate change [1].

Due to heightened interest by river-basin management agencies regarding "managed environmental flows" and other measures to alter flow regimes, we need a better understanding of the impacts of such measures on wetland ecology.

Our primary objective is to improve the understanding of the changes to the health of wetlands resulting from fluctuations in flow regimes such as drought-induced low flows, flooding, and managed environmental flows.

Key tools for this study include an Isotopic Ratio Mass Spectrometry (IRMS) laboratory and a suite of isotopic modelling software for simulating food-web relationships. ANSTO's capabilities are combined with those of the Office of Environment and Heritage, Department of Premiers and Cabinet, NSW to provide input to the sound management of Australia's riparian wetlands.

Stable isotopes as tools for wetland ecology

Stable isotopes of carbon and nitrogen make up the fundamental building blocks of wetland animals and plants, and therefore the carbon isotope ratios $^{13}\text{C}:^{12}\text{C}$ (designated as $\delta^{13}\text{C}$) are used as a tracer of food 'source' [2] while nitrogen isotope ratios $^{15}\text{N}:^{14}\text{N}$ (designated as $\delta^{15}\text{N}$) are indicative of consumers' trophic position in a food web [3].

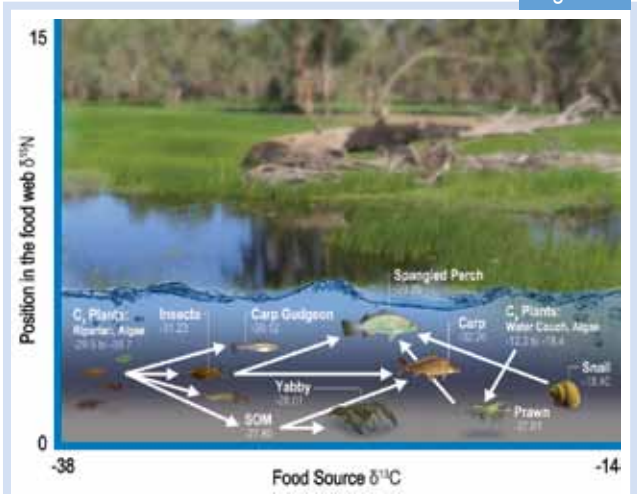
By measuring the relative abundance of stable isotope ratios ($\delta^{13}\text{C}$ and $\delta^{15}\text{N}$) in sediment, algae, invertebrates and fish, we determine food-web relationships that when mapped over a period of changing conditions reveal how the food web is impacted.

Samples were gathered from key ecological compartments, i.e. sediment organic matter, plants, macro-invertebrates, aquatic insects, and fish in three wetland water-bodies in the Lowbidgee floodplain wetland system within Yanga National Park, NSW, Australia.

We compared a wetter seasonal period following the release of a managed environmental flow with that from a later period of drier conditions and contracted water-pool levels and areas.

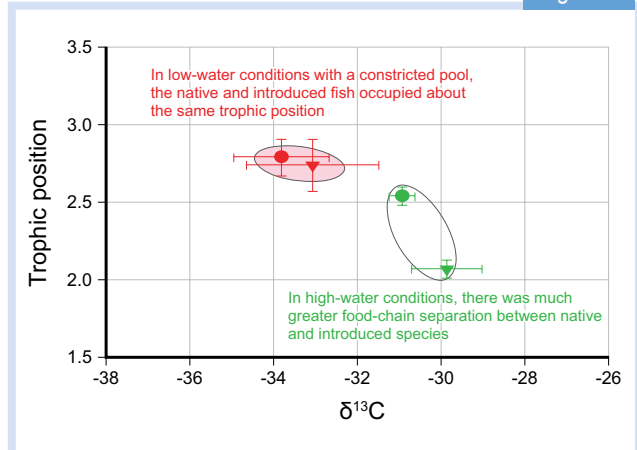
During this recession event, water volumes in the three water bodies reduced by 88-98%. Our study evaluated shifts of $\delta^{13}\text{C}$ and $\delta^{15}\text{N}$ data in the food web resulting from the reduced water-levels and in particular the potential impacts on native species.

Figure 1



Postulated food-web connections among species in the wetland ecosystem.

Figure 2



Food-chain positions of native carp gudgeon ● and introduced European carp ▼ during high-water conditions (green) and low-water conditions (red). Whiskers represent 5th and 95th percentiles on multiple samples.

Shift in the food web

The food web was altered during the change from high-water to low-water conditions in the Lowbidgee floodplain wetland, but in a different way than we expected. Although algae showed a relatively large depletion of -25‰ (the largest $\delta^{13}\text{C}$ shift) we found that higher-order animals do not show the same $\delta^{13}\text{C}$ shift. Apparently, algae do not represent the dominant food-chain base.

However, sediment organic matter shows a $\delta^{13}\text{C}$ ratio shift of about 2-4‰ that consistently tracks that of insects, fish, and other organisms higher up the food-chain. This has interesting implications as the makeup of the sediment organic matter is highly influenced by overland runoff which is in turn determined by the riparian biotic community and nearby land-use practices.

Native versus introduced species

During low-water conditions, heightened competition occurred for similar food items (insects) between native carp gudgeon (*Hypseleotris* spp), a small insectivorous fish, and an introduced European carp (*C. carpio*) a larger omnivore that preys opportunistically on insects.

The two species were well separated in their food-chain positions during high water levels, illustrated in Fig. 2 when comparing a plot of $\delta^{13}\text{C}$ and $\delta^{15}\text{N}$ values.

However, during low-water conditions they occupied almost the same food-web position suggesting the two species were competing for similar food items in food-scarce, constricted low-water pools.

The increased competition for insects was also indicated by a model analysis that considered the various food-sources available to European carp in the high-water and low-water conditions in three different wetland water-bodies. Fig. 3 shows modelling results of isotopic mixing that suggest the percentages of insects in the European carp diet increased by 18-30% in low-water conditions.

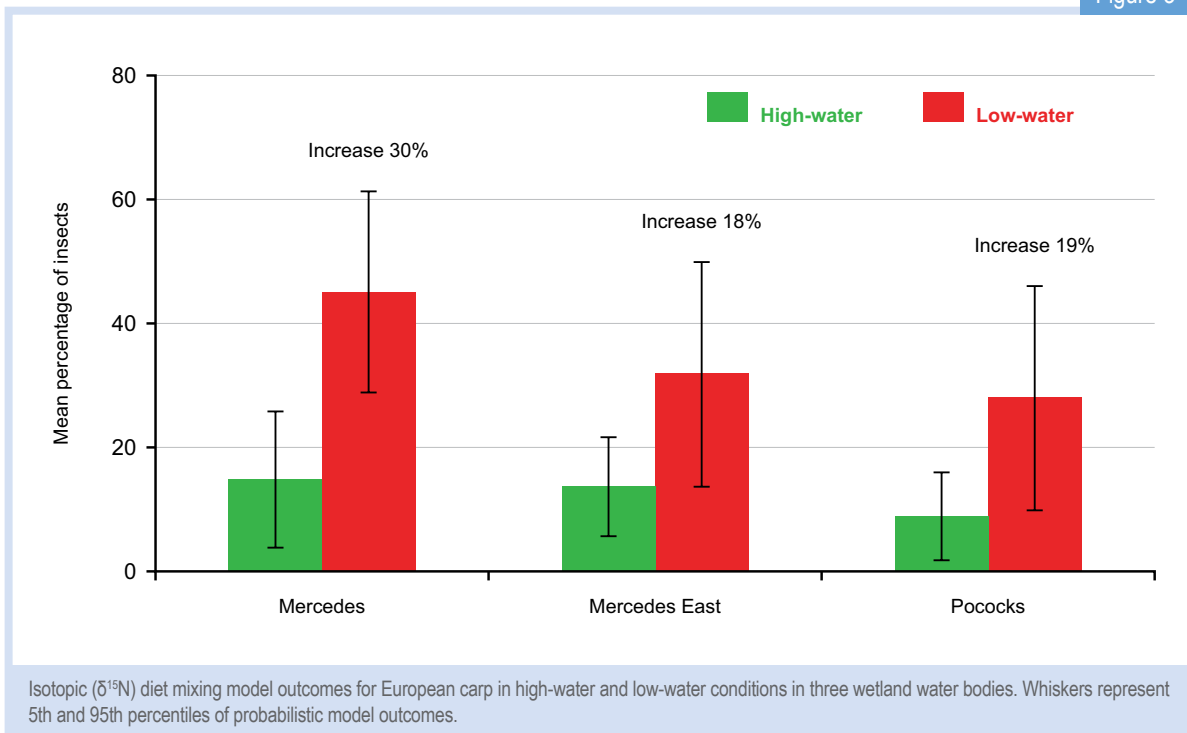
Consequently, European carp's increased consumption has a direct effect on native carp gudgeon as insects are the primary diet source of carp gudgeon.

Management Implications

We observed shifts in food chain relationships during changing (decreasing) water levels which indicate lower trophic aquatic animals relied on sediment organic matter as the dominant base of their food chain instead of algae or macrophytic plants.

Because the sediment organic matter is highly influenced by overland runoff from a variety of river floodplain activities, the land uses such as farming occurring on nearby floodplains and catchments have the potential to impact the wetland food chain directly.

Figure 3



River management strategies consider the length of low-flow periods between controlled releases and the degree to which wetlands are allowed to dry out.

Our observation of native fish species in the Murray-Darling basin show heightened competition between native and exotic fish species during periods of low water flows. This finding indicates that extended low-water conditions could reduce populations of native fish species in the Murray-Darling basin wetlands.

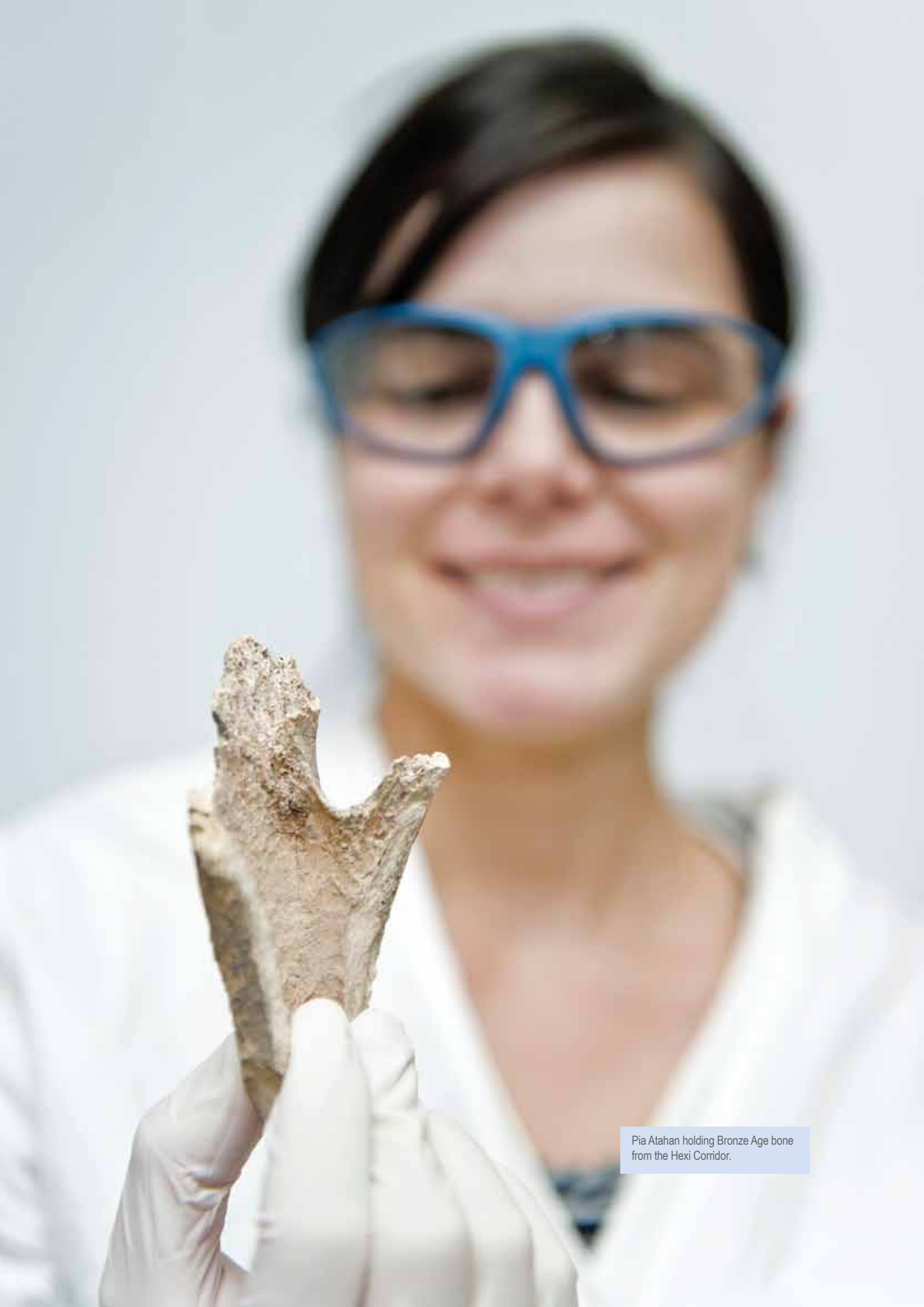
Further study is needed to determine the likelihood of displacing native species at large scales [4], and the impacts to other species including floodplain predators and birds that rely on native fish populations.



Researchers in the wetlands.

References

- [1] Kingsford, R. T. (2000). Ecological impacts of dams, water diversions and river management on floodplain wetlands in Australia. *Austral Ecology*, 25(2), 109-127.
- [2] Hecky, R. E., & Hesslein, H. R. (1995). Contributions of benthic algae to lake food webs as revealed by stable isotope analysis. *Journal of the North American Benthological Society*, 14(4), 631-653.
- [3] Zanden, V., Jake, M., & Rasmussen, J. B. (2001). Variation in $\delta^{15}\text{N}$ and $\delta^{13}\text{C}$ trophic fractionation: Implications for aquatic food web studies. *Limnology and Oceanography*, 46(8), 2061-2066.
- [4] Bunn, S. E., & Arthington, A. H. (2002). Basic principles and ecological consequences of altered flow regimes for aquatic biodiversity. *Environmental Management*, 30(4), 492-507.



Pia Atahan holding Bronze Age bone from the Hexi Corridor.

Unravelling farming and metallurgy in ancient China with nuclear science

Pia Atahan¹, Fiona Bertuch¹, John Dodson¹ and Xiaoqiang Li²

¹ANSTO, ²Institute of Vertebrate Paleontology and Paleoanthropology, Chinese Academy of Science, Beijing, China

Nuclear techniques are finding increasing utility in telling us who we are and where we have come from. Our research is shedding new light on early cultural connectivity across Eurasia by investigating sites in north-west China. Separate systems of agriculture emerged independently in eastern and western Asia around 8000 -10,000 years ago.

In the east, incipient agriculture centred on cultivating millet and rice, while in the west, it centred on wheat and barley.

We are applying isotopic methods and atom mass-spectrometry with radiocarbon dating to archaeological remains from Bronze Age sites in northern China in order to better understand cereal cultivation, animal husbandry and bronze metal-work technology.

Civilisations in the East and West

Some of the first significant human innovations in agriculture and technology were developed between 10,000 and 3000 years ago. This was when people learned to select and improve the characteristics of crops, to domesticate animals and to produce new tools using metallurgy.

These were the essential elements that enabled sedentary and then village life, and allowed societies to expand specialisations that produced writing, literature, music, politics, culture and innovation – essential ingredients that elevated achievement and improved life outcomes for humans generally. Of course most societies are still on this journey.

Archaeology and prehistoric records tell us that two of the greatest and earliest centres of urban life were in the East (in what is now recognised as part of China) and the West, centred on the Levant (including modern-day Syria, Lebanon and Jordan).

Agriculture emerged independently in both regions around 10,000 to 8000 years ago. In the Levant it was centred on wheat and barley, while in China it centred on millet and rice. Metal-work technology also represents a significant cultural advance, and it is sites in western Asia that yield the oldest metal tools. There, metal tools

were made from copper, until the technology of making bronze, by adding small amounts of tin and/or arsenic to copper in hotter smelting systems, was developed.

Links between eastern and western civilisations were well established 2000 years ago. By this time clear trading routes were established between the two major cities of the day namely, Baghdad in the west and Xi'an in the east with many staging posts between the two cities. This route became known as the Silk Road, deriving its name from the precious silken products made from a secret process in China that drove westerners mad with desire for the precious fabric.

The power of isotopic methods is shining new light on this view of history, and in recent years has demonstrated that the Silk Road has also been an Agriculture Road, a Bronze Road and more, and has been an East-West networking route for more than 4000 years.

Ancient bronze in the Hexi Corridor

Scientists at ANSTO and the Chinese Academy of Sciences in Xi'an and Beijing have been examining bronze metal-work remains at Huoshiliang site in the Hexi Corridor of north-west China (Fig. 1 and 2). The remains have now been dated in context to a

Figure 1

Location of field sites in the Guanzhong Basin and Hexi Corridor of northern and north-western China. The upper map shows the location of Xishanping, the lower map shows the location of Huoshiliang and Gangangwa.

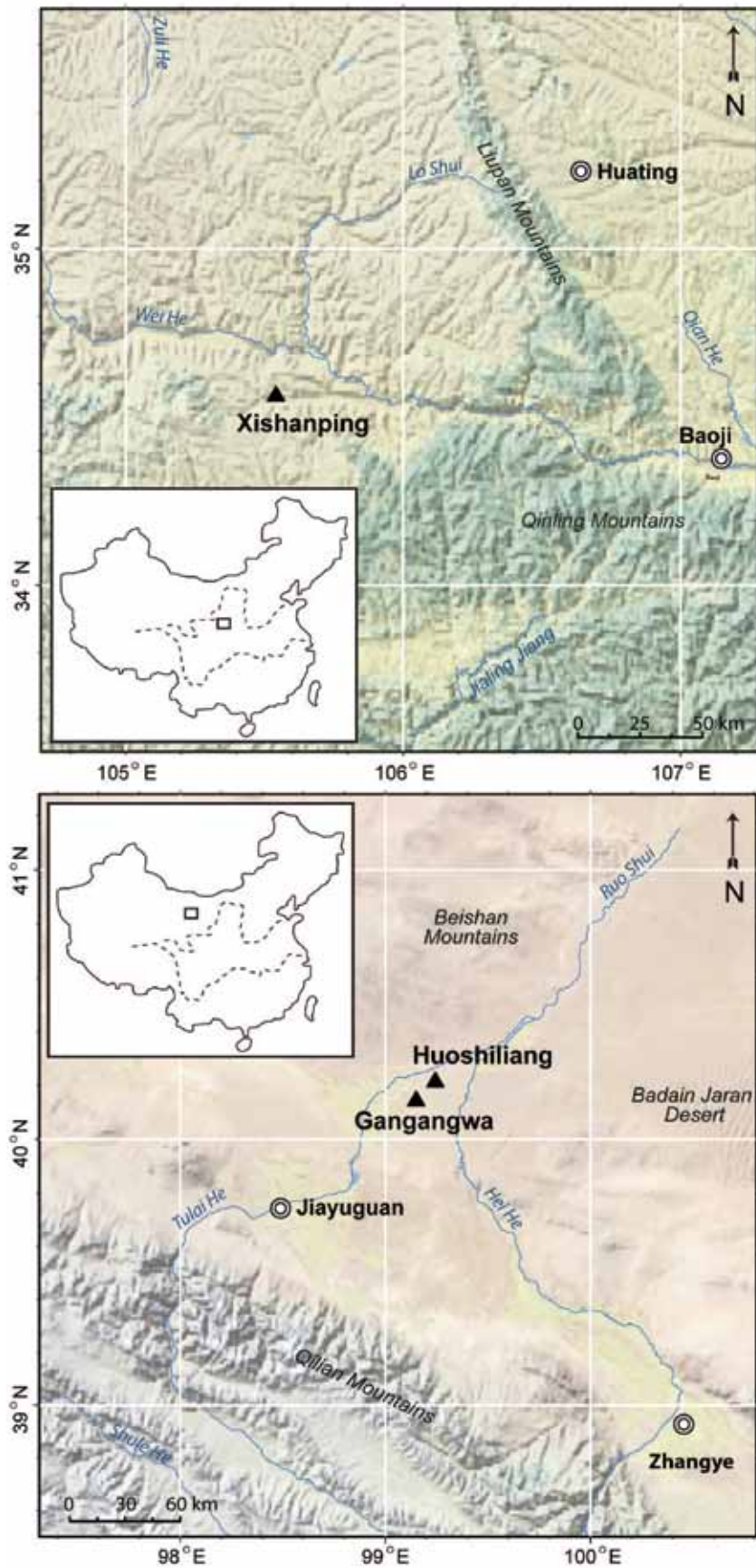


Figure 2



Photograph showing the surface scatter of cultural remains at Huoshiliang site. Inset shows pottery fragments *in situ* at the surface scatter.

bit before 4000 years ago placing Huoshiliang amongst the oldest bronze sites in China. Was this bronze imported with other western technologies such as wheat farming, or was it developed independently in China? Well, the ages from Huoshiliang are younger than those from Syria and suggest the technology may in fact have been imported from the West.

Can we determine if the bronze at Huoshiliang was made locally or carried east with the technology? The answer is yes we can and nuclear techniques are the key for doing this.

The bronze contains a large number of trace elements, such as lead and strontium. These metals have isotope mixes which are specific to individual ore bodies and arise from differences in the age and past geochemical processes at each ore site. These isotopic signatures carry through to the final metal objects.

We have measured the abundance of a range of lead and strontium isotopes from bronze slag, bronze tools and copper ore samples collected at Huoshiliang (Fig. 3), and from ore samples from a modern day copper mine at Baishantang, located about 50 km to the north-west [1]. These measurements were taken using

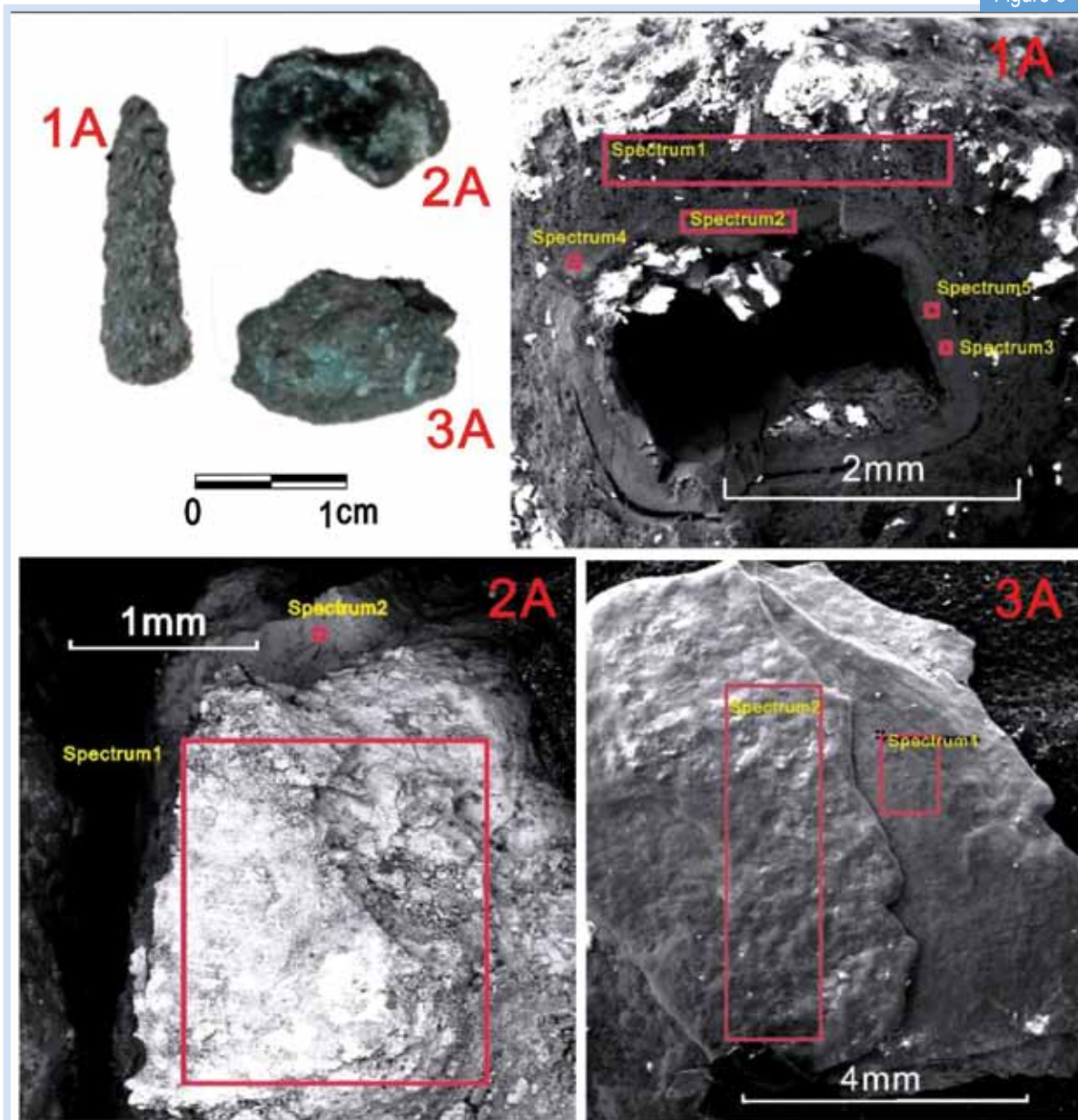


From Left to Right: Keliang Zhao, Pia Atahan, Xinying Zhou, John Dodson, Mr Zhao, Xiaoqiang Li and Mr Zheng.

inductively coupled plasma mass spectrometry (ICP-MS) which is capable of determining minute concentrations of metals.

Most of the site's samples produce isotope signatures that are statistically identical to the mine's samples, indicating the bronze was manufactured locally. One sample from Huoshiliang has a different isotope mix, and thus originated from a place at present unknown.

Figure 3



Three artefact pieces from Huoshiliang shown under a scanning electron microscope. The red rectangles indicate locations targeted for energy dispersive X-ray (EDS) analysis [1].

Western domesticates in ancient China

In order to better understand the antiquity of western domesticates in China, botanical remains from Huoshiliang, Gangangwa and Xishanping in north-west China (Fig. 1) are being examined.

Much evidence about early agricultural practices is in the form of charred seeds, and at these sites millet dominates. Rice, wheat and barley are also present.

At Xishanping, wheat remains have been radiocarbon dated, using ANSTO's STAR accelerator, to ca. 4650 calibrated years before present. This is the oldest confirmed wheat in eastern Asia, and is firm evidence that there was exchange between the West and East more than 2000 years before the Silk Road route, as is traditionally recognised in the history books.



John Dodson, Xiaoqiang Li and Xinying Zhou discussing sampling in the field.

Dietary clues from skeletal remains

Apart from seeds, abundant pottery, metal and stone artefacts and bone have been recovered from the ancient agro-pastoral sites of Huoshiliang and Gangangwa, in the Hexi Corridor.

At ANSTO, we are applying sophisticated treatments to extract bone protein and determining its integrity in order to provide reliable radiocarbon ages on bone from human, cattle, sheep/goat, rat, pig, dog and cat. To date, the ages of the bone fall around 4000 years ago.

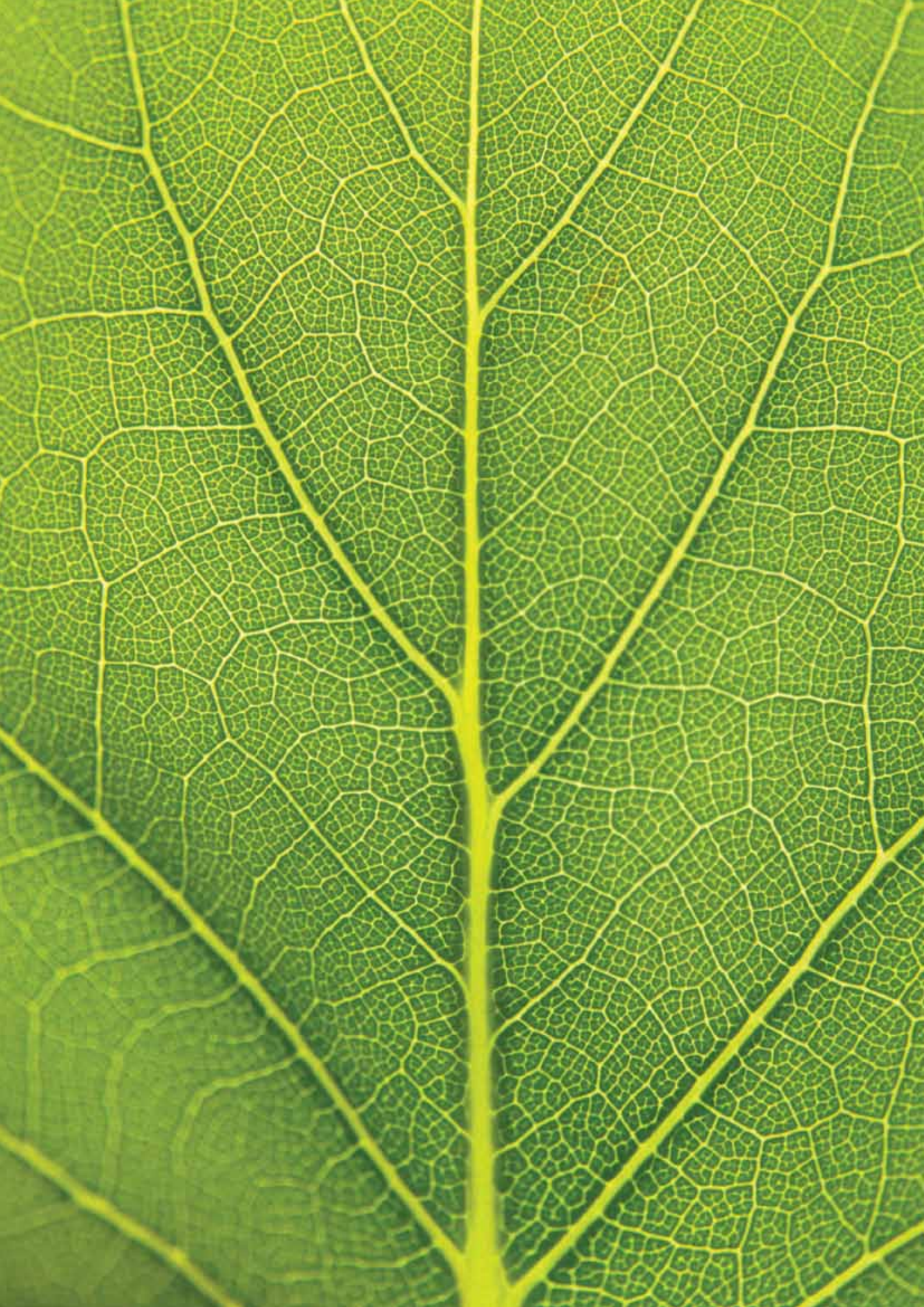
Stable isotope ratios of carbon and nitrogen, measured on an elemental analyser – isotope ratio mass spectrometer (EA-IRMS), are giving clues about the diets of the inhabitants of these ancient sites.

Stable carbon isotope ratios enriched in the heavier isotope (^{13}C) indicate millet was the principle component of human diets as well as some of the domestic animals, while herded animals yield carbon and nitrogen stable isotopic signatures suggesting grazing was well beyond the agricultural areas [2].

Further work at these sites will contribute to knowledge on the history of domestication, particularly of pig, sheep and cattle, to allow us to learn more about our ancient beginnings.

References

- [1] Dodson, J., Li, X., Ji, M., Zhao, K., Zhou, X., Levchenko, V., (2009). Early Bronze in two Holocene archaeological sites in Gansu, NW China. *Quaternary Research* 72, 309-314.
- [2] Atahan, P., Dodson, J., Li, X., Zhou, X., Hu, S., Bertuch, F., Sun, N. 2011. Subsistence and the isotopic signature of herding in the Bronze Age Hexi Corridor, NW Gansu, China. *Journal of Archaeological Science*, 38(7), 1747-1753.



Plants that can accumulate toxic metals

Rainer Siegele¹, Yaodong Wang², Anthony Kachenko³ and Mihail Ionescu¹

¹ANSTO, ²University of Melbourne, ³University of Sydney

Microanalytical techniques provide new insight into the understanding of biological and environmental processes, such as metal hyper-accumulation in plants. Measuring the elemental distribution in different plant tissue types, such as leaves, stems and roots can help us to understand the strategies they employ to tolerate high concentrations of metals, such as Ni and Co, that are toxic to other plants.

These plants have the potential to be used to remove metal contamination from soils, a process known as phyto-remediation.

Metal accumulation in plants

Heavy metal tolerance is the ability of a plant to grow in a heavy metal-enriched soil that is toxic to most other plants. Amazingly, some plants are tolerant species that can additionally concentrate metal(s) in their above-ground tissues to levels exceeding the concentration present in the soil or in the non-accumulating species growing nearby [1].

In some hyper-accumulating plants, the metal concentration can exceed $1000 \mu\text{g g}^{-1}$ (0.1%) in the dry matter of the above-ground tissue. Some plants (notably, *Stackhousia tryonii*) have been reported to contain exceptionally high levels of Ni (> 4%; dry weight basis).

Clearly, these properties make the plants useful in removing metal contamination from soils or to mine areas with low-yield surface deposits; technically this is called phyto-remediation of contaminated soils or phyto-mining.

Elemental imaging using nuclear methods

We can establish elemental maps of the plants using nuclear techniques such as micro Proton-Induced X-ray Emission (μ -PIXE) in order to understand the physiology of metal hyper-accumulation, and therefore study the distribution of the metals within the plant tissues.

The plants form organo-metallic complexes to hyper-accumulate toxic metals, and subsequently transport and compartmentalise these complexes within vacuoles of 'storage' cells. Using μ -PIXE the metals can be traced on their journey through the cell tissue.

Localisation of Ni in *Hybanthus Floribundus*

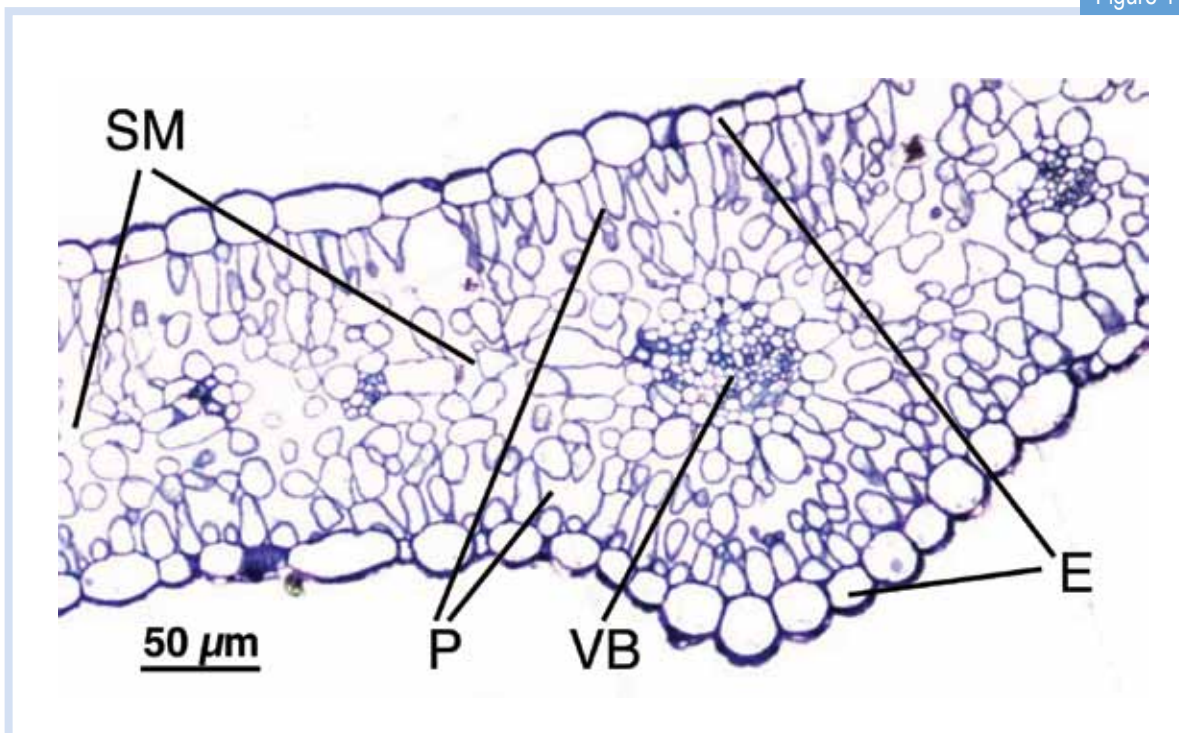
Hybanthus floribundus, commonly known as Australian shrub violet, is one of three Ni hyper-accumulating plants reported from Australia and is one of approximately 320 Ni hyper-accumulators worldwide. It is a native Australian perennial shrub and has been reported to hyper-accumulate up to $13,500 \text{ mg Ni kg}^{-1}$ of dry weight in leaf tissues. For comparison most other plants will show signs of toxicity at Ni concentrations of 100 mg kg^{-1} or less.

Fig. 1 shows an optical micrograph of a stained leaf section of *Hybanthus floribundus* showing the anatomical structure of the leaf. On both the upper and lower leaf surface a continuous single row of cells form the epidermis, outer layer. Below the epidermis is a layer of elongated cells, that form the palisade layer, which is followed by the spongy mesophyll that contains the vascular bundles, part of the plant's transport system.

Fig. 2 shows the elemental distributions of S, Ca, K and Ni of *Hybanthus floribundus* leaf section (Ca, K and S highlight the different structural parts of the leaf). Lighter colours indicate a higher concentration of the element in the area. Individual cells are clearly resolved showing the variation of the concentration of elements within the cells and in different cell layers [3,4].

Ni is highly concentrated in the upper and lower epidermis of the leaf, thus accumulating in the outer layer or skin of the leaf. However, high concentrations of Ni are also found in the vascular bundles, as Ni is being transported through the vascular tissue into the leaves. The Ni concentration in both the epidermis and the vascular tissue reaches up to $15,000 \text{ mg Ni kg}^{-1}$ on

Figure 1



Light micrograph of a Ni-treated leaf cross-section of *Hybanthus floribundus* subsp. *floribundus* (1 μm , magnification $\times 40$); where E, epidermis, the outer layer; P, palisade mesophyll, a layer of cells just below the upper surface; SM, spongy mesophyll and VB, vascular bundle; both located in the inner part of the leaf.

a dry weight basis (yellow areas). The high-resolution images show that Ni is mainly concentrated in the walls of the epidermis cells whereas in the vascular tissue Ni is evenly distributed throughout the cells.

This information is important for plant biologists to narrow down the processes that allow the plants to transport and store the metals.

Localisation of Co in *Haumaniastrum robertii*

Haumaniastrum robertii is a plant that thrives in areas with high concentrations of copper and cobalt in the soil. Its common name is copper flower, because it is often found in copper-rich soils.

However, some species can also accumulate high concentrations of cobalt, which has lead some researchers to speculate that its distribution is governed by cobalt rather than copper. Copper or cobalt concentrations in hyper-accumulating plants are much lower compared to Nickel concentrations.

Hence, the cobalt concentration found in this plant reaches a maximum concentration of around 2000-3000 mg kg^{-1} . Elemental maps taken on a leaf of *Haumaniastrum robertii*, using the Heavy Ion Microprobe are shown in Fig. 3: High concentrations of cobalt are present in the vascular tissue, with lower concentrations in the epidermis, i.e. little accumulation of Co.

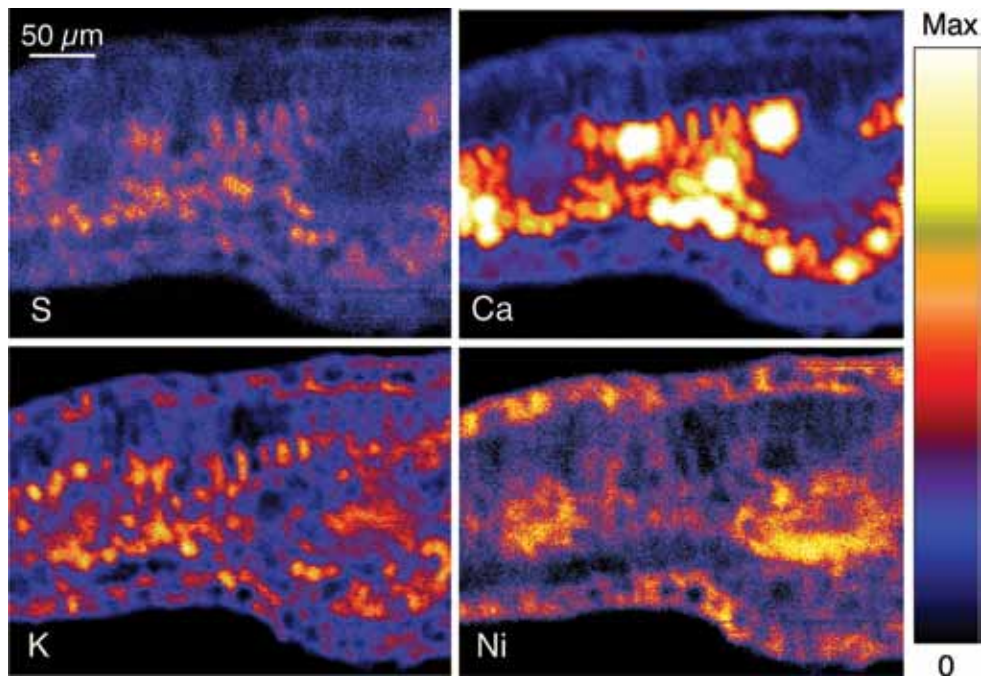
Clearly, there are different mechanisms for how these two species process these toxic metals. The cobalt results are similar to earlier findings for copper, which is also concentrated in the vascular bundles and to a lesser degree in the epidermis, indicating that in these plants the metals are to a lesser degree stored in the epidermis, but largely remain in the vascular bundles.

Further work is planned using synchrotron radiation and X-ray absorption spectroscopy (XAS) techniques which will help to better understand the molecular structure that binds the metals.

References

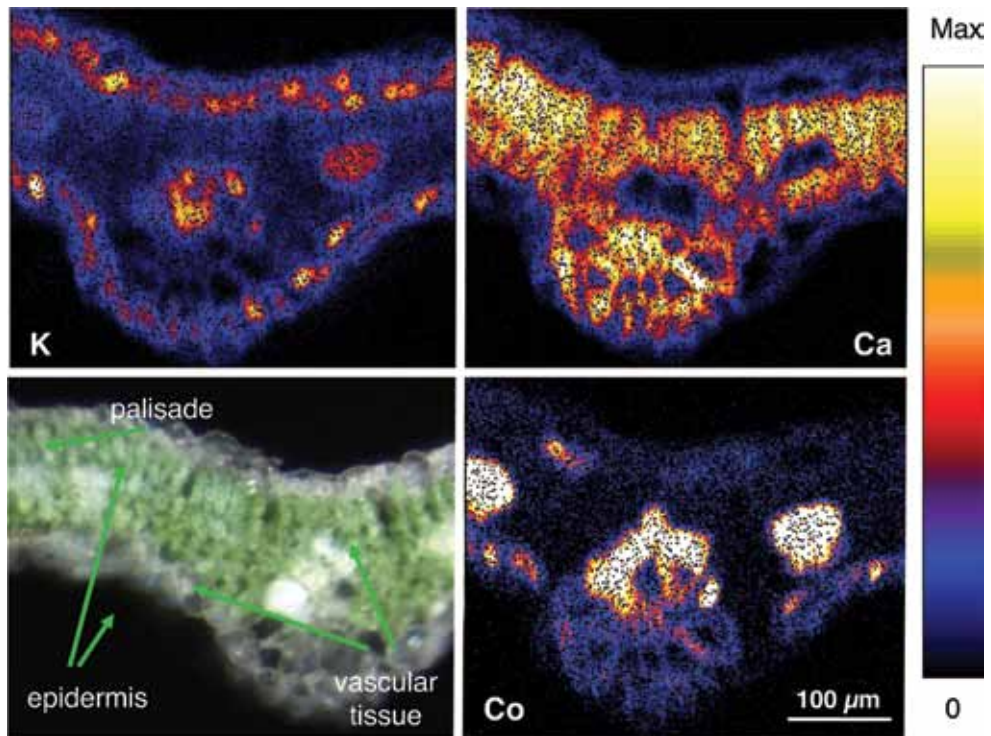
- [1] A.J.M. Baker and R.R. Brooks, *Biorecovery* 1 (1989) 81-126.
- [2] R. Siegele, N. Dytlewski and D.D. Cohen, *Nucl. Instr. and Methods* B158 (1999) 31-38.
- [3] A.G. Kachenko, B. Singh, N.P. Bhatia, R. Siegele, *Nucl. Instr. and Methods* B266 (2008) 667-676.
- [4] R. Siegele, A.G. Kachenko, M. Ionescu and D.D. Cohen, *Nucl. Instr. and Methods* B267 (2009) 2054-2059.

Figure 2



High resolution elemental maps showing distribution of S, K, Ca and Ni in a freeze-dried leaf cross-section of *Hybanthus floribundus* subsp. *floribundus*. The images show the relative concentration of the elements across the sample.

Figure 3



High resolution elemental maps showing distribution of K, Ca and Co in a freeze-dried leaf cross-section of *Haumaniastrum robertii*. The figure on the lower left shows an optical micrograph of the same sample.

LifeSciences



LifeSciences

From building knowledge about the behaviour of cell-membranes to designing new radiopharmaceuticals, ANSTO LifeSciences' research spans a broad and diverse field of studies concerned with the natural world.

Using nuclear and isotopic techniques, over the past year ANSTO has undertaken a range of studies including the development of a new radiopharmaceutical to more efficiently diagnose malignant melanoma, a cancer for which Australia has the highest incidence in the world. ANSTO's scientists have found new ways to optimise conditions to produce more effective radiopharmaceuticals.



(L-R) ANSTO LifeSciences' Andrew Katsifis, Naomi Wyatt, Cathy Jiang, Tien Pham and Ivan Greguric have played a central role in the development of this important new radiopharmaceutical.

Development of novel imaging radiopharmaceuticals for malignant melanoma

Ivan Greguric¹, Tien Pham¹, Stephen Taylor¹, Patrice Ballantyne¹, Christian Loc'h¹, Andrew Katsifis¹, Rob Ware², Marie Gregoire¹, Delphine Denoyer², Rodney J Hicks², Ron Weiner¹.

¹ANSTO, ²Centre for Molecular Imaging, Peter MacCallum Cancer Centre, Melbourne

Australia has the world's highest incidence rate for melanoma. Melanoma accounts for 10% of all cancers in Australia. Malignant melanoma is a very aggressive cancer, with a high rate of metastasis brought about by excessive ultraviolet (UV) exposure. A key feature of melanoma is the extensive pigmentation present in most tumour cells.

Accordingly, this pigmentation, melanin, is a very attractive target for both disease localisation and treatment. As part of our radiopharmaceutical optimisation program we have developed a series of nicotinamide structures to target melanin with high selectivity.

Preclinical animal studies indicated that [¹⁸F]N-(2-(diethylamino)ethyl)-6-fluoronicotinamide ([¹⁸F]MeI050) was the most promising Positron Emission Tomography (PET) radiotracer for clinical staging with great potential for personalising therapeutical treatments. Preliminary patient studies appear to confirm these results.

Why we study melanoma

Skin cancer is the third most common human malignancy with 2-3 million new cases estimated across the world each year. Although melanoma accounts for only about 130,000 of these, it is the most dangerous form and results in most of the deaths related to skin cancer.

Australia has the world's highest incidence rate for melanoma accounting for 10% of all cancers - the fourth most common. Survival largely depends on early detection and cure by surgical resection of primary melanomas. Extensive metastatic malignant melanoma is refractory to most therapies with a median survival of 6 months and a 5 year survival rate of less than 5% [1], although surgery may still be effective if metastases are localised.

Despite a paucity of effective treatments for advanced melanoma currently, improved diagnostic methods have considerably decreased mortality rates in early disease. Radiopharmaceuticals that can target the melanoma tumours may offer opportunities for better assessment of disease extent and thereby improve the selection of patients with metastatic disease for surgical resection, as well as potential radiotherapeutic applications [1].

A key feature of melanoma tumours is the extensive pigmentation present in most melanoma tumour cells, thus making melanin a very attractive target for both diagnosis and treatment.

To date, we and others have developed a considerable number of [¹²³I]benzamide derivatives that exhibited good uptake in melanoma tissue and could be used for single photon emission computed tomography (SPECT) imaging and disease localisation.

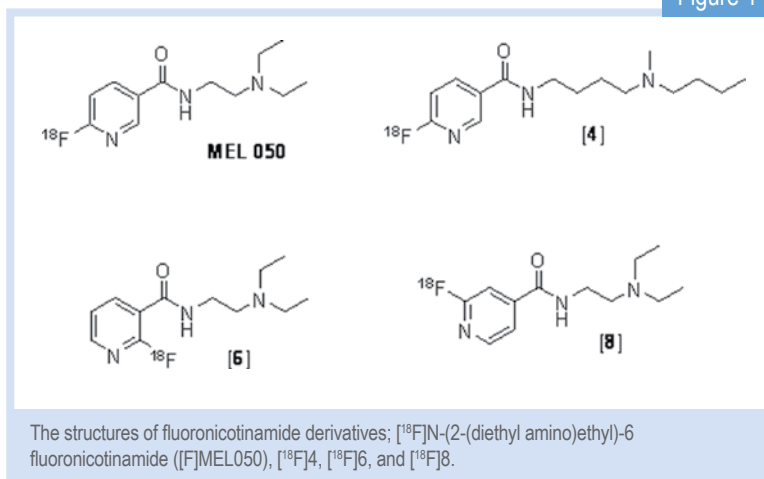
Our attempts to improve the tumour to background ratios and body clearance of iodobenzamides led to the development of iodonicotinamide analogues [2] which are readily taken up in melanoma tumours with subsequent melanin binding.

Our approach

Positron emission tomography (PET) has emerged as a valuable imaging tool due to its ability to provide high resolution and absolute quantitative uptake in tissue, with ease in background subtraction versus the older SPECT imaging.

At present, 2-[¹⁸F]fluoro-2-deoxy-D-glucose [¹⁸F]FDG PET imaging of melanoma is the only PET clinical radiotracer used routinely to localise melanoma tumours [3].

Figure 1



Although [¹⁸F]FDG is an effective tool for melanoma tumour detection, inflammation and infection decrease its specificity [4] and partial volume-effects limit its sensitivity for small-volume disease. Our objective was to improve specificity by incorporating fluorine-¹⁸F into the nicotinamide structure while retaining high melanin binding affinity and its rapid whole body clearance of unbound tracer, stability, and ease of radiolabelling.

We have developed a series of new PET [¹⁸F] fluoronicotinamide radiotracers that can be prepared in one simple radiosynthetic step [5-7]. One of them, [¹⁸F]N-(2-(diethylamino)-ethyl)-6-fluoronicotinamide ([¹⁸F]Mel050), displayed rapid clearance, superior *in vivo* stability, high tumour to background ratio in animal PET imaging and biodistribution studies and, in particular, high specificity for melanin.

Preliminary patient studies of [¹⁸F]Mel050 have demonstrated that the tracer is safe and can effectively demonstrate the location of normal melanin containing tissues and pigmented melanomas. If this data is confirmed in larger patient studies, [¹⁸F]Mel050 could be a useful PET tracer for clinical staging and metabolic characterisation.

This should enable more accurate patient selection and planning of treatment as well as better therapeutic monitoring in melanoma compared to existing standards including [¹⁸F]FDG.

Making and testing the radiopharmaceutical

The [¹⁸F]fluorine atom was added directly onto the nicotinic ring by direct [¹⁸F]fluorination of the chloronicotinamide precursor. Rapid radiosynthesis was achieved. This is critical since the ¹⁸F half-life is only 109 min. Various [¹⁸F]Fluoronicotinamides derivatives; [¹⁸F]Mel050, [¹⁸F]4, [¹⁸F]6, and [¹⁸F]8 (Fig. 1) were prepared to determine which had the best characteristics. These radiotracers were ready to use within 40 minutes.

This total process included purification and formulation from their chloronicotinamide precursors. High radiochemical yields, radiochemical purity and specific activity were obtained. The radiochemical stability was maintained at >98% over 3-4 hours in saline. The biodistribution of the [¹⁸F]fluoronicotinamides

were studied in two mice strains: black mice bearing the murine melanotic melanoma and nude mice bearing the human amelanotic tumour.

A skin lesion (abnormal areas of tissue on the body) that is amelanotic, lacks the pigment melanin and therefore is essentially colourless. It would be expected that the fluoronicotinamides, if specific, would localise in the melanotic, but not in the amelanotic tumours.

Melanoma patients were recruited that had [¹⁸F]FDG positive lesions. The patients were then imaged with a GE PET/CT camera using [¹⁸F] [¹⁸F] Mel050 at the Peter MacCallum Cancer Centre that was prepared at Cyclotek, a commercial provider of radiopharmaceuticals.

A pilot study: from animal to humans

Table 1 shows the uptake of the different [¹⁸F] fluoronicotinamides as a function of time. Eye and tumour concentration for all analogues were relatively stable in this time frame where as the compounds rapidly washed out of the non-melanotic tissue. Localisation in the eyes of mice was significant but similar to that of other melanin binding compounds [8,9].

Uptake values in the murine melanotic tumour and in the eyes of black mice at 3 h were more than 200 times greater than that observed in the nude mice bearing the amelanotic tumour. The large uptake differences between black and nude mice support the hypothesis that [¹⁸F]fluoronicotinamides are involved in a specific interaction with melanin.

High concentrations of melanin are present in the murine melanotic tumour and the pigmented eye structure of black mice, but are lacking in nude mice [2]. [¹⁸F]Mel050 was the best of the four compounds studied. It displayed the least bone uptake of all the derivatives and highest tumour to bone ratio at 0.25 and

3 hr PI (Table 1). Bone uptake was comparable to that reported for a study using [^{18}F]DAFBA [8].

Also, [^{18}F]Mel050 was very stable *in vivo*. Analysis demonstrated that more than 90% of activity in tumour, eyes, and urine and 70% in plasma remained [^{18}F]Mel050 for at least 2 h PI. The low bone uptake also suggested stability in rodents. Fluorine cleaved from the molecule would be expected to lodge in the bone.

The rapid uptake and fast normal tissue washout of [^{18}F]Mel050 is confirmed in the dynamic animal PET/CT image (Fig. 2). Initial images (Fig. 2b) demonstrated only renal uptake while later images show that only eyes, stomach, and tumour retain activity (Fig. 2c). Fig. 2a demonstrates that a high tumour to background ratio, ~10:1, was achieved at 80 min PI.

[^{18}F]Mel050 was further evaluated in experimental mouse models of melanoma metastases in the lungs and in the lymph nodes (see Fig. 3). A significant accumulation of the compound was shown in the lungs of mice bearing melanoma metastases.

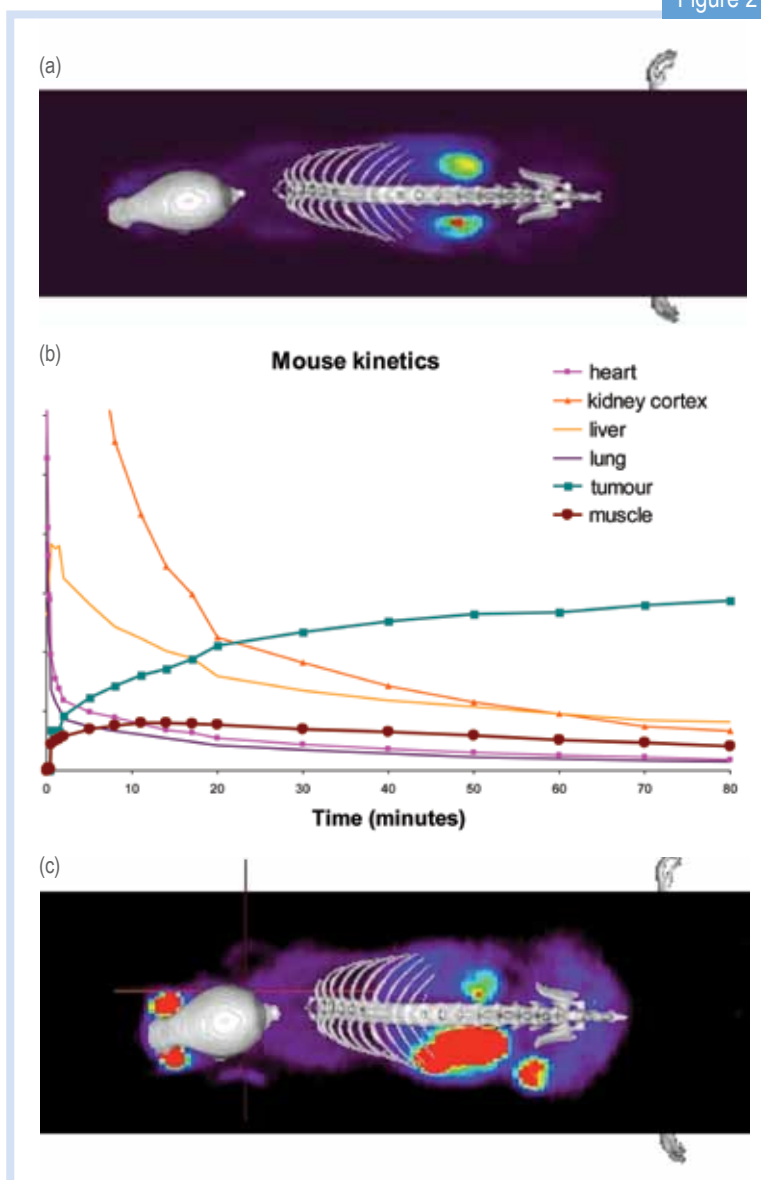
The level of [^{18}F]Mel050 signal in the images reflected the tumour burden with a strong link between [^{18}F]Mel050 signal and the presence of melanoma deposits at necroscopy (6). [^{18}F]Mel050 had also the ability to identify lymph node metastases when the tracer was injected intravenously.

In addition, [^{18}F]Mel050 allowed visualisation of nodal lesions below the theoretical spatial resolution of PET when administered locally into subcutaneous tissues around the primary lesion site (10).

All together, these results provide evidence that [^{18}F]Mel050 has the potential for whole-body staging of pigmented melanoma as well as for the sensitive and specific identification of lymph node involvement

when administered locally at the primary tumour site. Because of this successful pre-clinical data, animal toxicology studies of Mel050 were performed as a prerequisite for human clinical studies.

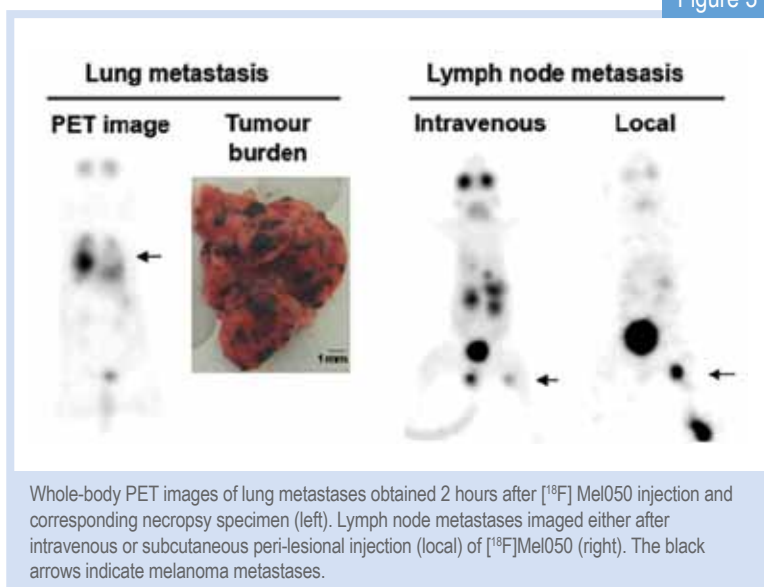
The lack of observable toxicity in rats at doses of Mel050 one thousand times that proposed for human studies supported the initiation of first in human studies to evaluate safety, biodistribution, tracer stability and to



[^{18}F]Mel050 PET/CT image analysis of murine melanoma.

- (a) 2 minute whole body image (kidney and skeleton visible) of a C57BL/6J black mouse bearing a melanotic (B16F0) tumour (left flank),
 (b) graphical representation of uptake in a variety of tissues as a function of time demonstrating normal tissue washout and rapid tumour uptake
 (c) whole body images (tumour, stomach and eyes visible) at 80 minute PI. Note: Green represents low and red high radioactive concentration.

Figure 3



obtain preliminary information about melanin targeting potential.

To date, five melanoma patients have been imaged in a pilot clinical study at the Peter MacCallum Cancer Centre supported by the Cooperative Research Centre for Biomedical Imaging Development (CRC-BID). Fig. 4 is an example of a patient image from this study and demonstrates the advantage of [¹⁸F]Mel050 compared to a CT scan. Of these five, two patients had no [¹⁸F]Mel050 retention in their [¹⁸F]FDG-positive metastatic melanoma lesions.

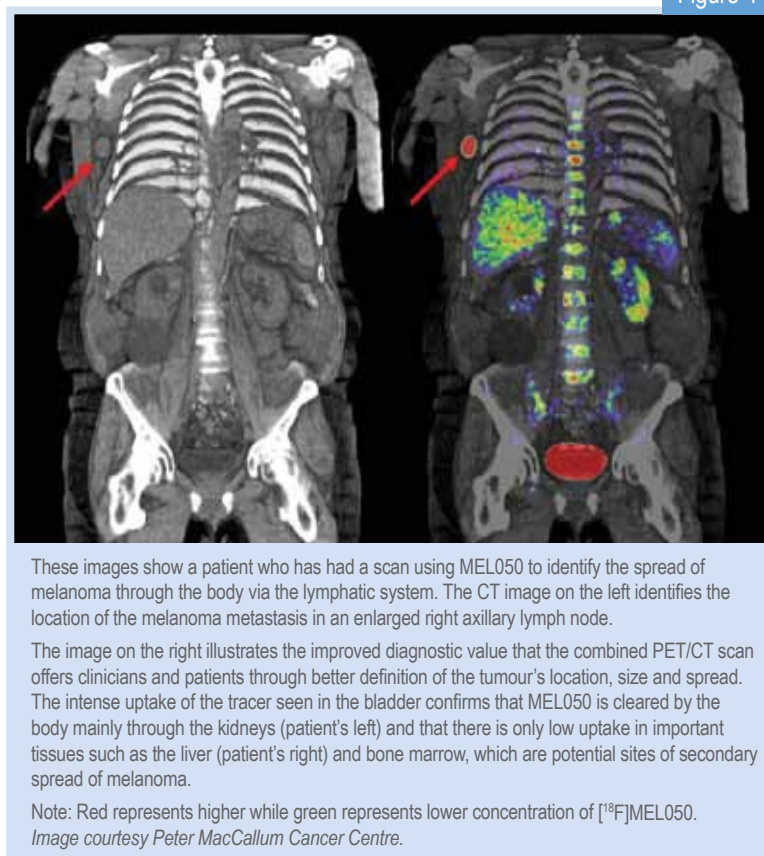
Histological examination of tumour samples indicated an absence of melanin. In contrast, three patients with melanin detected at pathological tumour evaluation had high [¹⁸F]Mel050 uptake in their [¹⁸F]FDG-positive lesions.

Next steps

It was somewhat surprising that our small patient study had a high percentage of patients with amelanotic tumours, however this finding may reflect the biology of the tumours at more advanced clinical stages. If identifying patients with amelanotic tumours had prognostic significance, i.e., had a poorer prognosis, [¹⁸F]Mel050 could provide additional critical staging information to the standard patient work-up. [¹⁸F] Mel050 could also be an effective means of following therapeutic efficacy of new therapies that are targeted to melanin.

Lastly, as indicated above, the survival rate for patients with metastatic melanoma is poor. Work has continued to develop a radiotherapeutic derivative of Mel050 to treat patients with melanoma. We are designing Mel050 analogues labelled with therapeutic radionuclides: ¹³¹I, ¹⁷⁷Lu or ⁹⁰Y to achieve favourable biodistribution characteristics.

Figure 4



This would be high tumour residence time (high radiation to the tumour) and low normal tissue uptake (low radiation to normal tissue). These new treatments could provide hope to the patients afflicted with this disease.

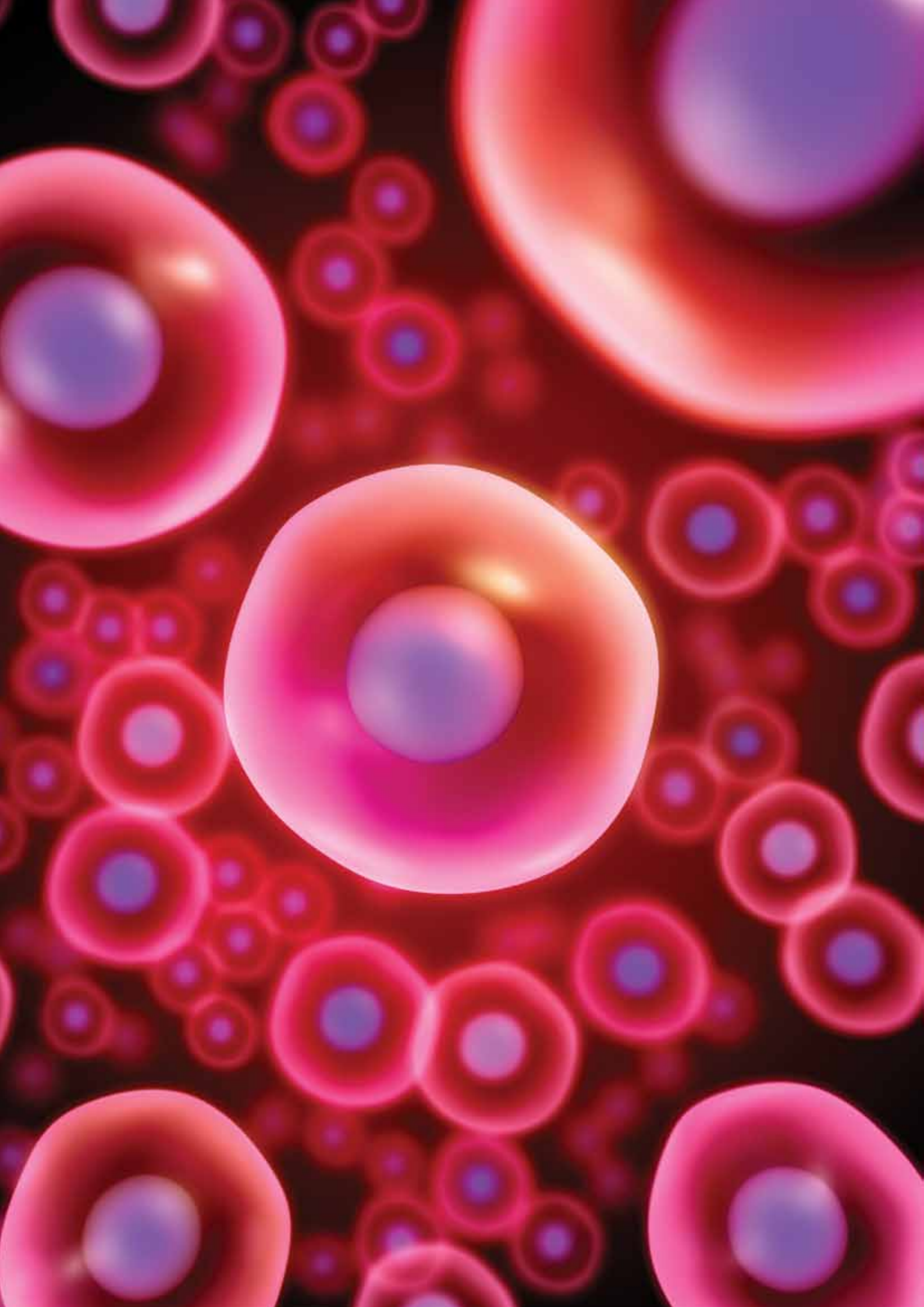
Table 1

Biodistribution of [¹⁸ F]Fluoronicotinamides ^a					
Compound	tumour	eye	thyroid	stomach	bone
[¹⁸ F]Mel050					
Time (h)					
0.25	7.0 ± 0.9	14.7 ± 0.5	5.5 ± 0.8	9.4 ± 1.1	3.5 ± 0.2
1	8.4 ± 1.5	18.8 ± 2.4	3.3 ± 3.7	3.4 ± 0.9	1.4 ± 0.3
3	7.8 ± 1.4	17.3 ± 3.1	0.49 ± 0.33	0.83 ± 0.55	0.62 ± 0.19
[¹⁸ F]4					
0.25	4.0 ± 1.4	11.3 ± 2.6	10.2 ± 6.7	8.5 ± 3.1	3.9 ± 0.5
1	4.8 ± 1.1	12.7 ± 1.2	5.4 ± 2.9	3.3 ± 0.9	2.0 ± 0.1
3	5.3 ± 1.3	14.3 ± 2.1	2.9 ± 1.3	2.4 ± 0.9	1.4 ± 0.3
[¹⁸ F]6					
0.25	10.6 ± 2.9	36.7 ± 7.1	4.5 ± 1.0	14.7 ± 1.6	4.8 ± 0.3
1	14.6 ± 5.1	38.0 ± 4.3	2.2 ± 0.4	6.8 ± 1.8	3.4 ± 0.2
3	17.3 ± 1.7	36.3 ± 2.8	2.1 ± 0.4	1.9 ± 1.4	4.6 ± 0.2
[¹⁸ F]8					
0.25	7.0 ± 0.9	17.3 ± 2.1	4.8 ± 0.4	13.2 ± 1.6	4.0 ± 0.3
1	12.2 ± 3.3	23.7 ± 1.2	2.2 ± 0.4	5.3 ± 1.5	1.5 ± 0.1
3	8.8 ± 3.0	18.8 ± 1.2	1.5 ± 0.5	0.82 ± 0.36	0.77 ± 0.13

^a Data are the means of %ID/g of tissue ±SD; n = 5. B16F0 melanoma tumour in C57BL/6J mice.

References

- [1] Cummins, D. L., Cummins, J. M., Pantle, H., Silverman, M. A., Leonard, A. L., & Chanmugam, A. (2006). Cutaneous malignant melanoma. *Mayo Clinic Proceedings*, 81(4), 500-507.
- [2] Liu, X., Pham, T. Q., Berghofer, P., Chapman, J., Greguric, I., Mitchell, P., et al. (2008). Synthesis and evaluation of novel radioiodinated nicotinamides for malignant melanoma. *Nuclear Medicine and Biology*, 35(7), 769-781.
- [3] Belhocine, T. Z., Scott, A. M., Even-Sapir, E., Urbain, J. L., & Essner, R. (2006). Role of nuclear medicine in the management of cutaneous malignant melanoma. *Journal of Nuclear Medicine*, 47(6), 957-967.
- [4] Hafner, J., Schmid, M. H., Kempf, W., Burg, G., Kunzi, E., Meuli-Simmen, C., et al. (2004). Baseline staging in cutaneous malignant melanoma. *British Journal of Dermatology*, 150(4), 677-686.
- [5] Greguric, I., Taylor, S. R., Denoyer, D., Ballantyne, P., Berghofer, P., Roselt, P., et al. (2009). Discovery of [¹⁸F]N-(2-(diethylamino)ethyl)-6-fluoronicotinamide: A melanoma positron emission tomography imaging radiotracer with high tumour to body contrast ratio and rapid renal clearance. *Journal of Medicinal Chemistry*, 52(17), 5299-5302.
- [6] Denoyer, D., Greguric, I., Roselt, P., Neels, O. C., Aide, N., Taylor, S. R., et al. (2009). High contrast PET imaging of melanoma using [¹⁸F]MEL050, a selective probe for melanin with predominantly renal clearance. *Journal of Nuclear Medicine*, 51(3), 441-447.
- [7] Greguric, I., Pham, T. Q., Liu, X., & Katsifis, A. (2008). Nicotinamide Derivatives for imaging and therapy of melanoma. Patent No: 2008901989.
- [8] Garg, S., Kothari, K., Thopate, S. R., Doke, A. K., & Garg, P. K. Design, synthesis, and preliminary in vitro and in vivo evaluation of N-(2-diethylaminoethyl)-4-[¹⁸F]fluorobenzamide ([¹⁸F]-DAFBA): a novel potential PET probe to image melanoma tumors. *Bioconjugate Chemistry*, 20(3), 583-590.
- [9] Pham, T. Q., Berghofer, P., Liu, X., Greguric, I., Dikic, B., Ballantyne, P., et al. (2007). Preparation and biologic evaluation of a novel radioiodinated benzylpiperazine, 123I-MEL037, for malignant melanoma. *Journal of Nuclear Medicine*, 48(8), 1348-1356.
- [10] Denoyer, D., Potdevin, T., Roselt, P., Neels, O. C., Kirby, L., Greguric, I., Katsifis, A., Dorow, D. S., Hicks, R. J. (2011). Improved detection of regional melanoma metastasis using 18F-6-fluoro-N-[2-(diethylamino)ethyl] pyridine-3-carboxamide, a melanin-specific PET probe, by perilesional administration. *Journal of Nuclear Medicine* Jan;52(1):115-22.



Understanding molecular mechanisms to aid in the protection of cell membranes in anhydro and cryo-biology

Christopher J. Garvey¹, Thomas Lenné^{2,3}, Ben Kent^{1,3}, Taavi Hunt³ and Gary Bryant³

¹ANSTO, ²ANU Canberra, ³RMIT Melbourne

Cell membranes exist as selective barriers between the cell cytoplasm, and various intracellular compartments and the extracellular world. Maintaining the correct functioning of this permeability barrier is a key issue in the viability of the cell after cooling and/or drying.

Our current work aims at understanding fundamental questions in membrane biophysics in the context of scientific problems arising around cell-membrane behaviour at low temperatures (cryo-biology) and at low water contents (anhydro-biology).

We looked into the effects of small solute molecules in terms of the stability of membranes and the redistribution of water and various sugars during both dry and cold environments.

Measurements resolving important intermolecular distances, have been used to build a theoretical model for effects of sugars on the rearrangement of lipids during dehydration and the consequential loss of membrane integrity under these conditions.

The effects of drying and freezing on membranes

In slow drying conditions, as is normally found in the natural environment, and at temperatures above the formation of a glassy state, molecular mobility comes to a halt. Small solute molecules, typically sugars, are used by organisms which live and reproduce in very cold and dry environments to protect their membranes from these deleterious phase transitions [1].

In this case one can assume that water potentials in a solution have come to equilibrium and solutes (substances dissolved in water) do not redistribute across the membrane appreciably during the drying process.

The effects of slow cooling are equivalent to slow drying. When ice forms in the extracellular solution the concentration of extracellular solutes is increased, and because the membrane is quite permeable to water, water may be drawn out of the cell much more quickly than solutes are transported in.

As further freezing occurs, more water is drawn out of the cell. Thus the net effect of freezing on slow timescales is to dehydrate and contract the volume of

the intracellular solution inside the cell and is in fact similar to the effects of drying. The most evident impact of this are changes in the way lipids are packed into bilayers and other structures.

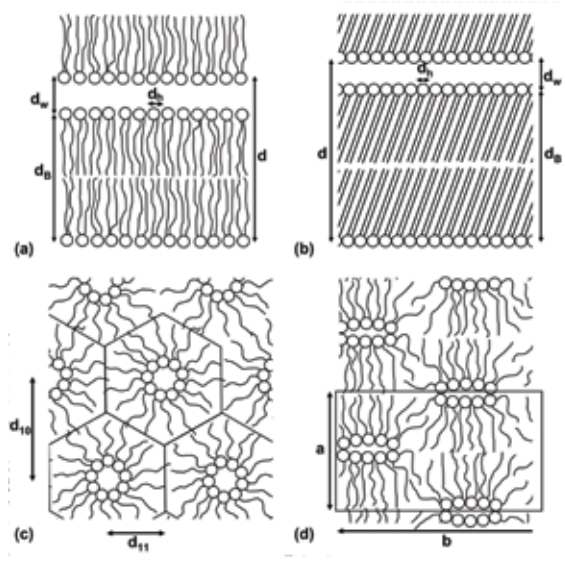
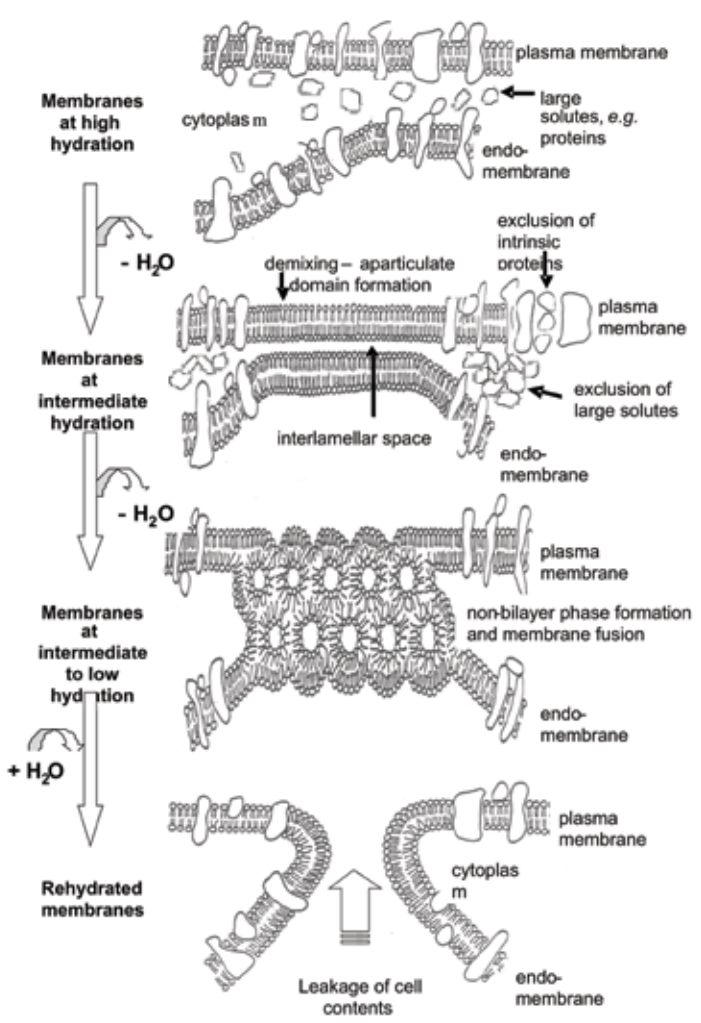
Lipids are the major structural components of cell membranes but also represent a broad group of important signalling molecules for biological functions such as energy storage. Fig. 1 depicts these effects and subsequent interactions.

Quantifying these effects with X-ray and neutron scattering

Scattering techniques, particularly X-rays and neutrons, can be used as diagnostic of the phase of the lipids providing a method for measuring the distances shown in the right-hand side of Fig. 1. In Fig. 2, we show X-ray measurements from which we can extract structural details relating to the shape and spatial relationships between coexisting phases, particularly when deuteration and contrast variation are applied [2-6].

Two very important structural parameters easily calculated from the position of diffraction peaks,

Figure 1



The left-hand side shows a diagram of the effects of slow drying and cooling on the cell membrane. The generation of compressive forces in the plane of the membrane by inter-membrane interactions, and subsequent phase transitions in the membrane lead to the loss of membrane integrity and functionality.

The dimensions of cells are 1/10's to micron size. The important length scales shown in the right-hand side, the lipids phases associated with freezing or desiccation induced cellular damage, are of the order of nanometers for a single bilayer:

- a) the fluid lamella phase is associated with normal functioning and consists of alternating layers of lipid bilayers (thickness, d_b) and water (thickness, d_w) and separation between head groups, d_h . In the fluid lamella phase the tail chains are packed rather randomly in the hydrophobic phase;
- b) the gel lamella phase is very similar in geometry with the difference being a closer packing of head groups and a more ordered lipid phase [1];
- c) the hexagonal phase causes loss of continuity of the lipid membrane and is characterised by a hexagonal symmetry with two characteristic repeat distances. Each hexagon has at its centre a circular channel projecting out of the page surface; and the ribbon phase where the unit cell is again characterised by two characterised by repeat distances [2];
- d) A ribbon-like channel is formed by lipid head-groups and projects out of the page [3].

see Fig. 2c, are: (i) the average chain-chain lateral spacing which can be used to estimate the average head-group spacing d_h – see Fig. 1a, and (ii) the bilayer repeat spacing d , which can be used to estimate d_w and d_b [1].

In addition, we used small-angle neutron scattering (SANS) with contrast variation (neutrons can distinguish between different elements and their isotopes) to investigate the partitioning of sugar molecules between the water between bilayers and the channels in the hexagonal phase (Fig. 1a) and a bulk aqueous phase which is not shown in the figure [5,6].

Fig. 2 shows how the scattering data can be interpreted to obtain the important information on the spacing in the lipid phases. Based on the distances measured and the partitioning of sugar we have developed a detailed and successful theoretical model to explain the effects of sugars in the bilayer system [2].

X-ray Scattering patterns from the area detector of a pin-hole SAXS camera (ID15 beam line, Advanced Photon Source, Argonne, USA) from dipalmitoylphosphatidylcholine:

- a) in the fluid phase at 70°C and
- b) in the gel phase at 20°C, both are the results of 10 second exposures.

The pin-hole scattering data is radially symmetric and together with the experimental geometry and wavelength of the scattered radiation we could produce the radial average shown in c).

The positions of the peaks are used to calculate the spacing of the inter-lamellar and lipid-packing shown in Figure 1 under conditions of dehydration and cooling, where cooling causes a more efficient packing of lipids and shift of peaks to the right.

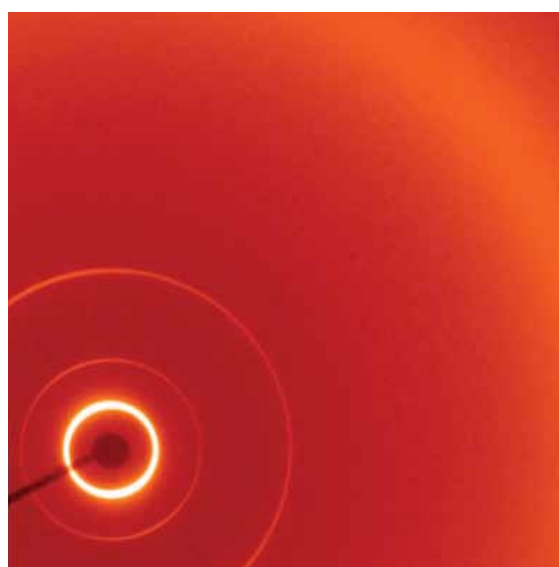
Next steps

We intend to further our understanding of physical changes in membranes, particularly lipid packing, in anhydro and cryo-biology by looking at the role of lateral phase separation (lipid rafts). With the ability to deuterate various biomolecules at the National Deuteration Facility combined with neutron-scattering techniques, we particularly develop techniques for studying large unit-cells (*cf* Fig. 1) at higher resolution than is available with conventional small-angle neutron scattering.

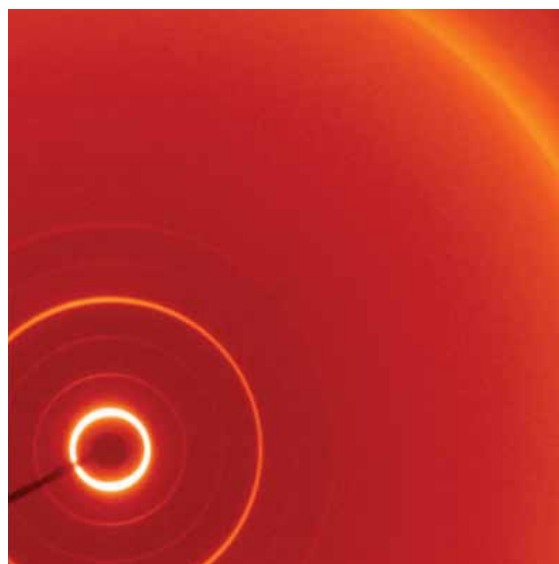
In addition, we study lateral order in oriented systems such as bilayers by grazing-incidence scattering and off-specular reflectivity techniques.

References

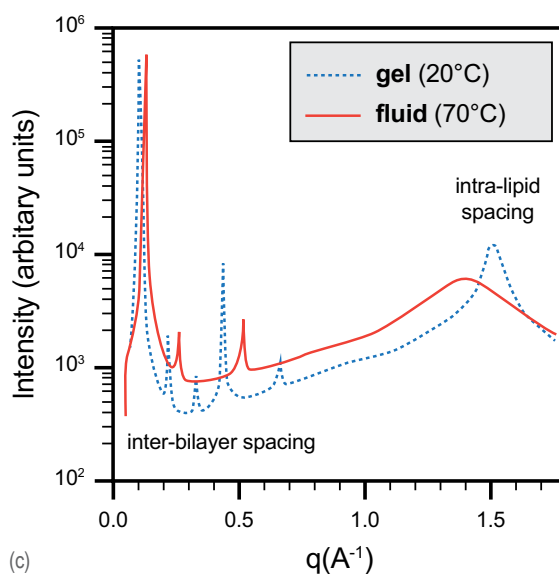
- [1] Andersen, H. D., Wang, C., Arleth, L., Peters, G. H., & Westh, P. (2011). Reconciliation of opposing views on membrane-sugar interactions. *Proceedings of the National Academy of Sciences (PNAS)*, 108(5), 1874-1878.
- [2] Lenné, T., Garvey, C. J., Koster, K. L., & Bryant, G. (2009). Effects of sugars on lipid bilayers during dehydration - SAXS/WAXS measurements and quantitative model. *Journal of Physical Chemistry B*, 113(8), 2486-2491.
- [3] Kent, B., Garvey, C. J., Lenné, T., Porcar, L., Garamus, V. M., & Bryant, G. (2010). Measurement of glucose exclusion from the fully hydrated DOPE inverse hexagonal phase. *Soft Matter*, 6(6), 1197-1202.
- [4] Kent, B., Garvey, C. J., Cookson, D., & Bryant, G. (2009). The inverse hexagonal - inverse ribbon - lamellar gel phase transition sequence in low hydration DOPC:DOPE phospholipid mixtures. *Chemistry and Physics of Lipids*, 157(1), 56-60.
- [5] Lenné, T., Bryant, G., Garvey, C. J., Keiderling, U., & Koster, K. L. (2006). Location of sugars in multilamellar membranes at low hydration. *Physica B: Condensed Matter*, 385-386(2), 862-864.
- [6] Lenné, T., Garvey, C. J., Koster, K. L., & Bryant, G. (2010). Kinetics of the lamellar gel-fluid transition in phosphatidylcholine membranes in the presence of sugars. *Chemistry and Physics of Lipids*, 163(2), 236-242.



(a)



(b)



(c)



Next generation radiopharmaceuticals will provide better health outcomes for Australians.

Identifying optimal conditions for the production of next generation radiopharmaceuticals

Van So Le

ANSTO

State-of-the-art radiopharmaceutical development requires radioisotopes of optimal specific radioactivity to maximize radiopharmaceutical uptake in the body. Specific radioactivity is the ratio of radioactive atoms to the sum of non-radioactive and radioactive atoms of the chemical element. Optimising specific radioactivity allows more radioactive atoms to be delivered to the tumour. This enhances the image quality in patient scanning and improves effectiveness of endo-radiotherapy (tumour cell killing using internally deposited radiation) treatments.

In general terms, high specific radioactivity is important because it increases the fraction of radioactive atoms bound to the radiopharmaceutical precursor. This increases labelling efficiency, and reduces the amount of precursor necessary to maintain efficiency. Additional precursor could have deleterious side effects when injected into patients. High specific radioactivity ^{177}Lu is a prerequisite to formulate radiopharmaceuticals targeting tumours for several different cancer treatments (neuroendocrine tumours, breast and colon cancer, and lymphomas).

Radioisotopes can be produced from a range of sources; cyclotrons, radionuclide generators and nuclear reactors. The advantages of nuclear reactors are large production capacity, easy target preparation and irradiation and robust operation.

The current expansion of targeted endo-radiotherapy is dependent on the availability of high specific radioactivity radioisotopes (such as $^{188}\text{W}/^{188}\text{Re}$, ^{90}Y and ^{177}Lu) which can be produced in nuclear research reactors.

The yield (activity produced for each target irradiation or generator elution) of radioisotope production from cyclotrons, radionuclide generators and nuclear reactors is usually the only parameter used to justify using a particular nuclear reaction [1].

While the conventional yield evaluation provides high quantities of activity, it is insufficient to set up the optimal conditions for producing radionuclide products of the desired radiochemical quality. It does not take account of undesirable effects, e.g. target impurities and unwanted radioactive transformations.

Alternatively, we can assess the specific radioactivity by dealing with the relationship between the affecting factors and the inherent properties of the target.

Assessing this relationship we can optimise the irradiation for production of the highest specific radioactivity radioisotopes for various applications. This is especially true for receptor/antigen targeted radiopharmaceutical preparation.

In addition, this method plays a complementary or even substantial role in the quality management and subsequent certification regarding the radioisotope product. For example, based on our theoretical specific radioactivity assessment results, we could calculate optimal conditions to produce ^{177}Lu suitable for radiopharmaceutical preparations for targeted endoradiotherapy.

Better technology performance of radioisotope production, example ^{177}Lu

The specific activity assessment of radioisotopes produced in a neutron-activated target is a complex issue and has not yet been fully solved. The targets used in the production of short-lived medical radioisotopes usually have high neutron-capture cross-sections. Neutrons are readily absorbed by the target atoms and facilitate the conversion to the radionuclide.

These high cross section will provide the highest possible SA values. This fact causes a high “real” burn-up (conversion) of the target element. In particular, the short half-life of the beta-emitting radioisotope produced in the target hastens the transformation of the target nuclide to the produced radioisotope which in turn strongly affects the SA.

Neutron-capture characteristics, target impurities, side nuclear reactions, target burn-up and post-irradiation processing/cooling time are the main parameters affecting the SA of the radioisotope product. As a result of our recent study, these parameters have been incorporated into the format of mathematical equations for the reaction yield and SA assessment [2].

In this study, SA assessment was performed on the production of ^{177}Lu from ^{176}Lu and ^{176}Yb enriched targets. The irradiation conditions required for achieving a maximum yield and maximum SA value and the effect of several factors (such as elemental Lu and $^{174}\text{Yb}/^{175}\text{Lu}$ isotopic impurities) on the reduction of ^{177}Lu

SA were evaluated. ^{177}Lu is a radioisotope of choice for endo-radiotherapy because of its favourable decay characteristics: a medium-energy beta decay of 497 keV with moderate range in tissue and half-life of 6.71 days. It also emits gamma rays of 113 keV and 208 keV which make it useful for imaging *in vivo* localisation with a gamma camera.

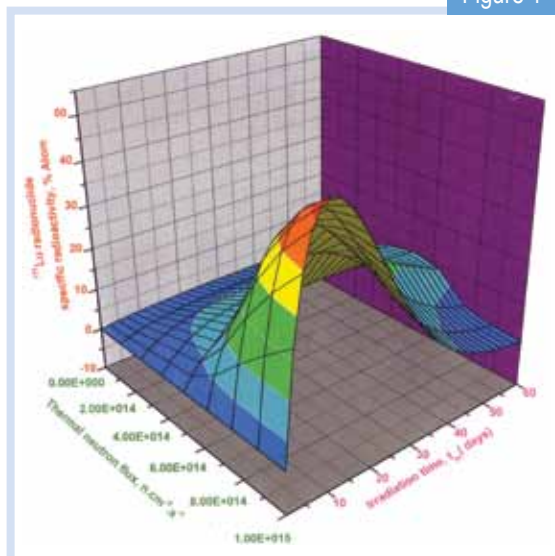
^{177}Lu can be produced by two different routes, a direct route with the $^{176}\text{Lu} (n, \gamma) ^{177}\text{Lu}$ reaction and an indirect route via the $^{176}\text{Yb} (n, \gamma) ^{177}\text{Yb} (\beta \text{ decay}) \rightarrow ^{177}\text{Lu}$ nuclear reaction-transformation. The direct route could be successfully performed in high neutron-flux nuclear reactors but these are available in only a handful of countries in the world.

Additionally, large burn-up of the target nuclide during high neutron-flux irradiation may cause a decrease in the specific radioactivity of the produced nuclide if the target contains isotopic impurities. The indirect route is used for production of “no carrier-added” ^{177}Lu of higher specific radioactivity. In this case, the same reduction in specific radioactivity can occur if the target contains isotopic and/or elemental Lu impurities.

While being the best theoretical way to produce no carrier-added ^{177}Lu with this reaction, we always obtain a ^{177}Lu product of much lower specific radioactivity due to the use of an isotopically/elementally impure target.

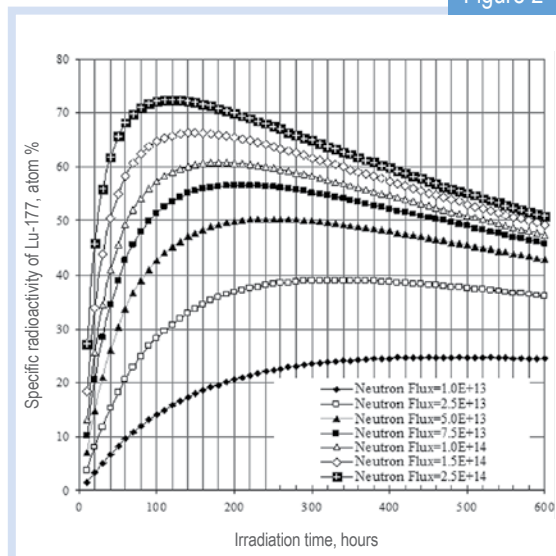
Based on the theoretical SA assessment results obtained in our report, the optimal conditions for ^{177}Lu production were set up to maximize the production of high specific radioactivity ^{177}Lu product [2].

Figure 1



Specific radioactivity of ^{177}Lu produced from ^{176}Lu targets as function of the irradiation time and thermal neutron flux, Target composition: 74.1% ^{176}Lu and 25.9 % ^{175}Lu .

Figure 2



Specific radioactivity of ^{177}Lu produced from ^{176}Yb target as function of the irradiation time and thermal neutron flux; target composition: 97.6% ^{176}Yb , 1.93% ^{174}Yb and 50 parts per million Lu impurities.

Figure 3



Equipment for production of ^{177}Lu solution of high SA from $^{176-175}\text{Yb}$ target bombarded with the OPAL reactor neutron flux.

Theoretical approach and methods of SA assessment [2]

Reactor-based radioisotope production usually involves two main nuclear reactions. The first one is the thermal neutron-capture (n, γ) reaction. This reaction (direct, see above example) does not lead to a radioisotope of another chemical element, but following radioactive β decay of this isotope during target activation results in a decrease in both the reaction yield and atom numbers of the target chemical element.

The second reaction (indirect, see above example) is thermal neutron-capture followed by radioactive transformation $S (n, \gamma) R_x (\beta\text{-decay}) R_1$ (S is non-radioactive target nuclide; (n, γ) neutron-capture nuclear reaction; R_x short-lived intermediate radioactive nuclide; R_1 product radioisotope). This reaction leads to a no carrier-added radioisotope (R_1) of another chemical element than the target chemical element (S). The specific radioactivity assessment in the radioisotope production using the first reaction (with a simple target system) is simple. Careful targetry could avoid the side reaction $S (n, \gamma) R_y (\beta\text{-decay}) R$ which could result in the isotopic impurities R for the radioisotope R_1 intended to be produced using the first reaction.

In this case, the specific radioactivity assessment can be simplified by investigation of the decline in specific radioactivity due to target nuclide burn-up, chemical element depression due to radioactive decay and isotopic impurities present in the target.

On the other hand the SA assessment in the radioisotope production using the second reaction (with complex target system) is more complicated. The complexity of this targetry requires an analysis of the combined reaction system.

We can assess the effect of side nuclear reactions in this target system in addition to the three above mentioned factors that are involved in the simple target system. In this case, the specific radioactivity assessment is best resolved by a comprehensive method of specific radioactivity calculation.

The complex target system is considered as a mixture of several radioactive sources of variable specific radioactivity; details on the method of specific radioactivity assessment for this mixture is formulated in reference [2].

Figures show the results of our calculations to determine the specific radioactivity of ^{177}Lu radioisotope produced by the direct (fig. 1) and indirect (fig. 2) route as a function of the elemental and isotopic impurities of the ^{176}Yb enriched target, the irradiation time t_{irr} and neutron flux [2].

A defined maximum specific radioactivity value for each target and its irradiation condition and neutron flux

was found for both production routes suggesting that the irradiation time could be optimised to obtain the highest specific radioactivity of ^{177}Lu . The maximum specific radioactivity value was affected by a combined effect of ^{174}Yb and elemental Lu impurities.

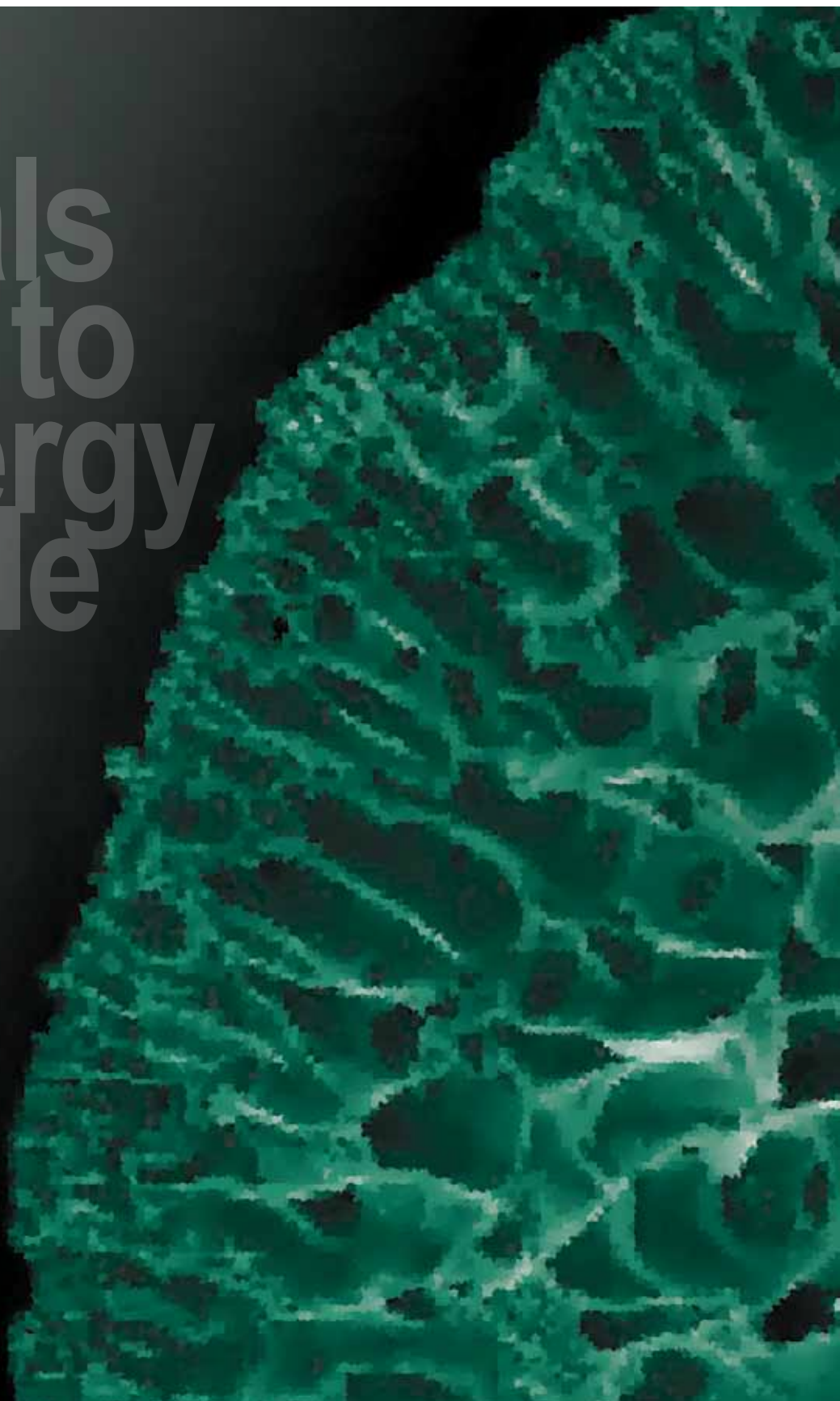
However, these results are only valid for a specific target composition and its neutron-irradiation conditions. This theoretical assessment of specific radioactivity maximization is critical before starting the neutron-activation process. The optimised process would avoid lowering the specific radioactivity of ^{177}Lu product by over-bombardment, and also avoid wasting expensive reactor-operation time.

Lastly, the post-irradiation processing time should be minimised to keep the specific radioactivity as high as possible. Fig. 3 shows an automated system for production of high specific radioactivity ^{177}Lu . Besides enhancing the speed of purification, this system has the added benefit of reducing operator absorbed dose. The details of this process have been presented in a number of previous publications [3-5].

References

- [1] Rubinson, W. (1949). The Equations of Radioactive Transformation in a Neutron Flux. *Journal of Chemical Physics*, 17(6), 542.
- [2] Le, V. S. (2011). Specific radioactivity of neutron induced radioisotopes: assessment methods and application for medically useful ^{177}Lu production as a case. *Molecules*, 16(1), 818-846.
- [3] Le, V. S. (2008). Alternative chromatographic processes for no-carrier added ^{177}Lu radioisotope separation. Part I. Multi-column chromatographic process for clinically applicable. *Journal of Radioanalytical and Nuclear Chemistry*, 277(3), 663-673.
- [4] Le, V. S., Morcos, N., Zaw, M., Pellegrini, P., Greguric, I., & Nevissi, A. (2008). Alternative chromatographic processes for no-carrier added ^{177}Lu radioisotope separation. Part II. The conventional column chromatographic separation combined with HPLC for high purity. *Journal of Radioanalytical and Nuclear Chemistry*, 277(3), 675-683.
- [5] Le, V. S., & Morcos, M. (2008). New SPE column packing material: Retention assessment method and its application for the radionuclide chromatographic separation. *Journal of Radioanalytical and Nuclear Chemistry*, 277(3), 651-661.

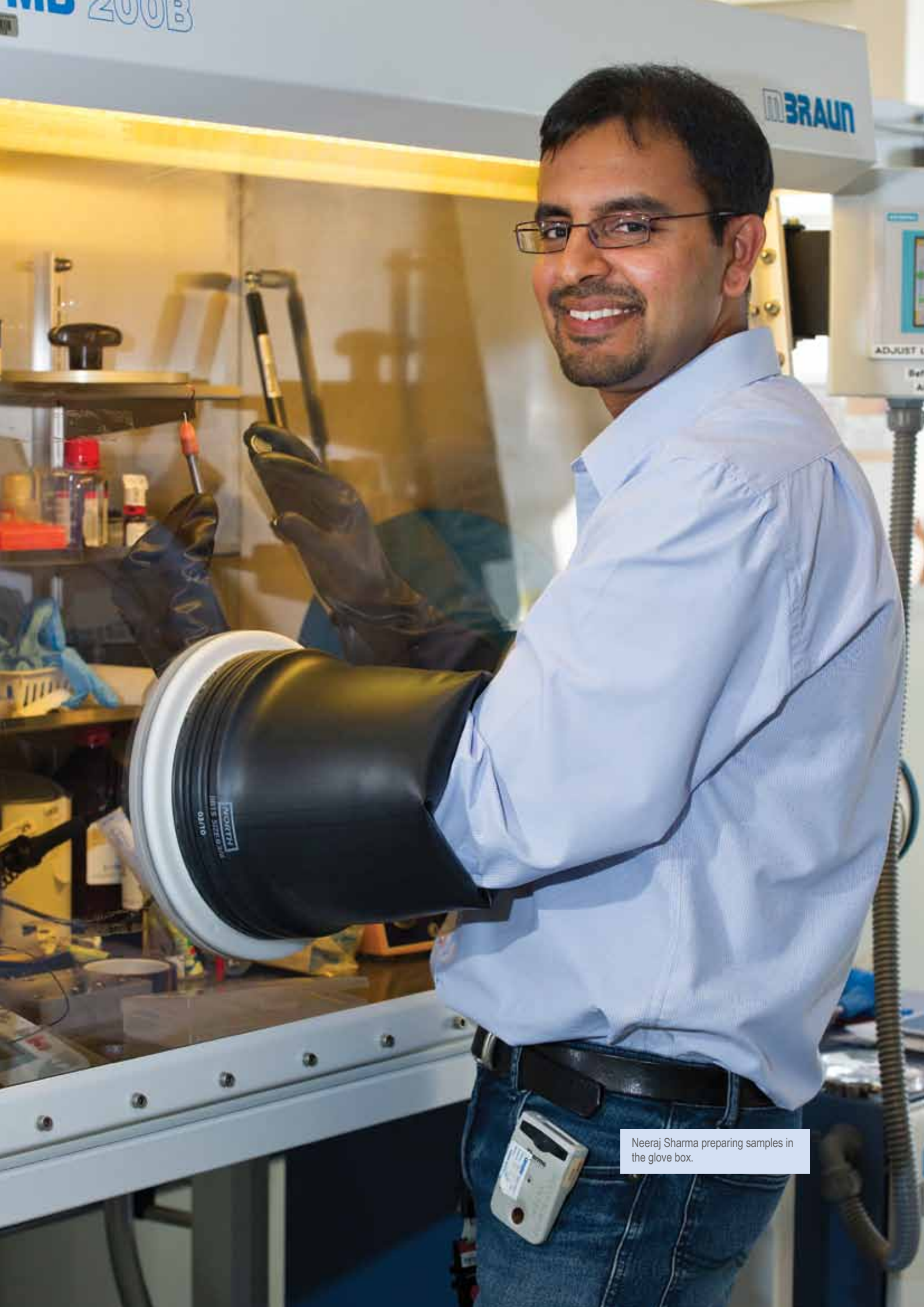
Materials related to the energy life-cycle



Materials related to the energy life-cycle

From improving the life of everyday lithium-ion batteries used to power mobile phones and laptop computers, to improving the flow of fuel in marine oil/gas pipelines on the ocean floor, ANSTO is using its world-class OPAL reactor and neutron beam instruments to undertake cutting-edge energy studies.

Although ANSTO does not produce nuclear power, our scientists are also working internationally to find ways of reducing the volume of nuclear waste produced by power reactors, and the amount of radiation damage caused during the nuclear energy production process.



Neeraj Sharma preparing samples in the glove box.

Making better Li-ion batteries using neutron diffraction

Neeraj Sharma and Vanessa K. Peterson

ANSTO

Most Australians own at least one Li-ion battery, usually in a mobile device, such as a mobile phone, portable media player, or a laptop computer. Soon Australians may be driving electric vehicles powered by Li-ion battery technology. Our research uses neutron diffraction to learn what happens to the molecular-scale structure of components within Li-ion batteries during use and re-charge.

We explore crystallographic features with respect to electrochemical properties and the mechanism of charge-transfer, in order to improve our understanding of the electrochemical performance of batteries. Here, we present some work undertaken with *in situ* and *ex situ* neutron diffraction on the instruments Wombat and Echidna, respectively, at the OPAL research reactor.

How do Li-ion batteries work?

We chose to investigate Li-ion batteries because of their current technological applications and due to their higher energy densities relative to other battery systems such as Ni-MH and Ni-Cd. Commercialisation of the first Li-ion battery began in the early 1990's in the form of a LiCoO₂ cathode and a graphite anode.

During charging, electricity is drawn into the battery from a power-point. The electrons induce a series of chemical reactions where positively charged Li-ions are transferred from the cathode material, via an electrolyte, to the anode material as a consequence.

During use of a battery (discharge) the reverse occurs and Li-ions are transferred back from the anode to the cathode, and electrons are provided to an external circuit, allowing us to power devices by using the stored electricity.

The relatively high energy-density of the Li-ion battery is a result of the low atomic mass of Li atoms and the ease at which Li can be transported into and out of electrodes and through electrolytes [1].

Presently, Li-ion battery research is focused on materials that show favourable electrochemical properties including investigations into new high-voltage cathode and low-voltage anode materials in order to enable the maximum voltage output.

For example, combining LiCoO₂ and graphite produces a 3.7 V battery, while combining LiMn₂O₄ and graphite produces a 4.5 V battery [2]. However, the practicality of a battery is not limited to its maximum voltage output.

Other factors that play a significant role in the useability of a battery include its ability to be re-charged and discharged thousands of times, its Li capacity, as well as the safety and environmental implications of the battery components.

What can neutron diffraction do for this research?

Neutrons are useful in Li-ion battery research as a result of their high sensitivity towards Li in comparison to other probes of matter such as X-rays. Furthermore, neutrons are highly penetrating, so the bulk materials are sampled rather than their surfaces. Using neutrons we can study whole commercially available batteries *in situ*.

Examples of batteries we have evaluated in charge-discharge cycles are shown in Fig. 1. There are two types of experiments that we routinely undertake using Echidna, the high-resolution powder diffractometer [3], and Wombat, the high-intensity powder diffractometer [4], and these are outlined below.

Figure 1



From left to right, a lithium battery using a metallic Li anode, a cylindrical or 18650 Li-ion battery with a graphite anode and LiCoO_2 cathode (a battery pack for electric vehicles is often composed of a number of 18650 batteries), a mobile phone (prismatic-type) Li-ion battery, a prismatic Li-ion battery with a graphite anode and LiMn_2O_4 cathode, and a laptop computer Li-ion battery.

Wombat experiments

In situ experiments undertaken on Wombat provide a method to directly link real-time changes in the crystal-structure of materials inside a battery to the electrochemical state of the battery. The compromise made to gain *in situ* capability comes in the form of our ability to resolve the structure of the battery components accurately. To help mitigate this, we use structural models determined *ex situ* (with Echidna) as a starting point and modify these as necessary to observe the affect of electrochemical activity (charge or discharge).

This approach has been used successfully to determine what happens to the electrode structures in a commercial Li-ion battery [5] during its use. In the discharged state, the anode consists of graphite, and as the battery was charged Li was inserted into the graphite resulting in an expansion of the anode.

This is observed by the reduction in the measured 2θ value of the (002) reflection for graphite shown in Fig. 2. The (002) reflection was found not to decrease in a continuous way during charging, but instead we find that the reflection position stabilises somewhat, before the relatively fast formation of a second phase, LiC_6 .

This indicates that the Li insertion mechanism into graphite does not correspond to a continuous linear expansion of graphite. One possible explanation for this behaviour is the formation of a surface layer that traps Li, inhibiting the flow of Li into the graphite.

Another possibility is that the first Li-ions inserted into graphite cause expansion of the material and the remaining Li-ions fill in the gaps. These possibilities will be investigated in future experiments.

At the cathode, which was composed of two types of LiCoO_2 , a series of reactions took place during charge-discharge of the battery, as shown in Fig. 3. Using *in situ* neutron diffraction we identified each phase as they changed with Li insertion and extraction (see top panels of Fig. 3) and followed these changes qualitatively through changes occurring to the lattice parameters of the crystal structure for each phase (corresponding to different forms of LiCoO_2).

We identified two reaction mechanisms for Li insertion. The first mechanism is solid-solution behaviour where Li is inserted and the lattice parameters increase or decrease to accommodate this. The second mechanism is two-phase behaviour where the first phase transforms into the second phase during Li insertion (see the regions labelled I+II and A+B in the top panels of Fig. 3).

Echidna experiments

Typically *ex situ* experiments are undertaken on Echidna, where we obtain high accuracy crystal-structure information. We can dope materials with a variety of cations and anions, aimed at improving the electrochemical performance of the material, and investigate how these dopants alter the material's structure.

Since the structural changes can be related to changes in the electrochemical performance (as measured using batteries assembled from these components) we can determine whether there is a structural reason why some of these materials show better electrical performance.

Another experimental approach using Echidna is to assemble an electrode and battery from the material after we have obtained high precision structural information. This way we can charge or discharge the electrode and then extract the electrode material from the battery and re-analyse it using Echidna to structurally characterise it in a different electrochemical state.

This approach is problematic as reactions can occur to the material during its extraction from the battery resulting in changes to its structure, limiting the validity of the relationship of the material's structure to its electrochemical state.

Next steps

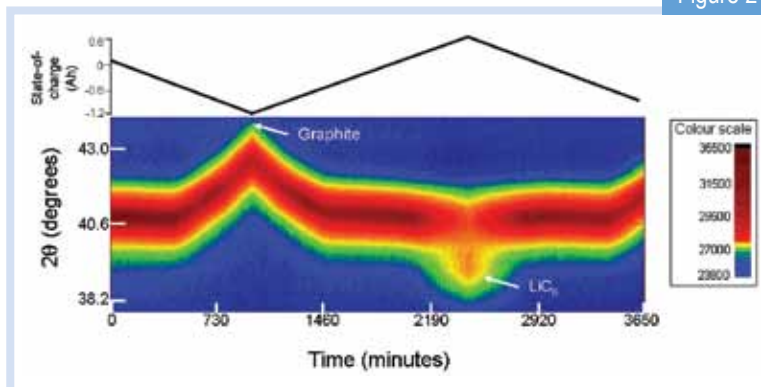
Our present focus is to develop designs for *in situ* electrochemical cells that resemble commercially available batteries but provide increased neutron-scattering signals from materials of interest. Using this approach we hope to gain more accurate structural information that will enable us to track Li in both known (as reported here) and new electrode materials (for which the crystal structures have not been previously characterised).

This is important as our *in situ* experiments have revealed transformation of electrode materials during battery operation to phases with crystal structures that are, at present, unknown.

References

- [1] Tarascon, J. -M., & Armand, M. (2001). Issues and challenges facing rechargeable lithium batteries. *Nature*, 414, 359-367.
- [2] Guyomard, D., & Tarascon, J. M. (1994). The carbon/Li_{1+x}Mn₂O₄ system. *Solid State Ionics*, 69(3-4), 222-237.
- [3] Studer, A. J., Hagen, M. E., & Noakes, T. J. (2006). Wombat: The high-intensity powder diffractometer at the OPAL reactor. *Physica B: Condensed Matter*, 385-386(2), 1013-1015.
- [4] Liss, K. D., Hunter, B., Hagen, M., Noakes, T., & Kennedy, S. (2006). Echidna—the new high-resolution powder diffractometer being built at OPAL. *Physica B: Condensed Matter*, 385-386(2), 1010-1012.

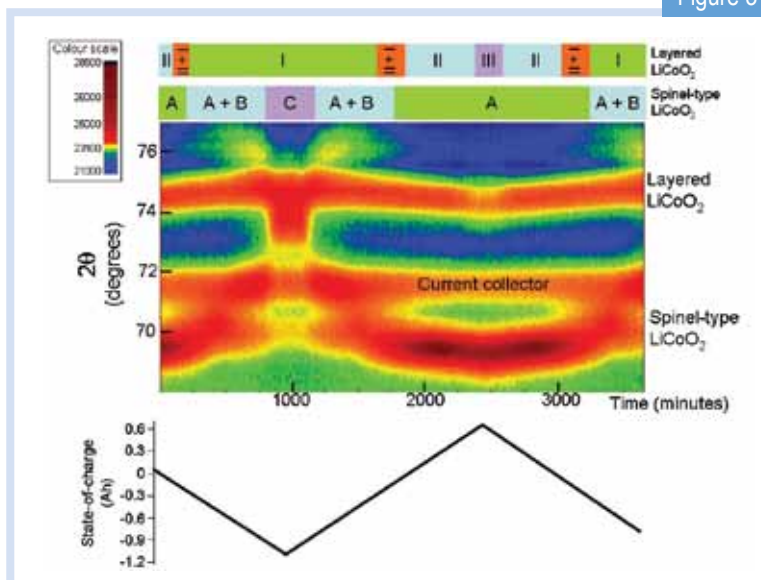
Figure 2



State-of-charge (top) and a selected 2D region of the *in situ* neutron diffraction patterns (bottom) highlighting the changes to the graphite (002) reflection. Pure graphite and LiC₁₂ are labelled, a colour scale is used to show peak intensity and the phases were identified and modelled using Rietveld analysis.

Rietveld analysis is used for modelling the crystal-structure of materials with the collected diffraction pattern [6-7]. There are 730 neutron diffraction patterns of 5 minute intervals in this figure. Figure taken from [5].

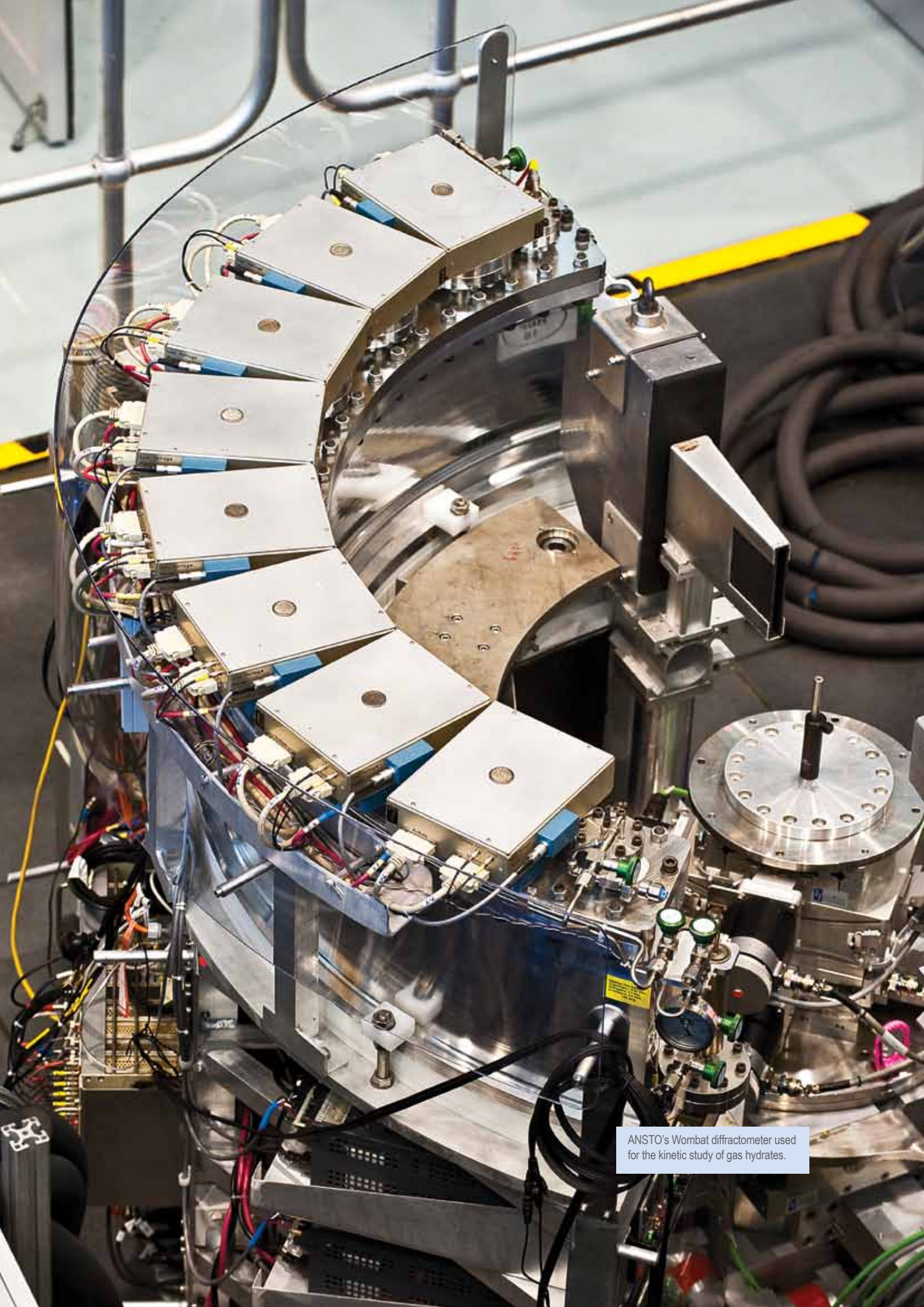
Figure 3



State-of-charge (bottom), selected 2D region of the *in situ* neutron diffraction patterns (middle) highlighting the changes to reflections assigned to the current collector, layered and spinel-type LiCoO₂, and the observed phase transitions (top).

A colour scale is used to show peak intensity and the phases were identified and modelled using Rietveld analysis. Figure taken from [5].

- [5] Sharma, N., Peterson, V. K., Elcombe, M. M., Avdeev, M., Studer, A. J., Blagojevic, N., et al. (2010). Structural changes in a commercial lithium-ion battery during electrochemical cycling: An *in situ* neutron diffraction study. *Journal of Power Sources*, 195(24), 8258-8266.
- [6] Rietveld, H. M. (1969). A profile refinement method for nuclear and magnetic structures. *Journal of Applied Crystallography*, 2(2), 65-71.
- [7] Young, R. A. (1993). *The Rietveld Method*. Chester, United States of America: Oxford University Press. 312p.



ANSTO's Wombat diffractometer used for the kinetic study of gas hydrates.

Understanding the kinetic processes of gas-hydrate formation in the marine environment

Shane Kennedy¹, Alice Klapproth^{1,2} and Ross Piltz¹

¹ANSTO, ²CSIRO

Gas-hydrates are found in nature, in deep ocean sediments and in permafrost, but are not stable at atmospheric temperature and pressure. They are also found in marine oil/gas pipelines on the ocean floor, where they can agglomerate into large solid plugs which stop the flow of fuel, and consequently are seen as a major risk for oil/gas industry exploitation.

Due to a lack of reliable information on the formation and dissociation of gas-hydrates, our understanding of the opportunities and risks presented by these compounds is limited. As neutrons are very sensitive to the structure and dynamics of hydrogenous media, we have embarked on an investigation of the kinetic processes of gas hydrates using the neutron-beam instruments at the OPAL research reactor.

The impact of gas-hydrates

Gas-hydrates (or clathrate hydrates) are inclusion compounds, which form at low temperature and elevated pressure from the action of water molecules encapsulating gases of suitable size and shape (e.g. methane, propane or carbon dioxide). Naturally occurring gas hydrates, containing mostly methane, are of particular interest in the energy sector as a potential future energy source, and environmental science as a geo-hazard.

Gas-hydrates pose a major risk of disruption to the marine oil and gas pipelines, see Fig. 1, through blockages and breakages. Due to a lack of understanding of hydrate formation and dissociation processes, the gas mining industry currently takes extreme measures to reduce the risk of hydrate formation. A clear understanding of these processes would allow implementation of effective strategies to avoid blockages in gas pipelines alleviating both economic and environmental concerns [1].

Neutrons scatter rather strongly from light elements like hydrogen and therefore they are a unique technique for investigating hydrates. In addition, they are a non-destructive probe for the study of the



Gas-hydrate shot plug being removed from a blocked pipeline.

structure and dynamics of hydrogenous media at the atomic and molecular scale. Consequently, ANSTO has initiated a comprehensive study of the kinetics of formation and dissociation of pure methane and methane-propane hydrates.

This joint research project with CSIRO aims to investigate the processes of formation and dissociation of gas-hydrates using the neutron-beam instruments at OPAL. Within that study we are comparing the effect of a range of known and potential inhibitors of gas hydrate formation processes using neutron diffraction and small-angle neutron scattering (SANS).

Figure 1

Figure 2

Hydrate formation

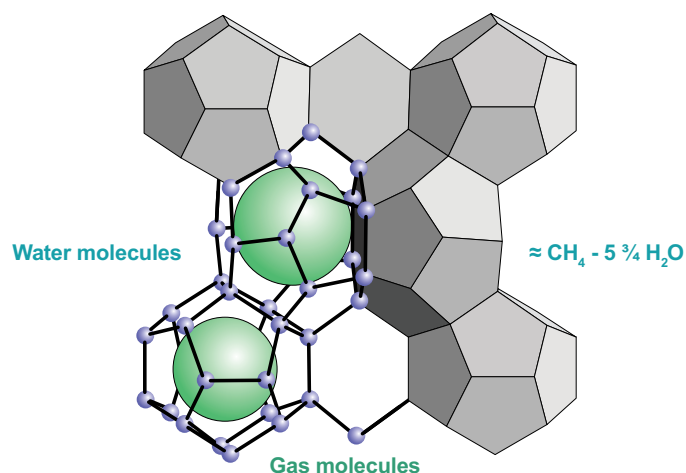
Fig. 2 (top) shows one of the known clathrate hydrate crystal structures with a methane guest molecule. There are several known hydrate structures stemming from different mixtures of cages that form around hydrocarbons of differing size and shape.

With increasing water depth, the temperature of the ocean decreases and the water pressure increases. Beyond depths of a few hundred meters, where the temperature drops to 4°C, the risk of gas hydrate formation in pipelines increases rapidly with depth (Fig. 2, bottom).

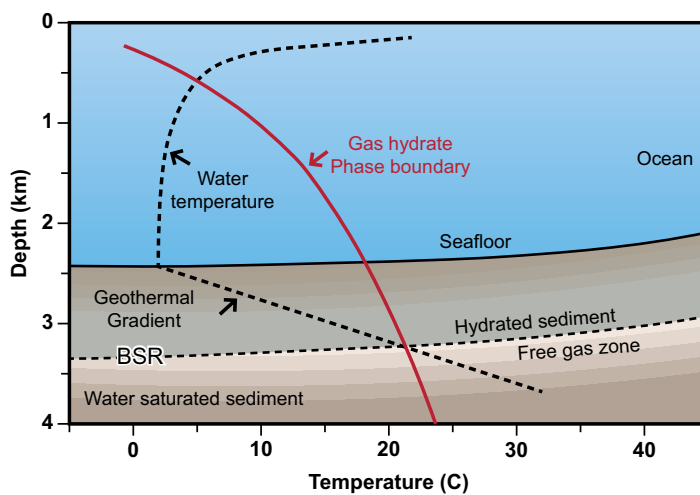
However, the probability of hydrate formation also depends on other factors, such as turbulence, or catalytic agents such as salts or other molecules that may be present in the gas or oil stream; hence posing a great challenge in view of replicating marine conditions.

Hydrate formation at the interface between water and hydrocarbon gases is quite rapid, but rates of gaseous diffusion into water are quite slow, and into solids are even slower. This means that, in the absence of turbulence gas hydrates only form thin layers (some microns in depth) on the surface of water droplets.

In the laboratory setting this means that gas hydrate will not form from bulk liquid water. Therefore we have seeded the hydrate formation process in the laboratory by starting with fine-ground ice crystallites. This forms hydrate crusts on the fine ice particles from which we can further study the formation process at the liquid-water interface by melting the remaining ice cores. Thus, we have been able to perform our experiments close to sub-sea geological conditions on the high-intensity neutron powder diffractometer Wombat, and the small-angle neutron scattering (SANS) instrument, Quokka.



Kuhs, W. F., Goettingen (Germany)



Kuhs, W. F., Goettingen (Germany)

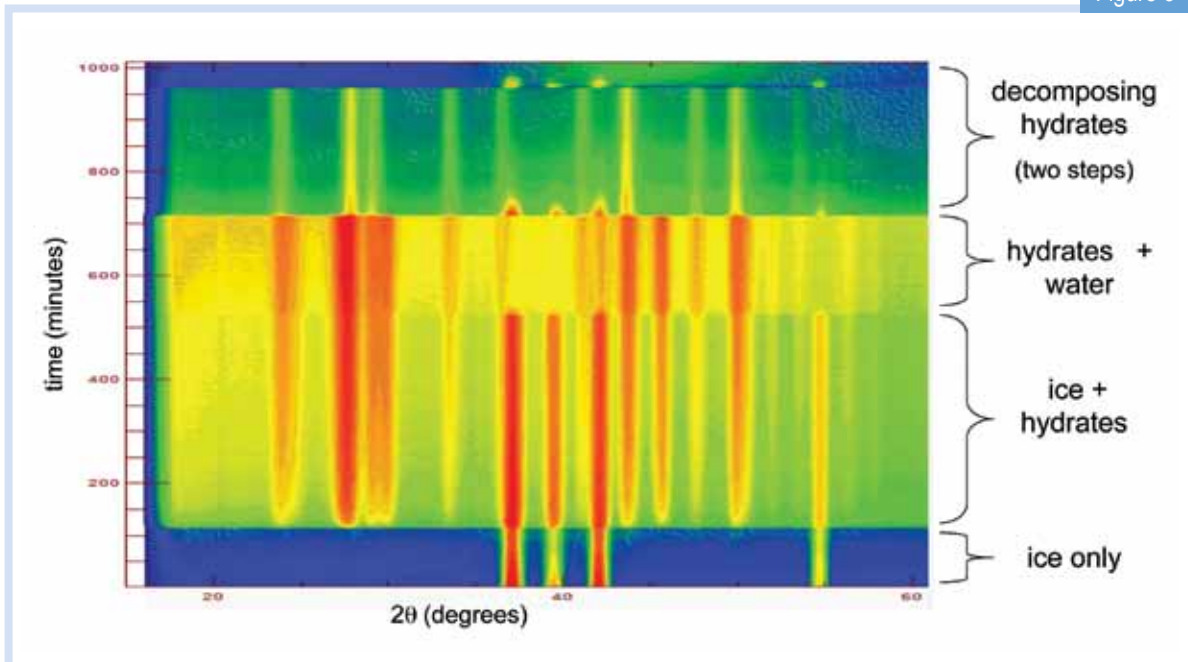
(Top) gas hydrate, where a methane guest molecule is caged by water molecules, and (bottom) chart showing the stability of gas-hydrate beneath the seafloor at mid-latitudes.

Experiments on Wombat

Our *in situ* experiments on *Wombat* provide insights into the kinetics of hydrate crystallite formation and dissociation, elucidating the thermodynamics of the reaction processes [2].

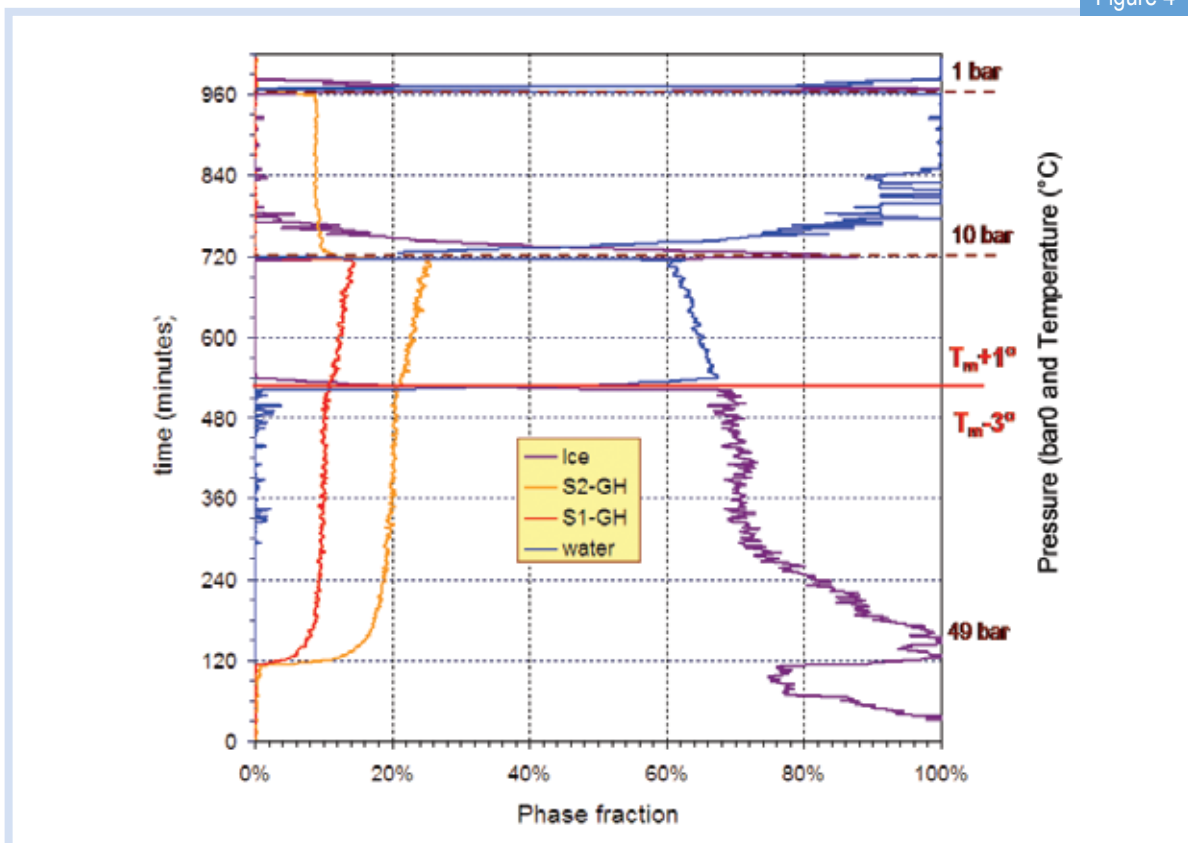
Fig. 3, which is a colour-contour map of the neutron diffraction patterns in a reaction between heavy water (D_2O) and high-pressure methane-propane gas, illustrates the formation process we observe.

Figure 3



Selected region of the Wombat diffraction patterns from hydrate formation by heavy water (D_2O) in methane-propane gas at pressures up to 49 bar.

Figure 4



Kinetics phase map of Ice, Type I & Type II hydrates and water, extracted from the neutron diffraction patterns of Figure 3.

Note D₂O is used instead of normal water due to its stronger diffraction signal, which leads to a higher sensitivity. In the figure, the stronger diffraction peaks are shown in red, and the green background indicates the presence on methane-propane gas at high pressure (49 bar).

Here, as we modify the temperature and pressure of the system, the diffraction reveals the kinetics of crystallisation of gas-hydrates; initially on the surface of ice crystallites and later from the interface between water and gas.

Finally, we see the dissociation of gas-hydrate on depressurisation, with a concomitant reformation of ice crystallites due to local cooling. In this example both hydrate structures Type I and Type II methane-propane hydrates form.

Fig. 4 displays the kinetics of the phase transformations that were extracted from the diffraction patterns shown in Fig. 3. In our neutron diffraction studies on Wombat, we have systematically varied temperature and pressure in a range of experiments to facilitate a mapping of dependencies of the chemical processes involved.

We observe a systematic increase in the rate of change of hydrate phase (either formation or dissociation) as we move away from the hydrate-H₂O phase boundary. We also note that the kinetics are more sensitive to temperature changes than to pressure changes. These observations hold for both Type I and Type II methane-propane hydrates.

Additional information on the role and efficacy of a thermodynamic inhibitor, mono-ethylene-glycol (MEG), and a kinetic inhibitor (Luvicap EG, BASF Corporation) were observed.

We note that the effect of the addition of MEG is in proportion to the shift in water-ice phase boundary, so that large concentrations (~ 10%) are needed to produce a noticeable change. In contrast, the kinetic inhibitor is more effective, such that even 0.5% of Luvicap EG added to the water, will retard the growth of crystallites from the liquid gas mixture. This is particularly noticeable for the Type I gas-hydrate phase.

Experiments on Quokka

Quokka is designed to detect structures and morphologies in the nanometre regime through SANS. With *in situ* SANS experiments we aim to probe the hydrate nucleation process, which precedes the crystallisation processes observed in diffraction experiments.

Our first SANS experiment on Quokka revealed rapid uptake of methane gas on ice crystallites well below the accepted phase boundary, offering the prospect of valuable insights in planned future experiments using a gas-liquid flow loop.

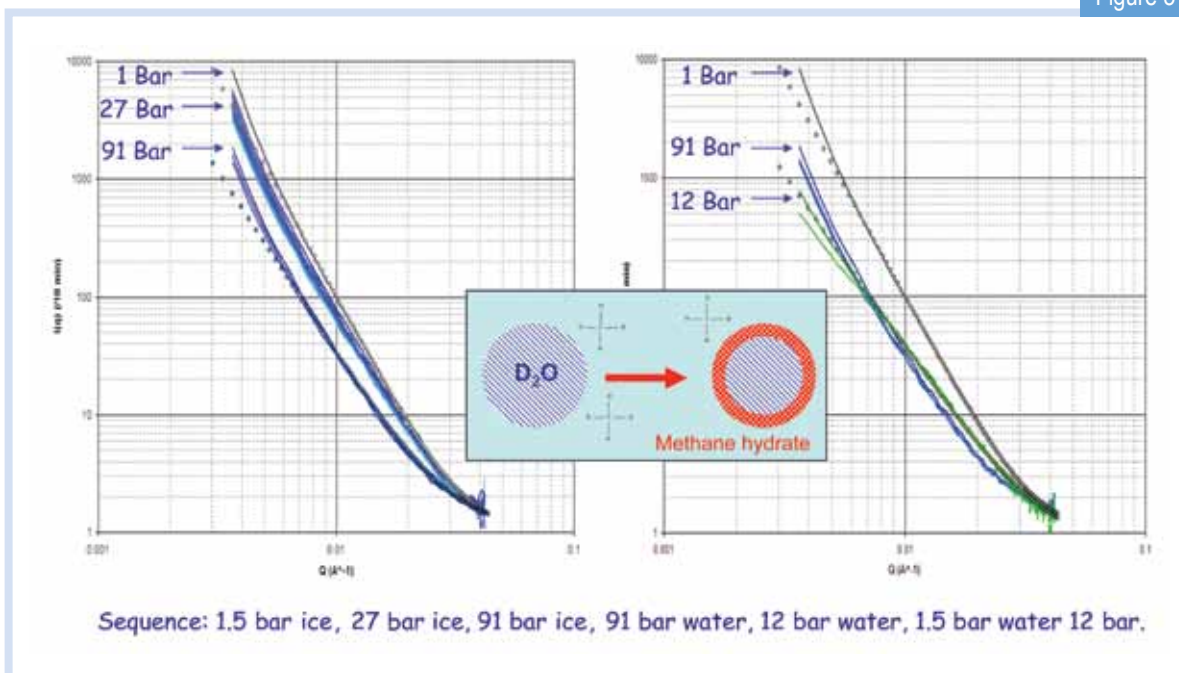
Initially, the SANS maps the rate of growth of hydrate on ice crystallites, and later the increase in growth rate on melting of the ice cores. Fig. 5 shows the changes in SANS pattern during methane hydrate formation (Fig. 5, left) and dissociation (Fig. 5, right).

In Fig. 5 on the left where the temperature is ~ 4°C below ice point for heavy water, the slope of SANS decreases from Q^{-3.7} (grey dotted line) at 1 bar gas pressure to Q^{-3.1} (blue dotted line) after 6 hrs at 27 bar and 1 hr at 91 bar; indicating formation and thickening of a crust of methane hydrate on near-spherical ice particles.

In Fig. 5 on the right where the temperature is ~ 2°C above ice point for heavy water, the slope decreases further to Q^{-2.9} (green dotted line) after ~2 hr at 91 bar; indicating further thickening of the methane hydrate crust. On depressurisation to 12 bar the methane hydrate slowly decomposes releasing methane gas to form water.

This provides an independent measure of the growth rate of methane hydrate and thereby on the diffusion rates of hydrocarbon gases through solid & liquid water and through solid hydrate material.

Figure 5



Log-log plots of the SANS patterns during methane hydrate formation & dissociation in heavy water.

(Left) Below the ice point, the slope of SANS decreases from $Q^{3.7}$ (grey dotted line) at 1 bar gas pressure to $Q^{3.1}$ (blue dotted line) after 6 hrs at 27 bar and 1 hr at 91 bar; indicating formation and thickening of a crust of methane hydrate on near-spherical ice particles.

(Right) Above the ice point, the slope decreases further to $Q^{2.9}$ (green dotted line) after ~2 hr at 91 bar; indicating further thickening of the methane hydrate crust. The insert is a schematic picture of the formation of a methane hydrate crust on a spherical D_2O core, consistent with the changing slope of the SANS pattern.

Future direction for our research

Our experiments so far enable us to differentiate between the dependencies of hydrate formation and dissociation on temperature and pressure, to gauge the effect of different hydrate inhibitors, and able to identify the differences in behaviour of Type I and Type II hydrates. Thus, we have established that this method can be used to evaluate potential new kinetic inhibitors.

Our major challenge remains to be able to initiate gas-hydrate nucleation and growth from the liquid-gas interface under turbulent conditions (as is experienced in the marine environment) in a manner accessible by neutron beams.

Currently, we are developing a gas-hydrate flow loop specifically for neutron-beam studies in order to replicate industry conditions, and thereby to probe hydrate nucleation processes at the atomic and molecular scale, a goal which has so far eluded scientists working with other techniques.

References

- [1] Sloan, E. D., Koh C. A. (2008). Clathrate Hydrates of Natural Gases, Third Edition by Taylor & Francis Group, LLC.
- [2] A. Klapproth, R.O. Piltz, S. J. Kennedy, V. K. Peterson, K. A. Kozielski, P. G. Hartley, Gas hydrate formation and decomposition close to subsea geological conditions, Proceedings of the 12th International Conference on the Physics and Chemistry of Ice (Sapporo, September 2010), edited by Yoshinori Furukawa, Gen Sasaki, Tsutomu Uchida, and Naoki Watanabe, Hokkaido University Press, 2011, Sapporo, ISBN978-4-8329-0361-6.



Ces Fabian setting up an experiment.

Waste – a resource when using selective separation

Tracey Hanley¹, Jessica Veliscek-Carolan¹, Nick Scales¹, Zaynab Aly¹, Ces Fabian¹ and Victor Luca²

¹ANSTO, ²Cómission Nacional de Energía Atómica, Argentina

Selective separation of aqueous elements is a vitally important and industrially significant process not only with regards to reducing the volumes of nuclear-waste materials, but also for extracting industrially important elements: all rely upon the ability to remove a specific element from a complex mixture of elements.

For this purpose, we create new functionally designed materials for selective separation, in particular, within the context of the nuclear industry.

Selective separation in relation to the nuclear industry

Nuclear energy increasingly represents an important option for generating clean CO₂-free electricity generating increased interest in innovative nuclear reactors such as “Gen (IV)” reactors [1]. The concept of these reactors implies recycling of irradiated fuel, waste-reduction strategies and improved waste technologies – also called closed fuel-cycles.

Currently, reprocessing of used nuclear-fuel is carried out in several countries including France, UK, Russia and Japan using the PUREX (Plutonium and Uranium Extraction) process.

However, recovery of the other transuranic elements, i.e. Neptunium (Np), Americium (Am) and Curium (Cm), from used fuel has not yet been achieved industrially. As Np, Am and Cm contribute significantly to the lifetime and radiotoxicity of nuclear waste they are targets for removal.

It may also be possible to recover and re-use some of the other fission products present in used nuclear-fuel, for example ¹³⁷Cs and ⁹⁰Sr are industrially relevant products (e.g. for use in gauges, as radioactive tracers and ⁹⁰Sr is used in medicine).

Thus, separation of ¹³⁷Cs and ⁹⁰Sr from used nuclear-fuel is under development - a topical area of research. Lanthanides (La, Ce, Pr, Nd, Sm, Eu, Gd, Tb, Dy, Ho, Er) are another industrially relevant product: used in magnets, hybrid cars, LEDs for TV and computer screens, and similar.

As the demand and cost for these elements has increased dramatically (up to 750%) over the last year their extraction is a potential new resource.

Elements can be separated by precipitation, fractional crystallisation, solvent-solvent extraction, liquid-solid extraction, electrochemical methods and others. Current commercial nuclear-separation technology is based upon solvent-solvent extraction, but this technology is inefficient and suffers complications due to radiation-induced decomposition.

Consequently, new separation methodologies are searched for. We are currently investigating two such methodologies: liquid-solid extraction and electrochemical methods. The latter involves investigation into the potential of pyroelectrochemical processes based on molten alkali salts; this is studied in partnership with the ACSEPT (Actinide reCYcling by SEPARation and Transmutation) programme of the European Union.

However, in the following we report on liquid-solid extraction where we develop new sorbent materials that can withstand the imposed radiation and improve separation efficiencies.

The separation-science strategies

Liquid-solid extraction via column chromatographic methods (solid phase is packed into a column and liquid phase is pumped through) offers a simple, safe and economical alternative to current solvent-solvent separation technologies (see Fig. 1).

However, the particular environments encountered in nuclear systems (temperature, acidity) and radioanalysis means that any promising materials need to pass rigorous testing for all these requirements. To address this complex mix of requirements a multifunctional material is required.

This demands an interdisciplinary approach to materials selection and evaluation. For example, the solid-sorbent material in a chromatographic column needs to have high selectivity and allow a non-restricted flow of the liquid through the column as well as chemical and radiolytic stability.

Once sorption has occurred the solid-matrix material can be either; (i) converted to a waste form suitable for safe disposal, or (ii) used to elute a pure form of the extracted element, particularly if the separated element is industrially useful.

From macro- to meso-porosity

Producing the solid matrix in the form of beads imparts the desired characteristics for large-scale ion-exchange applications with ease of use and ease of flow. We have manufactured mixed titanium-zirconium oxide beads with the desired wide range of porosities from macro-to-meso, illustrated in Fig. 2.

But why mixed titanium-zirconium oxide compositions? They allow potential inclusion in waste-form materials or can be used as transmutation matrices. The radial macroporous bead structure was imparted using polyacrylonitrile templating techniques and mesoporosity was generated using a secondary templating methodology.

The desired mesopore architecture can be built through evaporation-induced self-assembly technique (EISA) using a variety of supramolecular templates [2,3]. With this technique we tailor the binding sites through both channel size and surface charge and allowing the material and its properties to be tuned to a particular application.

Essentially, this results in a hierarchy of porosity from macro-to-meso materials with enhanced mass-transfer kinetics relative to materials that only had mesoporosity of one size regime [4]. It should be pointed out that rapid adsorption kinetics is highly desirable in nuclear and other separation applications.

Figure 1

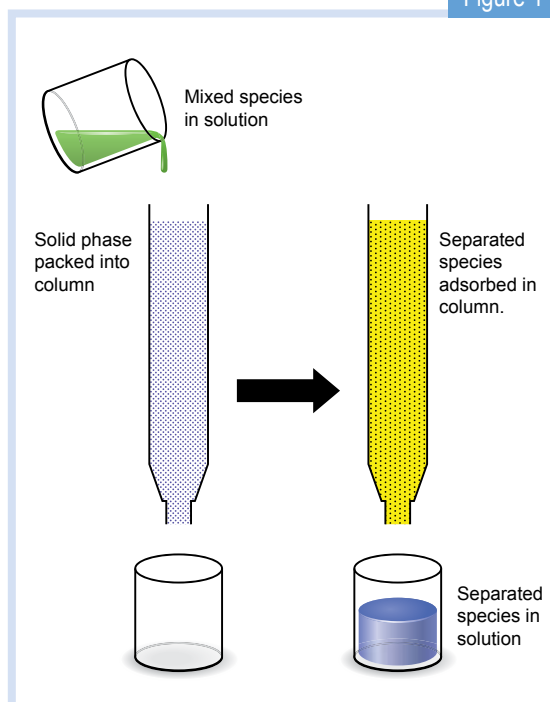


Illustration of column chromatographic separation process; a mixed solution is added to the top of a column of solid phase, as the solution passes through the column the element of interest is retained within the solid phase and all other components are eluted from the bottom of the column giving a means of separating components in a solution.

The key to selectivity

Mesoporous oxide materials can impart selectivity through size and charge, but greater chemical selectivity can be generated by attaching specific organic ligands to the surface, i.e. a surface offers a specificity (or preference) for the desired species to be attached.

For example, the use of amino tris-methylenephosphonic acid [5] on the mixed oxide beads proved promising for lanthanide adsorption. We call this 'functionalising' material and in this



Ces Fabian, Zaynab Aly, Tracey Hanley, Nick Scales and Jessica Veliscek-Carolan pictured in the laboratory.

particular case surface functionalisation. We are now working on establishing selectivity in the presence of competing cations.

An organic ligand for functionalisation consists of three distinct parts: the surface binding group to attach to the mesopore, a linker, and the functional ligand itself (see Fig. 3).

Consequently, our research is concentrated on three main areas: (i) surface binding, how we chemically react with the mesopore surface; (ii) self assembly processes for enabling the packing of the functional molecules inside the pores; and (iii) synthesis of selective ligands that, once bound to the surface, remain available for co-ordination to the metal species of interest.

We pursue organic synthesis of molecules that consist of all three parts. In addition, we continue to investigate the synthesis and structure of mesoporous oxides and initiate investigations into alternative mesoporous-structures based upon carbon, titanium carbides and zirconium carbides.

These chemical compositions are important to new waste-form structures currently under development, which have the potential to minimise reprocessing requirements of future nuclear fuels.

References

- [1] Olander, D. (2009). Nuclear fuels – present and future. *Journal of Nuclear Materials*, 389(1), 1-22.
- [2] Luca, V., Drabarek, E., Griffith, C. S., & Hanley, T. L. (2010). Understanding the supramolecular self-assembly of zirconium titanate mesophases formed from the poly(ethylene oxide) surfactant brij-58. *Chemistry of Materials*, 22(13), 3834-3842.
- [3] Luca, V., Soler-Illia, G. J. A. A., Angelomé, P. C., Steinberg, P. Y., Drabarek, E., & Hanley, T. L. Striving for order and compositional homogeneity in bulk mesoporous zirconium titanium mixed metal oxides from triblock copolymers and metal chlorides. *Microporous and Mesoporous Materials*, 118(1-3), 443-452.
- [4] Drisko, G. L., Kimling, M. C., Scales, N., Ide, A., Sizgek, E., Caruso, R. A., et al. (2010). One-pot preparation and uranyl adsorption properties of hierarchically porous zirconium titanium oxide beads using phase separation processes to vary macropore morphology. *Langmuir*, 26(22), 17581-17588.
- [5] Griffith, C. S., De Los Reyes, M., Scales, N., Hanna, J. V., & Luca, V. (2010). Hybrid inorganic-organic adsorbents Part 1: synthesis and characterisation of mesoporous zirconium titanate frameworks containing coordinating organic functionalities. *ACS Applied Materials and Interfaces*, 2(12), 3436-3446.

Figure 2

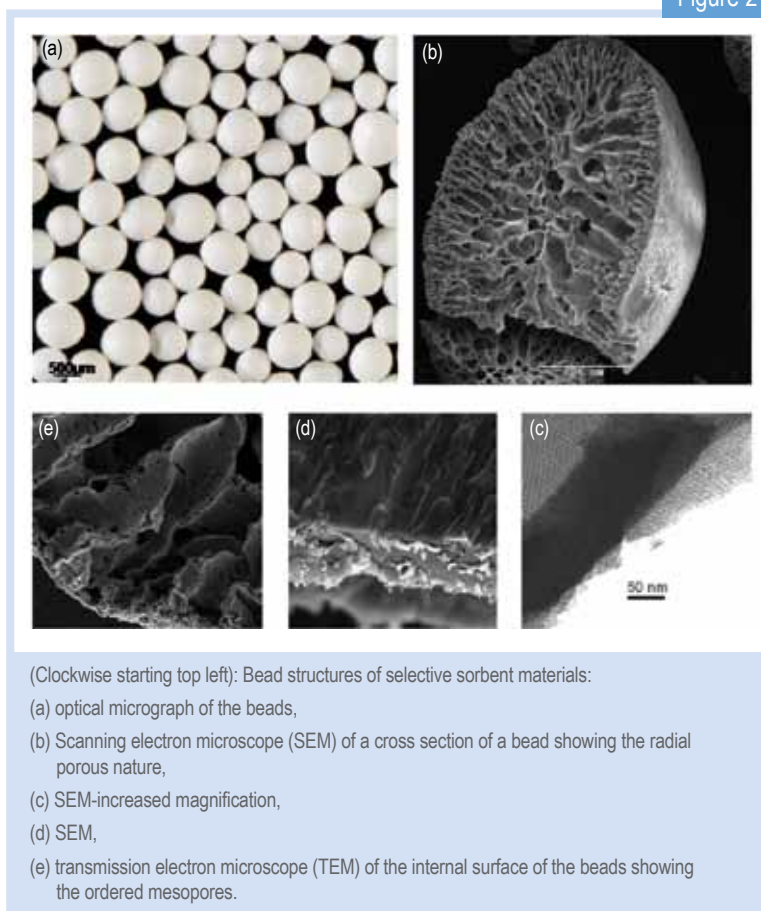
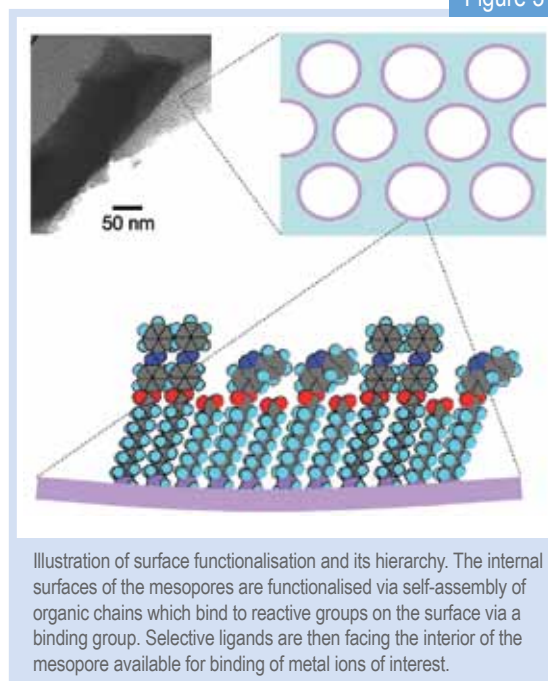
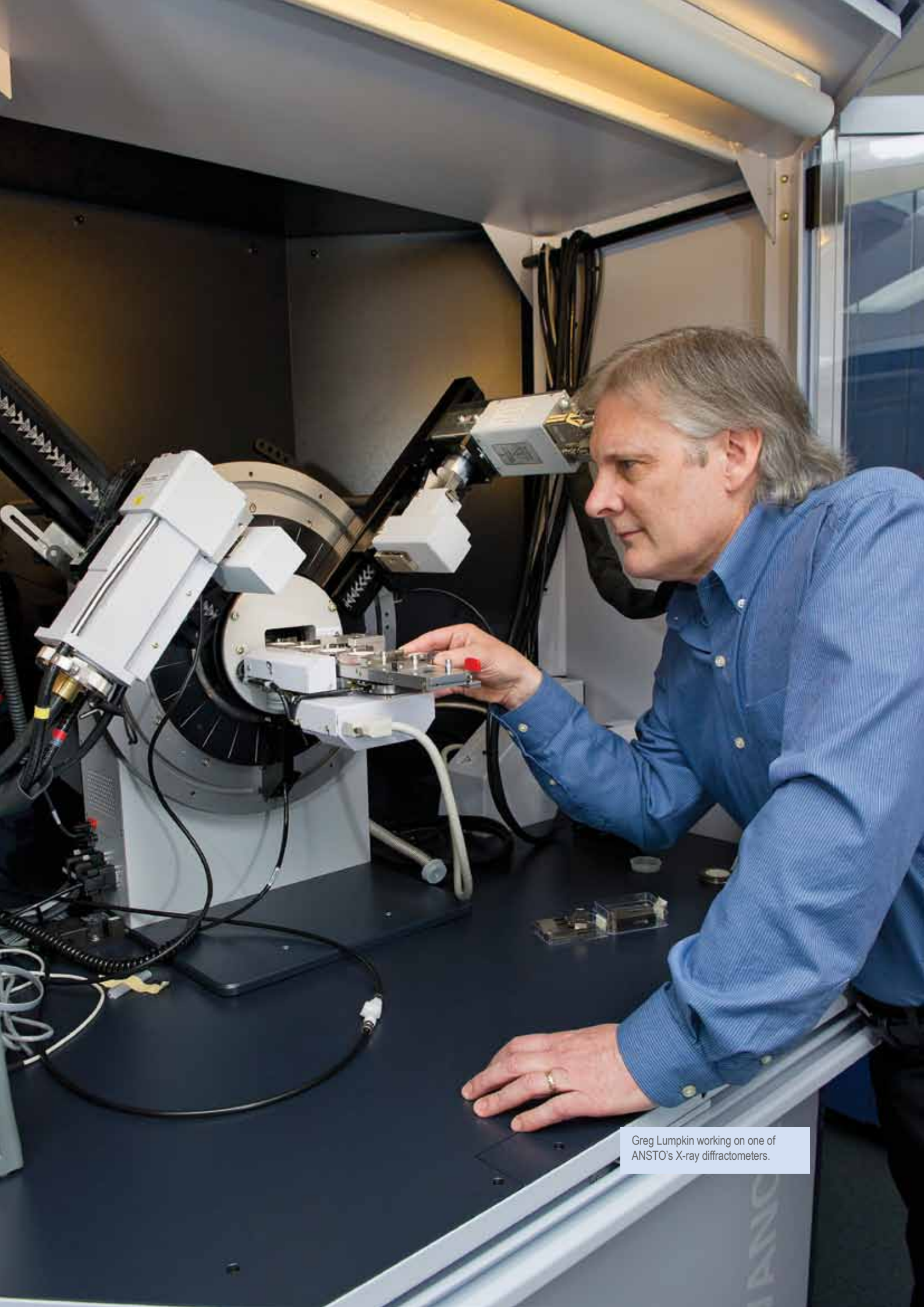


Figure 3





Greg Lumpkin working on one of ANSTO's X-ray diffractometers.

Developing radiation-tolerant materials

Greg Lumpkin, Kath Smith, Bronwyn Thomas, Zhaoming Zhang, and Karl Whittle

ANSTO

All materials for future energy production using nuclear energy will need to perform under extreme levels of irradiation and elevated temperature without significant degradation of properties for a specified service life. These advanced nuclear materials represent a material's life cycle and include structural load-bearing materials, radiation barriers, inert matrix fuels, transmutation targets, and specialised waste forms.

Our research investigates radiation damage in complex perovskite systems, where we test a theory that a coupling exists between the radiation damage recovery mechanism and a phase transition in the $\text{La}_x\text{Sr}_{1-1.5x}\text{TiO}_3$ system.

Why perovskite?

Many of the physical and chemical properties of high technology materials depend critically on the nature and concentration of defects. In crystalline solids, the types of defects present include point defects (e.g. vacancies and interstitials), impurity atoms, and extended defects (e.g. edge and screw dislocations).

In this work, we are mainly concerned with materials that must perform a specific function while being exposed to external irradiation, e.g. inert matrix fuel materials, transmutation targets, and nuclear waste forms.

The compound perovskite, with the ideal general formula ABO_3 , encompasses a large family of compounds with large A cations (e.g. La) and small B cations (e.g. Sr or Ca), but it also has a number of different structural phases and subsequent phase transitions that occur with changes in temperature.

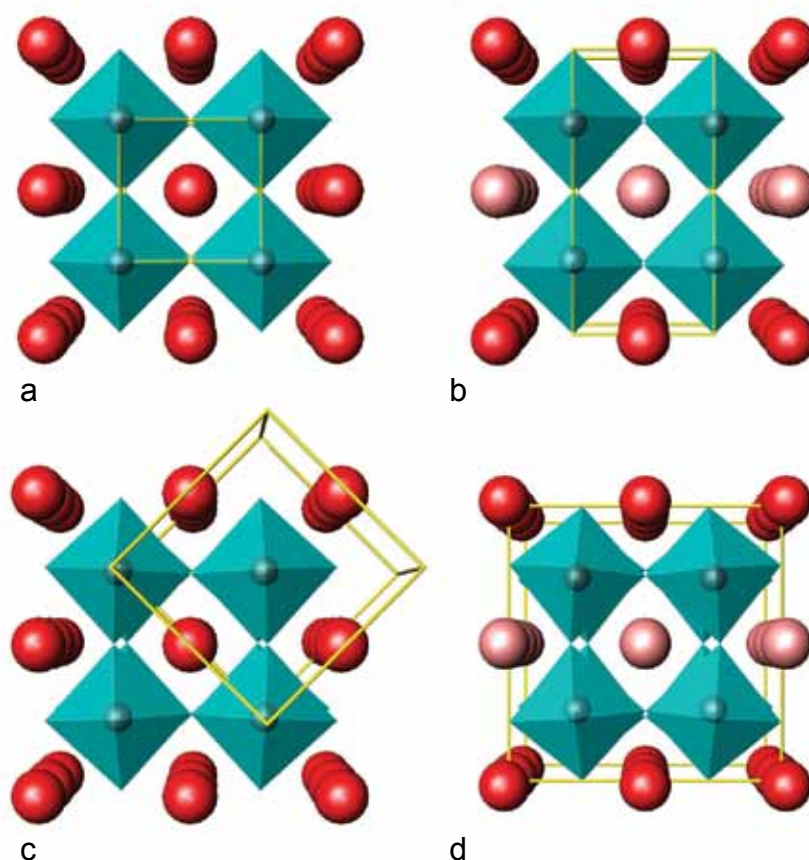
Perovskite is important as a component of high-technology devices and may also incorporate trivalent fission products (e.g. Ce, Nd, Pr) and actinides (e.g., Pu) on the A-site, making it very attractive in the field of nuclear science and technology.

The nature of the defects produced in these materials is related to the mass and energy of the irradiating particles and the ability of the solid to recover from structural damage (radiation tolerance).

However, crystal structure, composition, and the presence of pre-existing cation vacancies (unoccupied sites) also play an important role in the recovery from radiation damage. Some materials actually "heal" themselves very quickly during irradiation and remain crystalline to very high dose levels.

Combining both experimental and atomistic computer-simulation approaches – a truly multi-disciplinary effort – we can describe changes in radiation response as a function of composition and temperature.

This article is in essence a three-part story in which we describe unusual radiation response in Sr-La perovskites, apply computer simulations to understand the problem at the atomic scale, and then attempt to determine if damage recovery is related to a well-known structural phase transition.



Perovskite structures obtained in the system $\text{La}_x\text{Sr}_{1-1.5x}\text{TiO}_3$. In each structure, the Ti atoms are surrounded by six oxygen atoms, forming an octahedral coordination environment.

The two structures on the left, Pm3m (a) and I4/mcm (c), exist for compositions with less than 0.53 La atoms (to the left of the vertical red line in Fig. 2). Red spheres represent Sr, La, and vacancies (disordered in these two structures).

The two structures on the right, P4/mmm (b) and Cmmm (d), exist for compositions with more than 0.53 La atoms (to the right of the vertical red line in Fig. 2).

In these structures the Sr and La atoms (red spheres) and vacancies (pink spheres) are ordered into alternating layers. Phase transitions (black line in Fig. 2) between the structures in the upper (a, b) and lower structures (c, d) are due to tilting of the octahedra.

Structure and radiation tolerance in complex perovskites

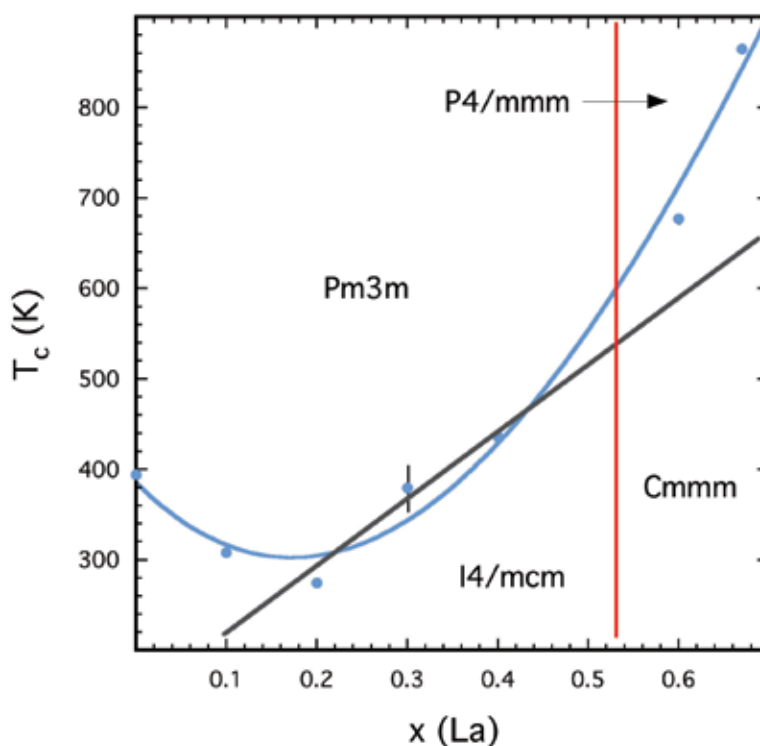
At first, we attempted to understand the radiation damage response of perovskite compounds with A-site vacancies in the system $\text{La}_x\text{Sr}_{1-1.5x}\text{TiO}_3$ [1]. This system is of interest because the replacement of Sr by La requires some vacancies, e.g. for every three Sr atoms, two La atoms and one vacancy are required to maintain charge balance.

Fig. 1 shows the four different crystal structures we found in this system and Fig. 2 shows the stability field for each structure over a range of temperature (vertical axis) and composition (horizontal axis). The diagonal black line in Fig. 2 represents the boundary between

structures due to octahedral tilting and the vertical red line at $x = 0.53$ is the boundary due to (Sr, La)-vacancy ordering. The two structures at the top of Fig. 1 (a and b) occur above the gray line in Fig. 2, the octahedra in these structures (Pm3m and P4/mmm) are not tilted.

Conversely, the two structures at the bottom of Fig. 1 (c and d) occur below the gray line in Fig. 2 and the octahedra in both structures (I4/mcm and Cmmm) show the tilting characteristic of many perovskites.

For any composition in the system, if you change the temperature above or below the black line, then the structure will change due to minor changes in the



This figure shows a portion of the system $\text{La}_x\text{Sr}_{1-1.5x}\text{TiO}_3$, [1], wherein we show how the critical temperature for amorphisation (T_c) changes with increasing La and vacancy content (indicated by the blue symbols and curve). Near coincidence of the blue data points for $x = 0.2, 0.3,$ and 0.4 suggests the possibility of a link between the octahedral phase transition (black line) and the damage recovery mechanism.

Remember that in these perovskites, one vacancy and two La atoms are introduced for every three Sr atoms. These measurements were obtained by ANSTO researchers at the IVEM-Tandem User Facility, Argonne National Laboratory.

positions of the oxygen atoms – they control the tilting of the octahedra. The ordering of Sr, La, and vacancies into layers is purely down to composition and does not change significantly with temperature.

A major question facing our team was: how does the radiation response change as a function of structure and composition in this complex system?

Smith et al. [2] provided an answer to the question above by irradiation of synthetic perovskite samples with 1.0 MeV Kr ions using the IVEM-Tandem User Facility at Argonne National Laboratory. All of the samples examined pass through the crystalline-amorphous transformation, as shown by the electron diffraction patterns in Fig. 3.

The unirradiated sample reveals the diffraction pattern of the undamaged structure (Fig. 3a), whereas the irradiated samples reveal the transformation from the crystalline to the amorphous state with increasing radiation dose (Fig. 3b-d).

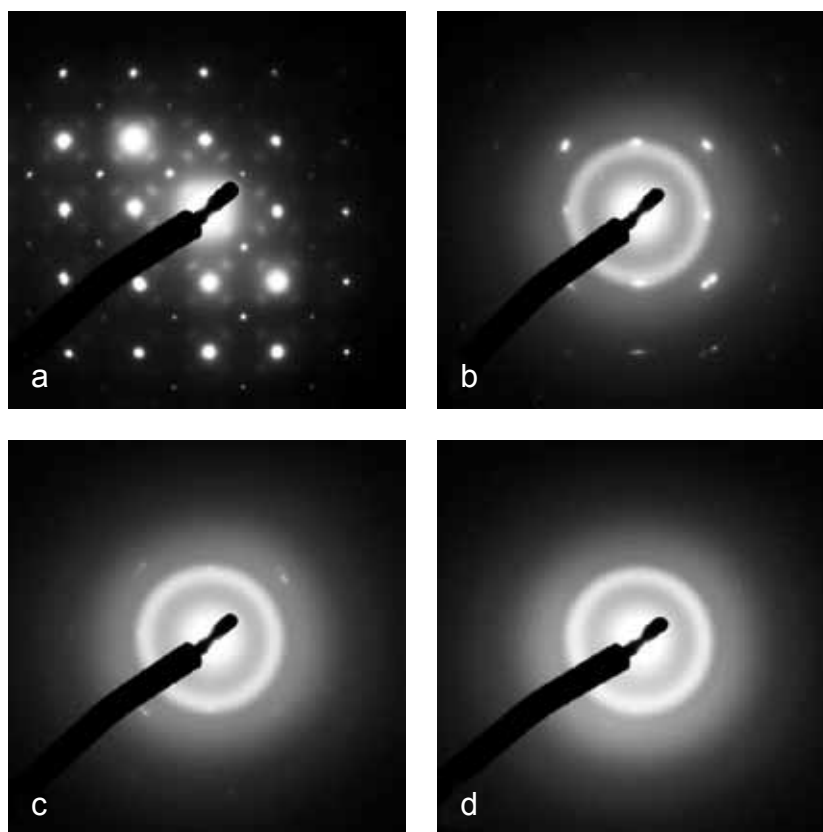
When this transformation is studied as a function of temperature, we can describe radiation tolerance by an

important parameter known as the critical temperature for amorphisation, T_c , which is the temperature above which the material remains crystalline due to thermal annealing of damage. In Figure 2, the blue curve shows how T_c changes with composition, with the lowest T_c being recorded at $x = 0.2$, the most radiation resistant composition in the system.

However, the most interesting observation is the non-linear change in T_c in the $\text{La}_x\text{Sr}_{1-1.5x}\text{TiO}_3$ perovskite system between $x = 0.0$ and 0.67 . At this point in the research project, we faced a major problem in trying to explain why the radiation tolerance changes the way it does.

The influence of electrostatic and strain energy on defect behaviour

In order to understand the $\text{La}_x\text{Sr}_{1-1.5x}\text{TiO}_3$ perovskites in greater detail, Thomas et al. [3] applied atomistic simulation methods to model the behaviour of vacancies as a function of composition. In this study, a combination



A set of electron diffraction patterns [2] illustrating the change in structure from crystalline to amorphous with increasing ion radiation dose from (a) to (d).

The critical dose for amorphisation is determined by the disappearance of Bragg diffraction spots, e.g., this sample becomes amorphous at a dose bracketed by (c) and (d).

This experimental procedure is repeated at different temperatures in order to determine the critical temperature for amorphisation. Diffuse rings in the diffraction patterns are due to the scattering of electrons by atoms in the amorphous structure.

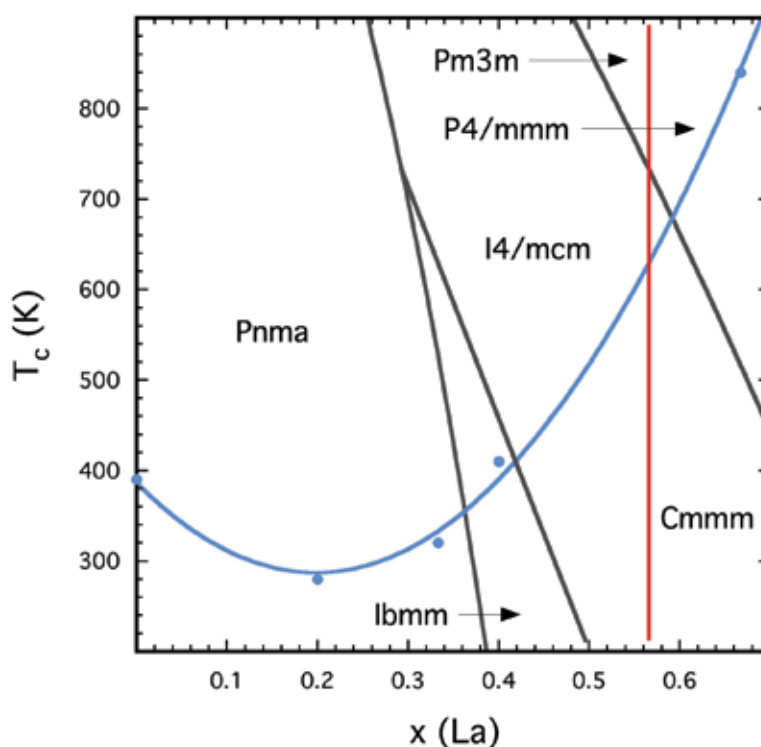
of *ab initio* (Latin, meaning “from the beginning”, this refers to simulations based on first principles) and classical simulation techniques were used to characterise the energetics of A-site vacancy and cation interactions.

When the La content is low, the A-site interactions follow intuitive electrostatic arguments, promoting association of La ions with vacancies and dissociation of vacancy-vacancy pairs. This mechanism explains why T_c decreases and the material becomes more radiation tolerant between $x = 0.0$ and 0.2 , e.g., the increasing number of A-site vacancies speeds up the recovery of atoms displaced by radiation damage by providing more available sites and by lowering the energy barrier for the migration of atoms through the material.

For samples with high La content, the defect interactions are inverted due to strain forces arising from cooperative atomic relaxations and it is more energetically favourable for La atoms and vacancies to dissociate into separate layers (see Fig. 1b, d).

Although the reasons for reduced radiation tolerance at high La content are still open to debate, we believe that energy barriers for defect migration are higher in the strain-dominated region of the system (above $x = 0.4$).

For intermediate compositions with $x = 0.2-0.4$, our colleagues at the University of Cambridge suggested that there may be a coupling between the radiation damage recovery mechanism and the octahedral tilting phase transition. This hypothesis was tested during recent experiments described below.



This figure shows a portion of the system $\text{La}_x\text{Ca}_{1-1.5x}\text{TiO}_3$ [4], showing the phase transformation boundaries due to octahedral tilting (black lines), the cation-vacancy ordering transformation (vertical red line near $x = 0.57$), and the critical temperature for amorphisation (blue line).

Note that in this system, the T_c curve is similar to that shown in Fig. 2 and it crosses all of the phase boundaries, therefore there is no direct coupling of any phase transformation with the damage recovery mechanism in this system.

Ion irradiation of Ca-La perovskites – the final chapter?

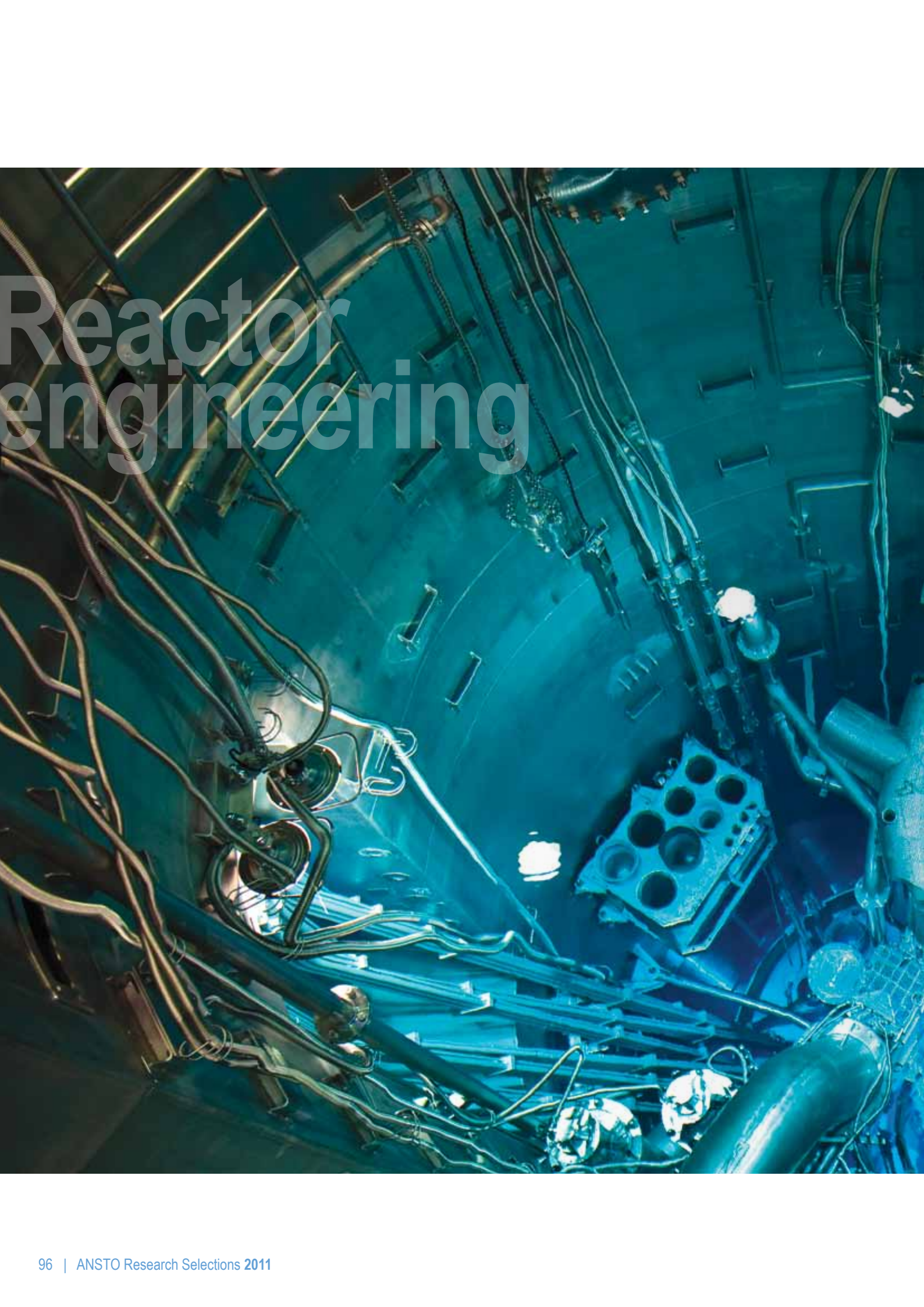
Zhang et al. [4] found that the system $\text{La}_x\text{Ca}_{1-1.5x}\text{TiO}_3$ has very different octahedral tilting transitions and two additional structures for $x < 0.5$, Pnma and Ibmm, both of which have tilted octahedra, although the La-vacancy ordering transition is still present at a slightly higher La content (Fig. 4).

Therefore, we chose this system as a test of the proposed coupling between radiation damage recovery and phase transition boundaries. Results of ion-irradiation experiments obtained in December 2010 on selected samples are shown in Fig. 4, where it is obvious that the T_c curve (blue line) mimics that found in the Sr-La system, but it cuts across all of the phase boundaries, thus providing evidence against the idea that damage recovery processes couple with phase transitions.

In future work, we will attempt to measure the ionic conductivity in both perovskite systems, as it may give a general indication of the barriers to atomic migration (e.g., higher ionic conductivity is related to lower migration barriers).

References

- [1] Howard, C. J., Lumpkin, G. R., Smith, R. I., & Zhang, Z. (2004). Crystal structures and phase transition in the system $\text{SrTiO}_3\text{-La}_{2/3}\text{TiO}_3$. *Journal of Solid State Chemistry*, 177(8), 2726-2732.
- [2] Smith, K. L., Lumpkin, G. R., Blackford, M. G., Colella, M., & Zaluzec, N. J. *In situ* radiation damage studies of $\text{La}_x\text{Sr}_{1-3x/2}\text{TiO}_3$ perovskites. *Journal of Applied Physics*, 103(8), 083531.
- [3] Thomas, B. S., Marks, N. A., & Harrowell, P. (2006). Inversion of defect interactions due to ordering in $\text{Sr}_{1-3x/2}\text{La}_x\text{TiO}_3$ perovskites: an atomistic simulation study. *Physical Review B*, 72(21), 214109.
- [4] Zhang, Z., Lumpkin, G. R., Howard, C. J., Knight, K. S., Whittle, K. R., & Osaka, K. (2007). Structures and phase diagram for the system $\text{CaTiO}_3\text{-La}_{2/3}\text{TiO}_3$. *Journal of Solid State Chemistry*, 180(3), 1083-1092.



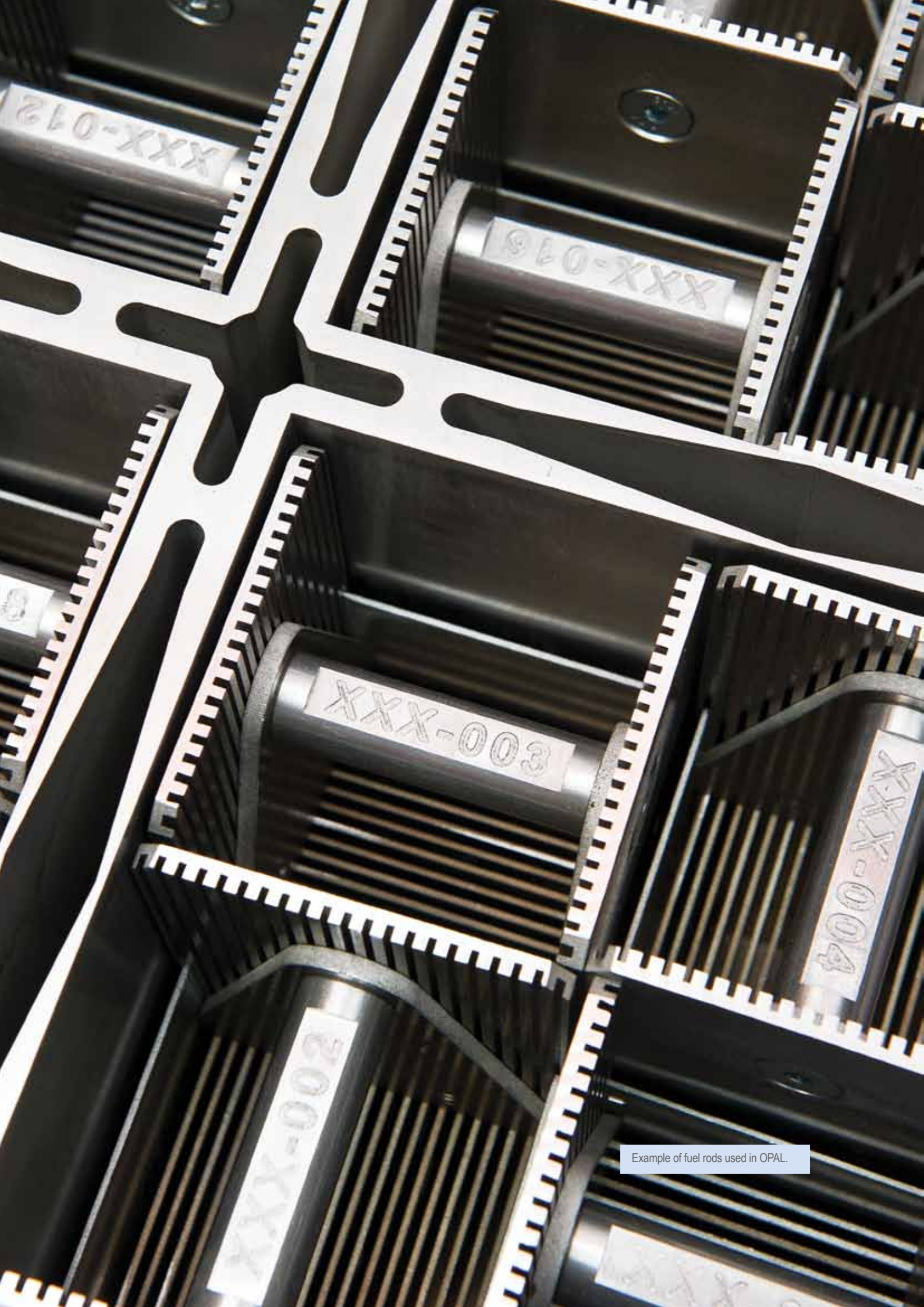
Reactor engineering

Reactor engineering

Reactor engineering seeks to improve the safety and increase the efficiency of nuclear reactors.

ANSTO's work in the field covers a broad range of research areas from the development of computer models to determine design and operational deficiency, to the creation of software to gauge the wear and tear on plant infrastructure, to structural integrity research and consultation.

The following two examples cover important ANSTO computer modelling research which will lead to improvements in the safety and efficiency of nuclear reactors around the world.



Example of fuel rods used in OPAL.

Understanding the vibrational response of thin plates secured using varying strength longitudinal connections

Mauro Caresta¹, David Wassink²

¹University of New South Wales (UNSW) Sydney, ²ANSTO

Plate-type nuclear fuel assemblies, such as those used in ANSTO's OPAL research reactor, consist of a number of thin aluminium plates containing a uranium-aluminium mixture. Typically, the fuel plates are secured into a box-type fuel assembly using a technique termed 'roll swaging'.

The strength of the roll swaged connections determines the integrity of the fuel assembly as a whole, therefore it is very important to have a non-destructive method to verify that the roll swaged connections are secure. Since the interaction between fuel assemblies and coolant flow during reactor operation can lead to flow-induced structural instabilities [1-3], it is crucial to be able to predict their dynamic characteristics and how these are affected by the strength of the roll swaged connections.

Previous research has investigated the instability of parallel plates due to fluid velocity, sometimes leading to plate collapse. The aim of the present work is to provide a computational and experimental justification for the model used in reference [7]. This will be the first step in achieving a qualitative test method for assessing the quality of plate-type nuclear fuel assemblies.

The results of this work will be used to model a whole fuel assembly made of multiple plates restrained by the roll swaging technique.

We performed experimental modal analysis on test swage specimens manufactured with different swaging parameters, resulting in varying swage strengths. The boundary conditions of the swage joint as modelled by a finite element model (FEM) were determined by matching the experimental values of the first natural frequencies measured with the results obtained from the FEM.

It was shown that the swage contact between the thin plates and side plates can be modelled assuming a perfect clamp in all the degrees of freedom except the rotational around the axis parallel to the swage, where an equivalent torsional spring stiffness can be applied.

Construction of a swaged joint

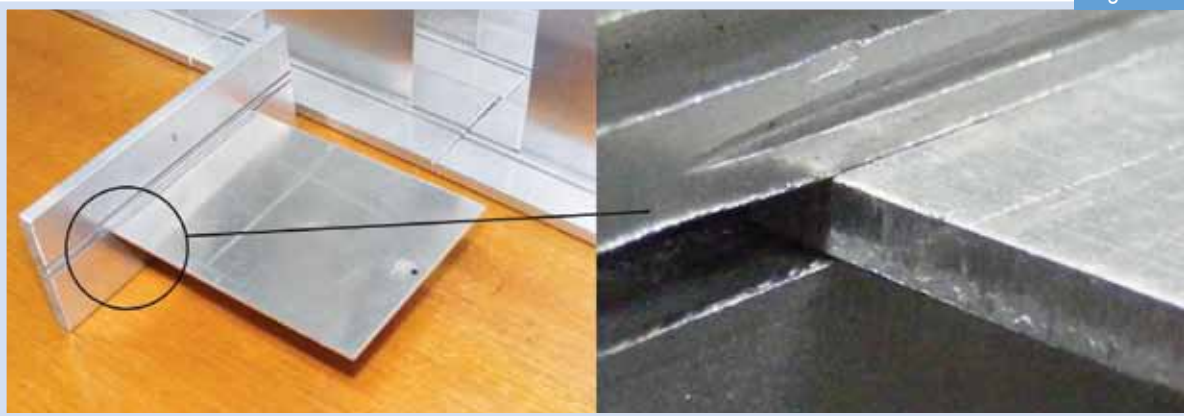
In a typical fuel assembly, the plates are inserted into slots machined into the side walls of the fuel box. The clamping of the plates to the box is generally

assured by a swage between adjacent plates. The swage is obtained by forcing the sharp edge of a swaging wheel into the aluminium ridge between the slots, resulting in plastic deformation of the ridge to create the clamp as shown in Fig. 1. The nature of the clamp is a key element in predicting the vibrational behaviour of a fuel assembly.

A perfect clamp completely constrains all six degrees of freedom at the edges of the fuel plates. In this present work it is shown that the swaging process results in a clamp that fixes all the degrees of freedom but the rotational around the axis parallel to the swage.

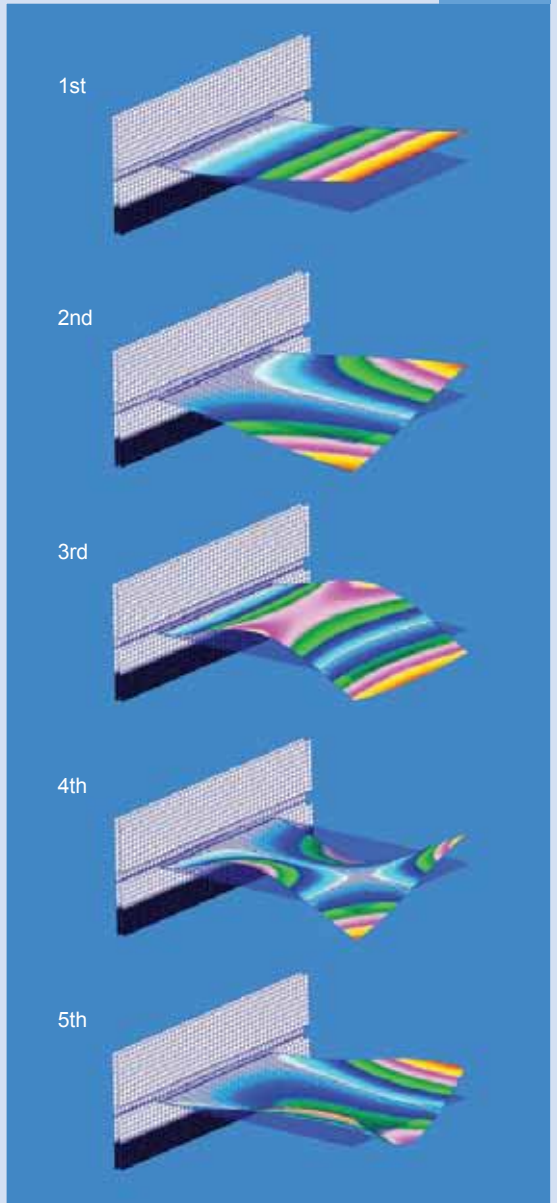
For small rotations, the effect of the swage joint is shown to be a torsion spring whose stiffness is related to the quality of the swage. A good swage leads to a very high stiffness that approaches the ideal case of a perfect clamp, while a poor swage results in a lower stiffness value tending to a simply supported case.

Figure 1



A swaged specimen used for the modal analysis tests detailing the swaged connection (right image)

Figure 2



The first five mode shapes for a perfectly clamped plate as calculated using the FEM.

Experimental aspect

The natural frequencies of the specimen plates were determined by clamping the bottom of the side plates in a vice and performing an impact hammer test to obtain the Frequency Response Function (FRF). A laser vibrometer was used to measure the response, focussed close to the corner of the plate to maximise the visibility of all the modes. We found that different swaging parameters shifted the natural frequencies, with a dependence on the integrity of the swage connection.

Computational aspect

Using data obtained from the experiments, an FEM of the specimen was built connecting the plate to the support using 6 degree of freedom elements with adjustable torsional stiffness K_s . The first five natural frequencies for a perfect clamp situation ($K_s \rightarrow \infty$) are shown in Fig. 2, represented as their vibrational mode shapes.

Different stiffness values for the torsion spring, simulated the conditions between a perfect clamp ($K_s \rightarrow \infty$) and a simple support ($K_s = 0$). The first five natural frequencies were normalised with respect to the perfect clamp case and plotted against spring stiffness (Fig. 3). The first natural frequency is the most sensitive to variations in spring stiffness. Sensitivity decreases approaching the ideal clamped case and with higher-order modes.

Arranging the data with respect to the natural frequency order, a characteristic stepwise variation between perfect clamp and simple support was observed (Fig. 4). The equivalent experimental results obtained by swaging at different distances from the plates, thus changing the strength of the swage, showed the same trend.

Matching theoretical and experimental data

Fig. 4 compares the first natural frequencies of two experimental results depicting a poor swage or loose connection and a good, but not perfect swage, with the FEM results obtained by updating the stiffness values of the torsion springs. The characteristic stepwise variation can be seen at the second order. The maximum error between experiment and FEM for higher-order natural frequencies is around 3%.

The matching of experimental and theoretical results confirm the validity of the FA model, showing that we can assess the dynamic behaviour of a swaged connection by means of torsion springs with adjustable stiffness.

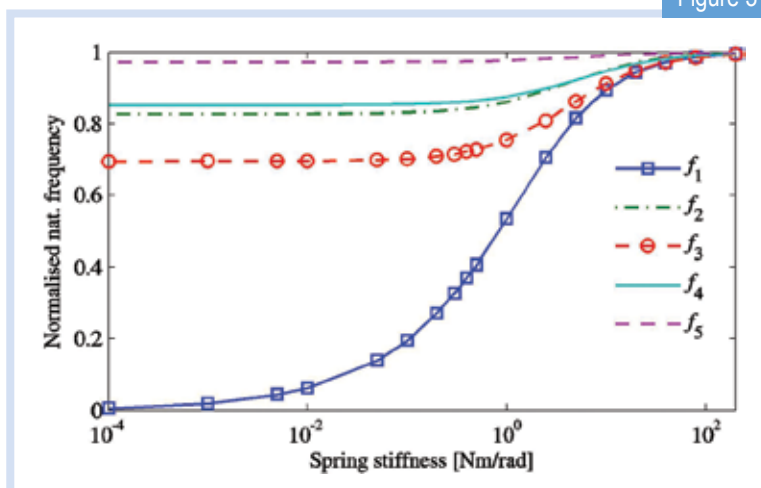
This is a first step to model the dynamic behaviour of thin plates secured by swage joints in nuclear fuel assemblies and opens a variety of issues to be studied in more depth. A more sophisticated FEM updating process able to match the results of higher orders of natural frequencies will give an improved value for the equivalent torsion spring.

Further validation of the results can be achieved by finding the sensitivity of the natural frequencies to additional swaging parameters such as depth of cut (swaging force) and the profile of the swage wheel. The results of this work will be used to model a whole fuel assembly made of multiple plates restrained by the technique of the roll swaging.

References

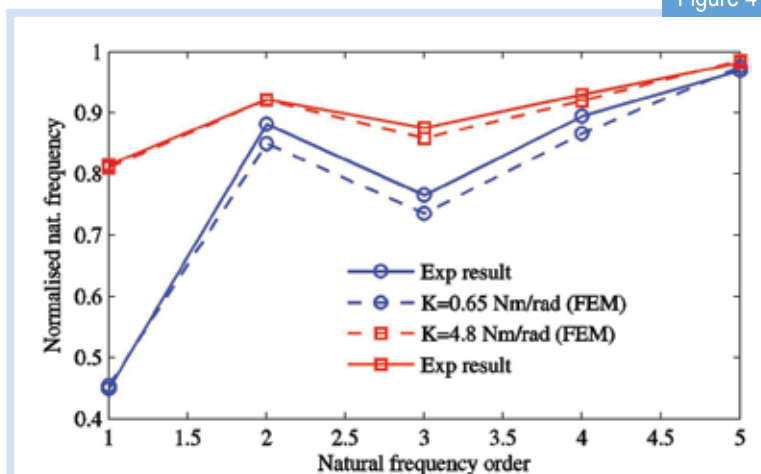
- [1] Blevins, R. D. (1979). Flow-induced vibration in nuclear reactors: a review. *Progress in Nuclear Energy*, 4(1), 25-49.
- [2] Paidoussis, M. (1980). Flow-induced vibrations in nuclear reactors and heat exchangers: practical experiences and state of knowledge. In E. E. Naudascher & D. Rockwell (Eds.), *Practical Experiences with Flow-Induced Vibrations* (volume 829-832, pp. 1-81). Berlin, Germany: Springer-Verlag.
- [3] Ho, M., Hong, G., & Mack, A. N. F. (2004). Experimental investigation of flow-induced vibration in a parallel plate reactor fuel assembly. 15th Australasian Fluid Mechanics Conference, 13th – 17th December 2004. Sydney, Australia: The University of Sydney.
- [4] Miller, D. R. (1960). Critical flow velocities for collapse of reactor parallel-plate fuel assemblies. *Journal of Engineering for Power-Transactions of the ASME*, 82, 83-95.
- [5] Pavone, S. J., & Scarton, H. A. (1983). Laminar flow induced deflections of stacked plates. *Nuclear Engineering and Design*, 74(1), 79-89.
- [6] Davis, D. C., & Scarton, H. A. (1985). Flow-induced plastic collapse of stacked fuel plates. *Nuclear Engineering and Design*, 85(2), 193-200.
- [7] Kim, G., & Davis, D. C. (1995). Hydrodynamic instabilities in flat-plate-type fuel assemblies. *Nuclear Engineering and Design*, 158(1), 1-17.

Figure 3

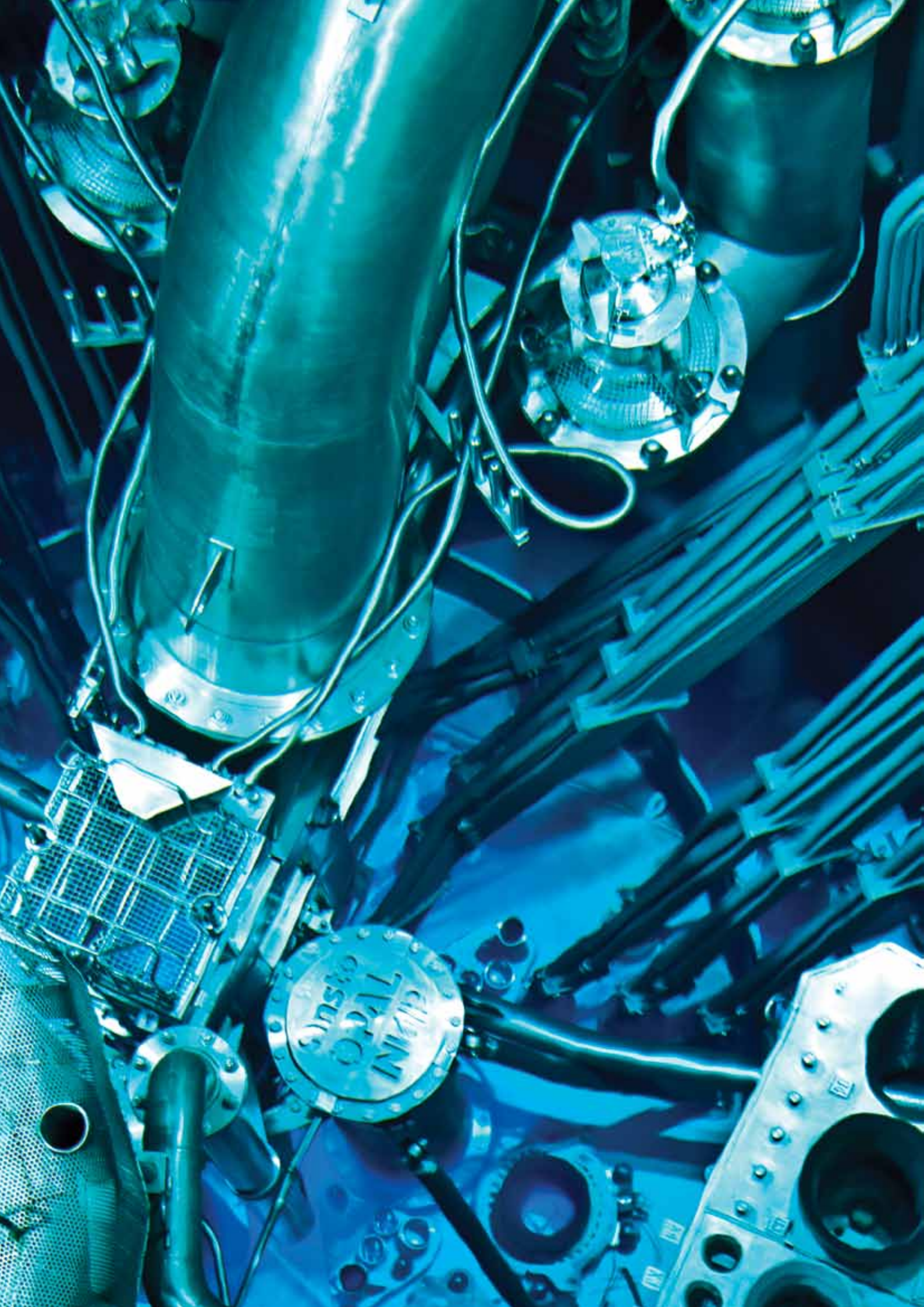


Variation of the natural frequencies calculated using the FEM with the spring stiffness applied to the joint.

Figure 4



Matching the natural frequencies obtained by experiment with the computational natural frequencies by FEM updating.



Bubbly flow regime and beyond – modelling gas-liquid flow using population balance

Guan Heng Yeoh¹, Sherman Chi Pok Cheung², Jiyuan Tu²

¹ANSTO, ²School of Aerospace, RMIT University

Many challenges remain in the development of physical models for gas-liquid flow for different flow regimes, an important aspect in the understanding of the cooling mechanism of a reactor for example. One approach to unravel such flows is the consideration of a two-fluid model based on the interpenetrating media framework where the inter-phase exchanges of mass, momentum and energy can be modelled as interfacial transfer term acting on each phase.

In this sense, two sets of conservations (one conservation equation for mass, momentum and energy of the gas phase as well as liquid phase) can be written in terms of phase-averaged properties. The dynamics of the interaction between the two phases are fully described by the constitutive relationships governing the inter-phase mass, momentum and energy exchange.

A standard method is modelling of population balance for the gas-liquid flow. In order to predict the complex hydrodynamics processes of various bubbly turbulent pipe-flow conditions we capture the bubble coalescence and bubble breakage mechanisms, making a complete three-dimensional two-fluid model.

Application of models

Mechanistic modelling of gas-liquid flows allows more realistic predictions of gas-liquid flows, circumventing the need to resort to flow regimes which are empirically determined and do not aptly account for the time and length scale for the flow regime transition between two flow regimes. Better safety analyses can be performed for gas-liquid flows in existing and advanced nuclear reactors.

Population balance modelling

To overcome the limitations represented by the flow regime approach, the bubble coalescence and break-up phenomena are directly simulated through the consideration of a population-balance equation. The fundamental development stems from the consideration of the Boltzman equation, which describes the particle-size distribution.

On the basis of this equation, different approaches are derived such as the Average Bubble Number Density (ABND) equation [1], MUSIG model [2] and Direct Quadrature Method of Moment (DQMOM) [3].

In Fig. 1, the major phenomenological mechanisms have been identified and appropriate mechanistic models have been established [4,5]:

- (i) Forming a unit, i.e. coalescence through random collision driven by turbulent eddies; eddies are the swirling of a fluid and the reverse current created when the fluid flows past an obstacle,
- (ii) coalescence due to the acceleration of the following bubble in the wake of the preceding bubble, and
- (iii) break-up due to the impact of turbulent eddies.

Figure 1

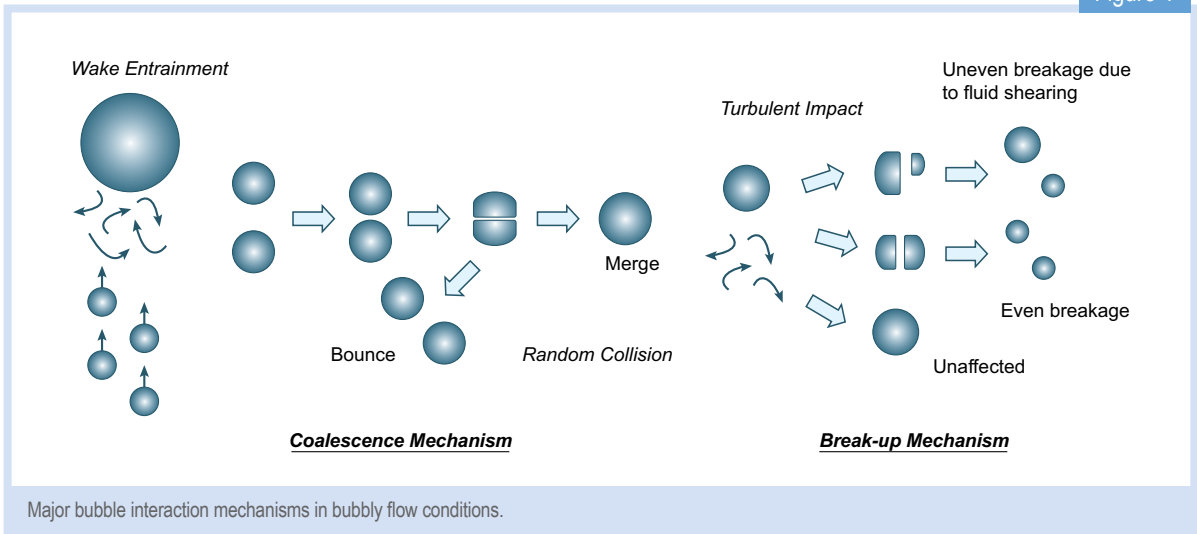
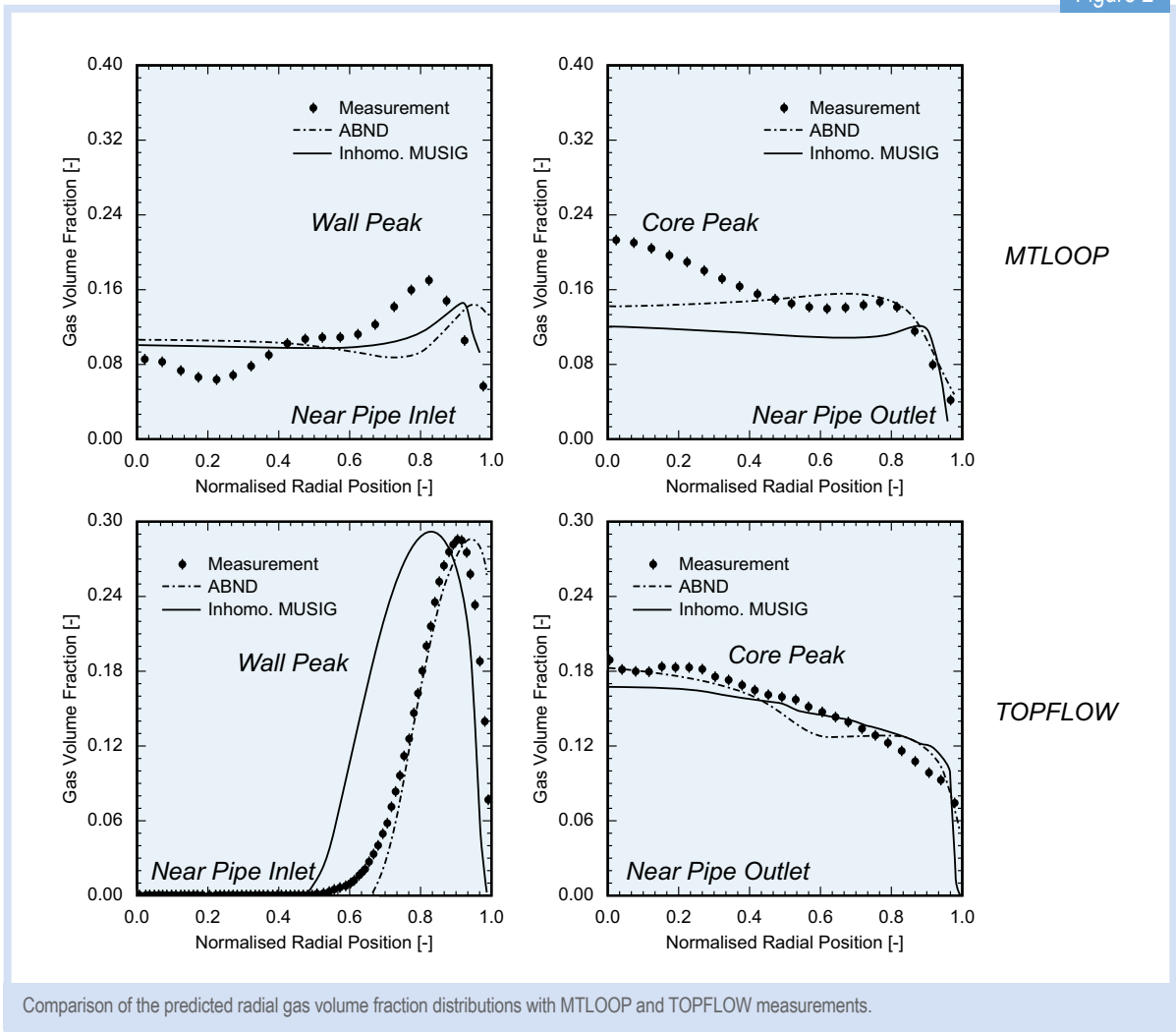


Figure 2



Assessment of models

Fig. 2 compares the predicted gas void fraction profiles for a vertical air-water flow against experimental data of MTLOOP [6] and TOPFLOW [7] obtained at Forschungszentrum Rossendorf, Germany.

It can be observed that population-balance models based on ABND and Inhomogeneous MUSIG have been able to capture the transition process from *wall peak* where the local volume fraction is maximum near the pipe wall to *core peak* where the local volume fraction is maximum at the pipe centre of the gas-volume fraction distribution.

Tomiya et al. [8] and Krepper et al. [9] have shown that the lift force which acts perpendicular to the vertical fluid flow is positive when the gas bubbles are small. These bubbles flow preferentially along the pipe wall.

However, the lift force becomes negative when the bubble size is greater than 5.5 – 6.0 mm. Because of the high bubble coalescence rate that can be experienced near the pipe outlet, the negative lift force pushes the large gas bubbles towards the pipe centre, resulting in the *core peak* distribution.

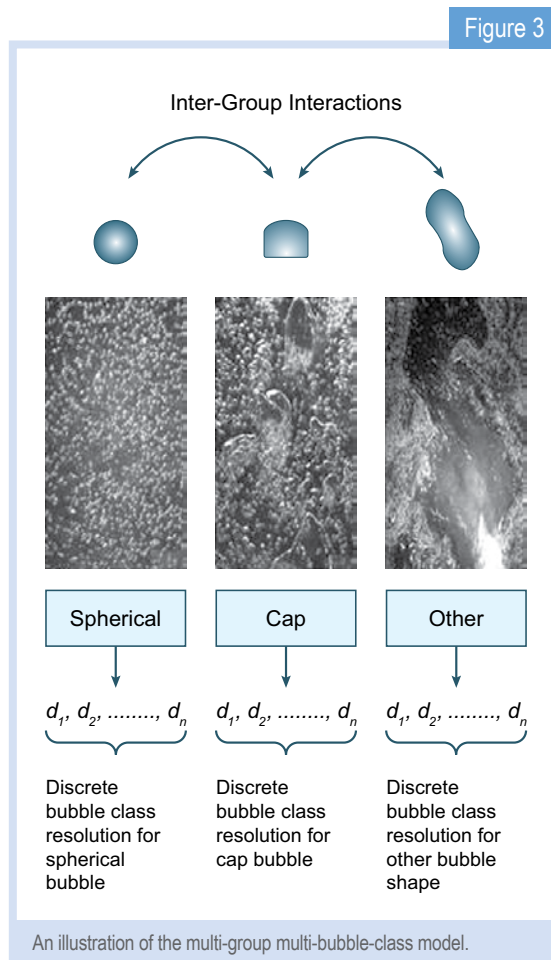
Modelling beyond bubbly flow regime

This modelling framework considers additional transport equations to characterise different groups of gas bubbles. For bubbly flow, the bubbles are normally categorised as spherical bubbles. For flows beyond the bubbly flow regime, the bubbles could be in the form of cap or slug or churn-turbulent.

By solving each transport equation to characterise the particular group of bubbles such as described in Fig. 3, such a framework presents great potential of accounting the wide spectrum of bubble sizes that may exist in different flow regimes.

References

[1] S. C. P. Cheung, G. H. Yeoh and J. Y. Tu (2007). On the modelling of population balance in isothermal vertical bubbly flows - Average bubble number density approach, *Chem. Eng. Process.*, 46, 742-756.
 [2] S. M. Lo (1996). Application of Population Balance to CFD Modelling of Bubbly Flow via the MUSIG model, AEA Technology, AEAT-1096.
 [3] D. L. Marchisio and R. O. Fox (2005). Solution of population balance equations using the direct quadrature method of moments, *J. Aerosol Sci.*, 36, 43-73.
 [4] M. J. Prince and H. W. Blanch, H. W. (1990). Bubble Coalescence and Break-up in Air-Sparged Bubble-Columns, *AIChE J.*, 36, 1485-1499.
 [5] H. Luo and H. Svendsen, H. (1996). Theoretical model for drop and bubble breakup in turbulent dispersions, *AIChE J.*, 42, 1225-1233.



Further work is required to formulate more comprehensive bubble coalescence and break-up models to handle gas-liquid flows beyond the bubbly flow regime.

[6] D. Lucas, E. Krepper and H.-M. Prasser, H.M. (2005). Development of co-current air-water flow in a vertical pipe, *Int. J. Multiphase Flow*, 31, 1304-1328.
 [7] H.-M. Prasser, M. Beyer, M., H. Carl, S. Gregor, D. Lucas, H. Pietruske, P. Schutz, F. P. Weiss (2007). Evolution of the structure of a gas-liquid two-phase flow in a large vertical pipe, *Nuc. Eng. Des.*, 237, 1848-1861.
 [8] A. Tomiyama, Struggle with computational bubble dynamics, *Proc. 3rd Int. Conf. Multiphase Flow*, Lyon, France (1998).
 [9] E. Krepper, D. Lucas, T. Frank, H.-M. Prasser and P. J. Zwart, P.J. (2008). The inhomogeneous MUSIG model for the simulation of polydispersed flows, *Nuc. Eng. Des.* 238, 1690-1702.

ANSTO facts and figures

Financial Statement (\$AUD'000)

	2010 Research		2010 Total ANSTO	
Expenditure				
Operations	44,966	62%	219,236	73%
Investments	27,903	38%	80,579	27%
Total	72,869	100%	299,815	100%
Exp according to source of income				
Federal Govt. funding	66,653	91%	156,513	69%
Third Party	6,216	9%	70,718	31%
Third Party revenue				
Private Industry	4,918	79%	67,196	95%
Grants #1	1,298	21%	3,522	5%
Total	6,216	100%	70,718	100%

#1 Includes grants from Government, Universities and CRCs

The total expenditure by ANSTO for the calendar year 2010 was AUD \$299.8 million. This represents a 39% increase from the previous year. Of this total amount, AUD \$72.9 million or 24.3% was utilised in scientific research. Federal Government (block) funding represented 91% of this revenue and 9% came from third parties.

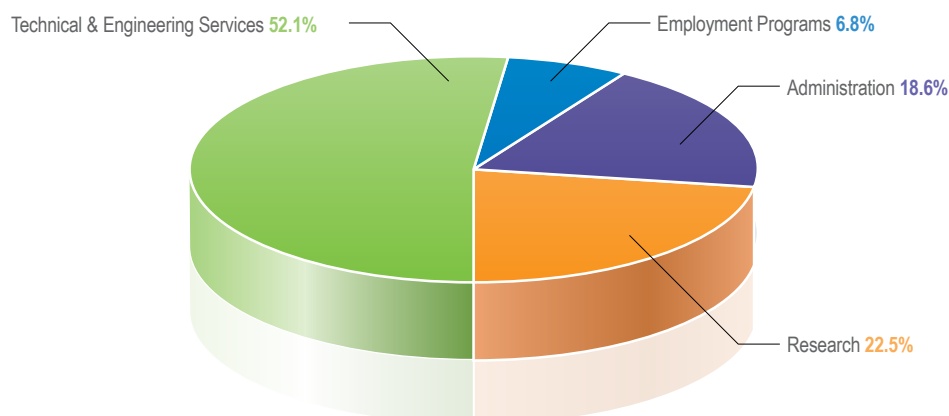
These third parties include significant private investment (79%) while the rest came through grants and Government, Universities and Co-operative Research Centres (CRCs).

ANSTO Employees

At the end of 2010, ANSTO had 1,085 full time equivalent employees of which 27.6% were women. The chart below shows ANSTO's reliance on Technical and Engineering Staff (52.1%) for a successful user-based research facility.

In addition, 36 postdoctoral fellows and 28 PhD students were involved in ANSTO's research activities.

ANSTO Employment Categories



User Facilities

2010 saw both the OPAL beam lines and the two accelerators (ANTARES and STAR) attract over 470 users with more than 1570 visits. These users came from more than 70 institutions in over 25 countries.

Invention Disclosures

In 2010 there were 3 'invention disclosures' to the patent office for the purposes of securing provisional patents.

- Anomaly Detection of Radiological Signatures
- Gallium 68 Purification
- Sorbent Material (for Radioactive Ions).

Awards 2010

- Professor David Cohen - Australian Nuclear Award (ANA) recipient
- Dr John Twining - National Programme Co-ordinator, International Atomic Energy Agency - Regional Co-operative Agreement, Project on Assessing Trends in Freshwater Quality Using Environmental Isotopes and Chemical Techniques for Improved Resource Management
- Dr Dioni Cendon - Full member of the International Quaternary Association (INQUA) group on Palaeogroundwater
- Dr Maxim Avdeev - Australian Neutron Beam Users Group "ANBUG Award" for outstanding science and leadership promoting the Australian neutron scattering community
- Dr Tamim Darwish - Fellowship by the Japan Society for the Promotion of Science in relation to the Deuterium Facility in order to collaborate with researchers at the University of Hokkaido
- Professor Jill Trehwella - Fellow of the Neutron Scattering Society of America "For her landmark experiments using small angle neutron scattering to study the structure of biological macromolecules in solution and service to the neutron scattering community."

Grants awarded in 2010 in which ANSTO collaborates

ARC Discovery Grants

- Characterising the tropical "heat engine" of global climate: combined coral, stalagmite and tree-ring records from the Indo-Pacific region (Univ. Sydney)
- Crystal-chemical tuning of order and disorder: a strategy for the discovery of novel solid state ionic conductors (Univ. Sydney)
- Novel multiferroic materials for the next generation of microelectronics: the effect of isotope substitution on magnetism (UNSW – ADFA)
- Mapping Antarctic climate change in space and time using mosses as biological proxies (Univ. Wollongong)
- Novel imaging technologies for continuous measurement of tracer kinetics in awake animals (Univ. Sydney)
- Integrated Ocean Drilling Program (IODP) drilling in the Great Barrier Reef: unlocking the causes, rates and consequences of abrupt sea level and climate change (Univ. Sydney).

ARC Linkage Infrastructure, Equipment and Facilities (LIEF) Grants

- Combined scanning tunnelling microscope system for nano-fabrication and characterisation (Univ. Wollongong)
- Facilities of Thermophysical Characterisations at Nanometre Scale for Development of Advanced Materials, Energy Technologies and Biomedical Components (Univ. NSW)
- Federated single crystal X-ray structural analysis facility (Univ. Sydney)
- A facility for sensitive and precise isotopic dating of the earth's and extraterrestrial rocks (Australian National University)
- Innovative Synchrotron Science - Access Program to the Australian National Beamline Facility and Cutting - Edge Beamlines at International Synchrotrons (Univ. Sydney)
- A mass spectrometer to analyse carbonate isotope records of Australia's climate, soil and groundwater history (Univ. of NSW)

- Sonic drilling to provide contamination-free core sampling of rock and unconsolidated sediment (Univ. Wollongong)
- An advanced characterisation facility for opaque multiphase flows (Curtin Univ. Technology)
- Biogeochemical controls on efficacy and sustainability of uranium heap leaching (Univ. NSW).

ARC Linkage Projects

- Biogeochemical controls on efficacy and sustainability of uranium heap leaching (Univ. NSW).

International Science Linkages Program

- Neutrons and Food Workshop: Addressing the challenges of food science in an evolving global environment
- A collaborative research project studying the adsorption of the fission product radionuclide (Strontium-90) on clay barrier materials at National Tsing Hua University in Taiwan
- SINAP (the Shanghai Institute for Applied Physics) Workshop
- Italian-Australian Cultural Heritage Workshop. New Scientific Techniques in Archaeology, Palaeo-Anthropology and Cultural Heritage.

Australian Government - Regional Support for National Security programme - Grant

- Research Support for Counter Terrorism.

Environmental Trust Grant

- A new approach to extracting hydrological history from River Red Gum (Macquarie Univ.).

European Union – Framework FP7

- MATTER (Materials Testing and Rules) – Fission Programme.

National Science Foundation, USA

- A “horizontal ice core” for large-volume samples of the past atmosphere, Taylor Glacier, Antarctica, Scripps Institute of Oceanography (UoC), Oregon State University, NIWA (NZ), ANSTO

- Is there cosmogenic radiomethane in polar firn? Scripps Institute of Oceanography (UoC), ANSTO, NIWA (NZ).

North Greenland Eemian Ice Drilling (NEEM), US Office of Polar Programs, National Science Foundation

- Greenland, Carbon-climate feedbacks in the palaeo record, ACE CRC, AAD, ANSTO, NIWA (NZ), University of Copenhagen, Centre for Ice and Climate, University of NSW, Oregon State University.

Australian Antarctic Division (ANARE)

- High resolution studies of cosmogenic beryllium isotopes (^{10}Be and ^7Be) at Law Dome, ANSTO, AAD, ACE CRC
- Historical atmospheric radio-methane, ANSTO, AAD, CSIRO, NIWA (NZ).

Macquarie University Grant

- Speleothems and Lakes.

Co-operative Research Centres (CRCs) and Equivalent 2010

CRCs and their equivalents are an integral part of the scientific research landscape in Australia today. From their inception, ANSTO has been involved in these centres and our current involvements are described below.

CRC for integrated engineering asset management (CIEAM)

- Sustainability and Organisational Performance
- Integration and Operability
- Capability Optimisation
- Structural Integrity.

Nuclear Structural Integrity Modelling

- Defence Materials Technology Centre (DMTC) - Non CRC.

CRC for Polymers III

- Functional Polymers for Photovoltaic devices
- Degradable Polymer films.

CRC for Biomedical Imaging and Development

- Protein Biosynthetic Pathway Targeting
- Neuroreceptor Ligand Targeting
- Development of Novel Receptor Based Radio-Pharma
- Apoptotic Pathway Targeting
- Development of Synthesis Mods for Tracer Product
- General
- CRC Revenue and Contributions
- Evaluation and Characterisation of Detector Materials.

CRC for Sustainable Resource Processing

- Geopolymers.

Partnerships and Collaboration

As reflected by the research presented here, collaboration is vital to productive and innovative science. Co-operation among the scientific community enables research institutions to combine and thus perform beyond individual capabilities and provide greater outcomes for society.

ANSTO continues to pursue collaborative agreements and memoranda of understanding with leading science and research institutions within Australia and around the world. The Australian Institute for Nuclear Science and Engineering (AINSE) is a key facilitator of collaboration between ANSTO and Australasian universities. Through AINSE, university scientists and researchers can access ANSTO's world class facilities, supporting high quality research, education and training in nuclear science and engineering.

In addition, 2010 marked the formation of the Australian Collaboration for Accelerator Science, of which ANSTO is a founding partner along with Australian National University (ANU), University of Melbourne and the Australian Synchrotron.

Since the beginning of 2010, ANSTO has broadened Australia's scientific reach, entering into formal co-operation with international research organisations including:

- CERN (European Organisation of Nuclear Research)
- French Atomic Energy Commission (CEA)
- KEK High Energy Research Organisation, Japan
- Korea Atomic Energy Research Institute (KAERI)
- Paul Scherrer Institute (PSI), Switzerland
- RIKEN SPring-8 Center, Japan.

Schools, workshops, reviews

Neutrons and Food Workshop



ACAS Workshop



51 ANSTO scientists were lecturing at Universities and higher education establishments across New South Wales and Australia.

Schools

- 4th Annual Neutron School for PhD students and Post Doctoral Fellows (33 participants) to learn about and perform experiments using ANSTO's neutron instrumentation 15 - 20 August ANSTO
- Australian Collaboration for Accelerator Science (ACAS) Workshop on Accelerator Feedback Systems 13 - 15 December, School for Accelerator Physics 13 - 17 December ACAS School
- Individual professional development days for secondary teachers: 74 teachers attended the 3 individual one-day courses on 6, 7 and 9 December. Overview of all areas of the science curriculum including Chemistry, Physics, Biology as well as Earth & Environmental Science that are covered (at a HSC level).

Workshops

- Advances in Radiopharmaceutical Sciences Conference (22 and 23 April 2010, Garvan Institute)
- Neutrons and Food Workshop (31 October to 3 November, 2010)
- Fusion Materials Workshop (4 November, 2010)
- Cyclotron Workshop (15 December 2010, ANSTO).

Reviews

- February, 2010 - ANSTO's Bragg Institute underwent an external review by an International Committee chaired by Professor Peter Colman (Walter and Eliza Hall Institute). Formal recommendations were made that are now being considered
- July 2010 - Program Advisory Committee (external review body) chaired by Prof. Anton Middelberg (University of Queensland), met to assess the scientific merit of beam-time and deuteration proposals submitted for time between October 2010 and March 2011.

ANSTO Executive

Mr Peter Arambatzis - Chief Financial Officer

Mr Robert Blissett - General Manager, Human Resources

Mr Doug Cubbin - Executive General Manager for Business and Enterprise

Professor John Dodson - Head, Institute for Environmental Research

Professor Lyndon Edwards - Head, Institute of Materials Engineering

Dr Marie-Claude Gregoire - Head, ANSTO LifeSciences

Mr Shaun Jenkinson - General Manager, ANSTO Health

Mr Paul Jones - General Manager, Security and Safeguards

Mr Con Lyras - General Manager, Engineering and Capital Programs

Mr Kobus Naude - Senior Manager Strategy

Dr Adrian (Adi) Paterson - Chief Executive Officer

Dr Robert (Bob) Ring - General Manager, ANSTO Minerals

Dr Robert (Rob) Robinson - Head, Bragg Institute

Dr Greg Storr - General Manager, Nuclear Operations

By Invitation:

Professor Richard Banati - Distinguished Research Fellow and ANSTO LifeSciences

Mr Michael Beckett - General Manager Support Services and Chief Information Officer

Ms Stephanie Cole - Senior Legal Counsel

Mr Hefin Griffiths - Manager, Safety Environment and Radiation Protection

Ms Nadia Levin - Head, Strategic Communications and Government Affairs



Pictured from left to right (back row) Kobus Naude, Rob Blissett, Hefin Griffiths, Michael Beckett, Stephanie Cole, John Dodson, Lyndon Edwards, Rob Robinson, Paul Jones, Richard Banati.

(front row) Peter Arambatzis, Nadia Levin, Adi Paterson, Greg Storr, Marie-Claude Gregoire.

Not present: Doug Cubbin, Shaun Jenkinson, Con Lyras, Bob Ring.

Australian Institute of Nuclear Science and Engineering (AINSE) - facts and figures 2010

Background

The Australian Institute of Nuclear Science and Engineering (AINSE) was established in 1958 to provide a mechanism for access to the special facilities at Lucas Heights (ANSTO) by universities and other tertiary institutions and to provide a focus for cooperation in the nuclear scientific and engineering fields.

Active membership includes 42 Universities as well as ANSTO and CSIRO.

Research Awards

Access to ANSTO's nuclear science and technology facilities as well as other AINSE supported facilities, is the primary purpose of these awards. These awards require close cooperation by both ANSTO and University staff and generally involve substantial use of both the accelerators and the reactor.

In 2010, 198 projects were supported with a total value of \$1,655,066.

International Conference and Travel Scholarships:

- 5 scholarships were awards to students and post-doctoral fellows to the value of \$900 each.

Postgraduate Research Awards

In 2010, AINSE supported 21 new postgraduate research projects with 12 finalised and submitted in receipt of their thesis. A total of 81 scholars are currently active in this programme.

Research Fellows

These are three year fellowships which can be extended to a total of five years where appropriate. In 2010 there were two recipients:

- Rachel Popelka-Filcoff – (Flinders University) 2010. Geochemical Characterisation of Australian ochre by k_0 – Neutron Activation Analysis for Characterisation and sourcing of aboriginal Australian Mines and Artefacts
- Roman Dronov – (Flinders University) 2010. Design of Advanced Optical Biosensors through Neutron-Based Surface Analysis.

Grants awarded in 2010 in which AINSE collaborates

ARC Linkage Infrastructure, Equipment and Facilities (LIEF) Grants:

- High-Resolution ITRAX Core Scanning for Global Change Research

Schools, Workshops and Reviews

(Run and held at AINSE only)

- AINSE ANBUG Neutron Scattering Symposium (AANSS – 2010) Neutron and X-ray Scattering – from Biology to Physics (1 to 3 December 2010)

AINSE supported in excess of 100 students and lectures through travel grants and bursaries to attend conferences and workshops held around Australia and internationally.

Publications

Notification was given of 329 publications that incorporated results from AINSE supported projects in 2010. Of these, 181 were in refereed journals and 113 were published with an ANSTO co-author.

ANSTO Publications 2010

	Page
Refereed Journal Publications (191)	115
Books (1), Book Chapters (7), Theses (1), Editing of Special Journal Issues (1), Other (Webpage) (1)	126
Published Conference Proceedings (85)	127

Refereed Journal Publications

Araujo, P. Z., Luca, V., Bozzano, P. B., Bianchi, H. L., Soler-Illia, G., and Blesa, M. A. Aerosol-assisted production of mesoporous titania microspheres with enhanced photocatalytic activity: the basis of an improved process. *ACS Applied Materials & Interfaces*, 2(6), 1663-1673. (2010).

Avdeev, M., Kharton, V. V., and Tshipis, E. V., Geometric parameterization of the YBaCo₄O₇ structure type: Implications for stability of the hexagonal form and oxygen uptake, *J. Solid State Chem.*, 183(10), 2506-2509 (2010).

Baldini, L. M., McDermott, F., Baldini, J. U. L., Fischer, M. J., and Mollhoff, M. An investigation of the controls on Irish precipitation $\delta^{18}\text{O}$ values on monthly and event timescales. *Climate Dynamics*, 35(6), 977-993. (2010).

Bali, R., Siegele, R., and Harris, A. T. Phytoextraction of Au: uptake, accumulation and cellular distribution in *Medicago sativa* and *Brassica juncea*. *Chemical Engineering Journal*, 156(2), 286-297. (2010).

Benesch, J. L. P., Aquilina, J. A., Baldwin, A. J., Rekas, A., Stengel, F., Lindner, R. A., Basha, E., Devlin, G. L., Horwitz, J., Vierling, E., Carver, J. A., and Robinson, C.V., The Quaternary Organization and Dynamics of the Molecular Chaperone HSP26 Are Thermally Regulated, *Chem. Biol.*, 17(9), 1008-1017 (2010).

Benson, S. J., Lennard, C. J., Hill, D. M., Maynard, P., and Roux, C. Forensic Analysis of Explosives Using Isotope Ratio Mass Spectrometry (IRMS)-Part 1: Instrument Validation of the DELTAplusXP IRMS for Bulk Nitrogen Isotope Ratio Measurements. *Journal of Forensic Sciences*, 55(1), 193-204. (2010).

Benson, S. J., Lennard, C. J., Maynard, P., Hill, D. M., Andrew, A. S., Neal, K., et al. Forensic Analysis of Explosives Using Isotope Ratio Mass Spectrometry (IRMS)-Part 2: Forensic Inter-Laboratory Trial: Bulk Carbon and Nitrogen Stable Isotopes in a Range of Chemical Compounds (Australia and New Zealand). *Journal of Forensic Sciences*, 55(1), 205-212. (2010).

Berecki, G., Motin, L., Haythornthwaite, A., Vink, S., Bansal, P., Drinkwater, R., Wang, C. I., Moretta, M., Lewis, R. J., Alewood, P. F., Christie, M. J., and Adams, D. J., Analgesic omega-Conotoxins CVIE and CVIF Selectively and Voltage-Dependently Block Recombinant and Native N-Type Calcium Channels, *Mol. Pharmacol.*, 77(2), 139-148 (2010).

Bignell, L. J., Mo, L., Alexiev, D., and Hashemi-Nezhad, S. R. Effect of multiple γ -ray interactions on ionisation quenching corrections in liquid scintillants. *Nuclear Instruments & Methods in Physics Research Section a-Accelerators Spectrometers Detectors and Associated Equipment*, 614(2), 231-236. (2010).

Blazek, J., and Copeland, L., Amylolysis of wheat starches. I. Digestion kinetics of starches with varying functional properties, *J. Cereal Sci.*, 51(3), 265-270 (2010).

Blazek, J., and Copeland, L., Amylolysis of wheat starches. II. Degradation patterns of native starch granules with varying functional properties, *J. Cereal Sci.*, 52(2), 295-302 (2010).

Blazek, J., and Gilbert, E. P., Effect of Enzymatic Hydrolysis on Native Starch Granule Structure, *Biomacromolecules*, 11(12), 3275-3289 (2010).

Boland, M. P., Hatty, C. R., Separovic, F., Hill, A. F., Tew, D. J., Barnham, K. J., Haigh, C. L., James, M., Masters, C. L., and Collins, S. J., Anionic Phospholipid Interactions of the Prion Protein N Terminus Are Minimally Perturbing and Not Driven Solely by the Octapeptide Repeat Domain, *J. Biol. Chem.*, 285(42), 32282-32292 (2010).

Bonyhady, S. J., Jones, C., Nembenna, S., Stasch, A., Edwards, A. J., and McIntyre, G. J., beta-Diketiminato-Stabilized Magnesium(I) Dimers and Magnesium(II) Hydride Complexes: Synthesis, Characterization, Adduct Formation, and Reactivity Studies, *Chem.-Eur. J.*, 16(3), 938-955 (2010).

Boyd, P., Edwards, A., Gardiner, M., Ho, C., Lemée-Cailleau, M. H., McGuinness, D., Riapanitra, A., Steed, J., Stringer, D., and Yates, B., Reduction of a Chelating Bis(NHC) Palladium(II) Complex to $[\{\mu\text{-bis(NHC)}\}_2\text{Pd}^{\text{II}}]^+$: A Terminal Hydride in a Binuclear Palladium(I) Species Formed under Catalytically Relevant Conditions, *Angew. Chem.-Int. Edit.*, 49(36), 6315-6318 (2010).

Brant, W. R., Schmid, S., Gu, Q. F., Withers, R. L., Hester, J., and Avdeev, M., Temperature and composition dependent structural investigation of the defect perovskite series $\text{Sr}_{1-x}\text{Ti}_{1-2x}\text{Nb}_{2x}\text{O}_3$, $0 \leq x \leq 0.2$, *J. Solid State Chem.*, 183(9), 1998-2003 (2010).

Caba, B. L., Zhang, Q., Carroll, M. R. J., Woodward, R. C., St Pierre, T. G., Gilbert, E. P., Riffle, J. S., and Davis, R. M., Nanostructure of PEO-polyurethane-PEO triblock copolymer micelles in water, *J. Colloid Interface Sci.*, 344(1), 81-89 (2010).

Callaghan, M. D., Humphries, S. R., Law, M., Ho, M., Bendeich, P., Li, H., et al. Energy-based approach for the evaluation of low cycle fatigue behaviour of 2.25Cr-1Mo steel at elevated temperature. *Materials Science and Engineering a-Structural Materials Properties Microstructure and Processing*, 527(21-22), 5619-5623. (2010).

Carroll, M. R.J., Woodward, R. C., House, M. J., Teoh, W. Y., Amal, R., Hanley, T. L., and St Pierre, T. G., Experimental validation of proton transverse relaxivity models for superparamagnetic nanoparticle MRI contrast agents, *Nanotechnology*, 21(3), Art. No. 035103 (2010).

Cartwright, I., Weaver, T. R., Simmons, C. T., Fifield, L. K., Lawrence, C. R., Chisari, R., et al. Physical hydrogeology and environmental isotopes to constrain the age, origins, and stability of a low-salinity groundwater lens formed by periodic river recharge: Murray Basin, Australia. *Journal of Hydrology*, 380(1-2), 203-221. (2010).

Cartwright, I., Weaver, T., Cendon, D. I., and Swane, I. Environmental isotopes as indicators of inter-aquifer mixing, Wimmera region, Murray Basin, Southeast Australia. *Chemical Geology*, 277(3-4), 214-226. (2010).

Cendon, D. I., Larsen, J. R., Jones, B. G., Nanson, G. C., Rickleman, D., Hankin, S. I., et al. Freshwater recharge into a shallow saline groundwater system, Cooper Creek floodplain, Queensland, Australia. *Journal of Hydrology*, 392(3-4), 150-163. (2010).

Cheetham, M. D., Keene, A. F., Erskine, W. D., Bush, R. T., Fitzsimmons, K., Jacobsen, G. E., et al. Resolving the Holocene alluvial record in southeastern Australia using luminescence and radiocarbon techniques. *Journal of Quaternary Science*, 25(7), 1160-1168. (2010).

Chen, D. H., Cao, L., Huang, F. Z., Imperia, P., Cheng, Y. B., and Caruso, R. A. Synthesis of Monodisperse Mesoporous Titania Beads with Controllable Diameter, High Surface Areas, and Variable Pore Diameters (14-23 nm). *Journal of the American Chemical Society*, 132(12), 4438-4444. (2010).

Child, D. P., Hotchkis, M. A. C., Whittle, K., and Zorko, B. Ionisation efficiency improvements for AMS measurement of actinides. *Nuclear Instruments & Methods in Physics Research Section B-Beam Interactions with Materials and Atoms*, 268(7-8), 820-823. (2010).

Chou, S. L., Wang, J. Z., Choucair, M., Liu, H. K., Stride, J. A., and Dou, S. X., Enhanced reversible lithium storage in a nanosize silicon/graphene composite, *Electrochem. Commun.*, 12(2), 303-306 (2010).

Chow, J. Y. H., Jeffries, C. M., Kwan, A. H., Guss, J. M., and Trewhella, J., Calmodulin Disrupts the Structure of the HIV-1 MA Protein, *J. Mol. Biol.*, 400(4), 702-714 (2010).

Cohen, D. D., Crawford, J., Stelcer, E. and Bac, V. Thu. Characterisation and Source Apportionment of Fine Particulate Sources at Hanoi from 2001 to 2008. *Atmos. Environ.*, 44 320-328. (2010).

Cohen, D. D., Crawford, J., Stelcer, E., & Bac, V. T. Long range transport of fine particle windblown soils and coal fired power station emissions into Hanoi between 2001 to 2008. *Atmospheric Environment*, 44(31), 3761-3769. (2010).

Cohen, T. J.; Nanson, G. C.; Larsen, J. R.; Jones, B. G.; Price, D. M.; Coleman, M.; Pietsch, T. J. Late Quaternary aeolian and fluvial interactions on the Cooper Creek Fan and the association between linear and source-bordering dunes, Strzelecki Desert, Australia. *Quaternary Science Reviews*, 29(3-4): 455-471. (2010).

Collins, R. N., and Kinsela, A. S. (2010). Aqueous phase speciation and chemistry of cobalt in terrestrial environments. *Chemosphere*, 79(8), 763-771. (2010).

Comoletti, D., Miller, M. T., Jeffries, C. M., Wilson, J., Demeler, B., Taylor, P., Trewhella, J., and Nakagawa, T., The Macromolecular Architecture of Extracellular Domain of alpha NRXN1: Domain Organization, Flexibility, and Insights into Trans-Synaptic Disposition, *Structure*, 18(8), 1044-1053 (2010).

Creighton, N. M., and Twining, J. R. Bioaccumulation from food and water of cadmium, selenium and zinc in an estuarine fish, *Ambassis jacksoniensis*. *Marine Pollution Bulletin*, 60(10), 1815-1821. (2010).

Cross, A.J., Jeffries, C. M., Trewhella, J., and Matthews, J. M., LIM Domain Binding Proteins 1 and 2 Have Different Oligomeric States, *J. Mol. Biol.*, 399(1), 133-144 (2010).

Darwish, T.A., Evans, R. A., James, M., Malic, N., Triani, G., and Hanley, T. L., CO₂ Triggering and Controlling Orthogonally Multiresponsive Photochromic Systems, *J. Am. Chem. Soc.*, 132(31), 10748-10755 (2010).

Deslandes, A., Jasieniak, M., Ionescu, M., Shapter, J. G., and Quinton, J. S. Hydrogenation of sp² - bonded carbon surfaces using methane plasma. *Applied Surface Science*, 256(6), 1888-1894. (2010).

Dong, Y. D., Tilley, A. J., Larson, I., Lawrence, M. J., Amenitsch, H., Rappolt M., Hanley T., and Boyd, B. J., Nonequilibrium Effects in Self-Assembled Mesophase Materials: Unexpected Supercooling Effects for Cubosomes and Hexosomes, *Langmuir*, 26(11), 9000-9010 (2010).

Drisko, G. L., Imperia, P., de los Reyes, M., Luca, V., and Caruso, R. A. Size matters: incorporation of poly(acrylic acid) and small molecules into hierarchically porous metal oxides prepared with and without templates. *Langmuir*, 26(17), 14203-14209. (2010).

Drisko, G. L., Kimling, M. C., Scales, N., Ide, A., Sizgek, E., Caruso, R. A., et al. One-pot preparation and uranyl adsorption properties of hierarchically porous zirconium titanium oxide beads using phase separation processes to vary macropore morphology. *Langmuir*, 26(22), 17581-17588. (2010).

Fenton, A. W., Williams, R., and Trehwella, J., Changes in Small-Angle X-ray Scattering Parameters Observed upon Binding of Ligand to Rabbit Muscle Pyruvate Kinase Are Not Correlated with Allosteric Transitions, *Biochemistry*, 49(33), 7202-7209 (2010).

Fernando, D. R., Mizuno, T., Woodrow, I. E., Baker, A. J. M., and Collins, R. N. Characterization of foliar manganese (Mn) in Mn (hyper)accumulators using X-ray absorption spectroscopy. *New Phytologist*, 188(4), 1014-1027. (2010).

Fong, W. K., Hanley, T. L., Thierry, B., Kirby, N., and Boyd, B. J., Plasmonic Nanorods Provide Reversible Control over Nanostructure of Self-Assembled Drug Delivery Materials, *Langmuir*, 26(9), 6136-6139 (2010).

Gao, Y., Heinemann, A., Knott, R., and Bartlett, J., Encapsulation of Protein in Silica Matrices: Structural Evolution on the Molecular and Nanoscales, *Langmuir*, 26(2), 1239-1246 (2010).

Garcia-Fernandez, M., Staub, U., Bodenthin, Y., Pomjakushin, V., Mirone, A., Fernandez-Rodriguez, J., Scagnoli, V., Mulders, A. M., Lawrence, S. M., and Pomjakushina, E., Doping and temperature dependence of Mn 3d states in A-site ordered manganites, *Phys. Rev. B*, 82(23), Art. No. 235108 (2010).

Goossens, D. J., Studer, A. J., and Stachurski, Z. H., Microstructure of Horseshoe Nails Using Neutron Diffraction, *J. Mater. Eng. Perform.*, 19(3), 380-384 (2010).

Grey, I. E., Madsen, I. C., Mills, S. J., Hatert, F., Peterson, V. K., and Bastow, T. J., A new type of cubic-stacked layer structure in anthoinite, AlWO₃(OH)₃, *Am. Miner.*, 95(4), 639-645 (2010).

Griffiths, A. D., Zahorowski, W., Element, A. and Werczynski, S. Map of radon flux at the Australian land surface. *Atmospheric Chemistry and Physics Discussions*, 10(6), 14313–14346. (2010).

Griffiths, M. L., Drysdale, R. N. and 8 other authors (including M. J. Fischer). Evidence for Holocene changes in Australian-Indonesian monsoon rainfall from stalagmite trace element and stable isotope ratios. *Earth and Planetary Science Letters*, 292, 27-38. (2010).

Guralnik, B., Matmon, A., Avni, Y., and Fink, D. Be-10 exposure ages of ancient desert pavements reveal Quaternary evolution of the Dead Sea drainage basin and rift margin tilting. *Earth and Planetary Science Letters*, 290(1-2), 132-141. (2010).

Hameed, N., Guo, Q. P., Hanley, T., and Mai, Y. W., Hydrogen Bonding Interactions, Crystallization, and Surface Hydrophobicity in Nanostructured Epoxy/Block Copolymer Blends, *J. Polym. Sci. Pt. B-Polym. Phys.*, 48(7), 790-800 (2010).

Hameed, N., Guo, Q. P., Xu, Z. G., Hanley, T. L., and Mai, Y. W., Reactive block copolymer modified thermosets: highly ordered nanostructures and improved properties, *Soft Matter*, 6(24), 6119-6129 (2010).

He, L. Z., Wang, H., Garamus, V. M., Hanley, T., Lensch, M., Gabius, H. J., Fee, C. J., and Middelberg, A., Analysis of MonoPEGylated Human Galectin-2 by Small-Angle X-ray and Neutron Scattering: Concentration Dependence of PEG Conformation in the Conjugate, *Biomacromolecules*, 11(12), 3504-3510 (2010).

Hoile, R., Banos, C., Colella, M., Walsh, S. J., and Roux, C. Gamma Irradiation as a Biological Decontaminant and Its Effect on Common Fingerprint Detection Techniques and DNA Profiling. *Journal of Forensic Sciences*, 55(1), 171-177. (2010).

Htoon, A. K., Uthayakumar, S., Piyasiri, U., Appelqvist, I. A. M., López-Rubio, A., Gilbert, E. P., and Mulder, R. J., The effect of acid dextrinisation on enzyme-resistant starch content in extruded maize starch, *Food Chem.*, 120(1), 140-149 (2010).

Huang, T. W., Chen, T. K., Yeh, K. W., Ke, C. T., Chen, C. L., Huang, Y. L., Hsu, F. C., Wu, M. K., Wu, P. M., Avdeev, M., and Studer, A. J., Doping-driven structural phase transition and loss of superconductivity in $M_x\text{Fe}_{1-x}\text{Se}_2$ ($M=\text{Mn, Cu}$), *Phys. Rev. B*, 82(10), Art. No. 104502 (2010).

Humphries, S. R., Snowden, K. U., and Yeung, W. The effect of repeated loadings on the stress relaxation properties of 2.25Cr-1Mo steel at 550°C and the influence on the Feltham 'a' and 'b' parameters. *Materials Science and Engineering a-Structural Materials Properties Microstructure and Processing*, 527(13-14), 3240-3244. (2010).

Iles, J., Kelleway, J., Kobayashi, T., Mazumder, D., Knowles, L., Priddel, D., et al. Grazing kangaroos act as local recyclers of energy on semiarid floodplains. *Australian Journal of Zoology*, 58(3), 145-149. (2010).

Itakura, T., Airey, D. W., Leo, C. J., Payne, T., and McOrist, G. D. Laboratory studies of the diffusive transport of ^{137}Cs and ^{60}Co through potential waste repository soils. *Journal of Environmental Radioactivity*, 101(9), 723-729. (2010).

Jacques, D. A., and Trehwella, J., Small-angle scattering for structural biology-Expanding the frontier while avoiding the pitfalls, *Protein Sci.*, 19(4), 642-657 (2010).

James, M., Carter, M. L., Zhang, Z. M., Zhang, Y. J., Wallwork, K. S., Avdeev, M., and Vance, E. R., Crystal Chemistry and Structures of (Ca,U) Titanate Pyrochlores, *J. Am. Ceram. Soc.*, 93(10), 3464-3473 (2010).

Karatchevtseva, I., Astoux, M., Cassidy, D. J., Yee, P., Bartlett, J. R., and Griffith, C. S. Synthesis and Characterization of Functionalized Silica-Based Nanohybrid Materials for Oxyanions Adsorption. *Langmuir*, 26(11), 8327-8335. (2010).

Kealley, C. S., Sokolova, A. V., Kearley, G. J., Kemner, E., Russina, M., Faraone, A., Hamilton, W. A., and Gilbert, E. P., Dynamical transition in a large globular protein: Macroscopic properties and glass transition, *BBA-Proteins Proteomics*, 1804, 34-40 (2010).

Kearley, G. J., and Johnson, M. R., Vibrational spectroscopy with neutrons-Where are we now?, *Vib. Spectrosc.*, 53(1), 54-59 (2010).

Kelleway, J., Mazumder, D., Wilson, G. G., Saintilan, N., Knowles, L., Iles, J., et al., Trophic structure of benthic resources and consumers varies across a regulated floodplain wetland. *Marine and Freshwater Research*, 61(4), 430-440. (2010).

Kent, B., Garvey, C. J., Lenne, T., Porcar, L., Garamus, V. M., and Bryant, G., Measurement of glucose exclusion from the fully hydrated DOPE inverse hexagonal phase, *Soft Matter*, 6(6), 1197-1202 (2010).

Khan, M. K., Hainsworth, S. V., Fitzpatrick, M. E., and Edwards, L. Combined experimental and finite element approach for determining mechanical properties of aluminium alloys by nanoindentation. *Computational Materials Science*, 49(4), 751-760. (2010).

Kharton, V. V., Patrakee, M. V., Tsipis, E. V., Avdeev, M., Naumovich, E. N., Anikina, P. V., and Waerenborgh, J. C., Oxygen nonstoichiometry, chemical expansion, mixed conductivity, and anodic behavior of Mo-substituted $\text{Sr}_3\text{Fe}_2\text{O}_7$ -delta, *Solid State Ion.*, 181(21-22), 1052-1063 (2010).

Kiernan, K., Fink, D., Greig, D., and Mifud, C., Cosmogenic radionuclide chronology of pre-last glacial cycle moraines in the Western Arthur range, Southwest Tasmania. *Quaternary Science Reviews*, 29(23-24), 3286-3297. (2010).

Kimber, S. A. J., Ling, C. D., Morris, J. P., Chemseddine, A., Henry, P. F., and Argyriou, D. N., Interlayer tuning of electronic and magnetic properties in honeycomb ordered $\text{Ag}_3\text{LiRu}_2\text{O}_6$, *J. Mater. Chem.*, 20(37), 8021-8025 (2010).

Kinsela, A. S., Tjitradjaja, A., Collins, R. N., Waite, T. D., Payne, T. E., Macdonald, B. C. T., et al., Influence of calcium and silica on hydraulic properties of sodium montmorillonite assemblages under alkaline conditions. *Journal of Colloid and Interface Science*, 343(1), 366-373. (2010).

- Kisi, E. H., Zhang, J. F., Kirstein, O., Riley, D. P., Styles, M. J., and Paradowska, A. M., Shear stiffness in nanolaminar Ti_3SiC_2 challenges ab initio calculations, *J. Phys.-Condes. Matter*, 22(16), Art. No. 162202 (2010).
- Kong, P., Huang, F. X., Liu, X. H., Fink, D., Ding, L., & Lai, Q. Z., Late Miocene ice sheet elevation in the Grove Mountains, East Antarctica, inferred from cosmogenic ^{21}Ne - ^{10}Be - ^{26}Al . *Global and Planetary Change*, 72(1-2), 50-54. (2010).
- Kruglova, O., Mulder, F. M., Kearley, G. J., Picken, S. J., Stride, J. A., Paraschiv, I., and Zuilhof, H., Dispersive kinetics in discotic liquid crystals, *Phys. Rev. E*, 82(5), Art. No. 051703 (2010).
- Kuang, X. J., Li, Y. D., Ling, C. D., Withers, R. L., and Evans, I. R., Oxide Ion Conductivity, Phase Transitions, and Phase Separation in Fluorite-Based $Bi_{38-x}Mo_{7+x}O_{78+1.5x}$, *Chem. Mat.*, 22(15), 4484-4494 (2010).
- Ladd, B., Larsen, J. R., and Bonser, S. P. Effect of two types of tree guards (with and without weed control) on tree seedling establishment. *Ecological Management & Restoration*, 11(1), 75-76. (2010).
- Lauw, Y., Horne, M. D., Rodopoulos, T., Nelson, A., and Leermakers, F. A. M., Electrical Double-Layer Capacitance in Room Temperature Ionic Liquids: Ion-Size and Specific Adsorption Effects, *J. Phys. Chem. B*, 114(34), 11149-11154 (2010).
- Lauw, Y., Rodopoulos, T., Gross, M., Nelson, A., Gardner, R., and Horne, M. D., Electrochemical cell for neutron reflectometry studies of the structure of ionic liquids at electrified interface, *Rev. Sci. Instrum.*, 81(7), Art. No. 074101 (2010).
- Law, M., Kirstein, O., and Luzin, V., An assessment of the effect of cutting welded samples on residual stress measurements by chill modelling, *J. Strain Anal. Eng. Des.*, 45(8), 567-573 (2010).
- Law, R. M. Steele, L.P., Krummel, P.B., and Zahorowski, W., : Synoptic variations in atmospheric CO2 at Cape Grim: a model intercomparison', *Tellus 62B*, 810-820. (2010).
- Lee, J., Metson, J., Evans, P. J., Pal, U., and Bhattacharyya, D., Comparison of implantation and diffusion behavior of Ti, Sb and N in ion-implanted single crystal and polycrystalline ZnO: A SIMS study. *Applied Surface Science*, 256(7), 2143-2146. (2010).
- Lenne, T., Garvey, C. J., Koster, K. L., and Bryant, G., Kinetics of the lamellar gel-fluid transition in phosphatidylcholine membranes in the presence of sugars, *Chem. Phys. Lipids*, 163(2), 236-242 (2010).
- Levy, E., Chan, L. K., Yu, D. H., Koza, M. M., Mastai, Y., Ford, R. C., and Li, J. C., Neutron scattering study of water confined in periodic mesoporous organosilicas, *J. Solid State Chem.*, 183(7), 1691-1696 (2010).
- Li, X. L., Cai, K. F., Li, H., Yu, D. H., Wang, X., and Wang, H. F., Alumina template-assisted electrodeposition of $Bi_2Te_{2.7}Se_{0.3}$ nanowire arrays, *Superlattices Microstruct.*, 47(6), 710-713 (2010).
- Li, Y., Baledent, V., Yu, G., Barisic, N., Hradil, K., Mole, R. A., Sidis, Y., Steffens, P., Zhao, X., Bourges, P., and Greven, M., Hidden magnetic excitation in the pseudogap phase of a high-Tc superconductor, *Nature*, 468(7321), 283-285 (2010).
- Liljedahl, C. D. M., Zanellato, O., Fitzpatrick, M. E., Lin, J., and Edwards, L., The effect of weld residual stresses and their re-distribution with crack growth during fatigue under constant amplitude loading. *International Journal of Fatigue* 32(4), 735-743. (2010).
- Lilly, K., Fink, D., Fabel, D., and Lambeck, K., Pleistocene dynamics of the interior East Antarctic ice sheet. *Geology*, 38(8), 703-706. (2010).
- Ling, C. D., Avdeev, M., Kharton, V. V., Yaremchenko, A. A., Macquart, R. B., and Hoelzel, M., Structures, Phase Transitions, Hydration, and Ionic Conductivity of $Ba_4Ta_2O_9$, *Chem. Mat.*, 22(2), 532-540 (2010).
- Ling, C. D., Kennedy, B. J., Zhou, Q. D., Spencer, J. R., and Avdeev, M., Synthesis, structures, and phase transitions of barium bismuth iridium oxide perovskites Ba_2BilrO_6 and $Ba_3Bilr_2O_9$, *J. Solid State Chem.*, 183(3), 727-735 (2010).
- Liss, K. D., and Yan, K., Thermo-mechanical processing in a synchrotron beam, *Mater. Sci. Eng. A-Struct. Mater. Prop. Microstruct. Process.*, 528(1), 11-27 (2010).
- Lock, N., Wu, Y., Christensen, M., Cameron, L. J., Peterson, V. K., Bridgeman, A. J., Kepert, C. J., and Iversen, B. B., Elucidating Negative Thermal Expansion in MOF-5, *J. Phys. Chem. C*, 114(39), 16181-16186 (2010).

Lovelock, C. E., Sorrell, B. K., Hancock, N., Hua, Q., and Swales, A., Mangrove forest and soil development on a rapidly accreting shore in New Zealand. *Ecosystems*, 13(3), 437-451. (2010).

Luca, V., Drabarek, E., Griffith, C. S., and Hanley, T. L., Understanding the Supramolecular Self-Assembly of Zirconium Titanate Mesophases Formed from the Poly(ethylene oxide) Surfactant Brij-58, *Chem. Mat.*, 22(13), 3832-3842 (2010).

Lumpkin, G. R., Blackford, M. G., Smith, K. L., Whittle, K. R., Zaluzec, N. J., Ryan, E. A., et al. Ion irradiation of the TiO₂ polymorphs and cassiterite. *American Mineralogist*, 95(1), 192-195. (2010).

Macquart, R. B., Kennedy, B. J., and Avdeev, M., A primitive tetragonal intermediate in the orthorhombic-cubic phase transition of perovskite-type strontium niobate Sr_{0.92}NbO₃, *J. Solid State Chem.*, 183(10), 2400-2405 (2010).

Macquart, R. B., Kennedy, B. J., and Avdeev, M., Neutron diffraction study of phase transitions in perovskite-type strontium molybdate SrMoO₃, *J. Solid State Chem.*, 183(1), 250-255 (2010).

Mazumder, D. and Saintilan, N., Mangrove leaves are not an important dietary source of carbon and nitrogen for crabs in temperate Australian mangroves, *Wetlands*, 30:375-380. (2010).

Mazumder, D., Iles, J., Kelleway, J., Kobayashi, T., Knowles, L., Saintilan, N., et al. Effect of acidification on elemental and isotopic compositions of sediment organic matter and macro-invertebrate muscle tissues in food web research. *Rapid Communications in Mass Spectrometry*, 24(20), 2938-2942. (2010).

McGlenn, P. J., de Beer, F. C., Aldridge, L. P., Radebe, M. J., Nshimirimana, R., Brew, D. R. M., et al., Appraisal of a cementitious material for waste disposal: neutron imaging studies of pore structure and sorptivity. *Cement and Concrete Research*, 40(8), 1320-1326. (2010).

Miller, W., Causeret, L., and Ling, C. D., Frustrated magnetism and local structural disorder in pyrochlore-type Bi_{1.89}Fe_{1.16}Nb_{0.95}O_{6.95}, *J. Phys.-Condes. Matter*, 22(48), Art. No. 486004 (2010).

Minakshi, M. and Blackford, M. G., Electrochemical characteristics of B₄C or BN added MnO₂ cathode material for alkaline batteries. *Materials Chemistry and Physics*, 123(2-3), 700-705. (2010).

Minakshi, M., Blackford, M. G., Thorogood, G. J., and Issa, T. B., The effect of B₄C addition to MnO₂ in a cathode material for battery applications. *Electrochimica Acta*, 55(3), 1028-1033. (2010).

Mistry, M. K., Choudhury, N. R., Dutta, N. K., and Knott, R., Inorganic modification of block copolymer for medium temperature proton exchange membrane application, *J. Membr. Sci.*, 351(1-2), 168-177 (2010).

Mistry, M. K., Choudhury, N. R., Dutta, N. K., and Knott, R., Nanostructure Evolution in High-Temperature Perfluorosulfonic Acid Ionomer Membrane by Small-Angle X-ray Scattering, *Langmuir*, 26(24), 19073-19083 (2010).

Mitchell, M.R., Reader, S.W., Johnston, K.E., Pickard, C.J., Whittle, K.R., and Ashbrook, S.E., "¹¹⁹Sn MAS NMR and first principles calculations for the investigation of disorder in stannate pyrochlores". *Physical Chemistry Chemical Physics*, 13, 488-497 (2010).

Mulders, A. M., Lawrence, S. M., Princep, A. J., Staub, U., Bodenthin, Y., Garcia-Fernandez, M., Garganourakis, M., Hester, J., Macquart, R., and Ling, C. D., Circularly polarized soft X-ray diffraction study of helical magnetism in hexaferrite, *Phys. Rev. B*, 81(9), Art. No. 092405 (2010).

Muransky, O., Barnett, M. R., Carr, D. G., Vogel, S. C. and Oliver, E. C., Investigation of deformation twinning in a fine-grained and coarse-grained ZM20 Mg alloy: Combined *in situ* neutron diffraction and acoustic emission. *Acta Materialia*, 58(5), 1503-1517. (2010).

Muransky, O., Barnett, M. R., Luzin, V., and Vogel, S., On the correlation between deformation twinning and Luders-like deformation in an extruded Mg alloy: *In situ* neutron diffraction and EPSC.4 modelling, *Mater. Sci. Eng. A-Struct. Mater. Prop. Microstruct. Process.*, 527(6), 1383-1394 (2010).

Musumeci, A. W., Schiller, T. L., Xu, Z. P., Minchin, R. F., Martin, D. J. and Smith, S. V., Synthesis and Characterization of Dual Radiolabeled Layered Double Hydroxide Nanoparticles for Use in In Vitro and In Vivo Nanotoxicology Studies. *Journal of Physical Chemistry C*, 114(2), 734-740. (2010).

Musumeci, A. W., Xu, Z. P., Smith, S. V., Minchin, R. F. and Martin, D. J., Layered double hydroxide nanoparticles incorporating terbium: applicability as a fluorescent probe and morphology modifier. *Journal of Nanoparticle Research*, 12(1), 111-120. (2010).

Nadeem, M. A., Bhadbhade, M., and Stride, J. A., Four new coordination polymers constructed from benzene tricarboxylic acid: synthesis, crystal structure, thermal and magnetic properties, *Dalton Trans.*, 39(41), 9860-9865 (2010).

Nadeem, M. A., Bhadbhade, M., Bircher, R., and Stride, J. A., Controlled Synthesis of Isomorphous Coordination Polymers via *in Situ* Ligand Transformation Reaction: Crystal Structure, Thermal and Magnetic Properties, *Cryst. Growth Des.*, 10(9), 4060-4067 (2010).

Nadeem, M. A., Bhadbhade, M., Bircher, R., and Stride, J. A., Three isolated structural motifs in one crystal: penetration of two 1D chains through large cavities within 2D polymeric sheets, *Crystengcomm*, 12(5), 1391-1393 (2010).

Nadeem, M. A., Craig, D. J., Bircher, R., and Stride, J. A., Magneto-structural correlations of a three-dimensional Mn based metal-organic framework, *Dalton Trans.*, 39(18), 4358-4362 (2010).

Nguyen, T. H., Hanley, T., Porter, C. J. H., Larson, I., and Boyd, B. J., Phytantriol and glyceryl monooleate cubic liquid crystalline phases as sustained-release oral drug delivery systems for poorly water soluble drugs I. Phase behaviour in physiologically-relevant media, *J. Pharm. Pharmacol.*, 62(7), 844-855 (2010).

Nguyen, T. H., Hanley, T., Porter, C. J. H., Larson, I., and Boyd, B. J., Phytantriol and glyceryl monooleate cubic liquid crystalline phases as sustained-release oral drug delivery systems for poorly water-soluble drugs II. In-vivo evaluation, *J. Pharm. Pharmacol.*, 62(7), 856-865 (2010).

Niga, P., Wakeham, D., Nelson, A., Warr, G. G., Rutland, M., and Atkin, R., Structure of the Ethylammonium Nitrate Surface: An X-ray Reflectivity and Vibrational Sum Frequency Spectroscopy Study, *Langmuir*, 26(11), 8282-8288 (2010).

Nigam, R., Pan, A. V., Dou, S. X., Kennedy, S. J., Studer, A. J., and Stuesser, N., Magnetic field dependent neutron powder diffraction studies of Ru_{0.9}Sr₂YCu₂O_{7.9}, *J. Appl. Phys.*, 107(9), 3 (2010).

Olsen, S. R., Pullen, S. A., and Avdeev, M., A 100-position robotic sample changer for powder diffraction with low-background vacuum chamber, *J. Appl. Crystallogr.*, 43, 377-379 (2010).

Pang, W. K., Low, I. M., Kennedy, S. J., and Smith, R. I., *In situ* diffraction study on decomposition of Ti₂AlN at 1500-1800 degrees C in vacuum, *Mater. Sci. Eng. A-Struct. Mater. Prop. Microstruct. Process.*, 528(1), 137-142 (2010).

Parkinson, A., Colella, M. and Evans, T., The Development and Evaluation of Radiological Decontamination Procedures for Documents, Document Inks, and Latent Fingermarks on Porous Surfaces. *Journal of Forensic Sciences*, 55(3), 728-734. (2010).

Payten, W. M., Dean, D. W. and Snowden, K. U., A strain energy density method for the prediction of creep-fatigue damage in high temperature components. *Materials Science and Engineering a-Structural Materials Properties Microstructure and Processing*, 527(7-8), 1920-1925. (2010).

Payten, W. M., Snowden, K. U. and Bendeich, P., The use of a simplified analytical expression for metastable thermal stress analysis and its application to creep-fatigue damage of a 2.25Cr 1Mo thick walled component. *International Journal of Fatigue*, 32(2), 368-375. (2010).

Pearce, D. C., Dowling, K., Gerson, A. R., Sim, M. R., Sutton, S. R., Newville, M., Russell, R., and McOrist, G., Arsenic microdistribution and speciation in toenail clippings of children living in a historic gold mining area, *Sci. Total Environ.*, 408(12), 2590-2599 (2010).

Peterson, V. K., Kearley, G. J., Wu, Y., Ramirez-Cuesta, A. J., Kemner, E., and Kepert, C. J., Local Vibrational Mechanism for Negative Thermal Expansion: A Combined Neutron Scattering and First-Principles Study, *Angew. Chem.-Int. Edit.*, 49(3), 585-588 (2010).

Petrenko, V. V., Etheridge, D. M., Weiss, R. F., Brook, E. J., Schaefer, H., Severinghaus, J. P., et al., Methane from the east Siberian arctic shelf. *Science*, 329(5996), 1146-1147. (2010).

Photongkam, P., Zhang, Y. B., Assadi, M. H. N., Li, S., Yu, D., Ionescu, M., and Pan, A. V., Enhancement of Co substitution induced by Eu codoping in ZnO-based diluted magnetic semiconducting thin films, *J. Appl. Phys.*, 107(3), Art. No. 033909 (2010).

Pramanick, A., Prewitt, A. D., Cottrell, M. A., Lee, W., Studer, A. J., An, K., Hubbard, C. R., and Jones, J. L., *In situ* neutron diffraction studies of a commercial, soft lead zirconate titanate ceramic: response to electric fields and mechanical stress, *Appl. Phys. A-Mater. Sci. Process.*, 99(3), 557-564 (2010).

- Prokopovich, D. A., Reinhard, M. I., Cornelius, I. M. and Rosenfeld, A. B., Geant4 simulation of the CERN-EU high-energy reference field (CERF) facility. *Radiation Protection Dosimetry*, 141(2), 106-113. (2010).
- Radhi, M., Box, M. A., Box, G. P., and Cohen, D. D., Size-resolved chemical composition of the September 2009 Sydney dust storm. *Air Quality and Climate Change*, 44(3), 25-30. (2010).
- Radhi, M., Box, M. A., Box, G. P., Mitchell, R. M., Cohen, D. D., Stelcer, E., et al., Size-resolved mass and chemical properties of dust aerosols from Australia's Lake Eyre Basin. *Atmospheric Environment*, 44(29), 3519-3528. (2010).
- Rahlenbeck, M., Wagenknecht, M., Tsukada, A., Koelle, D., Kleiner, R., Keimer, B., and Ulrich, C., Raman light scattering study and microstructural analysis of epitaxial films of the electron-doped superconductor $\text{La}_{2-x}\text{Ce}_x\text{CuO}_4$, *Eur. Phys. J. B*, 75(4), 461-467 (2010).
- Ramachandran, S., Taraban, M. B., Trehwella, J., Gryczynski, I., Gryczynski, Z., and Yu, Y. B., Effect of Temperature During Assembly on the Structure and Mechanical Properties of Peptide-Based Materials, *Biomacromolecules*, 11(6), 1502-1506 (2010).
- Rekas, A., Knott, R. B., Sokolova, A., Barnham, K. J., Perez, K. A., Masters, C. L., Drew, S. C., Cappai, R., Curtain, C. C., and Pham, C. L. L., The structure of dopamine induced alpha-synuclein oligomers, *Eur. Biophys. J. Biophys. Lett.*, 39(10), 1407-1419 (2010).
- Ricciardo, R. A., Cuthbert, H. L., Woodward, P. M., Zhou, Q. D., Kennedy, B. J., Zhang, Z. M., Avdeev, M., and Jang, L. Y., Structure and Properties of $\text{Sr}_{1-x}\text{Ca}_x\text{Mn}_{0.5}\text{Ru}_{0.5}\text{O}_3$ Perovskites: Using Chemical Pressure to Control Mn/Ru Mixed Valency, *Chem. Mat.*, 22(11), 3369-3382 (2010).
- Rickard, W. D. A., van Riessen, A. and Walls, P., Thermal Character of Geopolymers Synthesized from Class F Fly Ash Containing High Concentrations of Iron and alpha-Quartz. *International Journal of Applied Ceramic Technology*, 7(1), 81-88. (2010).
- Roberts, D.J., Gregg, D.J. and Fitchett, C.M., Draper, S.M. Ferrocenyl-polyphenylenes: Toward Metallo-organic Polyaromatics. *Organometallics*, 29 (23), pp 6541-6547. (2010).
- Saerbeck, T., Klose, F., Lott, D., Mankey, G. J., Lu, Z., LeClair, P. R., Schmidt, W., Stampfl, A. P. J., Danilkin, S., Yethiraj, M., and Schreyer, A., Artificially modulated chemical order in thin films: A different approach to create ferro/antiferromagnetic interfaces, *Phys. Rev. B*, 82(13), Art. No. 134409 (2010).
- Saines, P. J., Hester, J. R., and Cheetham, A. K., Neutron diffraction study of the magnetic structures of manganese succinate $\text{Mn}(\text{C}_4\text{H}_4\text{O}_4)$: A complex inorganic-organic framework, *Phys. Rev. B*, 82(14), Art. No. 144435 (2010).
- Saintilan, N. and Mazumder, D., Fine-scale variability in the dietary sources of grazing invertebrates in a temperate Australian saltmarsh. *Marine and Freshwater Research*, 61(5), 615-620. (2010).
- Salim, N. V., Hanley, T., and Guo, Q. P., Microphase Separation through Competitive Hydrogen Bonding in Double Crystalline Diblock Copolymer/Homopolymer Blends, *Macromolecules*, 43(18), 7695-7704 (2010).
- Schmoelzer, T., Liss, K. D., Zickler, G. A., Watson, I. J., Droessler, L. M., Wallgram, W., Buslaps, T., Studer, A., and Clemens, H., Phase fractions, transition and ordering temperatures in TiAl-Nb-Mo alloys: An in- and ex-situ study, *Intermetallics*, 18(8), 1544-1552 (2010).
- Sharma, N., Macquart, R. B., Avdeev, M., Christensen, M., McIntyre, G. J., Chen, Y. S., and Ling, C. D., Re-investigation of the structure and crystal chemistry of the $\text{Bi}_2\text{O}_3\text{-W}_2\text{O}_6$ 'type (Ib)' solid solution using single-crystal neutron and synchrotron X-ray diffraction, *Acta Crystallogr. Sect. B-Struct. Sci.*, 66, 165-172 (2010).
- Sharma, N., Peterson, V. K., Elcombe, M. M., Avdeev, M., Studer, A. J., Blagojevic, N., Yusoff, R., and Kamarulzaman, N., Structural changes in a commercial lithium-ion battery during electrochemical cycling: An *in situ* neutron diffraction study, *J. Power Sources*, 195(24), 8258-8266 (2010).
- Shrestha, A. K., Ng, C. S., Lopez-Rubio, A., Blazek, J., Gilbert, E. P., and Gidley, M. J., Enzyme resistance and structural organization in extruded high amylose maize starch, *Carbohydr. Polym.*, 80(3), 699-710 (2010).
- Shulmeister, J., Fink, D., Hyatt, O. M., Thackray, G. D., and Rother, H., Cosmogenic ^{10}Be and ^{26}Al exposure ages of moraines in the Rakaia Valley, New Zealand and the nature of the last termination in New Zealand glacial systems. *Earth and Planetary Science Letters*, 297(3-4), 558-566. (2010).

- Siddiqui, K. S., Poljak, A., De Francisci, D., Guerriero, G., Pilak, O., Burg, D., Raftery, M. J., Parkin, D. M., Trehwella, J., and Cavicchioli, R., A chemically modified alpha-amylase with a molten-globule state has entropically driven enhanced thermal stability, *Protein Eng. Des. Sel.*, 23(10), 769-780 (2010).
- Smith, M. L., Bignell, L. J., Alexiev, D. and Mo, L., Sipping test: checking for failure of fuel elements at the Opal Reactor. *Nuclear Engineering and Technology*, 42(1), 125-130. (2010).
- Sokolova, A., Kealley, C. S., Hanley, T., Rekas, A., and Gilbert, E. P., Small-Angle X-ray Scattering Study of the Effect of pH and Salts on 11S Soy Glycinin in the Freeze-Dried Powder and Solution States, *J. Agric. Food Chem.*, 58(2), 967-974 (2010).
- Sprouster, D. J., Giulian, R., Araujo, L. L., Kluth, P., Johannessen, B., Cookson, D. J., Foran, G. J., and Ridgway, M. C., Structural and vibrational properties of Co nanoparticles formed by ion implantation, *J. Appl. Phys.*, 107(1), Art. No. 014313 (2010).
- Steuwer, A., Rahman, M., Shterenlikht, A., Fitzpatrick, M. E., Edwards, L. and Withers, P. J., The evolution of crack-tip stresses during a fatigue overload event *Acta Materialia*, 58(11), 4039-4052. (2010).
- Stevenson, A. W., Mayo, S. C., Hausermann, D., Maksimenko, A., R. F. Garrett, A., Hall, C. J., Wilkins, S. W., Lewis, R. A., and Myers, D. E., First experiments on the Australian Synchrotron Imaging and Medical beamline, including investigations of the effective source size in respect of X-ray imaging, *J. Synchrot. Radiat.*, 17, 75-80 (2010).
- Stevenson, J., Gillespie, R., Jacobsen, G., Fallon, S. and Levchenko, V. The archaic and puzzling record of Lake Xere Wapo, New Caledonia. *Terra Australis* 32 381-394 (2010).
- Stevenson, J., Siringan, F., Finn, J., Madulid, D., and Heijnis, H., Paoay Lake, northern Luzon, the Philippines: a record of Holocene environmental change. *Global Change Biology*, 16(6), 1672-1688. (2010).
- Sun, Y. L., Qu, D.D., Sun, Y. J., Liss, K. D., and Shen, J., Inhomogeneous structure and glass-forming ability in Zr-based bulk metallic glasses, *J. Non-Cryst. Solids*, 356(1), 39-45 (2010).
- Taylor, D. J. M., and Mazumder, D., Stable isotopes reveal post-release trophodynamic and ontogenetic changes in a released finfish, mulloway (*Argyrosomus japonicus*), *Marine and Freshwater Research*, 61:302-308. (2010).
- Telford, A. M., James, M., Meagher, L., and Neto, C., Thermally Cross-Linked PNVP Films As Antifouling Coatings for Biomedical Applications, *ACS Appl. Mater. Interfaces*, 2(8), 2399-2408 (2010).
- Thorogood, G. J., Avdeev, M., and Kennedy, B. J., Structural studies of the aeschynite-euxenite transformation in the series Ln(TiTa)O-6 Ln = Lanthanide, *Solid State Sci.*, 12(7), 1263-1269 (2010).
- Thorogood, G. J., Kennedy, B. J., Griffith, C. S., Elcombe, M. M., Avdeev, M., Hanna, J. V., Thorogood, S. K., and Luca, V., Structure and Phase Transformations in the Titanosilicate, Sitenakite. The Importance of Water, *Chem. Mater.*, 22(14), 4222-4231 (2010).
- Ting, J., Kennedy, B. J., Zhang, Z., Avdeev, M., Johannessen, B., and Jang, L. Y., Synthesis and Structural Studies of the Transition-Metal-Doped Rh Perovskites LaMn_{0.5}Rh_{0.5}O₃ and LaCu_{0.5}Rh_{0.5}O₃, *Chem. Mat.*, 22(5), 1640-1646 (2010).
- Treweek, T. M., Rekas, A., Walker, M. J., and Carver, J. A., A quantitative NMR spectroscopic examination of the flexibility of the C-terminal extensions of the molecular chaperones, α A- and α B-crystallin, *Exp. Eye Res.*, 91(5), 691-699 (2010).
- Triani, G., Campbell, J. A., Evans, P. J., Davis, J., Latella, B. A. and Burford, R. P., Low temperature atomic layer deposition of titania thin films. *Thin Solid Films*, 518(12), 3182-3189. (2010).
- Tsai, P. H., Donelson, R., Tan, T. T., Avdeev, M., Yu, D. H., Strassle, T., and Li, S., Oxygen Level Dependent Lattice Dynamics of Na_{0.73}CoO₂- δ , *J. Phys. Chem. C*, 114(49), 21848-21850 (2010).
- Vance, E. R., Zhang, Y. and Zhang, Z., Diffuse reflectance and X-ray photoelectron spectroscopy of uranium in ZrO₂ and Y₂Ti₂O₇. *Journal of Nuclear Materials*, 400(1), 8-14. (2010).
- Wang, C. H., Lawrence, J. M., Christianson, A. D., Goremychkin, E. A., Fanelli, V. R., Gofryk, K., Bauer, E. D., Ronning, F., Thompson, J. D., de Souza, N. R., Kolesnikov, A. I., and Littrell, K. C., Kondo behavior, ferromagnetic correlations, and crystal fields in the heavy-fermion compounds Ce₃X (X = In, Sn), *Phys. Rev. B*, 81(23), Art. No. 235132 (2010).
- Wang, H. F., K. F. Cai, H. F., Li, H., Yu, D. H., Wang, X., Zhou, C. W., Li, X. L., Wang, Y. Y., An, B. J., and Du, Y., Synthesis and thermoelectric properties of single crystalline and polycrystalline Ba₈Ga₁₆Ge₃₀. *J. Alloy. Compd.*, 491(1-2), 684-688 (2010).

Webster, N. A. S., Madsen, I. C., Loan, M. J., Knott, R. B., Naim, F., Wallwork, K. S., and Kimpton, J. A., An investigation of goethite-seeded $\text{Al}(\text{OH})_3$ precipitation using *in situ* X-ray diffraction and Rietveld-based quantitative phase analysis, *J. Appl. Crystallogr.*, 43, 466-472 (2010).

Wehr, J. B., Blamey, F. P. C., Hanna, J. V., Kopittke, P. M., Kerven, G. L. and Menzies, N. W., Hydrolysis and Speciation of Al Bound to Pectin and Plant Cell Wall Material and Its Reaction with the Dye Chrome Azurol S. *Journal of Agricultural and Food Chemistry*, 58(9), 5553-5560. (2010).

Wen, G., Naik, R., Cookson, P. G., Smith, S. V., Liu, X. and Wang, X. G., Wool powders used as sorbents to remove Co^{2+} ions from aqueous solution. *Powder Technology*, 197(3), 235-240. (2010).

Whittle, K. R., Blackford, M. G., Aughterson, R. D., Moricca, S., Lumpkin, G. R., Riley, D. P., et al., Radiation tolerance of $\text{M}_{n+1}\text{AX}_n$ phases, Ti_3AlC_2 and Ti_3SiC_2 . *Acta Materialia*, 58(13), 4362-4368. (2010).

Whittle, K. R., Lumpkin, G. R., Blackford, M. G., Aughterson, R. D., Smith, K. L. and Zaluzec, N. J., Ion-beam irradiation of lanthanum compounds in the systems $\text{La}_2\text{O}_3\text{-Al}_2\text{O}_3$ and $\text{La}_2\text{O}_3\text{-TiO}_2$. *Journal of Solid State Chemistry*, 183(10), 2416-2420. (2010).

Winton, B. R., Ionescu, M., Dou, S. X., Wexler, D., and Alva rez, G. A., Structural and morphological modification of PDMS thick film surfaces by ion implantation with the formation of strain-induced buckling domains. *Acta Materialia*, 58(5), 1861-1867. (2010).

Wolfson, E. J., Caspi, E. N., Ettetdgui, H., Shaked, H., and Avdeev, M., The effect of non-magnetic dilution of the Tb sublattice in TbCo_3B_2 , *J. Phys.-Condes. Matter*, 22(2), Art. No. 026001 (2010).

Wood, K., Tobias, D. J., Kessler, B., Gabel, F., Oesterhelt, D., Mulder, F. A. A., Zaccai, G., and Weik, M., The Low-Temperature Inflection Observed in Neutron Scattering Measurements of Proteins Is Due to Methyl Rotation: Direct Evidence Using Isotope Labeling and Molecular Dynamics Simulations, *J. Am. Chem. Soc.*, 132(14), 4990-+ (2010).

Wood, S. W., Hua, Q., Allen, K. J., and Bowman, D. M. J. S., Age and growth of a fire prone Tasmanian temperate old-growth forest stand dominated by *Eucalyptus regnans*, the world's tallest angiosperm. *Forest Ecology and Management*, 260(4), 438-447. (2010).

Woodroffe, C.D., Brooke, B.P., Linklater, M., Kennedy, D.M., Jones, B.G., Buchanan, C., Mlecko, R., Hua, Q. and Zhao, J.-x., Response of coral reefs to climate change: Expansion and demise of the southernmost Pacific coral reef, *Geophysical Research Letters*, 37, L15602. (2010).

Wu, H., Simmons, J. M., Liu, Y., Brown, C. M., Wang, X. S., Ma, S., Peterson, V. K., Southon, P. D., Kepert, C. J., Zhou, H. C., Yildirim, T., and Zhou, W., Metal-Organic Frameworks with Exceptionally High Methane Uptake: Where and How is Methane Stored?, *Chem.-Eur. J.*, 16(17), 5205-5214 (2010).

Xia, F., O'Neill, B., Ngothai, Y., Peak, J., Tenailleau, C., Etschmann, B., Qian, G., Brugger, J., Studer, A., Olsen, S., and Pring, A., A thermosiphon-driven hydrothermal flow-through cell for *in situ* and time-resolved neutron diffraction studies, *J. Appl. Cryst.*, 43(3), 511-519 (2010).

Xia, F., Qian, G., Brugger, J., Studer, A., Olsen, S., and Pring, A., A large volume cell for *in situ* neutron diffraction studies of hydrothermal crystallizations, *Rev. Sci. Instrum.*, 81(10), Art. No. 105107 (2010).

Xia, Y., Sartorius, H., Schlosser, C., Stoeckler, U., Conen, F., and Zahorowski, W., 'Comparison of one- and two-filter detectors for atmospheric ^{222}Rn measurements'. Accepted for publication in: *Atmospheric Measurement Techniques*. 3, 723-731 (2010).

Xu, X., Dou, S. X., Wang, X. L., Kim, J. H., Stride, J. A., Choucair, M., Yeoh, W. K., Zheng, R. K., and Ringer, S. P., Graphene doping to enhance the flux pinning and supercurrent carrying ability of a magnesium diboride superconductor, *Supercond. Sci. Technol.*, 23(8), Art. No. 085003 (2010).

Yan, K., Carr, D. G., Callaghan, M. D., Liss, K. D., and Li, H. J., Deformation mechanisms of twinning-induced plasticity steels: *In situ* synchrotron characterization and modeling, *Scr. Mater.*, 62(5), 246-249 (2010).

Yee, L. H., Hanley, T., Evans, R. A., Davis, T. P., and Ball, G. E., Photochromic Spirooxazines Functionalized with Oligomers: Investigation of Core-Oligomer Interactions and Photomerocyanine Isomer Interconversion Using NMR Spectroscopy and DFT, *J. Org. Chem.*, 75(9), 2851-2860 (2010).

Yu, G., Li, Y., Motoyama, E. M., Hradil, K., Mole, R. A., and Greven, M., Two characteristic energies in the low-energy magnetic response of the electron-doped high-temperature superconductor $\text{Nd}_{2-x}\text{Ce}_x\text{CuO}_{4+\delta}$, *Phys. Rev. B*, 82(17), Art. No. 172505 (2010).

Yu, K., Hua, Q., Zhao, J.-x., Hodge, E., Fink, D. and Barbetti M., Holocene marine ^{14}C reservoir age variability: evidence from ^{230}Th -dated corals from South China Sea, *Paleoceanography*, 25, PA3205. (2010).

Yun, S. I., Lo, V., Noorman, J., Davis, J., Russell, R. A., Holden, P. J., and Gadd, G. E., Morphology of composite particles of single wall carbon nanotubes/ biodegradable polyhydroxyalkanoates prepared by spray drying, *Polym. Bull.*, 64(1), 99-106 (2010).

Zbiri, M., Johnson, M. R., Haverkate, L., Mulder, F. M., and Kearley, G. J., Molecular Modelling of Ground- and Excited-States Vibrations in Organic Conducting Devices: Hexakis(n-hexyloxy)triphenylene (HAT(6)) as Case Study, *Aust. J. Chem.*, 63(3), 388-395 (2010).

Zbiri, M., Johnson, M. R., Kearley, G. J., and Mulder, F. M., Density functional calculations of potential energy surface and charge transfer integrals in molecular triphenylene derivative HAT(6), *Theor. Chem. Acc.*, 125(3-6), 445-451 (2010).

Zhang, Z. M. and Carter, M. L., An X-ray Photoelectron Spectroscopy Investigation of Highly Soluble Grain-Boundary Impurity Films in Hollandite. *Journal of the American Ceramic Society*, 93(3), 894-899. (2010).

Zhang, Z., Kennedy, B. J., Howard, C. J., Jang, L.-Y., Knight, K. S., Matsuda, M and Miyake, M. X-ray absorption and neutron diffraction studies of $(\text{Sr}_{1-x}\text{Ce}_x)\text{MnO}_3$: transition from coherent to incoherent static Jahn–Teller distortions. *J. Phys.: Condens. Matter* 22 445401. (2010).

Zhou, Q. D., Kennedy, B. J., and Avdeev, M., Structural studies of the disorder and phase transitions in the double perovskite Sr_2YTaO_6 , *J. Solid State Chem.*, 183(8), 1741-1746 (2010).

Zhu, H. L., Zhang, X. Q., Couper, M. J. and Dahle, A. K., The Formation of Streak Defects on Anodized Aluminum Extrusions. *Jom*, 62(5), 46-51. (2010).

Books, Edited Book Chapters, Special Journal Issues and Web Pages

Book

Dodson, J. R. (Ed.). *Changing climates, earth systems and society*. Warren, Michigan, United States of America: Springer. 360p (2010).

Book Chapters

Dodson, J. Setting the scene: how do we get to a fitting future? In: Dodson J., (editor) *Changing Climates, Earth Systems and Society*. Springer. Pages 1-4 (2010).

Fearnely, E., Weinstein, P. and Dodson, J. R., Climate change, societal transitions and changing infectious disease burdens. In J. R. Dodson (Ed.), *Changing Climates, Earth Systems and Society* (chapter 9). Warren, Michigan, United States of America: Springer (2010).

Fifield, K. and Fink, D., Environmental applications of accelerator mass spectrometry. In D. Beauchemin & D. Matthews (Eds.), *The Encyclopaedia of Mass Spectrometry, Vol. 5 - Elemental and Isotope Ratio Mass Spectrometry*, (chapter 6). Maryland Heights, United States of America: Elsevier (2010).

Fujioka, T. and Chappell, J., History of Australian aridity – chronology in the evolution of arid landscapes. In: Bishop, P. and Pillans, B. eds., *Australian Landscapes*. Geological Society, London, Special Publications, 346, pp. 121-139. DOI: 10.1144/SP346.8 - 2010.

Haberlah, D., Glasby, P., Williams, M. A. J., Hill, S. M., Williams, F., Rhodes, E. J., et al., 'Of droughts and flooding rains': an alluvial loess record from central South Australia spanning the last glacial cycle. In P. Bishop & B. Pillans (Eds.), *Geological Society of London, Special Publication - Australian Landscapes* (vol. 346, pp. 185-223). Piccadilly, London, United Kingdom: Geological Society of London (2010).

Kelleway, J., Mazumder, D., Wilson, G., and Kobayashi, T., Using isotopic techniques to assess trophic structure in northern Murray-Darling Basin wetlands. In N. Saintilan & I. Overton (Eds.), *Ecosystem Response Modelling in the Murray-Darling Basin* (chapter 6, pp. 85-101). Collingwood, Victoria, Australia: CSIRO Publishing (2010).

Vandenhove, H., Hurtgen, C., and Payne, T. E., Uranium. In D. Atwood (Ed.), *Radionuclides in the Environment* (pp. 261-272). Chichester, United Kingdom: John Wiley & Sons (2010).

Theses

Ashford, M. The Development and SAR of Selective Sigma-2 Receptor Ligands for the Diagnosis of Cancer (PhD Thesis) – University of Wollongong, Australia (2010).

Special Journal Issues

Buttner, H. G. (Ed). *Neutron News, 21(1-4) with 21.1. special issue: 20 Years of Neutron News*. Philadelphia, USA: Taylor & Francis Group. (2010).

Web Page

Hua, Q. Radiocarbon calibration. Online vignette supporting: Berman, P. and Montgomery, D. (Eds.) *Key concepts in Geomorphology*. W.H. Freeman, Vermont. URL: <http://serc.carleton.edu/vignettes/collection/35379.html> (2010)

Published Conference Proceedings

Atahan, P., Dodson, J. R., Li, X. Q., Zhou, X. Y., Chen, L., and Grice, K., Millet agriculture in north-central China: evidence from human remains. Australasian Quaternary Association (AQUA) Biennial Conference, 11th – 16th July 2010. Dunwich, North Stradbroke Island, Southeast Queensland: University of Queensland Moreton Bay Research Station (2010).

Burn-Nunes, L., Rosman, K. J. R., Vallelonga, P., Loss, R. D., Curran, M., and Smith, A. M., Measurement of Pb in ancient Antarctic ice: implications for source regions of aerosols and past environmental conditions. 20th Annual V.M. Goldschmidt Conference (Goldschmidt 2010) - "Earth, Energy, and the Environment", 13th - 18th June 2010. Knoxville, Tennessee: Knoxville Convention Center. In *Geochimica et Cosmochimica Acta*, 74(12), A130 (2010).

Callaghan, M. D., Humphries, S. R., Law, M., Li, H., and Yeung, W. Y., Evaluation of high temperature fatigue behaviour of P22 by miniature specimen testing. International Conference on Processing & Manufacturing of Advanced Materials (Thermech' 2009), 25th – 29th August 2009. Maritim Hotel: Berlin, Germany. In *Materials Science Forum*, 638-642, 3937-3942. (2010).

Cendon, D. key note at workshop "Methods for the study of long-term groundwater dynamics" jointly organised by UNESCO International Hydrological Programme, International Union for Quaternary Research, International Association of Hydrogeologists and Laboratory of Radio-Analysis and Environment, Tunisia (1-5 November, 2010).

Cendon, D., Pueyo, J. J., Ayora, C., Garcia Veigas, J., and Blanc-Valleron, M. M., Exploring the hydrochemical evolution of brines leading to sylvite precipitation in ancient evaporite basins. 7th European Geosciences Union (EGU) General Assembly, 2nd – 7th May 2010. Vienna, Austria: Austria Center. In *Geophysical Research Abstracts*, 12, EGU2010-3807-1 (2010).

Chambers, S., Williams, A. G., Zahorowski, W., and Griffiths, A. D., Evaluating radon-derived mixing depth as a potential length scale for nocturnal mixing processes over land. 7th European Geosciences Union (EGU) General Assembly, 2nd – 7th May 2010. Vienna, Austria: Austria Center. In *Geophysical Research Abstracts*, 12, EGU2010-3839 (2010).

Child, D. P., Hotchkis, M. A. C., Whittle, K., and Zorko, B., Ionisation efficiency improvements for AMS measurement of actinides. 11th International Conference on Accelerator Mass Spectrometry (AMS-11), 14th – 19th September 2008. Spazio Etoile, Rome. In *Nuclear Instruments & Methods in Physics Research Section b-Beam Interactions with Materials and Atoms: Proceedings of the Eleventh International Conference on Accelerator Mass Spectrometry*, 268(7-8), 820-823 (2010).

Clarke, L.J., Robinson, S.A., Ayre, D.J., Hua, Q., and Fink, D., Impacts of a changing climate on growth rates of Antarctic mosses, the American Society of Plant Biologists Meeting – Plant Biology, 31 Jul – 4 Aug 2010, Montreal, Canada 2010.

Comarmond, M. C. J., Payne, T., Harrison, J., Thiruvoth, S., and Muller, K., Uranium sorption on various forms of TiO₂ - influence of surface area, surface charge and impurities. 16th Radiochemical Conference (Radchem 2010), 18th – 23rd April 2010. Czech Republic: Mariánské Lázně. In *Chemicke Listy*, 104, s178-s262(REG.L17(Id: 194)) (2010).

Dalton, V.S., Walker, A., Hodgson, D.M. and Zavitsanou, K. (2010). Cannabinoid impact on serotonin receptors in an animal model of prenatal psychosis-related susceptibility. Oral presentation, Australasian Schizophrenia Conference, 22-24 September 2010, Sydney, Australia.

Danilkin, S. A., Yethiraj, M., and Kearley, G. J., Phonon dispersion in superionic copper selenide - observation of soft phonon modes in superionic phase transition. The 3rd International Conference on Physics of Solid State Ionics, ICPSSI-3, 25th – 28th October 2009. Kumamoto University: Japan. In *Journal of the Physical Society of Japan*, 79(Suppl. A), 25-28 (2010).

Delzescaux, T., Leberberg, J., Raguet, T., Hantraye, P., Souedet, N. and Gregoire, M. C. (2010). Segmentation of small animal PET/CT mouse brain scans using an MRI-based 3D digital atlas: application in a neuroinflammation mouse model. 32nd Annual International Conference of the IEEE Engineering in Medicine and Biology Society (EMBC'10) - "Merging Medical Humanism and Technology", 31st August - 4th September 2010. In *Proceedings of the 2010 Annual International Conference of the IEEE Engineering in Medicine and Biology Society* (pp. 3097-3100, ThDPo06.5). Buenos Aires, Argentina: Buenos Aires Sheraton Hotel. (2010)

Dodson, J. Paradise lost: tools and lessons on how human-kind shaped the world. Royal Society of Victoria, Melbourne, 1 November 2010.

Dunne, N., Ormsby, R., McNally, T., Mitchell, C. A., Martin, D., Halley, P., et al., Nanocomposite bone cements for orthopaedic applications. International Conference on Orthopaedic Biomechanics, Clinical Applications and Surgery (OBCAS 2010), 6th - 9th June 2010. Brunel University: London, United Kingdom. In *Journal of Biomechanics*, 43(S1), S53 (2010).

Eberl, S., Katsifis, A., Wen, L., Bourdier, T., Henderson, D., Loc'h, C., Mohamed, A., Gregoric, I., Pham, T., and Fulham, M J., Quantitative analysis of the peripheral benzodiazepine receptor ligand [¹¹C] PBR170 in baboons with PET. 57th Annual Meeting of the Society of Nuclear Medicine, 5-9 June, Salt Lake City, UT, USA. *J Nucl Med*. 2010; 51 (Supplement 2):33 (2010).

Felton, E. A., Switzer, A. D., Fink, D., and Crook, K. A. W., Overturned cliff-top mega-boulders at Little Beecroft Head, Jervis Bay, NSW, Australia: a mega-tsunami or aboveground bolide impact about 20ka BP? Australian Earth Sciences Convention 2010 (AESC 2010), 4th – 8th July 2010. Canberra, Australia: National Convention Centre (2010).

Fink, D., AMS-11 in Rome, 2008: past achievements, current and future trends. 11th International Conference on Accelerator Mass Spectrometry (AMS-11), 14th – 19th September 2008. Spazio Etoile, Rome. In *Nuclear Instruments & Methods in Physics Research Section b-Beam Interactions with Materials and Atoms: Proceedings of the Eleventh International Conference on Accelerator Mass Spectrometry*, 268(7-8), 1334-1342. (2010).

Fink, D. and Shulmeister, J., Late-glacial re-advance during the Last Glacial-Interglacial transition; revisiting the Misery moraines in the Southern Alps of New Zealand. International Glaciological Conference (VICC 2010) - "Ice and Climate Change: A View from the South", 1st - 3rd February 2010. Valdivia, Chile: Centro de Estudios Científicos (CECS) (2010).

Fink, D. and Williams, P., Southern Hemisphere millennial glaciations during the past 30 ka driven by Antarctic ice sheet variability. International Glaciological Conference (VICC 2010) - "Ice and Climate Change: A View from the South", 1st - 3rd February 2010. Valdivia, Chile: Centro de Estudios Científicos (CECS) (2010).

Fink, D. and Augustinus, P., Glacial history of Tasmania from mid-Pleistocene to the Last Glacial Maximum – new challenges and new ideas for hemispheric glacial climate correlations. International Glaciological Conference (VICC 2010) - "Ice and Climate Change: A View from the South", 1st - 3rd February 2010. Valdivia, Chile: Centro de Estudios Científicos (CECS) (2010).

Fink, D., Anne, F. E., Crook, K. A. W., Switzer, A. D. Cliff-top boulders on coastal platforms at Little Beecroft Head, southeast Australia – Holocene tsunami deposits or ancient relics of platform weathering? EGU, Vienna, Geophysical Research Abstracts, Vol 12, EGU2010-6564 (2010).

Fink, D., Storey, B., Hood, D., Joy, K., and Shulmeister, J., Constraints on ice volume changes of the WAIS and Ross Ice Shelf since the LGM based on cosmogenic exposure ages in the Darwin-Hatherton glacial system of the Transantarctic Mountains. 7th European Geosciences Union (EGU) General Assembly, 2nd – 7th May 2010. Vienna, Austria: Austria Center. In *Geophysical Research Abstracts*, 12, EGU2010-6551 (2010).

Fischer, M. J. and Treble, P.C., Holocene Climate Reconstructions and modelling from Australian Speleothems. Australian Earth Sciences Convention 2010, Cabnberra, 4-8 July (<http://www.aesc2010.gsa.org.au/>). (2010).

Fischer, M. J. and Treble, P.C., Reconstructing climate modes from Australian speleothems. First Aus2K Workshop, School of Earth Sciences, University of Melbourne, 31 May- 2 June <http://www.pages-igbp.org/science/2k/aus2k/aus2kmeeting2010.html> (2010).

Fong, N., Musumeci, A., Guagliardo, P., Williams, J., Martin, D., and Smith, S. V., Clay Particles for Drug Delivery - Potential of Positron Annihilation Lifetime Spectroscopy (PALS) for Studying Interlayer Spacing. 12th International Workshop on Slow Positron Beam Techniques. 1-6 August, Magnetic Island, Australia (2010).

Francey, R., van der Schoot, M., Krummel, P., Steele, P., Trudinger, C., and Zadorowski, W., 2010: 'Recent Slowing in Global CO₂ Growth: Reducing Uncertainty in the CO₂ Growth Trend'. Invited oral presentation at: Greenhouse gases in the Earth system: setting the agenda to 2030 conference. The Royal Society, London. 22-23 February 2010.

Fruchter, N., Matmon, A., Zilberman, E., Avni, Y., and Fink, D., Sediment source and mixing and the cycle of sediment transport: an example from NE Negev Desert, Israel. 7th European Geosciences Union (EGU) General Assembly, 2nd – 7th May 2010. Vienna, Austria: Austria Center. In Geophysical Research Abstracts, 12, EGU2010-1391(2010).

Fuchs, A., Greguric, I., and Roe, G., Evaluation of radioisotope quality aspects for preparation of high specific activity [Ga-68]-NOTA-AnnexinA1. International Symposium on Technetium and Other Radiometals in Chemistry and Medicine (TERACHEM 2010), 8th - 11th September 2010. Forum Brixen: Bressanone (Bolzano), Italy. In Nuclear Medicine and Biology, 37(6), 692 (2010).

Fujioka, T., Fifield, L.K., Chappell, J., Pillans, B. and Tims, S., A new cosmogenic isotope, manganese-53, for exposure dating: preliminary results from iron-rich rocks in arid-semiarid Australia (oral). Australasian Quaternary Association (AQUA) biennial meeting, Stradbroke Is., QLD, 11-18 July 2010.

Griffiths, M., Drysdale, R., Hua, Q., Hellstrom, J., Frisia, S., Gagan, M., et al., Assessment of climatic influences on 14C activity in a Holocene stalagmite from Flores, Indonesia. 3rd Dated Speleothems - Archives of the Paleoenvironment (DAPHNE) Workshop, 30th June – 2nd July 2010. Kranebitter Hof: Innsbruck, Austria (2010).

Hamilton, W. A., and Porcar, L., Neutron scattering study of a membrane phase miscibility gap: Coexistence of L3 “sponge” and La Lamellar phases, J. Phys.: Conf. Ser., 251(1), Art. No. 012034, International Conference on Neutron Scattering 2009, 3–7 May 2009, Knoxville, Tennessee, USA (2010).

Hotchkis, M. A. C., Child, D. P., & Zorko, B., Actinides AMS for nuclear safeguards and related applications. 11th International Conference on Accelerator Mass Spectrometry (AMS-11), 14th – 19th September 2008. Spazio Etoile, Rome. In Nuclear Instruments & Methods in Physics Research Section b-Beam Interactions with Materials and Atoms: Proceedings of the Eleventh International Conference on Accelerator Mass Spectrometry, 268(7-8), 1257-1260 (2010).

Hua, Q., Drysdale, R., McDonald, J., Redwood, D and Fallon, S. Chronological reconstruction for young speleothems by radiocarbon, the Paleochronology Building Workshop, San Miguel de Allende, Guanajuato, Mexico, 17-21 Aug 2010.

Hua, Q., Williams, A., Levchenko, V., and Ying, B., Developments in micro-sample 14C AMS at the ANTARES AMS facility. 11th International Conference on Accelerator Mass Spectrometry (AMS-11), 14th – 19th September 2008. Spazio Etoile, Rome. In Nuclear Instruments & Methods in Physics Research Section b-Beam Interactions with Materials and Atoms: Proceedings of the Eleventh International Conference on Accelerator Mass Spectrometry, 268(7-8), 919-923 (2010).

Iles, J., Kobayashi, Y., Knowles, L., Saintilan, N., Mazumder, D., et al., Environmental flow water and aquatic consumer food web structure: temporal aspects. Ecosystem Response Modelling in the Murray-Darling Basin: Better Use of Environmental Water, 11th - 12th May 2010. Sydney Olympic Park, Australia: Waterview Conference Centre (2010).

Imperia, P., Zhang, Z., Stampfl, A., “Paramagnetic to ordered magnetic phase transition of He+ ions irradiated stainless steel studied by XMCD: A new perspective for early stage detection of defects in solids, Journal of Physics Conference Series, p. 200., 112001doi://dx.doi.org/10.1088/1742-6596/200/11/112001 (2010).

Ionescu, M., Photongkam, P., Yu, D., Siegele, R., Li, S., & Cohen, D. D., Doping of ZnO thin film with Eu using ion beams. International Conference on Processing & Manufacturing of Advanced Materials (Thermec' 2009), 25th – 29th August 2009. Maritim Hotel: Berlin, Germany. In Materials Science Forum, 638-642, 2962-2969 (2010).

Joy, K., Atkins, C., Storey, B., and Fink, D., Darwin / Hatherton glacial system: preliminary results of geomorphological mapping and cosmogenic sampling in 2009/10. Annual Antarctic Conference 2010 - “a Taste of the Ice”, 5th – 7th July 2010. In Proceedings of the Annual Antarctic Conference 2010 (p. 58). Christchurch, New Zealand: University of Canterbury (2010).

Joy, K., Storey, B., Fink, D., and Shulmeister, J., Diamond Hill, Darwin Glacier. A proxy for the West Antarctic ice sheet? Annual Antarctic Conference 2010 - “A Taste of the Ice”, 5th – 7th July 2010. In Proceedings of the Annual Antarctic Conference 2010 (p. 57). Christchurch, New Zealand: University of Canterbury (2010).

Larsen, J., Cendon, D., Nanson, G., and Jones, B., Radiocarbon and geochemical constraints on shallow groundwater recharge in a large arid zone river, Cooper Creek, SW Queensland, Australia. 7th European Geosciences Union (EGU) General Assembly, 2nd – 7th May 2010. Vienna, Austria: Austria Center. In Geophysical Research Abstracts, 12, EGU2010-14002 (2010).

Law, M., Luzin, V., and Kirstein, O., Effects of cutting and specimen size on neutron measurement of residual stresses, *J. Phys.: Conf. Ser.*, 251(1), Art. No. 012044, International Conference on Neutron Scattering 2009, 3–7 May 2009, Knoxville, Tennessee, USA (2010).

Law, M., Luzin, V., and Kirstein, O., Measurement of Residual Stress in a Welded Branch Connection and Effects on Fracture Behaviour, *J. Phys.: Conf. Ser.*, 251(1), Art. No. 012045 (2010). International Conference on Neutron Scattering 2009, 3–7 May 2009, Knoxville, Tennessee, USA (2010).

Lee, W.-T., Tong, X., Pierce, J., Fleenor, M., Ismaili, A., Robertson, J.L., Chen, W. C., Gentile, T. R., Hailamariam, A., Goyette, R., Parizzi, A., Lauter, V., Klose, F., Kaiser, H., Lavelle, C., Baxter, D. V., Jones, G. L., Wexler, J., and McCollum, L., In-situ Polarized ³He-Based Neutron Polarization Analyzer for SNS Magnetism Reflectometer, *J. Phys.: Conf. Ser.*, 251(1), Art. No. 012086. International Conference on Neutron Scattering 2009, 3–7 May 2009, Knoxville, Tennessee, USA (2010).

Lumpkin, G.R., Smith, K.L., Whittle, K.R., Thomas, B.S., and Marks, N.A., “Mechanisms of radiation damage and properties of nuclear materials”, *Materials Research Needs to Advance Nuclear Energy*, Mater. Res. Soc. Symp. Proc., Volume 1215, 19-26 (2010).

Mackintosh, A., Gолledge, N., Domack, E., Dunbar, R., Leventer, A., White, D., Pollard, D., DeConto, R., Fink, D., Gore, D., and Lavoie, C. Peripheral recession of Antarctic ice sheets forced by sea level rise and ocean warming. International Physical Year Conf, Oslo, July 2010.

Mazumder, D., Johansen, M., Saintilan, N., Iles, J., Knowles, L., Kobayashi, Y., et al., Isotopic and modelling studies of food web structure in wet and dry conditions, Yanga wetlands NSW, Australia. Ecosystem Response Modelling in the Murray-Darling Basin: Better Use of Environmental Water, 11th - 12th May 2010. Sydney Olympic Park, Australia: Waterview Conference Centre (2010).

Mazumder, D., Johansen, M., Saintilan, N., Iles, J., Knowles, L., Kobayashi, T., et al., Food webs in freshwater floodplain wetlands inundated with environmental flows during drought conditions. 7th International Conference on Applications of Stable Isotope Techniques to Ecological Studies (ISOECOL VII), 9th - 13th August 2010. Fairbanks, Alaska: University of Alaska Fairbanks (2010).

McDonald, J., R. Drysdale, E. Hodge, Q. Hua, M. Fischer, P. Treble, A. Greig, and J. Hellstrom, A 1,000 year rainfall record for SE Australia using speleothem hydrological proxies, 4-8 Jul 2010, Canberra, Australian Earth Sciences Convention 2010.

McGregor, H. V., Phipps, S. J., Woodroffe, C. W., Gagan, M. K., and Fink, D. (2010). El Niño-Southern Oscillation (ENSO) from 0-2 ka. The 1st Aus2k Regional Workshop - “Towards Data Synthesis”, Fritz Loewe Theatre, School of Earth Science, University of Melbourne: Melbourne, Australia, 31st May - 2nd June 2010.

Minami, M., Y. Miyata, T. Nakamura, and Q. Hua, A first step toward small-mass AMS radiocarbon analysis, The 12th Japanese Accelerator Mass Spectrometry (AMS) Conference, Nagoya, Japan, 23-24 May 2010.

Mo, L., Bignell, L. J., Steele, T. and Alexiev, D., Activity measurements of H-3 using the TDCR method and observation of source stability. 17th International Conference on Radionuclide Metrology and its Applications (ICRM 2009), 7th - 11th September 2009. Slovak Institute of Metrology: Bratislava, Slovak Republic. In *Applied Radiation and Isotopes*, 68(7-8), 1540-1542 (2010).

Mume, E., Uedono, A., Mizunaga, G., Lynch, D. E., and Smith, S.V. The Role of Positrons Annihilation Lifetime Studies and Nuclear Sensors for Characterising Porous Materials. *Journal of Physics: Conference Series* Accepted. 12th International Workshop on Slow Positron Beam Techniques (SLOPOS12), Magnetic Island, North Queensland, Australia” 1–6 August 2010.

Nelson, A., Motofit integrating neutron reflectometry acquisition, reduction and analysis into one, easy to use, package, *J. Phys.: Conf. Ser.*, 251(1), Art. No. 012094, International Conference on Neutron Scattering 2009, 3–7 May 2009, Knoxville, Tennessee, USA (2010).

Nguyen, V.H., Wang, H., Verdurand, M., Dedeurwaerdere, S. Small animal pet with [18F]FDG after a single dose of the synthetic cannabinoid HU210. ANS/AuPS Joint Meeting • Sydney • 31 January - 3 February 2010. POS-MON-064 13:30 - 14:30, 2010.

Othman, M. A. R., Marinaro, D. G., Petasecca, M., Guatelli, S., Cutajar, D. L., Lerch, M. L. F., et al. (2009). From imaging to dosimetry: GEANT4-based study on the application of Medipix to neutron dosimetry. 11th Neutron and Ion Dosimetry Symposium (NEUDOS-11), 11th - 16th October 2009. iThemba Laboratory for Accelerator-Based Sciences: Cape Town, South Africa. In *Radiation Measurements*, 45(10), 1355-1358 (2010)

P.C.Treble, Speleothem palaeo-rainfall archives in southwest and southeast Australia First Aus2K Workshop, School of Earth Sciences, University of Melbourne, 31 May- 2 June (<http://www.pages-igbp.org/science/2k/aus2k/aus2kmeeting2010.html>) (2010),

Pang, W. K., Low, I. M., O'Connor, B. H., Studer, A. J., Peterson, V. K., Sun, Z. M., and Palmquist, J.-P., Comparison of thermal stability in MAX 211 and 312 phases, *J. Phys.: Conf. Ser.*, 251(1), Art. No. 012025, International Conference on Neutron Scattering 2009, 3–7 May 2009, Knoxville, Tennessee, USA (2010).

Parkes, S., Griffith, D., Williams, A. G., Element, A., Chambers, S., and McCabe, M., In-situ measurements of the stable isotopes composition of atmospheric water vapour using FTIR spectroscopy. Workshop on the Water Isotopologues in the Atmosphere, 27th – 30th April 2010. Paris, France: University Pierre et Marie Curie (2010).

Parkes, S.D., Williams, A.G., Element, A., Chambers, S., Griffiths, A.D., and Griffith, D.W.T., 2010: 'The stable isotope signal of atmospheric water vapour in Sydney, Australia.' *Geophysical Research Abstracts*, Vol. 12, EGU2010-7429, EGU General Assembly Vienna, 2-7 May 2010,

Perkins, G. and Smith, S.V. (2010). Multiple patient batch production of 195mPt cisplatin and 195mPt carboplatin for use in drug risk assessment and optimisation of patient dose. International Symposium on Technetium and Other Radiometals in Chemistry and Medicine. TE.RA.CHE.M.-2010. Forum-Brixen, Bressanone (Bz) - Italy, Sept. 8-11, 2010.

Pham, B., Guagliardo, P., Williams, J., Samarin, S., and Smith, S. V. A Study of Porosity of Synthetic Polymer Nanoparticles using PALS. 12th International Workshop on Slow Positron Beam Techniques (SLOPOS12) 1–6 August 2010, Magnetic Island, North Queensland, Australia. *Journal of Physics, Conference Series*. *J. Phys.: Conf. Ser.* 262 012048" (2010).

Robinson, S. A., Clarke, L. J., King, D., Ayre, D. J., Hua, Q., Fink, D., et al., Monitoring impacts of a changing climate on plant communities of Continental Antarctica. British Ecological Society (BES) Annual Meeting 2010, 7th - 9th September 2010. University of Leeds: Leeds, United Kingdom (2010).

Rodriguez, D. M., Kennedy, S. J., and Klose, F., Upgrade of the neutron guide system at the OPAL Neutron Source, *J. Phys.: Conf. Ser.*, 251(1), Art. No. 012065, International Conference on Neutron Scattering 2009, 3–7 May 2009, Knoxville, Tennessee, USA (2010).

Selliayan, S., Smith, S.V., Hughes, T., Miller, T., Jenkins, D.R. and Uedono, A. Understanding the Effect of Nanoporosity on Optimizing the Performance of Self-Healing Materials for Anti-Corrosion. Applications . 12th International Workshop on Slow Positron Beam Techniques. 1-6 August 2010, Magnetic Island, Australia. *J. Phys.: Conf. Ser.* 262 012054, (2010).

Sharma, N., Söhnle, T., McIntyre, G. J., Piltz, R., and Ling, C. D., Structure of BiRe2O6 re-investigated using single-crystal neutron Laue diffraction, *J. Phys.: Conf. Ser.*, 251(1), Art. No. 012028 (2010). International Conference on Neutron Scattering 2009, 3–7 May 2009, Knoxville, Tennessee, USA (2010).

Smith, K.L., Lumpkin, G.R., Whittle, K.R., Blackford, M.G., and Zaluzec, N.J., Investigating radiation damage in ceramics: the role of *in situ* microscopy, *Microscopy and Microanalysis*, 16, 1618-1619 (2010).

Smith, S. V. The role of Nuclear Sensors and Positrons for Engineering Nano and Microtechnologies. 12th International Workshop on Slow Positron Beam Techniques (SLOPOS12) 1–6 August 2010, Magnetic Island, North Queensland, Australia. *J. Phys.: Conf. Ser.* 262 012055 " (2010).

St Pierre, E., J.-x. Zhao, K. Aplin, R. Drysdale, S. Golding, M. Griffiths and Q. Hua, A multi-proxy record of Late Holocene palaeoenvironmental change and human impact on the environment in Western Flores, Indonesia, The Australian Archaeology Association conference, Batemans Bay, NSW, Australia, 9-13 Dec 2010.

Storey, B., Fink, D., Joy, K. and Shulmeister, J., Constraints on Antarctic ice volume changes since the LGM based on cosmogenic exposure ages in the Darwin-Hatherton glacial system of the Transantarctic Mountains, 31st Scientific Conf on Antarctic Research, Meeting, Argentina, August, 2010.

Stroeven, Arjen P., Hattestrand, Clas, Fabel, Derek, Fink, David et al. Retreat pattern of the Fennoscandian ice sheet since the Younger Dryas based on geomorphology and multiple proxies for deglaciation age (^{14}C , ^{10}Be , OSL), APEX 4th Fourth International conference and workshop - Arctic paleoclimate proxies and chronologies, Iceland, May 2010.

Tibby, J., J. Marshall, J. Lobegeiger, T. Myburgh, and Q. Hua, Waterhole sedimentation in the dryland Moonie River and the loss of drought refugia for fish, AQUA (Australasian Quaternary Association) Biennial Meeting, 11-18 Jul 2010, North Stradbroke Island, southeast Queensland (2010).

Twining, J. R., and Johansen, M., Environmental studies in Australia: current radioecological priorities. IRPA Regional Congress (AOCR-3): the Third Asian and Oceanic Congress on Radiation Protection, 24th – 28th May 2010. Tokyo, Japan: Tower Hall Funabori (2010).

Verdurand, M., Nguyen, V., Stark, D., Zahra, D., Gregoire, M. C., Greguric, I. and Zavitsanou, K. Feasibility of imaging the ontogeny of CB1 receptors in adolescent and adult rats in vivo with $[^{18}\text{F}]\text{MK 9470}$ and PET. Foundation Meeting for the Biological Psychiatry, Melbourne Australia, 6 September 2010.

Verdurand, M., Nguyen, V., Stark, D., Zahra, D., Gregoire, M. C., Greguric, I., et al. Feasibility of imaging the ontogeny of CB1 receptors in adolescent and adult rats in vivo with $[^{18}\text{F}]\text{MK 9470}$ and PET: a pilot study. 11th Biennial Australasian Schizophrenia Conference (ASC2010) - "Molecules to Mind", 22nd - 24th September 2010. Sydney, Australia: Sheraton on the Park. In Australian and New Zealand Journal of Psychiatry, 44(Suppl. 1), A55 (2010).

Wang, J. L., Campbell, S. J., Studer, A. J., Kennedy, S. J., and Zeng, R., (2009). Magnetic properties of $\text{Ho}_2\text{Fe}_{17-x}\text{Mn}_x$ - influence of Mn substitution. 18th International Conference on Magnetism (ICM 2009) Section 11 - "Measuring Techniques and Instrumentation", 26th - 31st July 2009. The Congress Center Karlsruhe: Karlsruhe, Germany. In Journal of Physics: Conference Series, 200, 082025 (2010).

White, D., Fink, D., and Winkler, S., GRACE satellite data and cosmogenic exposure ages in Enderby Land, Antarctica: ice mass increase or uncorrected post-glacial rebound? 7th European Geosciences Union (EGU) General Assembly, 2nd – 7th May 2010. Vienna, Austria: Austria Center. In Geophysical Research Abstracts, 12, EGU2010-6562 (2010).

Whitfield, R. E., Goossens, D. J., and Studer, A. J., Study of phase formation in metal injection moulding through real time neutron diffraction, J. Phys.: Conf. Ser., 251(1), Art. No. 012048 (2010). International Conference on Neutron Scattering 2009, 3–7 May 2009, Knoxville, Tennessee, USA (2010).

Whittle, K.R., Blackford, M.G., Aughterson, R.D., Smith, K.L., Lumpkin, G.R., and Zaluzec, N.J. Ion beam irradiation of compounds in the series $\text{La}_2\text{O}_3\text{-TiO}_2$ Scientific Basis for Nuclear Waste Management XXXIV, Mater. Res. Soc. Symp. Proc., Volume 1265, 1265-AA08-05-BB07-05. (2010).

Whittle, K.R., Blackford, M.G., Smith, K.L., Lumpkin, G.R., and Zaluzec, N.J., Radiation Tolerance and Disorder - Can They Be Linked? Materials Research Needs to Advance Nuclear Energy, Mater. Res. Soc. Symp. Proc., Volume 1215, 71-79 (2010).

Williams, A. G., Zahorowski, W., Chambers, S., Element, A., Werczynski, S., and Griffiths, A. D., Improved estimation of total boundary layer radon for budget studies and regional integrations. 7th European Geosciences Union (EGU) General Assembly, 2nd – 7th May 2010. Vienna, Austria: Austria Center. In Geophysical Research Abstracts, 12, EGU2010-3823 (2010).

Woodroffe, C. D., Brooke, B. P., Linklater, M., Kennedy, D. M., Jones, D. M., Buchanan, C., et al. (2010). Morphology and formation of relict coral reef on the shelf around Lord Howe Island. Marine Geological and Biological Habitat Mapping Annual Forum (GEOHAB 2010), Town Hall: Wellington, New Zealand - 4th – 7th May 2010.

Zahorowski, W., Vermeulen, A., Williams, A. G., Chambers, S., and Verheggen, B., Continuous hourly radon gradient observations at Cabauw, the Netherlands - a review of main features of the 2007-2009 dataset. 7th European Geosciences Union (EGU) General Assembly, 2nd – 7th May 2010. Vienna, Austria: Austria Center. In Geophysical Research Abstracts, 12, EGU2010-3840 (2010).

Zahorowski, W., Chambers, S., Griffiths, A. D., Crawford, J., and Williams, A. G., Seasonal variability of the radon-222 flux density from the Southern Ocean derived from atmospheric radon-222 measurements at the Cape Grim baseline station in Tasmania. 7th European Geosciences Union (EGU) General Assembly, 2nd – 7th May 2010. Vienna, Austria: Austria Center. In Geophysical Research Abstracts, 12, EGU2010-3828 (2010).

Zhang, X., Heijnis, H., Dodson, J. R., and Zawadzki, A., Environmental changes indicated by grain-size and trace-metal analysis over the past 700 years at Annaburroo Lagoon, NT, Australia. Australasian Quaternary Association (AQUA) Biennial Conference, 11th – 16th July 2010. Dunwich, North Stradbroke Island, Southeast Queensland: University of Queensland Moreton Bay Research Station (2010).

Zorko, B., Child, D. P., and Hotchkis, M. A. C., Fast switching electrostatic deflector system for actinide isotopic ratio measurements. 11th International Conference on Accelerator Mass Spectrometry (AMS-11), 14th – 19th September 2008. Spazio Etoile, Rome. In Nuclear Instruments & Methods in Physics Research Section b-Beam Interactions with Materials and Atoms: Proceedings of the Eleventh International Conference on Accelerator Mass Spectrometry, 268(7-8), 827-829 (2010).

ANSTO Research Selections 2011

Published by

The Australian Nuclear Science and Technology Organisation (ANSTO)

Available from

PDF version is available on the ANSTO website

www.ansto.gov.au

Reproducing any part of the great science in this publication is welcomed provided the source is acknowledged and an archive copy sent to ANSTO Strategic Communications and Government Affairs Locked Bag 2001, Kirrawee DC NSW 2232.

ANSTO October 2011



Australian Government

Ansto

Nuclear-based science benefiting all Australians

www.ansto.gov.au

